ANL-6648
Chemical Separations
Processes for
Plutonium and Uranium
(TID-4500, 20th Ed.)
AEC Research and
Development Report

ARGONNE NATIONAL LABORATORY
9700 South Cass Avenue
Argonne, Illinois

CHEMICAL ENGINEERING DIVISION SUMMARY REPORT

October, November, December, 1962

Stephen Lawroski, Division Director
R. C. Vogel, Associate Division Director
Milton Levenson, Associate Division Director
V. H. Munnecke, Assistant Division Director

May 1963

Preceding Summary Reports:
ANL-6596 July, August, September, 1962
ANL-6569 April, May, June, 1962
ANL-6543 January, February, March, 1962

Operated by The University of Chicago
under
Contract W-31-109-eng-38
with the
U. S. Atomic Energy Commission

DISCLAIMER

TABLE OF CONTENTS

TABLE OF CONTENTS

LIST OF TABLES

LIST OF TABLES

LIST OF TABLES

LIST OF FIGURES

LIST OF FIGURES

LIST OF FIGURES

LIST OF FIGURES

LIST OF FIGURES

LIST OF FIGURES

SUMMARY

CHEMICAL ENGINEERING DIVISION SUMMARY REPORT

1. Chemical-Metallurgical Processing (pages 31 to 123)

Fission product-decontamination data have been obtained from the fifth and final small-scale melt refining experiment with highly irradiated uranium-fissium fuel alloy. A 382-g charge of EBR-II prototype fuel (ten percent enriched uranium alloyed with five percent fissium) irradiated to 1.75 total atom percent and cooled for 25 days was melt refined for one hour at 1400 C. Individual fission product removals were virtually identical with those found in the first four experiments. An analysis of the yield data for all five experiments and for control experiments shows that the product yields were consistently lower for the irradiated alloy than for a similar unirradiated alloy used in control experiments. There was no significant difference in the quantity of uranium oxidized during melt refining. Instead, the reduced yields resulted from a lower pouring efficiency and a correspondingly larger amount of metallic uranium retained in the skulls.

The use of molten chloride and oxide fluxes in melt refining was investigated briefly. Flux combinations of beryllia with strontia or baria, which contained also uranium oxide as a rare earth oxidant, provided good extraction of cerium from molten uranium metal, but severely attacked the only known possible container materials, beryllia and alumina. Use of a flux of calcium chloride containing magnesium fluoride as a rare earth oxidant also resulted in excellent cerium removal (about 99 percent) in one hour at 1100 to 1300 C without apparent attack of the beryllia crucible. On a 700-g-uranium scale, metal pouring yields ranged between 95 and 98 percent. In the melt refining of plutonium-containing fuels under salt fluxes, as yet uninvestigated, plutonium may be extracted into the flux phase. This would constitute a process drawback.

A study of the rate of removal of nitrogen from argon by titanium sponge is underway to provide design data for a nitrogen-removal system for the argon atmosphere of the EBR-II Fuel Cycle Facility. Engineering-scale equipment for removal of nitrogen from argon is also being designed, and will be built and operated to provide information on equipment and process performance.

The skull reclamation process is under development for the recovery of skull material which remains in a zirconia crucible after melt refining. In the previous summary report (ANL-6596), it was reported that in a series of process demonstration runs conducted in an argon atmosphere glove box, poor extraction of ruthenium had been realized in the noble metal extraction step (in which noble metals are extracted into zinc from uranium oxides

suspended in a halide flux phase). This was attributed to a loss of oxidizing power in the halide flux phase through elimination of reactions with air and water which produce chlorine, hydrogen chloride, and oxychlorides. Very good (up to 100 percent) ruthenium extractions have been achieved by addition to the salt phase of: zinc chloride to a two percent concentration, moisture to a 0.7 percent concentration, or both. Although extraction of ruthenium has been improved considerably, differences in the extent of removal between different batches of skull oxides were noted. Construction of large-scale integrated equipment for the skull reclamation process is nearly complete.

Thixotropically cast beryllia crucibles continue to show promise for use in the final three steps of the skull reclamation process (two uranium precipitation steps and a retorting step). A crucible of this type has now undergone 400 hr of process use at temperatures above 450 C without noticeable deterioration.

Other potential materials have thus far failed. A less-expensive, ram-molded alumina crucible, having an apparent porosity of 19 percent, was penetrated by a zinc-50 percent magnesium solution. In a separate 48-hr test in a similar ram-molded alumina crucible, reduction of alumina of the crucible by the magnesium-zinc solution introduced 1000 ppm aluminum into the metal solution. This should be compared with a pickup of 200 ppm of beryllia from a beryllia crucible and a pickup of 200 to 300 ppm of aluminum from high-density alumina crucibles. A thin oxide coating on beryllium metal, produced by anodizing the beryllium, was not sufficiently adherent to protect the beryllium from attack by zinc-magnesium-flux systems at 800 C.

Development work has continued on separations processes for uranium-plutonium-fissium alloys which show promise as fast reactor fuels. A critical separation for this type of fuel is that between plutonium and the rare earth fission products, since they behave similarly in many pyrometallurgical processes. One procedure under investigation involves an equilibration of the fuel constituents between liquid magnesium-zinc alloys and molten halide salts. Recent studies have been devoted primarily to the effects of temperature and salt composition on the codistribution behavior of plutonium and praseodymium. The distribution coefficients for plutonium and praseodymium between liquid magnesium-zinc alloy and equimolar lithium chloride-magnesium chloride or sodium chloride-potassium chloride-magnesium chloride eutectic tend to increase as the temperature is raised. Further distribution studies with vanadium show that it strongly favors the metal phase, with distribution coefficients in the vicinity of 10^{-2} at 800 C.

A separation of zirconium from uranium and plutonium by titration with magnesium in a two-phase salt-metal system has been demonstrated in a laboratory-scale experiment. Uranium, plutonium, and mildly irradiated zirconium were dissolved by the addition of excess zinc chloride in lithium

chloride-potassium chloride eutectic containing a small amount of lithium fluoride. By controlled additions of magnesium metal to a liquid cadmium phase in contact with the salt, it was possible to reduce the zirconium selectively into the metal phase, thereby effecting a relatively sharp separation from uranium and plutonium.

An alternative separation procedure entails a reduction of uranium, plutonium, and fission products from a salt phase into a calcium-rich zinc solution. The uranium and plutonium coprecipitate as the metals, while the Group IA, IIA, and IIIA fission product elements remain in solution. A coreduction-coprecipitation experiment of this type was conducted with a salt consisting mainly of lithium chloride-potassium chloride eutectic. Although some of the salt was reduced by the calcium, the procedure showed considerable promise as a process step. All of the uranium and 95 percent of the plutonium were precipitated in the calcium-zinc solution.

In accord with previous demonstration runs, a sixth demonstration run of the blanket process for recovery of plutonium from EBR-II blanket material has shown high recovery of plutonium (greater than 95 percent) and good separation of plutonium from uranium (from one percent plutonium in the feed material to 70 percent or more in the product). In this process, separation of plutonium from uranium is based on the low solubility of uranium in magnesium-rich zinc solutions and the contrasting high solubility of plutonium in such solutions. An engineering-scale study of the separation of the supernatant phase from precipitated uranium has shown phase-separation efficiencies of 95 percent to be easily achievable with insignificant entrainment of uranium. Plutonium, if it had been present, would have been separated from uranium in the supernatant phase.

Tungsten and certain tungsten alloys are among the promising materials for containment of flux and metal systems of the skull reclamation process. Sintered and rolled tungsten sheet exposed for 400 or 500 hr to noble metal extraction conditions underwent no detectable changes in size, weight, or structure. Physical tests of the exposed specimens indicated an apparently increased strength and ductility after exposure. Under the same conditions, a molybdenum-30 w/o tungsten alloy was attacked somewhat (to a depth of from 2 to 8 mils in 500 hr). There was a slight decrease in the strength of the alloy after exposure. However, the molybdenum-tungsten alloy is suitable for applications such as agitators and transfer lines.

Stainless steels are severely attacked by molten zinc systems, but suffer relatively little attack by zinc vapor. Because of a possible limited use of stainless steels for equipment items to be exposed only to zinc vapor, corrosion resistance of various stainless steels to zinc vapor has been determined. In 500-hr exposures to zinc vapor at 900 C, two austenitic 300 series stainless steels (Types 304 and 347) underwent severe attack.

Good corrosion resistance to zinc vapor was exhibited by a 400 series stainless steel, Type 405, a ferritic steel. Another 400 series stainless steel, Type 440C, a martensitic steel, also exhibited good corrosion resistance, but suffered some loss in weight.

A soluble uranium(V) species, believed to be UO_2^+ ion, is formed upon the addition of the higher uranium oxides to molten chloride salts. The same distinctive absorption spectrum assigned to UO_2^+ has been observed on the addition of uranyl chloride to molten chloride solvents at temperatures in the region of 500 to 800 C. This result is attributed to the thermal decomposition reaction

$$UO_2Cl_2 \text{ (solution)} \rightleftharpoons UO_2Cl \text{ (solution)} + 1/2\ Cl_2(g) \quad .$$

The calcium-zinc phase diagram has been redetermined by means of thermal analysis techniques supplemented with X-ray diffraction data and vapor effusion measurements. Evidence was found for the following compounds: Ca_3Zn, Ca_7Zn_4, $CaZn$, $CaZn_2$, Ca_7Zn_{20}, $CaZn_5$, $CaZn_{11}$, and $CaZn_{13}$. Three eutectics appear in the system: at 391 C (27.4 a/o zinc), 638 C (76.4 a/o zinc), and 690 C (86.4 a/o zinc).

Metal-distillation studies are being pursued in two ways: (1) distillation of cadmium in large-scale equipment, and (2) a fundamental study of liquid metal boiling and entrainment phenomena. Considerable entrainment of liquid cadmium in cadmium vapor has occurred at high rates of cadmium distillation (greater than 95 kg/hr). In the fundamental study, factors affecting the rate of nonturbulent vaporization of mercury (vaporization from vapor-liquid interface) are being examined. The use of a flat induction coil for heating and mixing shallow pools of mercury allowed nonturbulent vaporization to proceed at rates as high as 103,000 Btu/(hr)(sq ft). Rates as high as 110,000 Btu/(hr)(sq ft) were achieved with deep pools of mercury.

In work on the influence of agitation on the rate of solution of small (4- and 7-mm) uranium cylinders in molten cadmium, solution rate coefficients were found to increase sharply when the agitation intensity became great enough to begin suspending the uranium particles. Thereafter the coefficients increased slowly as agitator speed was further increased.

The construction and installation of equipment for the synthesis of materials under consideration as high-performance reactor fuels, i.e., uranium carbide, plutonium carbide, uranium sulfide, and plutonium sulfide, is continuing.

Further studies on the direct reduction of thorium dioxide to the metal by zinc-magnesium alloys in the presence of halide fluxes were completed. The importance of efficient agitation was confirmed by an experiment in which increasing the stirring speed to 1000 rpm improved the

reduction rate. Calcination of the thorium dioxide proved to have little effect on the rate of reduction. It was also learned that increase of the thorium loading in the final metal phase from 1.0 w/o to 9.1 w/o requires the magnesium chloride concentration in the flux to be raised to about 50 m/o to achieve complete reduction (the other flux constituents were 10 m/o calcium fluoride and the balance calcium chloride). Another study revealed that the rate and extent of thorium dioxide reduction were highly dependent on the magnesium concentration in the zinc phase, reaching a maximum between 5 and 10 w/o magnesium. The effect of the quantity of flux used was also studied. Variations in the amount used to reduce a fixed amount of thorium dioxide did not affect the reduction rate significantly, although it is clear that a minimum amount of flux must be present.

The solubility of thorium in zinc-magnesium solutions was determined within the region of process interest (750 to 850 C, and magnesium concentrations up to 20 w/o). The solubility approximately doubled with a temperature increase of 50 C, and also increased with increasing magnesium concentrations.

The technique of reduction in zinc-magnesium-flux is being applied to the direct reduction of uranium ore concentrates to uranium metal. Preliminary experiments indicated that silicon is the principal gangue element impurity appearing in the uranium metal product. Pretreatment of the ore concentrate with fluorides to remove the silicon as the tetrafluoride has shown promising results.

The construction of the Fuel Cycle Facility is essentially complete. The work necessary to correct deficiencies in construction and vendor-fabricated items is nearing completion.

The shielding of the Argon and Air Cells was radiographed to establish its integrity and adequacy. Radiation leakage was detected in three areas. A detailed analysis of the radiographic data is being made.

The correction of deficiencies in the operation of the process cell cranes and manipulators is continuing. Process cell cranes and manipulators are being used for the remote installation of equipment in the Air and Argon Cells.

A final inspection of all the shielding windows has shown them to have high transmittance, clarity, and resolution. Four wide-angle viewers were installed to view locations in the Argon Cell not readily visible from the windows. A periscope was installed in the wall of the Air Cell.

A diesel-generator was installed to provide electrical power for critical equipment items in the event of an electrical power failure.

Corrective work on the transfer locks and associated equipment is essentially complete. The transfer locks are being used for remote transfer operations. The valves in the transfer lock vacuum systems leak and may require replacement.

One of the two 20-ton transfer coffins to be used to transfer fuel subassemblies between the Reactor Building and the Fuel Cycle Facility was shipped to Idaho by the vendor. The second coffin is being designed and built at Argonne National Laboratory. A system has been designed for the removal of sodium from the fuel subassemblies while in the transfer coffin.

Exploratory tests of the effect of radiation upon the operation of oil-impregnated bearings have shown no specific desirable characteristics of this type of bearing. The testing has been discontinued.

Equipment is being developed in which to oxidize the skull material resulting from the melt refining operation. Assembly of the oxidation furnace and associated control equipment is nearly complete. Experiments with a similar furnace demonstrated that the furnace could be used to oxidize massive (10 kg) pieces of scrap fuel material.

The first model of the furnace for skull oxide reclamation was successfully tested in heatup tests with an empty crucible.

Experiments are continuing to develop a satisfactory condenser of metal vapor and distillate collector to permit adaption of the melt refining furnace to the distillation step of the skull reclamation process. A condenser and distillate collector design has been tested and is promising. The magnesium-zinc distillate collector will be discarded after each run. The condenser and crucible, however, would be used for more than one run.

Low-frequency inductive heating and mixing of molten metals and salts is being investigated for use in the skull reclamation process. Results of tests indicate that vigorous agitation can be obtained.

Fundamental studies of the chemistry of liquid metal systems are being made in conjunction with the work in the field of pyrometallurgical fuel reprocessing. Basic to these practical processes is knowledge of the solubilities of fission product elements, fissionable elements, and structural elements in metallic solvents. Study has shown that the solubility of technetium in liquid zinc may be represented by the empirical equations

$$\text{(428 to 544 C) Technetium: } \log(\text{atom percent}) = 6.431 - 7159\ T^{-1}$$

and

$$\text{(544 to 758 C) Technetium: } \log(\text{atom percent}) = 9.413 - 15690\ T^{-1} + 4.979 \times 10^{6}\ T^{-2} \quad .$$

The existence of at least five different intermetallic phases has been found in the tantalum-zinc system. Thermal analysis of tantalum-zinc alloys has indicated that some of these phases undergo peritectic reactions.

Metallographic examination of compacts prepared from powdered tungsten and zinc which were held at 430 C for two weeks and at 650 C for one month revealed no evidence of the existence of intermetallic phases in the tungsten-zinc system.

Data have been summarized for the solubility of uranium in liquid zinc-magnesium solutions containing 15.6, 24.4, 26.1, 47.1 and 67.7 w/o magnesium in the temperature range in which metallic uranium is the equilibrium solid phase. The solubility of 800 C was found to vary from 12 w/o uranium in the 15.6 w/o magnesium solution to 0.12 w/o uranium in the 67.7 w/o magnesium solution. The temperature coefficient of the solubility was found to increase with increasing magnesium concentration.

The ternary intermediate phase in the uranium-magnesium-zinc system has been shown to have the composition $UZn_{10.3}Mg_{4.3}$ and to have a hexagonal lattice.

The neodymium-zinc system has been studied by means of the continuous weighing effusion balance and by X-ray examination. Intermetallic phases having the following compositions were found: $NdZn_{8.5-12}$, $NdZn_{11}$, $NdZn_{8.5}$, $NdZn_{6.5}$, $NdZn_{4.3}$, $NdZn_{3.5}$, $NdZn_3$, $NdZn_2$, and NdZn.

The magnetic susceptibility of the intermetallic compound $ThCd_{11}$ has been found to be temperature independent. The susceptibility due to thorium in the compound was found to be 0.54×10^{-6} emu/g.

III. Fuel Cycle Applications of Volatility and Fluidization Techniques (pages 124 to 175)

Laboratory development work was continued on the Direct Fluorination Volatility Process for the recovery of uranium and plutonium from oxide fuels. This process depends on the conversion of the oxides of uranium and plutonium to hexafluorides in a bed of fluidized inert solids and the subsequent separation of these compounds. This separation will probably be brought about by conversion of plutonium hexafluoride to the nonvolatile tetrafluoride.

Laboratory studies have been concerned with the development of a fluorination scheme whereby optimum removals of uranium and plutonium from the inert solids can be achieved. This phase of the investigation is economically important since the inert solids will be discarded as waste.

Thus far, the laboratory work on the fluorination step of the process has been carried out with static beds and uranium-plutonium mixtures simulating those which are likely to be encountered in plant processing.

From the data obtained thus far on the fluorination of uranium-plutonium dioxide solid solutions mixed with an inert solid, several observations can be made regarding the optimum conditions for the removal of plutonium. Of the materials tested, Alundum (refractory grain alumina) has been found to be best suited for use as an inert solid, since its use results in the lowest retention of plutonium on the solid residue. For the initial period of fluorination, in which most of the uranium is removed from the solid mixture, a low temperature (450 C) and a low concentration of fluorine (10 v/o) are desirable. However, to obtain satisfactory removals of plutonium in the last portion of the fluorination period, it is desirable to use a higher temperature (550 C) and a higher fluorine content of the gas mixture (75 v/o). A two-step procedure involving an initial oxidation followed by two fluorination periods, one at 450 C and the other at 550 C, has resulted in plutonium removals of 99 percent or greater.

Another phase of the laboratory development work is now being started in which fluorinations will be carried out in a fluidized bed. A $1\frac{1}{2}$-in.-diameter fluid-bed fluorination reactor will be employed in these experiments. Initially, all experiments will be made with uranium dioxide. The procedure will consist of oxidizing the uranium dioxide to powdered uranosic oxide (U_3O_8), which will then be fed into the fluidized bed of the fluorination reactor either by gas transport or by a mechanical feeding device. Based on the results obtained in this work, a two-zone oxidation-fluorination reactor will be designed for studies of the overall process. Experiments with materials containing plutonium will begin after the apparatus has been tested and the experimental conditions have been defined.

Development of the Direct Fluorination Process applied to uranium dioxide fuel has continued. In this process, the uranium and plutonium dioxides from discharged reactor fuel are reacted with fluorine directly to produce hexafluoride products, which are then decontaminated by volatility techniques. Engineering-scale studies thus far have been directed toward process optimization of the primary fluorination of uranium dioxide pellets. The system used consists of pellets (or pellet fragments) which form a packed bed, with inert solid (alumina grain) fluidized in the space above and in the voids of the pellet bed. The fluidization aids in the heat transfer and in the mixing of solid fines formed as intermediates or residues in the system. Oxygen influences the reaction behavior by the formation of uranosic oxide fines.

Currently a two-zone process technique is being evaluated as a means of avoiding caking tendencies. In this scheme, a mixture of oxygen and nitrogen is introduced into the lower reaction zone formed by the uranium dioxide pellet bed, and fluorine is introduced into the upper zone, which

consists of a fluidized bed of alumina grain. The alumina, which also fills the voids of the pellet bed, is fluidized by the mixture of oxygen and nitrogen introduced into the system at the bottom of the pellet zone. Fluorine is introduced at the top of the pellet zone. Uranium oxide (U_3O_8) fines are formed in the lower zone and transported into the upper zone where they are removed by fluorination.

In the present period, two runs have been completed successfully, without caking, using a reduced reaction temperature in the pellet zone. Heaters were used to maintain the upper fluidized bed at 500 C or above for fluorination, while cooling of the bottom of the column was used to achieve an axial temperature gradient of 260 C for the oxidation in the pellet zone (i.e., the top layer of pellets was maintained at 400 C while the bottom layer was held at 140 C). The lower-temperature oxidation appears to allow closer matching of the oxidation and fluorination rates. In both runs a 12-in. pellet-bed charge of 8.8 kg uranium dioxide and an amount of alumina grain sufficient to form a 24-in. upper zone under static conditions were used. Total processing time for complete fluorination was about 17 hr in the 3-in.-diameter air-cooled reactor. Overall fluorine efficiencies were about 50 percent with a once-through gas flow. However, efficiencies of nearly 80 percent were obtained in one 5.7-hr period. Probably similar or higher efficiencies can be obtained with closer fluorination control and/or with gas recycle.

A high-alpha facility is being installed for pilot plant-scale studies of steps in the Direct Fluorination Process applied to uranium oxide-plutonium oxide fuel. Structural changes of the room and process cell have been completed, together with the installation of the glove boxes and various services to the operating and cell areas. Most of the equipment and accessories concerned with the fluorination step have been fabricated and delivered. Detailing of the ventilation and instrument connections is being carried out by Plant Engineering personnel. Detailed layout of the fluorination equipment is being done, and detailed design of the distillation column and a plutonium hexafluoride decomposer has started.

Tests of a uranium hexafluoride condenser were carried out before final mounting in the alpha enclosure. Uranium hexafluoride trapping efficiency and condenser capacity were measured for various temperature conditions at a total gas rate of 1 cfm nitrogen and about 3 lb uranium hexafluoride/hr. The condenser, made of Monel, is U-shaped, 10 ft long, and consists of a 4-in-diameter tube containing an internally finned tube through which trichloroethylene coolant flows. The best efficiency was obtained at the lowest finned tube temperature employed, -75 C. The best combination of efficiency and capacity was obtained when the outer wall was heated to 50 C while the finned tube was maintained at -75 C. Collection efficiencies of better than 99 percent were obtained for capacities up to about 50 lb uranium hexafluoride.

Supporting studies are also underway to obtain design data and to clarify fluidization mechanisms involved in particular equipment configurations used in the Direct Fluorination Process. In this process, inert fluidized particles of alumina are used as an aid for the removal of heat from the highly exothermic reaction of uranium dioxide pellets and fluorine gas. While the pellets are too massive to be fluidized, the alumina particles can be fluidized in the voids of the pellet bed. This configuration has been termed a fluidized-packed bed.

In the present study, axial heat-transfer in a fluidized-packed bed was studied as a function of the size and composition of the fluidized material, gas velocity, and packing shape. Two types of packing were used in these studies, $\frac{3}{8}$ x $\frac{3}{8}$-in. brass cylinders and $\frac{1}{2}$-in. steel spheres. The heat-transfer coefficient for the latter was found to be greater by a factor of 4 than that of the former. Three types of fluidizing material were used: 70 mesh glass beads, 120 mesh glass beads, and 60-140 mesh alumina. The finer glass particles produced coefficients greater by a factor of 3 than those for the coarser particles. The alumina and the 120 mesh glass particles had the same values for the effective axial thermal conductivity k_a. In all cases, the values of k_a rose as a function of superficial velocity to a maximum value between 0.4 to 0.7 ft/sec and then decreased. The highest value of k_a obtained was about 600 Btu/(hr)(sq ft)(F/ft). These axial heat transfer coefficients appear higher by a factor of 10 or more than radial heat transfer coefficients in similar fluidized-packed bed systems.

Additional studies on a fluidization-volatility scheme for reprocessing enriched uranium-zirconium alloy fuels were carried out. This processing scheme involves first a direct hydrochlorination (or chlorination) reaction while the alloy is submerged in an inert fluid-bed medium (currently Norton Type RR Alundum). This step produces volatile zirconium tetrachloride and permits ready separation of the uranium from the bulk alloying material. A subsequent fluorination step to volatilize the uranium as the hexafluoride provides the means of product recovery.

In current work, basic process reactions are being studied to determine the effect of various reaction cycles on uranium recovery. These experiments are being conducted in a 1 $\frac{1}{2}$-in-diameter nickel reactor. Continuous off-gas analysis by thermal conductivity techniques (Gow-Mac Co. cells) and/or intermittent analysis of the fluidized-bed solids for key components are methods employed for following the course of the reactions.

A major change in the cycle, involving the introduction of a hydrofluorination step between the chlorination and fluorination steps, was studied. Also, a sequence was tried involving the successive hydrochlorination of several batches of alloy, followed by a single fluorination. Results show that a significant savings in processing time and reagents can be achieved by the

use of the latter cycle, instead of performing both chlorination and fluorination steps for individual batches. For a run which included hydrochlorination of three batches of alloy followed by treatment with phosgene, hydrofluorination, and fluorination, the total time required was about 28.3 hr, whereas a single charge required a cycle time of 12 hr.

Effluent gases from the fluid bed pass to a down-flow fixed-bed filter wherein particulate solids are collected. Losses of uranium in the filter continue to be low, about 0.3 and 0.4 percent. The inert solids (both in the fluid bed and the filter bed) retained about one percent of the uranium in the original charge in the case in which a single batch of alloy was processed and only about 0.4 percent when three batches of alloy were processed. In the latter case, satisfactory product collection (over 98 percent of the uranium as the hexafluoride) was demonstrated. In two runs carried out during the quarter, overall uranium material balances were 101 and 100.1 percent.

Current results show no specific effects or benefits from the hydrofluorination step, which had been expected to permit elimination of the chlorine associated with the bed before fluorine was introduced and thereby to prevent the collection of undesirable chlorine compounds, such as chlorine trifluoride, in the uranium hexafluoride cold traps. Apparently, neither the chloride content of the final uranium hexafluoride product nor the retention of uranium by the inert solids was reduced. Values of the mole ratio of chlorine to uranium in the product were maintained at about 0.01 to 0.02. The uranium in Alundum remained at 0.02 w/o in current work as in previous work.

Work continued in the 6-in.-diameter fluid-bed unit on the study of the pyrohydrolysis reaction of zirconium tetrachloride with steam. This reaction is being considered as a method of converting the volatile zirconium tetrachloride produced during hydrochlorination of zirconium-based fuels to a more convenient form (namely, the solid dioxide) for ultimate waste disposal. As this step is being incorporated into the new pilot-scale alloy-processing facility, efforts are currently being directed to simulate pilot-plant conditions and simultaneously investigate the limits of satisfactory operation by broadening the range of operating conditions. In studies to date, satisfactory operation (that is, maintaining of fluidizable conditions in the bed and little pressure buildup at the exit gas filters due to accumulation of excessive amounts of fines) has been demonstrated over the following ranges of conditions:

a) bed temperatures from 250 to 500 C;

b) nominal starting-bed average particle sizes of 60, 90, and 120 mesh;

c) inert starting-bed materials including zirconium dioxide, Alundum, and sand;

d) zirconium tetrachloride feed rates up to 3 $\frac{1}{4}$ kg/hr;

e) run durations up to 11 $\frac{1}{2}$ hr.

Since the rate of feed (zirconium tetrachloride) to the fluid-bed unit has been limited by the size of the screw on the solids feeder, a larger feed screw is being incorporated to facilitate operations at higher rates which will be commensurate with those expected in the pilot plant.

Installation of the pilot-plant facility intended to demonstrate the recovery of uranium from zirconium-based fuels was started November 1, 1962, and is expected to be completed in three to four months. Testing of components will continue during the installation period.

Plans have been initiated for a study at high radiation levels of the chlorination-fluorination reaction sequence of the fluid bed-volatility process scheme for enriched uranium-zirconium alloy fuel. The purposes will be to determine fission product distribution in each step of the process and to determine the effect of radiation on reaction rates, yields, etc. The equipment will include a 1 $\frac{1}{2}$-in.-diameter fluid-bed column similar to that in use in studies of inactive alloys.

High-density spheroidal uranium dioxide particles were prepared directly by simultaneous reaction of uranium hexafluoride with steam and hydrogen at a temperature of 650 C in a fluid-bed system in a 3-in.-diameter Monel column. The product is intended for use in the preparation of compaction or dispersion-type fuels. Current studies investigating the effect on particle density of bed height (18-inch deep beds as compared with 8- to 10-inch beds used previously) and reduced hydrogen excess (about 4 times stoichiometric* as compared to about 17 times stoichiometric) at a constant steam rate of 1.15 times stoichiometric gave results similar to those achieved previously. Particles with a density** of about 9.6 g/cc were produced. The lower hydrogen excess appeared to result in a residual fluoride content of 650 ppm in the product as compared with about 380 ppm at the higher hydrogen excess. The quantity of fine material (believed to be produced by gas phase reaction) elutriated into the filter chamber averaged about 14 percent by weight of the hexafluoride fed.

Exploratory studies were initiated on the production of relatively large particles, about 14 mesh or greater, which constitute one of the sizes considered desirable for compaction. Through use of a starting bed containing particles in the range -18 +60 mesh, reasonable overall growth was achieved (the average bed particle size of 620 μ in the starting bed increased to 704 μ in the final bed), but the largest particles produced, which amounted to 2.2 percent of the final bed, were only +16 mesh after about 15 hr of operation. During this period, the superficial gas velocity was increased (by nitrogen addition) from 1.5 to 3.5 ft/sec to maintain fluidization.

* Based on the reaction $UF_6 + 2H_2O + H_2 \rightarrow UO_2 + 6HF$.

** Density determinations by mercury displacement method.

III. Calorimetry (pages 176 to 185)

Techniques and results are reported for a series of combustions of uranium in fluorine. The standard enthalpies of formation, ΔHf°_{298}, of uranium hexafluoride were found to be -522.8_7 kcal/mole for the crystalline and -511.0_0 for the gaseous state. The uncertainty interval of the values is $\pm 0.4_8$ kcal/mole.

The standard enthalpy of formation of crystalline aluminum trifluoride found from a series of combustions of aluminum in fluorine was $\Delta Hf^{\circ}_{298} = -356.5 \pm 0.7$ kcal/mole.

Preliminary determinations were made of the heat of formation of zirconium diboride, by combustion of the sample in fluorine. The products of the reaction are zirconium tetrafluoride and boron trifluoride, the heats of formation of which have previously been determined in this Laboratory. Final values for the heat of formation of zirconium diboride will be reported when obtained.

A series of calorimetric combustions of ruthenium in fluorine has been completed and calculations are currently in progress. Calorimetric combustions in fluorine are being carried out with zinc and tantalum, and combustions with niobium will be started soon.

The assembly and testing of components of the high-temperature enthalpy calorimeter is continuing. Control equipment for the furnace of the calorimeter has been installed, and controlled heating tests are being performed.

IV. Reactor Safety (pages 186 to 212)

The oxidation, ignition, and combustion processes of metals and compounds used in nuclear technology are being studied to provide information to aid in minimizing the hazards associated with handling these materials.

The program of theoretical studies designed to relate quantitatively ignition results with isothermal oxidation data is continuing. A mathematical model of ignition was described in a previous summary (see ANL-6569, page 136), in which isothermal rate laws for the uranium oxidation were combined with simple heat-transfer expressions. During this quarter, the equations were solved numerically to yield sample temperature-time curves, referred to as burning curves, which could be compared with experimental burning curves. It was evident from the calculations that the unusual transition from an accelerating to a decelerating oxidation rate at 450 C played an important role in the ignition process. The transition

resulted in a sharp break in calculated ignition temperatures between uranium samples having specific areas of 5 sq cm/g (ignition temperature, 510 C) and 7 sq cm/g (ignition temperature, 388 C). Experimental ignition temperatures also showed the break, but over the range of specific areas from 2 to 10 sq cm/g. Differences in the values obtained by experiment and by calculation for the "critical" specific area were attributed to differences in the impurity content and metallurgical history of the specimens. Foils, wires, and cubes from various sources were used as ignition specimens, whereas the equations used for calculations were derived from data on isothermal oxidation specimens (β-quenched uranium cubes). Calculated ignition temperatures were from 0 to 80 C higher than experimental values. The discrepancy was very likely due to thermal insulation afforded by the oxide coating which was not considered in the calculations. The similarity of the principal features of computed and experimental ignitions suggests that the mathematical model correctly considers the important factors in uranium ignitions.

A study of oxidized uranium surfaces with an X-ray diffractometer was completed. It had been reported previously that only uranium dioxide is present in thin, adherent oxide films. Recent studies at other laboratories, however, have indicated the existence of tetragonal phases, designated as α-U_3O_7, β-U_3O_7, and $UO_{2.3}$, which can be detected only by asymmetrical broadening of uranium dioxide diffraction lines. Studies were made with uranium surfaces oxidized at 100, 200, 300, 400, 500, and 600 C until the surfaces contained from 400 to 1100 μg O_2/sq cm. The diffractometer patterns suggested the presence of oxide phases higher than uranium dioxide (but not U_3O_8) in oxide formed at 100, 200, 300, and 400 C. Oxide formed at 500 and 600 C had sharp peaks, suggesting that only cubic uranium dioxide was present. These differences between oxides prepared at 400 C and at 500 C correlate with differences in the oxidation of uranium above and below 450 C.

Studies of the ignition of plutonium are continuing. Burning curve ignition experiments in oxygen and air have now been completed with 0.7 sq cm/g specimens of pure plutonium and 20 binary plutonium alloys. Samples of pure plutonium ignited between 494 and 520 C. Alloying additions to plutonium had relatively minor effects on the ignition temperature, the greatest effects being as follows: the ignition temperature of a 3.4 a/o aluminum alloy was 60 degrees higher than that of the base metal. The ignition temperatures of a 2.4 a/o copper alloy and a 1.2 a/o silicon alloy were 30 degrees higher than the ignition temperature of the base metal, whereas those of a 1.8 a/o cobalt alloy and a 1.8 a/o nickel alloy were 30 to 40 degrees lower.

The experimental program to determine rates of reaction of molten reactor fuel and cladding metals with water is continuing. One method being used involves the rapid melting and dispersion of metal wires in a water environment by a surge current from a bank of condensers. A series of runs

with stainless steel-316 wires in 315 C water (1500 psi vapor pressure) has been completed. The amount of metal-water reaction was nearly identical with that observed in similar runs with water at 100 C (15 psi) and 200 C (225 psi). The results indicate that the high-temperature oxidation of stainless steel by water is independent of pressure over a wide range. A similar finding was reported previously for the zirconium-water reaction (see ANL-6548).

The levitation melting method of studying the reaction of molten metal pellets with steam has been applied to aluminum. In each run, an aluminum sphere of nominal 8-mm diameter was suspended by a radio-frequency field in an environment of flowing steam. Pellet temperature was rapidly raised to a preset value between 1200 and 1700 C as determined by a recording, two-color optical pyrometer. Temperature was maintained for periods of time ranging between 5 and 100 min, after which the temperature was decreased rapidly to that of the steam environment. The quantity of aluminum oxidized during each exposure was determined gravimetrically by selective dissolution of the metal.

The aluminum-steam reaction could be described by the cubic rate law at 1200 and 1300 C. This was consistent with previous results obtained by the pressure-pulse method (ANL-6413, page 178) which indicated that the cubic rate law applied over the temperature range between 800 and 1200 C. The quantity of reaction obtained by the pressure-pulse method was approximately twice as great as that obtained by the levitation method. The higher values reported in studies by the pressure-pulse method were attributed to diffusion of water vapor through the slightly porous crucibles used to contain the molten aluminum.

The aluminum-steam reaction was found to follow a linear rate law at 1400, 1500, and 1600 C. An Arrhenius plot of the rate constants indicated an activation energy of 73.5 kcal/mole. Delayed ignitions occurred at 1600 C or slightly above; immediate ignitions occurred when the surface of the specimen reached 1750 C. Ignitions were believed to occur when aluminum vapor is able to penetrate the oxide film. The ensuing burning probably occurred by a vapor phase mechanism.

The use of the TREAT reactor at the NRTS, Idaho, to study the reaction of various metals with water is continuing. In these studies, small samples of an aluminum-uranium alloy reactor fuel were submerged in water in high-pressure autoclaves and then placed in TREAT, where they were subjected to severe nuclear transients. In-pile studies with 2S aluminum-clad, 77 w/o aluminum-23 w/o uranium (fully enriched) core material in a plate geometry were conducted. The cladding and core were each 20 mils thick, and the plate specimens tested had the nominal dimensions of 0.06 in. by 0.5 in. by 1.4 in. Nine separate experiments were conducted with the reactor energy input to the plate at various levels from

174 cal/g to 794 cal/g (based on the total weight of cladding and core). The reactor period varied from 104 to 42 msec with increasing energy input. When the nuclear energy input was less than 430 cal/g, the extent of reaction (determined from a hydrogen analysis of gas samples taken from the autoclaves) was found to be slight, of the order of 0.5 percent. Above this energy input, the extent of reaction increased to approximately 11 percent. A plateau in the plot of percent reaction versus nuclear energy input occurred up to an energy input of 794 cal/g, for which a single experiment indicated that the amount of reaction increased markedly; 36.9 percent of the plate reacted.

V. Energy Conversion (pages 213 to 231)

Work was continued on the development of a regenerative cell for the conversion of heat into electricity in a closed cyclic system. A lithium hydride cell and several bimetallic cells are being investigated.

Work on the regenerative cell is being carried out in three glove boxes in which a helium atmosphere of very high purity is maintained. The impurities and their concentrations in the helium atmosphere are as follows: oxygen, less than 10 ppm; nitrogen, less than 10 ppm; and water, less than 1 ppm.

The study of bimetallic cells received major attention during the quarter. The electromotive force of the cell Li/LiCl-KCl(eutectic)/Li-Bi (liquid alloy) was measured over a temperature range from 625 to 839 K for one cell and over 633 to 720 K for a second cell. The electromotive forces of the two cells were found to differ to some extent. The slopes of the electromotive force-temperature curves, however, were found to be the same for the two cells.

Presently, work on the lithium hydride cell is concerned mainly with the fabrication at Battelle Memorial Institute of metal diaphragms with suitable properties of hydrogen diffusion.

Fundamental studies in support of the work on the regenerative cells led to the establishment of a tentative phase diagram for the lithium hydride-lithium chloride system. A eutectic melting at 494 C was observed at 33 m/o lithium hydride.

Thermoelectric materials for direct conversion of nuclear reactor heat energy into electrical power are being investigated. Measurements are being made for liquid and for refractory solid thermocouple systems.

Enough data on the liquid antimony-bismuth, indium-antimony, and indium-bismuth systems have been accumulated to allow for a preliminary comparison. The Seebeck coefficient of the antimony-bismuth system has

a simple linear dependence on composition in terms of atom fractions, whereas the dependence for the indium-antimony and indium-bismuth systems is complex, but quite similar for the two systems. A simple correlation has been suggested based on the elementary electronic relationships among these elements.

It has been found that the relative values of the Seebeck coefficient for uranium monosulfide had been assigned incorrect signs in previous reports. Correction leads to positive absolute values of decreased magnitudes and to the consequent decrease in the figure-of-merit values. Measurements of the thermoelectric parameters of arc-melted and sintered specimens of uranium monosulfide, thorium monosulfide, and a 50-50 m/o uranium monosulfide-thorium monosulfide solid solution have been made at various temperatures. The results indicated that these substances behave somewhat like metals. The Seebeck coefficient was found to decrease with increasing thorium monosulfide content. The figure-of-merit value for uranium monosulfide was calculated to be approximately 1.2×10^{-4} K^{-1} through use of recent thermal conductivity data obtained at Oak Ridge National Laboratory in the temperature range from 40 to 125 C.

VI. Determination of Nuclear Constants (pages 232 to 238)

Several runs carried out in TREAT were designed to measure the rate of double neutron capture by rhodium to form 36-hr rhodium-105 and to derive the pile neutron cross sections of the short-lived intermediates, rhodium-104m and rhodium-104. Separation of rhodium from iridium was made necessary by the large amounts of iridium-192 and iridium-194 activities present. The calculation of the double capture cross section of rhodium has not yet been completed.

Radiochemical results of isotope buildup and fission studies in EBR-I (Mark III) are reported. Data are given for uranium-238 capture and fission cross sections as a function of reactor position. Data on plutonium-240 capture supplement the information previously reported for plutonium-239, uranium-233, and uranium-235 in the same loading.

VII. Routine Operations (pages 239 to 240)

The operation of the radioactive waste-processing facility and the gamma-irradiation facility continued without incident.

CHEMICAL ENGINEERING DIVISION
SUMMARY REPORT

October, November, December, 1962

I. CHEMICAL-METALLURGICAL PROCESSING*

Pyrometallurgical processes for the recovery of fissionable material from discharged reactor fuels offer promise of achieving a reduction in the reprocessing costs associated with nuclear power because of the simplicity, compactness, low-volume dry wastes, and capability for handling short-cooled fuels, with an attendant reduction in fuel inventories. Among the pyrometallurgical processes that are being developed are melt refining (a simple melting procedure for metallic fuels), and various processes for core and blanket materials which utilize liquid metal solvents as processing media. Pyrometallurgical techniques also show promise for the preparation of various reactor-fuel materials, including metals and carbides. The melt refining process is presently in the most advanced state of development and will be used for recovery of enriched uranium from the first core loading of the second Experimental Breeder Reactor (EBR-II).

A. Pyrometallurgical Development

1. Melt Refining
(L. Burris, Jr., R. K. Steunenberg)

The melt refining process will be used to recover uranium from the first core loading of EBR-II. The fuel consists of approximately 50 percent enriched uranium alloyed with about 5 w/o noble metal fission product elements. The fuel pins are clad with stainless steel, thermally bonded by a small amount of sodium. The pins are declad mechanically, chopped, and charged to a lime-stabilized zirconia crucible in which they are melted and maintained in a liquid state at 1400 C for a period of 3 to 4 hr. Approximately two-thirds of the fission products are removed through volatilization and selective oxidation. The purified metal product is poured to form an ingot from which new pins are prepared by injection casting. A mixture of oxidized and unpoured metal remaining in the crucible as a skull is recovered by a separate process employing liquid metal solvents. Experimental results for the quarter are reported on (1) the product yields of small-scale melt refining experiments with highly irradiated fuel alloy, and (2) the use of fused salt fluxes in the melt refining process.

---

*A summary of this section is given on pages 13 to 19.

Nitrogen removal from the argon atmosphere of the Argon Cell of the EBR-II Fuel Cycle Facility may ultimately be required to provide safer conditions under which to handle fuel and process materials. A program has been started on the removal of nitrogen from argon by gettering the nitrogen with hot titanium.

a. Melt Refining Experiments at High Activity Levels (V. G. Trice, W. H. Spicer)

Five demonstration experiments with highly irradiated ten percent enriched uranium-fissium alloys have been carried out in order to reveal any unexpected problems in the melt refining process which might arise from intense radiation fluxes and typical fission product concentrations. Because of limitations due to equipment size and activity levels, it was necessary to conduct the high activity level experiments on a reduced scale (about 0.4 kg) whereas approximately 10 kg would be utilized in the EBR-II plant facility. Although small-scale studies have contributed much useful information about the behavior of irradiated fuel during melt refining and the handling of radioactive fission products, geometric factors exert a strong influence on the product obtained from the melt refining process. It must be emphasized further that the small-scale results cannot be extrapolated directly to the plant-scale operation.

In the five demonstration experiments, the charge consisted of between 362 and 392 g of fuel pins, each pin about 0.144 in. in diameter. The irradiated alloy (varying from 0.22 to 1.75 total atom percent burnup) was melt refined at 1400 C under argon for 1 or 3 hr in order to determine the effect of duration of melt refining on the efficiency of fission product removal. Prior to melt refining, the pins were abraded with silicon carbide grit to remove any oxide coating that might have formed on the surface. The activity levels, which depend on the irradiation rate, the total irradiation, and the amount of radioactive decay before processing, varied from 2.6 to 12.6 curies of total beta and gamma activity per gram of alloy. In all five experiments, the fission product removals were virtually identical (See ANL-6413, page 35, and ANL-6477, page 31, for results of Experiments 1 through 4). Although identical results were obtained from small-scale melt refining experiments of 1- and 3-hr duration, the 3-hr period specified for the plant operation is believed to be necessary because of the longer diffusion paths traversed by the fission products to reach the crucible wall.

The results of control experiments with unirradiated alloy permitted the evaluation of the effect of irradiation on the melt refining yield.* The unirradiated pins were of approximately the same dimensions and composition as the irradiated alloy prior to irradiation. The principal differences were that the unirradiated alloy contained natural uranium instead of ten percent enriched uranium, and that about 0.6 w/o cerium was added to the unirradiated alloy to simulate the reactive fission product elements in the irradiated material.

* The yield is the amount of purified metal recovered by pouring and is expressed as percentage of the amount of metal charged.

The yields obtained in the demonstration experiments at high activity levels and the control experiments are shown in Table 1. The yields with the irradiated alloy were consistently lower than the yields with unirradiated fuel pins. The average yield was 85 percent in the control experiments, but the yields were 15 percent lower in Experiments 1, 2, 4, and 5, and 35 percent lower in Experiment 5. Control Experiment 4, in which unirradiated pins were melt refined in a radioactive crucible, had a relatively high yield (87.2 percent). This result suggests that the phenomena which lead to lower yields are related to irradiation of the fuel and not to the presence of a source of high activity.

Table 1

YIELDS OBTAINED IN HIGH-ACTIVITY-LEVEL AND CONTROL MELT REFINING EXPERIMENTS PERFORMED AT 1400 C[a]

Experiment	Charge Weight[b] (g)	Burnup (atom %)	Activity Level of Charge (curies/g)	Duration of Melt Refining (hr)	Yield (% of charge)
1	387 6	0 56	5 1	3	72 4
2	392 3	0 22	2 6	3	69 3
3	362 5	0 74	12 6	1	52 2
4	364 2	0 87	8 9	1	73 6
5	382 2	1 75	12 3	1	72 7
Control (1)[c]	359 6	0	0	3	86 7
Control (2)[d]	419 4	0	0	3	84 0
Control (3)[e]	397 5	0	0	1	84 2
Control (4)[f]	398 1	0	0	3	87 2

[a]Charges of irradiated alloy pins were abraded with silicon carbide grit before melt refining

[b]Alloy compositions prior to irradiation (w/o) as follows Experiments 1, 2 and 3 - U^{238} (84 00), U^{235} (10 73), Mo (2 58) Ru (2 11), Rh (0 26), Pd (0 19), Zr (0 12) Nb (0 01) carbon 25 ppm Experiments 4 and 5 - U^{238} (84 94) U^{235} (9 44), Mo (2 80) Ru (2 25), Rh (0 27) Pd (0 20), Zr (0 09), Nb (0 01)

[c]The charge of unirradiated alloy pins was polished with emery cloth to a bright, shiny finish and then melt refined in a crucible reclaimed from a low-activity-level exploratory experiment

[d]The charge of unirradiated alloy pins was soaked in NaK, washed with organic solvents, and abraded with silicon carbide grit before melt refining

[e]The charge of unirradiated alloy pins was held in air at 150 C for 16 hr, soaked in NaK, washed with organic solvents and abraded with silicon carbide grit before melt refining

[f]The charge of unirradiated alloy pins was soaked in NaK, washed with organic solvents, abraded with silicon carbide grit, and then melt refined in a radioactive crucible reclaimed from Experiment 2

The difference in yields is interpreted most readily by examining the behavior of uranium in these experiments. Since uranium was the major constituent (about 95 percent) of both the charge and the purified product, the percentage of uranium recovered was nearly equivalent to the yield. The uranium that was not recovered by pouring was retained in the crucible, and it constituted the major portion of the skull.*

It is convenient to consider that the uranium which was retained in the crucible after pouring consisted of three components, i.e., unpoured uranium metal, oxidized uranium, and absorbed uranium (retained

*For the purpose of this discussion, the skull is defined as the total amount of material retained in the crucible after pouring, exclusive of any material absorbed in the body of the crucible.

because of the porosity of the crucible). It is not known whether the absorbed uranium is present as the metal or as oxide. Since it is not available for recovery in either case, it is not included in the total metallic uranium present at the completion of melt refining. The total amount of metallic uranium present after melt refining is then defined as the sum of the recovered uranium and the unpoured uranium metal in the skull. The separation efficiency is the quotient, expressed as a percentage, which is obtained by dividing the amount of recovered uranium by the total amount of uranium metal present at the completion of melt refining.

The amount of unpoured uranium metal in the skull can be calculated (see ANL-6287, pp. 32-38) on the basis of two assumptions: (1) the composition of the unpoured metal in the skull is identical with the composition of the metal in the product ingot, and (2) the noble metal content of the skull results solely from the unpoured metal present. The amount of unpoured metal in the skull is then expressed as a fraction α of the total uranium in the skull (as metal and oxide) by the equation

$$\alpha = U_i Mo_s / U_s Mo_i \quad . \qquad (1)$$

The subscripts i and s refer to the ingot and skull, and the symbols U and Mo represent concentrations of these elements in weight percent. Using the appropriate combinations of direct experimental data, material balances, and Equation 1, the distribution of uranium was computed in terms of recovered uranium metal, unpoured uranium metal, oxidized uranium, and absorbed uranium. Where alternative methods of computation were available, the procedure was selected that would yield the minimum uncertainty in the result.

Complete data for the uranium distribution in the five demonstration experiments and for Control Experiment 1 are presented in Table 2. By means of the methods of small sample statistics, the following conclusions can be derived with a certainty corresponding to the 95 percent confidence level: (1) The amount of uranium recovered as metal in the product ingot (Table 2, Column 2) was decreased when irradiated fuel alloy was used. (2) The total amount of metallic uranium present at the conclusion of melt refining (Table 2, Column 6) was not affected significantly by irradiation of the alloy. A corollary which follows from Items 1 and 2 is that the separation efficiency (Table 2, Column 7) was adversely affected by irradiation of the alloy, indicating that in small-scale experiments the top-pouring technique used for the recovery of the melt refined metal was less efficient in the case of the irradiated alloy.

Yields in the plant-scale operation are expected to be higher than those found in the small-scale experiments with irradiated fuel. Full-scale melt refining runs with unirradiated alloy have generally resulted in yields exceeding 95 percent, which may be compared with yields of about

85 percent for the small-scale control experiments with unirradiated alloy. The 15 percent reduction in yield associated with irradiation of the fuel in the small-scale experiments has been shown to result from inefficient pouring related to the presence of an oxide film on the surface of the molten metal. This film is apparently composed mainly of fragments of uranium oxide from the irradiated pins which had to be handled in an air atmosphere prior to melt refining. Since no air exposure will be involved in the Argon Cell of the EBR-II Fuel Cycle Facility, a reduction in melt refining yields from this cause is not expected.

Table 2

URANIUM DISTRIBUTION IN DEMONSTRATION EXPERIMENTS

Experiment	Uranium Recovered as Metal in the Ingot (% of charge)	Uranium Retained in Crucible (% of charge)[a]			Total Metallic Uranium Present[a] (% of charge)	Separation Efficiency (%)
		Unpoured Metal[b]	Oxidized[b]	Absorbed[c]		
1	72.6	20.5 ± 2.9	5.4 ± 2.9	1.5	93.1 ± 2.9	78.3 ± 2.4
2	69.1	23.1 ± 3.2	6.3 ± 3.2	1.5	92.2 ± 3.2	74.9 ± 2.4
3	52.3	38.9 ± 5.5	7.3 ± 5.5	1.5	91.2 ± 5.5	57.3 ± 3.5
4	73.9	22.4 ± 2.2	2.2 ± 2.2	1.5	96.3 ± 2.2	76.7 ± 1.8
5	73.5	22.6 ± 2.4	2.4 ± 2.4	1.5	96.1 ± 2.4	76.5 ± 1.9
Control (1)	86.7	9.3 ± 1.3	2.5 ± 1.3	1.5	96.0 ± 1.3	90.3 ± 1.2

[a]Uncertainties are presented at the 95 percent confidence level.

[b]Method of computation outlined in text.

[c]Uranium retained in the crucible by absorption was determined experimentally in Experiment (5) only; the datum observed, 1.5 percent, was assumed to be representative of all experiments.

The 1.5 percent loss of uranium absorbed in the melt refining crucible has not been observed in full-scale melt refining runs with unirradiated fuel. It has been found during the oxidation of melt refining skulls in full-scale crucibles that the inside surface of the crucible is sloughed off, and the material is recovered along with the oxidized skull. Nitric acid leaching of the large-scale crucibles after removal of the skull by oxidation has indicated no retained uranium. The small-scale crucibles, on the other hand, show little or no degradation during the skull-oxidation procedure.

The extent of the effects discussed above in the plant-scale melt refining of highly irradiated fuel alloy can be determined with certainty only when the EBR-II Fuel Cycle Facility is placed in operation. However, the results of the small-scale experiments should be of considerable value in developing preventive or corrective measures if difficulties are encountered in the plant-scale equipment.

b. Use of Salt Fluxes in Melt Refining
(G. A. Bennett, W. A. Pehl)

The possibility of melt refining under salt fluxes has previously been considered during development of melt refining processes (see ANL-5466, page 42). The possible advantages in using salt fluxes are

high product yields, relatively low operating temperatures, and short processing times. By using a suitable oxidant in the salt flux, rare earth and alkaline earth fission product elements can be selectively oxidized, thereby effecting their transfer from the molten metal to the molten salt phase. It may ultimately be possible to test such alternative melt refining processes in the Fuel Cycle Facility, which is, in effect, a pilot plant for various pyrometallurgical processes.

Both chloride and oxide salt fluxes have been considered. The use of oxide fluxes has inherent difficulties. Chief among these are finding combinations of stable oxides with sufficiently low melting points for practical use and finding container materials which are resistant to attack by the molten flux and molten uranium. Constituents of the oxide flux must be more stable than uranium dioxide, and the flux should have a reasonably low melting point (<1400 C). Since all oxides more stable than uranium dioxide have very high melting points, only binary and ternary combinations of oxides can have sufficiently low melting points. As early as 1955, a search for such oxide combinations was made by the Chemical Engineering Division at Argonne (see ANL-5466, page 42, and ANL-5494, page 54).

Petit and co-workers in France have discussed[1] several low-melting (<1400 C) combinations of beryllium oxide with calcium oxide, barium oxide, and strontium oxide. They reported that containment of a molten oxide flux-molten uranium system was effected in high-fired beryllia crucibles, despite some dissolution of beryllia in the molten flux. In a search for alternative container materials, only aluminum oxide gave promise.

Since it may be possible to contain molten oxide flux-molten uranium systems in beryllia crucibles, three experiments were conducted in which uranium-5 percent fissium alloys containing 0.5 to 0.8 w/o cerium were melt refined under an oxide flux. The oxide combinations employed, their melting points, and other experimental details are given in Table 3.

Table 3

MELT REFINING OF URANIUM-5 PERCENT FISSIUM ALLOYS[a] IN THE PRESENCE OF OXIDE FLUXES

Crucible: Beryllia

	Flux				Fissium Alloy Charge		Operating Conditions			
Run No.	Composition (m/o)	Est Melting Point (C)	Wt (g)	UO_2 Added to Flux (g)	Wt (g)	Cerium (w/o)	Liquation Temp (C)	Liquation Time (hr)	Ingot Yield (%)	Cerium Removal (%)
OF4	63 BeO 37 SrO	1380	300	15	1965	0.82	1400	1	88	47
336	42 BeO 58 BaO	1140	300	15	1138	0.49	1300	3	78	95
337	66.5 BeO 33.5 BaO	1500	397	25	1250	0.54	1580[b]	1	93	97

[a]The uranium-fissium alloy contained about 2.5 w/o molybdenum, 1.9 w/o ruthenium, 0.3 w/o rhodium, 0.2 w/o palladium, and 0.1 w/o zirconium.

[b]By optical pyrometer; other temperatures were obtained through use of a tungsten/rhenium thermocouple.

[1] R Peray, A Auriol, and J. F. Petit, "Pyrometallurgical Treatment of Irradiated Uranium by Oxide Fluxes," Presented as Paper B2-2 at XVIIIth International Congress of Pure and Applied Chemistry, Montreal, Canada. August 1961. Abstracts Published by University of Toronto Press (Aug 1961).

Uranium dioxide was added to each flux (to a concentration of about 5 w/o) to oxidize cerium into the flux phase. A liquation time of 1 or 3 hr was employed at temperatures (between 1300 and about 1600 C) well above the estimated melting point of the oxide flux mixtures which were used.

A flux nearly saturated with beryllium oxide was employed in Run 337 in an attempt to reduce dissolution of the beryllia crucible in the flux. Later examination at the end of the run indicated that this flux was not completely molten.

Excellent cerium removal from the fissium alloy (>95 percent) was obtained with the beryllia-baria mixtures, but not with the beryllia-strontia mixture (47 percent). Pouring yields were low with the two lower-melting fluxes (78 and 88 percent) because of excessive attack of the beryllia crucible by the molten flux. The final run, in which the amount of beryllia in the flux had been increased to 66.5 m/o, gave a higher yield (92.5 percent) and resulted in much less reaction with the crucible; however, the high liquation temperature makes this approach unattractive.

Excessive corrosion was found to occur when alumina crucibles were used to contain the lower-melting oxide fluxes. Because a suitable container material is lacking, the use of oxide fluxes in a melt refining operation has been dropped.

The use of chloride fluxes, which generally have low melting points (<1000 C), was briefly investigated. Beryllia, which is resistant to attack by uranium, chloride fluxes, and combinations of these, was used as a containment material.

In the five runs made, two different chloride fluxes were used: calcium chloride containing 13 m/o magnesium fluoride, and calcium chloride containing two m/o uranium tetrachloride. Cerium in concentrations of between about 0.5 and 0.8 w/o was employed in the 700-g charges of uranium-five percent fissium alloy (see composition of this alloy in Table 3). The liquation temperatures were varied between 1100 and 1300 C.

With the uranium tetrachloride oxidant, cerium removals were about 94 percent; with the magnesium fluoride oxidant (in effect, a magnesium chloride oxidant because of the ionized character of the flux), a cerium removal of 99 percent or better was obtained.

When it was noted in the first run that a poor product yield (90 percent) was obtained on pouring at 1100 C, subsequent pours were made at 1300 C. Yields on pouring at 1300 C varied between 95.7 and 97.6 percent. Before the metal was poured, the flux was removed by freezing the metal, pouring off the flux, and vaporizing the residual flux under reduced pressure. The loss of uranium in the flux was 0.03 percent or less at a liquation temperature of 1100 C. A single isopressed beryllia crucible was used for three runs without apparent damage.

Although chloride fluxes may be useful for processing uranium fuels, application to plutonium-containing fuels is questionable, since McKenzie and co-workers[2] have shown that plutonium is oxidized (along with the rare earth elements) when in contact with a magnesium chloride flux phase. Therefore, the amount of plutonium that would be lost to a flux phase containing a limited amount of oxidant must be determined before this process can be seriously considered for plutonium-containing fuels. A few such runs will be made with plutonium present to ascertain the feasibility of the process for plutonium-containing fuels.

2. Removal of Nitrogen from Argon by Reaction with Titanium Sponge
(M. Kyle, J. Arntzen, L. Western)

The presence of nitrogen in the atmosphere of the Argon Cell of the EBR-II Fuel Cycle Facility could cause problems in processing fuel materials. Formation of a nitride coating or "pin shell" on the enriched uranium fuel pins to be used in the first EBR-II core could cause a decrease in the melt refining pouring yield (see ANL-6333, page 40). The full extent of problems caused by the presence of nitrogen in the cell atmosphere is not known, but previous data have shown that, by restricting the exposure of the fuel to the nitrogen-bearing atmosphere and by keeping fuel temperatures below 300 C to reduce the nitridation rate of the fuel, melt refining yields will not be seriously affected by nitrogen concentrations up to five percent (see ANL-6569, page 31, and ANL-6596, page 42).

Although the Argon Cell includes equipment for the removal of oxygen and water, no provisions have thus far been made for the removal of nitrogen from the argon atmosphere. It is planned to control the cell nitrogen content by intermittently purging a portion of the cell atmosphere with pure argon. Measurements of the rate of inleakage of air into the Argon Cell are currently being made. Although the rate has not yet been definitely established, it is believed that the resulting equilibrium content of nitrogen will be well under five percent.

Nevertheless, there is the possibility that for other fuel materials and other fuel-recovery processes, the removal of nitrogen from the Argon Cell atmosphere will be required. This has prompted the initiation of a project to investigate the removal of nitrogen from argon by gettering with titanium sponge. Titanium sponge was chosen as the gettering material because of its low cost per mole of nitrogen-removal capacity. The present study is being carried out in two parts: (1) the study of the kinetics of the titanium-nitrogen reaction, and (2) construction and operation of a scale model of the proposed plant system to test equipment designs, to obtain data on equipment reliability, and to obtain operating experience.

---

[2] D. E. McKenzie, W. L. Elsdon, and J. W. Fletcher, Can. J. Chem., 36, 1233 (1958).

A preliminary study of reaction kinetics has been made with the aid of a thermobalance. A 20-g sample of titanium sponge was held in a container made of stainless steel screen and supported in the thermobalance furnace by a rod connected to one arm of the balance beam. Argon gas containing a known concentration of nitrogen (380 ppm, 1160 ppm, or 4 v/o) was passed through molecular sieves to remove water, through copper turnings at 600 C to remove oxygen, and finally into the thermobalance and over the titanium sample at 900 C. The weight increase of the sample was used as a measure of the rate and extent of reaction. The argon flow rate was maintained high enough to provide about twenty times the rate of nitrogen required for the prevailing reaction rate, or enough to prevent backflow of air into the thermobalance.

At the low nitrogen concentrations of interest (50 to 5000 ppm), the reaction rate is so slow that several weeks are required to reach 50 percent conversion of the titanium to titanium nitride. In order to reduce the time required for high conversion, the nitrogen concentration was increased (during part of the run) to 4 v/o. After each resulting sharp increase in the extent of conversion, gas having low nitrogen concentrations was passed over the titanium sample and the reaction rate was again measured.

After achieving the desired conversion of the titanium with a four percent nitrogen-argon gas mixture, it was found that two or more hours of operation with argon of low nitrogen contents (380 or 1160 ppm) were required before a relatively constant reaction rate was obtained. This pattern of reaction indicates a strong influence of solid-state diffusion of nitrogen on the reaction rate. Because the nitrogen gradient established in the solid phase is directly related to the nitrogen partial pressure in the reacting gas, accurate reaction rates over a titanium conversion range from zero to 50 percent (as titanium nitride) can be established only with a gas of constant partial pressure of nitrogen. Operation of a thermobalance for long periods of time at low and constant partial pressures of nitrogen is considered impractical. Therefore, new experimental apparatus has been designed and is being built to obtain the necessary kinetic data.

In this equipment, an argon-nitrogen mixture of carefully controlled composition (50 to 5000 ppm of nitrogen) will be continuously circulated through a series of small titanium beds. The circulating rate will be such that only a small fraction of the nitrogen in the gas will react in a single pass. The entire nitrogen content of the gas will be removed in each pass by a large titanium bed and then will be replaced to the original controlled concentration by a slow bleed of nitrogen into the system just in front of the titanium test beds. The nitrogen concentration will be controlled by careful regulation of the flow rates of the argon and nitrogen streams. The extent of reaction of the titanium test material will be determined at various time intervals. The first titanium bed in the series will be removed

and analyzed for nitrogen. The bed will not be replaced, nor will succeeding beds as they are successively removed. Therefore, the number of values obtained will be equal to the number of test beds initially used. The rate of reaction for a particular titanium conversion will be determined by differentiation of the curve which gives the relationship between the extent of reaction and time.

3. Processes Utilizing Liquid Metal Solvents
(R. K. Steunenberg, L. Burris, Jr.)

Several processes are under development in which liquid metals and salts are employed as processing media. One such is the skull reclamation process for recovering the fissionable material remaining in the crucible residue (skull) after a melt refining operation. Small-scale runs demonstrating this process are now in progress, and large, integrated process equipment is now being installed for conducting runs and evaluating equipment performance at near plant scale.

A process has also been developed in which liquid metal solutions are used to achieve the isolation of plutonium bred into the EBR-II blanket material. Laboratory work is in progress on the development of processes for other fuel materials, especially future EBR-II fuels, which will contain plutonium as a fissionable material.

Fundamental studies of molten metal and salt systems are also in progress. These include studies of reactions in molten salts and studies of various unit operations in liquid metal systems (e.g., distillation and mass transfer).

a. Demonstration of the Skull Reclamation Process
(R. D. Pierce, K. R. Tobias)

The skull reclamation process is being developed as an auxiliary process to the melt refining process of the EBR-II fuel cycle in order (1) to recover the fissionable material from melt refining crucible residues, and (2) to obtain sufficient separation of this fissionable material from fission products to allow return to the main EBR-II fuel cycle. A series of small-scale (130-g uranium) demonstrations of this process is being performed to identify and resolve problems prior to the operation of large, integrated process equipment. During these studies, a problem in the noble metal extraction step of the process was revealed. To allow concentrated study of this problem, demonstration runs of the entire process were suspended during this quarter.

In the noble metal extraction step which follows oxidation of the crucible skull material and removal of the oxidized skull from a melt refining crucible, the skull oxides are suspended in a chloride flux

(composition in w/o: 47.5 magnesium chloride, 47.5 calcium chloride, and 5 magnesium fluoride), and this flux-oxide suspension is vigorously contacted with molten zinc at 800 C in order to leach or extract from the flux the following noble metal fission products: ruthenium, rhodium, palladium, molybdenum, and technetium (see flowsheet in last quarterly report: Figure 6, page 46, ANL-6596). As pointed out in ANL-6596, page 45, when all noble metal extraction operations were conducted within an inert atmosphere, noble metal extraction was unsuccessful, as typified by poor extraction of ruthenium. These operations were carried out in new equipment installed in an inert atmosphere glove box (ANL-6543, page 33).

Whereas ruthenium extractions of 75 to 85 percent were experienced in runs performed outside the glove box, ruthenium extractions of less than ten percent were realized when all operations were conducted within the inert atmosphere glove box (compare Runs SD-126 and SD-127 with Runs BJ-4A through BJ-10A in Table 4). All runs (both inside and outside the glove box) were made in closed furnaces under an argon atmosphere; however, for Runs SD-126 and SD-127 the metal and skull oxides were exposed to an air atmosphere during storage, and salt, metal, and skull oxides were exposed to air during loading of the equipment.

The poor extractions of ruthenium in runs made in the inert atmosphere glove box were initially attributed to the lack of oxidizing power which had existed in previous runs as a result of water absorption from air during loading operations. This hypothesis appeared to be confirmed when good ruthenium removals (near 100 percent) were achieved in runs in the inert atmosphere glove box by the addition of a small quantity of water or zinc chloride oxidant to the flux phase in the noble metal extraction step. However, in the runs in which good ruthenium extraction was obtained, less than the normal amount of zinc was used in order to increase the concentration of ruthenium in the zinc extract and thereby effect an improvement in the accuracy of ruthenium analyses. The resultant change in zinc volume lowered the flux-metal interface from a location several inches above the agitator blade to a location near the agitator blade. This change in mixing conditions may have contributed to the improvement in ruthenium extraction, and the effect of this change is currently being determined. Nevertheless, sufficient zinc chloride (concentrations up to 10 percent) will be employed as a standard constituent in the flux phase in the noble metal extraction step to oxidize into the flux phase any metallic uranium that might be present, such as, for example, any unoxidized uranium in the skull oxide. Thereby, loss of uranium in the waste zinc phase will be prevented.

Filtered samples were taken at 800 C at the conclusion of each run by pressurizing a portion of the zinc solution into tantalum tubes through tantalum filter frits. In the course of this work it was discovered that some ruthenium was retained on the tube wall after dissolving out the

sample with aqua regia. The amount retained was significant only when the percentage of ruthenium removed was small, as in Runs BJ-4A through BJ-10A. The less-than-10 percent ruthenium removals in these runs (see Table 4) include a liberal allowance for ruthenium retention on the tube walls.

Table 4

RUTHENIUM REMOVAL IN NOBLE METAL EXTRACTION RUNS

Runs SD-126 and SD-127 were performed outside the glove box; all other runs were performed in equipment located in an argon atmosphere glove box. Noble metal extractions were performed under argon at 800 C for 4 hr in $4\frac{1}{4}$-in. tungsten or tantalum crucibles.

	Charge (g)					
Run	Skull Oxide[a]	Flux[b]	Zinc	Zinc Chloride	Water Added	Percentage of Ruthenium Extracted into Zinc
SD-126	235	1000	4000	0	0	90
SD-127	223	1000	2000	0	0	95
BJ-4A	191	750	3005	0	0	<10
BJ-6A	162	751	3003	0	0	<10
BJ-7A	164	749	3002	0	0	<10
BJ-8A	162	944	3006	0	0	<10
BJ-9A	160	515	3002	0	0	<10
BJ-10A	162	755	3000	0	0	<40
BJ-10A-1	Recharge of BJ-10A		+	7.5	0	63
BJ-11A	138	751	2003	0	0	<20
BJ-12A	132	752	2000	0	1.0	<40
BJ-13A	142	750	1015	16.0	0	90
BJ-14A	142	750	1006	15.5	4.9	100
BJ-15A	140	750	1004	0	5.0	90
BJ-16A	115[a]	750[b]	3308	0	0	50
BJ-16A-3	Recharge of BJ-16A		+	15.8	0	50
BJ-17A	170[a]	750[b]	3301	0	0	48

[a]The skull oxide employed in all runs except BJ-16A through BJ-17A was from a single batch (SO-68). The skull oxide used in Run BJ-16A and thereafter was from batch SO-73 and contained ruthenium-106 tracer. Skull material from several melt refining runs was oxidized at between 700 and 800 C with argon containing approximately 25 percent oxygen. The compositions in weight percentages of two blends were, excluding oxygen which makes up most of the balance, as follows:

	Batch SO-68	Batch SO-73
Uranium	70	60
Cerium	4	4.6
Zirconium	1	10.4 (high because of large inclusion of melt refining crucible fragments)
Ruthenium	1.1	1.3
Molybdenum	1.5	1.6

[b]The flux composition in mole percent (exclusive of added zinc chloride and water) was: 47.5 calcium chloride, 47.5 $MgCl_2$, and 5.0 MgF_2. A common batch was used for Runs SD-126 and SD-127 and Runs BJ-4A through BJ-15A. The same batch of flux was used in Run BJ-16A and succeeding runs. All batches of flux were prepared in the same way.

Two runs (Runs BJ-4A and BJ-7A) were continued through the remaining process steps. Analyses of the uranium products of these two runs for ruthenium also showed no detectable ruthenium removal had been achieved. The analytical difficulty mentioned above was rectified by rinsing the sample tubes with hydrofluoric acid after the sample had been dissolved out with aqua regia. Accuracies of colorimetric ruthenium analyses in Runs BJ-10A-1 through 15A are estimated to be ±10 percent. These accuracies were in part achieved by increasing the ruthenium concentration in the zinc extract to a concentration more suitable for ruthenium colorimetric analyses by reducing the amount of zinc employed in the runs. By use of ruthenium-106 tracer, accuracies were improved, and were ±2 percent in Runs BJ-16A, BJ-16A-3, and BJ-17A.

Separation of the zinc extract (to be disposed as a waste) from the flux is accomplished by cooling to 525 C to freeze the flux and then removing the zinc (melting point 420 C) by pressure siphoning. At 525 C, most of the noble metals are insoluble in the zinc and, therefore, precipitate. In recent runs, the zinc phase was not stirred prior to and during transfer, and poor transfer of the noble metals along with the zinc phase occurred.* However, it has been shown that the noble metals can easily be suspended in the zinc throughout the phase-transfer operation by stirring; henceforth the zinc phase will be stirred while being transferred.

Although more study of noble metal extraction is required, results have been sufficiently encouraging to warrant performing new demonstration runs of the entire skull reclamation process.

b. Construction of Large-scale Integrated Equipment for the Skull Reclamation Process
(J. C. Hesson, I. O. Winsch, D. E. Grosvenor, G. L. Rogers, N. P. Quattropani)

Construction of integrated equipment for large-scale (2.5 kg of skull oxide) demonstrations of the skull reclamation process is continuing. It is expected that construction of this equipment will be completed in December 1962. It should be possible to commence processing runs in January. Preliminary equipment check-out will be done using cadmium.

c. Retorting of Uranium Concentrates
(J. F. Lenc, M. A. Bowden, P. Mack)

In a late stage of the skull reclamation process, uranium metal is produced by decomposition of the "epsilon" uranium-zinc

*The transferred zinc metal is sampled at 800 C at which temperature the zinc has adequate solubility for the quantities of ruthenium, rhodium, and palladium which are present. Molybdenum, however, has a very low solubility in zinc at 800 C. Its overall removal is subsequently determined by analysis of the uranium product.

intermetallic compound (approximate composition: U_2Zn_{23}) when sufficient magnesium is added to bring its concentration in the zinc-magnesium solution to 50 w/o magnesium. After removal of the supernatant metal liquid, the uranium precipitate remains enveloped in the residual magnesium-zinc liquid. Work has been aimed at achieving easy removal of the uranium in high yield, both before and after retorting to vaporize the residual magnesium and zinc. The high yield before retorting will be necessary if the uranium precipitate is transferred to separate retorting equipment. After the retorting operation, the uranium product will be recycled to the melt refining process and therefore must be in a form amenable to such recycle.

Previous experiments have shown that only ceramic crucibles permit easy recovery of the uranium in high yield either as an isolated product after retorting or as a concentrate after decomposition of the intermetallic compound. Because beryllia has a high thermal conductivity (and consequent low susceptibility to thermal shock) and a high chemical stability, it has been investigated more extensively than other ceramics for use as a crucible material in the precipitation and final retorting steps of the process. Other less expensive ceramics, such as alumina and magnesia, are also being tested as alternative crucible materials.

(1) Performance of an Unjacketed, Thixotropically Cast Beryllia Crucible

Beryllia crucibles are being subjected to repetitive process operations in order to determine their probable lifetime in plant use. Four 150-g-uranium-scale runs were conducted during the quarter in an unjacketed, thixotropically cast beryllia crucible (4-in. OD by 9 in. high by $\frac{3}{8}$-in. wall). This brings the total number of runs conducted in this crucible to seven and the total time at temperatures above 450 C to about 400 hr (see previous runs in ANL-6596, page 54). All runs were conducted in general accord with the "three-step" procedure* described in ANL-6379, page 62. One of the recent runs was a long-term test, similar to one shown schematically in ANL-6596, Figure 7, in which the products of the first two steps were repeatedly thermally cycled between approximately 450 and 800 C.

The uranium concentrate (enveloped in residual zinc and magnesium) did not adhere to the crucible in any of these tests. Isolation of uranium metal was achieved by vacuum evaporation of the residual zinc and magnesium in a final retorting step. In each run essentially 100 percent of the uranium was easily recovered from the crucible.

*The three steps, all of which are conducted in the same crucible, simulate the last three steps of the skull reclamation process, namely, (1) precipitation of the uranium-zinc intermetallic compound and removal of supernatant liquid metal, (2) decomposition of this compound with magnesium to precipitate the uranium, and, following removal of the supernatant liquid metal, (3) retorting to drive off residual zinc and magnesium.

No serious deterioration of the thixotropically cast beryllia is yet evident. In the seven runs, the crucible was subjected to conditions simulating 19 intermetallic compound precipitation steps, 20 intermetallic compound decomposition steps, and 5 retorting steps. The 400 hr of accumulated exposure to process conditions may be compared with an estimated 20 hr of exposure in processing a single batch of material on a plant scale. Runs will be continued in the crucible until its useful life has been determined. The retorted uranium products from these tests are being analyzed to identify impurities and to determine their concentrations.

(2) Performance of Ram-molded Alundum* Crucibles

Alumina is being considered as an alternative crucible material to beryllia for the last three steps of the skull reclamation process. To date, one run has been conducted in each of two different Alundum* (99 percent fused alumina) crucibles, each crucible having an apparent porosity of 19 percent. The procedure described in the footnote on page 44 was employed. In the first run, performed on a 100-g-uranium scale in a crucible having dimensions of $4\frac{1}{4}$-in. OD by 7 in. high by $\frac{3}{8}$-in. wall thickness, the crucible remained intact, but a small amount of the zinc-magnesium process solution leaked through the crucible wall. More severe leakage occurred from the second crucible, which was slightly larger and which had a slightly thicker wall ($\frac{7}{16}$ in. instead of $\frac{3}{8}$ in.). Despite the liquid metal leakage experienced in these runs, the uranium concentrate from the intermetallic compound decomposition step (precipitated uranium enveloped in residual zinc and magnesium) was easily removed from the crucible. Isolation of the uranium in the concentrate recovered from each of the two runs was accomplished in a tantalum crucible by vacuum evaporation of the residual zinc and magnesium.

Because of the ease with which the uranium concentrates were removed from the ram-molded Alundum crucibles in these recent tests, a more extensive investigation of similar, inexpensive ceramic crucible materials is being pursued. Various crucible-forming methods (such as thixotropic casting, isostatic pressing, and slip casting) also will be evaluated.

d. Processes for Plutonium Reactor Fuels
(R. K. Steunenberg)

The following alloy is considered to be typical of metallic fuels which may be used in fast breeder reactors: uranium, 70 percent; plutonium, 20 percent; fissium elements, 10 percent. A critical separation in the processing of irradiated fuels of this type is the adequate removal of rare earth fission products from the plutonium. Two promising methods for achieving this separation are being investigated. One involves selective extraction of the rare earths from a zinc-magnesium solution of uranium and plutonium by means of a molten halide flux. The other entails the use of a calcium-zinc solution in which the rare earths are soluble and the uranium and plutonium are relatively insoluble.

* Manufactured by the Norton Co., Worcester, Mass

The work completed during the past quarter includes (1) further data on the distribution behavior of various elements between liquid magnesium-zinc alloys and various molten halide fluxes, (2) the separation of uranium and plutonium from zirconium by controlled reduction from a molten halide phase into cadmium-zinc-magnesium alloy, and (3) simultaneous coreduction and coprecipitation of uranium and plutonium from a molten halide phase into a calcium-zinc alloy.

(1) Separation of Rare Earths from Uranium and Plutonium by Molten Salt Extraction
(J. B. Knighton, J. D. Schilb, J. W. Walsh)

The possibility of separating the various elements that may be present in spent reactor fuels by equilibration between liquid zinc-magnesium alloys and molten halide fluxes is being investigated. The recent work has been concentrated principally on the effects of temperature and the composition of the salt phase on the codistribution behavior of praseodymium and plutonium, but distribution data have also been obtained for vanadium and iron, which are likely to be constituents of cladding alloys.

Effect of Temperature on the Praseodymium-Plutonium Separation Factor

The effect of temperature (from 620 to 850 C) on the praseodymium-plutonium separation factor between an equimolar lithium chloride-magnesium chloride flux (m.p. ~600 C) and a 50 w/o zinc-50 w/o magnesium alloy was presented in the previous quarterly report (see ANL-6596, page 63). The data have been extended to include the temperature range from 425 to 850 C through use of a flux with a lower melting point, i.e., 30 m/o sodium chloride, 20 m/o potassium chloride, and 50 m/o magnesium chloride (m.p. 396 C). Results from these two experiments are compared in Figure 1. These data show the distribution coefficients for both praseodymium and plutonium to be lower in the ternary flux system. Also included in Figure 1 are single points showing the distribution coefficients for plutonium and praseodymium for an equimolar cesium chloride-magnesium chloride flux and a 50 w/o zinc-50 w/o magnesium metal phase. These points fall somewhat below the distribution curves for praseodymium and plutonium in the other two salt systems.

Comparison of the data for the three different fluxes suggests that the distribution coefficients vary in a systematic manner with the atomic weight of the alkali metal cation used in the flux. Previous experiments (see ANL-6596, page 64) have shown that the distribution coefficients vary with the amount of magnesium ion in the flux. It is also evident from the data in Figure 1 that the distribution coefficients for plutonium and praseodymium tend to increase as the temperature is raised.

Figure 1

EFFECT OF TEMPERATURE ON CODISTRIBUTION OF PRASEODYMIUM AND PLUTONIUM

Temperature:	As indicated
Mixing Rate:	300 rpm
Metal:	400 g of 50 w/o Zn-50 w/o Mg
Flux:	300 g (of indicated composition)
Atmosphere:	argon
Crucible:	tantalum

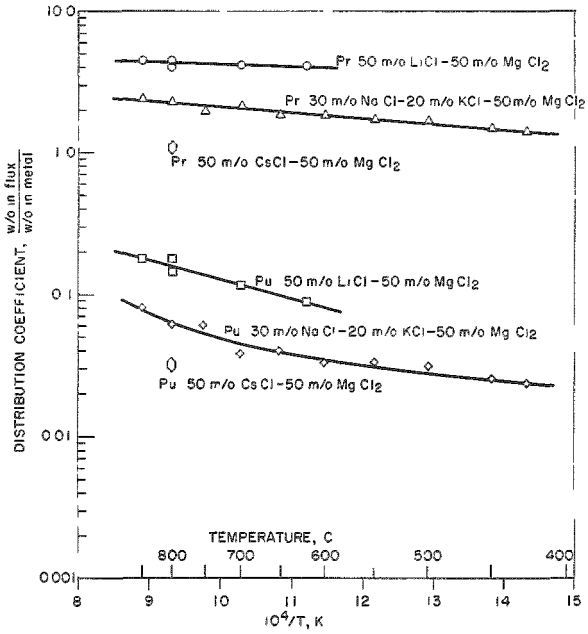

Separation factors for plutonium and praseodymium are shown as a function of temperature in two flux systems in Figure 2. The separation factor increases to about 60 as the temperature is lowered to 425 C in the 30 m/o sodium chloride-20 m/o potassium chloride-50 m/o magnesium chloride flux.

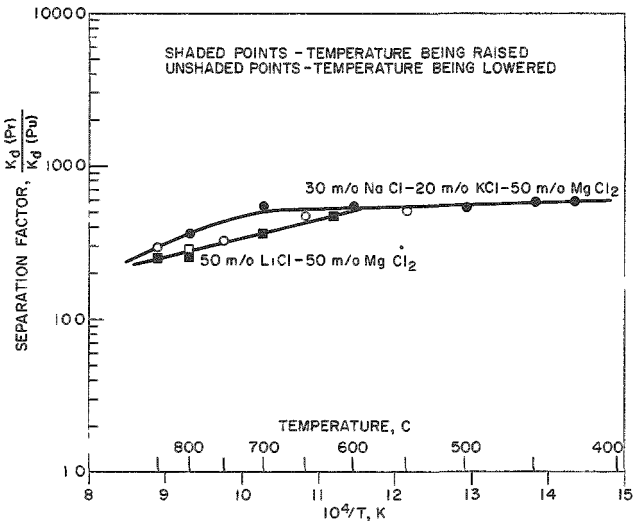

Figure 2

EFFECT OF TEMPERATURE ON PRASEODYMIUM-PLUTONIUM SEPARATION FACTOR

Temperature:	As indicated
Mixing Rate:	300 rpm
Flux:	300 g (of indicated composition)
Metal:	400 g of 50 w/o Zn-50 w/o Mg
Atmosphere:	argon
Crucible:	tantalum

Codistribution of Plutonium and Praseodymium between Zinc-Magnesium Alloy and Magnesium Chloride-Magnesium Fluoride Flux

The effect of fluoride anion on the distribution coefficients of plutonium and praseodymium was determined in an experiment with a flux composed of 10 m/o magnesium fluoride and 90 m/o magnesium chloride. The conditions and results of this experiment are shown in Figure 3. The new data (represented by points) are in good agreement with the curves, previously obtained, which represent the distribution coefficients for the individual elements in pure magnesium chloride. This indicates that the presence of 10 m/o fluoride anion in the flux has a negligible effect on the distribution coefficients.

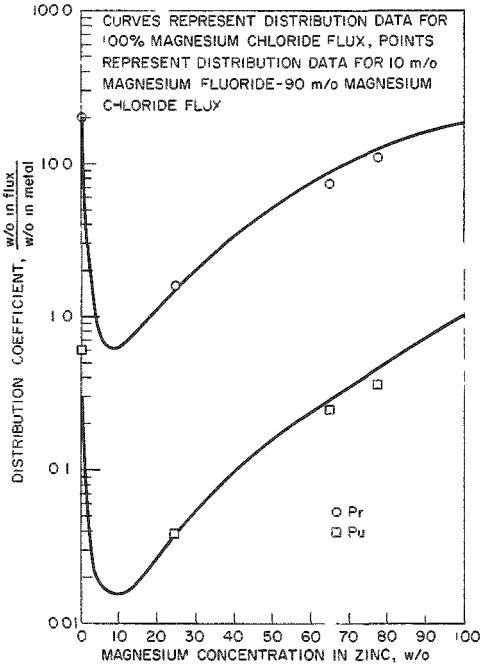

Figure 3

CODISTRIBUTION OF PRASEODYMIUM AND PLUTONIUM BETWEEN ZINC-MAGNESIUM ALLOY AND 10 m/o MAGNESIUM FLUORIDE-90 m/o MAGNESIUM CHLORIDE FLUX

Temperature:	800 C
Mixing Rate:	300 rpm
Atmosphere:	argon
Crucible:	tantalum

Codistribution of Plutonium and Praseodymium between Zinc-Magnesium Alloy and Magnesium Bromide Flux

In a further investigation of the effect of flux composition on the distribution behavior of plutonium and praseodymium, magnesium bromide was substituted for magnesium chloride. The results are presented in Figure 4. The praseodymium distribution coefficients, indicated by circles in Figure 4, differ little from the curve obtained with the magnesium chloride flux. The plutonium distribution coefficient, however, is increased by a factor of about 20 over that for a magnesium chloride flux at a magnesium concentration of 10 w/o in the zinc phase. The plutonium-praseodymium separation factors for the magnesium bromide flux range between 2.4 and 25.

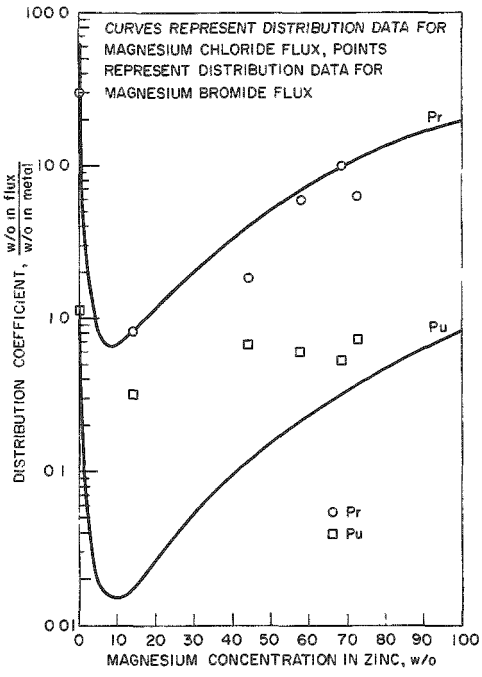

Figure 4

CODISTRIBUTION OF PRASEODYMIUM AND PLUTONIUM BETWEEN ZINC-MAGNESIUM ALLOY AND MAGNESIUM BROMIDE

Temperature:	800 C
Mixing Rate:	300 rpm
Crucible:	tantalum
Atmosphere:	argon

Codistribution of Plutonium and Praseodymium between Zinc-Magnesium Alloy and Magnesium Chloride-Barium Chloride Flux

The codistribution coefficients for plutonium and praseodymium between zinc-magnesium alloy and equimolar magnesium chloride-barium chloride flux are presented, with the experimental conditions, in Figure 5. The data for a magnesium chloride flux are represented by curves; data for the magnesium chloride-barium chloride flux are represented by points. The distribution coefficients for both plutonium and praseodymium are lowered by the presence of barium chloride in the magnesium chloride flux. The plutonium-praseodymium separation factor varies from 17 to 43, depending on the magnesium concentration in the metal phase.

Codistribution of Plutonium and Praseodymium between Zinc-Magnesium Alloy and Cesium Chloride-Magnesium Chloride Flux

The effect of a heavy alkali metal cation, cesium, on the codistribution coefficients of plutonium and praseodymium between zinc-magnesium alloy and chloride flux has been determined by using an equimolar cesium chloride-magnesium chloride flux. The results and conditions of this experiment are presented in Figure 6. These data show that the distribution coefficients for both plutonium and praseodymium are lowered by the presence of cesium chloride in the magnesium chloride flux. The plutonium-praseodymium separation factors for this system at 800 C vary from 36 to 38. They are in agreement with the separation factors calculated from distribution data for plutonium and praseodymium obtained individually with a pure magnesium chloride flux (see ANL-6596, p. 64).

Figure 5

CODISTRIBUTION OF PRASEODYMIUM AND PLUTONIUM BETWEEN ZINC-MAGNESIUM ALLOY AND 50 m/o MAGNESIUM CHLORIDE-50 m/o BARIUM CHLORIDE FLUX

Temperature:	800 C
Mixing Rate:	300 rpm
Crucible:	tantalum
Atmosphere:	argon

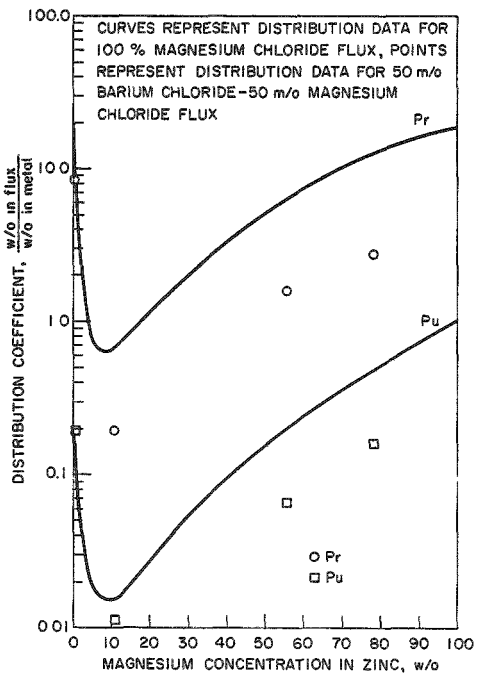

Figure 6

CODISTRIBUTION OF PRASEODYMIUM AND PLUTONIUM BETWEEN ZINC-MAGNESIUM ALLOY AND 50 m/o CESIUM CHLORIDE-50 m/o MAGNESIUM CHLORIDE FLUX

Temperature:	800 C
Mixing Rate:	300 rpm
Crucible:	tantalum
Atmosphere:	argon

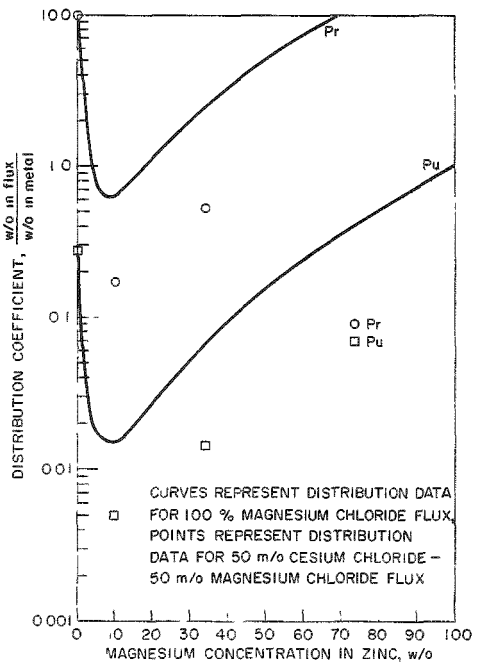

Distribution of Vanadium between Zinc-Magnesium Alloy and Magnesium Chloride

Vanadium is of process interest since it may be a constituent of fuel cladding metals. Earlier distribution data for vanadium (see ANL-6596, p. 60) showed very little vanadium in a magnesium chloride flux phase and a continuous decrease in the vanadium content of the metal phase as magnesium concentration was increased. It was suspected that the disappearance of vanadium resulted either from volatilization of vanadium pentachloride, or from the very low solubility of vanadium in the zinc-magnesium alloy.

An additional experiment was performed, with zinc-4.8 w/o magnesium in the metal phase and magnesium chloride as the flux phase, to determine the behavior of vanadium after various periods of time. The entire experiment lasted 24 hr. Filtered samples of the metal phase were taken after 70, 140, and 164 min, and after 24 hr. Unfiltered flux samples were taken after 70 min and 24 hr.

The results, shown in Table 5, indicate a slight decrease in the vanadium concentration in the metal phase after 24 hr. This decrease is within the analytical uncertainty, however, and is not considered significant. The bottom portion of the zinc-magnesium-vanadium ingot resulting from the experiment showed a segregated phase of a vanadium-zinc intermetallic compound. Thus, vanadium was not removed from the system through volatilization of the chloride, but by precipitation of a relatively insoluble intermetallic compound.

Table 5

DISTRIBUTION OF VANADIUM BETWEEN ZINC-MAGNESIUM ALLOY AND MAGNESIUM CHLORIDE

Metal Phase:	zinc-4.8 w/o magnesium (total: 400 g)
Flux Phase:	magnesium chloride (200 g)
Temperature:	800 C
Mixing Rate:	300 rpm
Atmosphere:	argon
Crucible:	tantalum
Vanadium:	2.2 g high-purity metal

Time after Vanadium Introduction (hr)	Metal Phase		Vanadium in Flux Phase (ppm)
	Magnesium (w/o)	Vanadium (ppm)	
1.1	4.81	1175	$\leq$ 0.02
2.3	4.80	1185	-
2.7	4.72	1115	-
24.0	4.76	1032	$\leq$ 0.02

Distribution of Iron between Zinc-Magnesium Alloy and Magnesium Chloride

Iron is of interest as a possible impurity from stainless steel, a potential cladding material for nuclear fuel. Two experiments were performed to determine the distribution behavior of iron between zinc-magnesium alloys and magnesium chloride. The experimental results are presented in Table 6 and Figure 7. The distribution data from the two experiments are in fair agreement, despite the considerable scatter resulting from the analytical uncertainty in determining the low iron concentrations in the flux. The iron concentrations in the metal phase in the two experiments are in good agreement (see Figure 8). Probably these values represent the solubilities. The value obtained in pure zinc, however, is lower by a factor of three or four than the literature value.[3] The iron

[3]Truesdale, E. C., Wilcox, R. L., and Rodda, J. L., Trans. AIME 122, 192 (1936).

strongly favors the metal phase and does not revert to the flux phase at low magnesium concentrations.

Table 6

DISTRIBUTION OF IRON BETWEEN ZINC-MAGNESIUM ALLOY AND MAGNESIUM CHLORIDE

Metal Phase:	zinc-magnesium (concentration as indicated)
Flux Phase:	magnesium chloride
Temperature:	800 C
Mixing Rate:	300 rpm
Crucible:	tantalum
Atmosphere:	argon

Experiment	Metal Phase: Magnesium (w/o)	Metal Phase: Iron (w/o)	Iron in Flux Phase (w/o)	Distribution Coefficient K_d; w/o Fe in flux / w/o Fe in metal
FeE-1	$<4 \times 10^{-3}$	2.94	8.4×10^{-3}	2.9×10^{-3}
	10.42	1.72	1.7×10^{-2}	9.9×10^{-3}
	41.49	0.24	4.8×10^{-3}	2.0×10^{-2}
	68.4	0.14	1.0×10^{-2}	7.2×10^{-2}
FeE-2	0.04	2.38	1.0×10^{-2}	4.3×10^{-3}
	6.12	1.76	6.1×10^{-3}	3.5×10^{-3}
	29.88	0.51	a	-
	61.2	0.16	1.5×10^{-2}	9.4×10^{-2}

[a]Sample lost

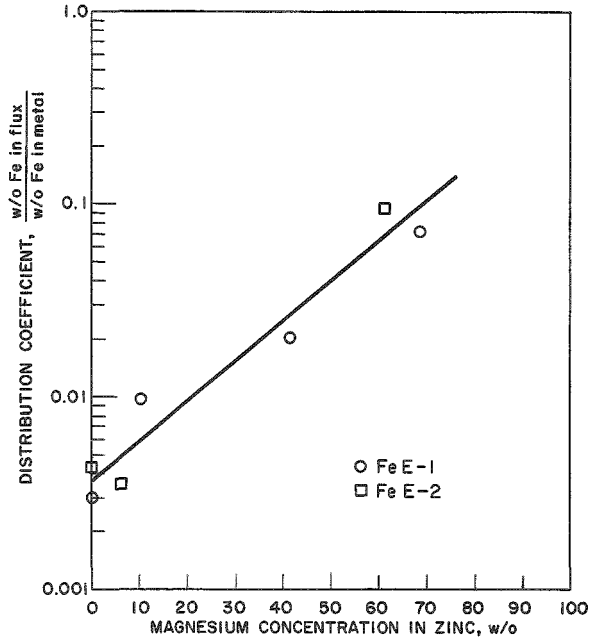

Figure 7

DISTRIBUTION OF IRON BETWEEN ZINC-MAGNESIUM ALLOY AND MAGNESIUM CHLORIDE

Temperature:	800 C
Mixing Rate:	300 rpm
Crucible:	tantalum
Atmosphere:	argon

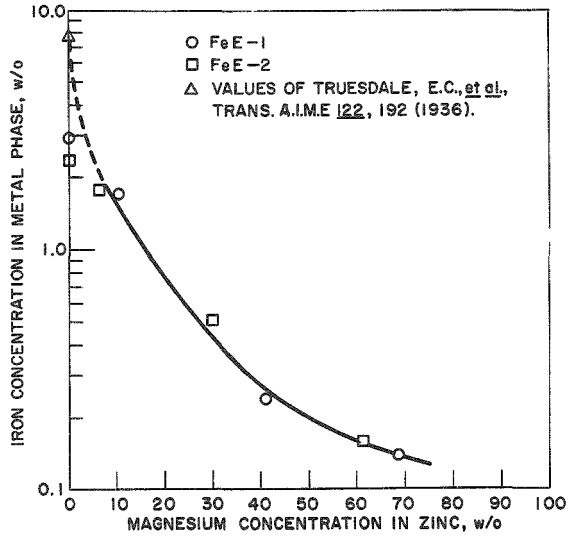

Figure 8

CONCENTRATION OF IRON IN MAGNESIUM-ZINC ALLOYS AFTER EQUILIBRATION WITH MOLTEN MAGNESIUM CHLORIDE

Temperature:	800 C
Mixing Rate:	300 rpm
Crucible:	tantalum
Atmosphere:	argon

The results show that relatively noble metals, such as vanadium and iron, favor the zinc-magnesium phase, along with uranium and plutonium, in this type of system. In a process involving vanadium or iron (a constituent of stainless steel) as fuel-cladding materials, separation from uranium and plutonium must therefore be accomplished in another process step. If the fuel were dissolved in liquid zinc, for example, the uranium and plutonium could first be oxidized selectively into a molten chloride phase by means of zinc chloride, leaving the cladding metals in the zinc phase. The salt phase would then be separated and contacted with the zinc-magnesium alloy, which would reduce the excess zinc chloride.

Preliminary Evaluation of Distribution Data

In process terms, the distribution results indicate that a separation of praseodymium from uranium and plutonium is possible. Since yttrium, cerium, and neodymium have larger separation factors than praseodymium (ANL-6569, page 40), a process employing this type of separation should be capable of removing the Group IIIB and rare earth fission products from fast breeder reactor fuels containing uranium and plutonium. Because certain variations in the composition of the salt phase do not affect the separation factors significantly, it is possible to lower the operating temperature well below the melting point of magnesium chloride (714 C). Preliminary evaluations of process applications have indicated that two or three extraction stages would be required to effect satisfactory fission product removals and recoveries of uranium and plutonium.

(2) Separation of Zirconium from Uranium and Plutonium in the Lithium Chloride-Potassium Chloride-Lithium Fluoride/Cadmium System
(M. Ader, J. T. Feeney)

Decontamination of zirconium from a typical fast breeder reactor fuel alloy, which consists of 20 percent plutonium, 70 percent uranium, and 10 percent fissium, is a key step in fuel processing. Studies at Ames Laboratory[4] on oxidation-reduction reactions in the lithium chloride-potassium chloride eutectic-zinc system showed that cerium, uranium, and zirconium metals are oxidized into the salt phase by zinc chloride in the sequence given. Reduction of the salts of these metals by magnesium proceeds in the reverse sequence, but in both directions some overlap of the redox reactions occurs. The Ames data indicate excellent separability of uranium and zirconium. Plutonium redox behavior is known to lie between that of cerium and uranium. Thus, it was believed that a magnesium titration would be capable of effecting separation of zirconium from plutonium contained in chloride melts.

Processes for uranium-plutonium alloy fuels appear to be readily adaptable to process control during titration, i.e., preventing magnesium overshoot which would result in reduction of plutonium chloride. If the amount of excess oxidant (e.g., zinc chloride) in the salt phase is known, only a slight excess of magnesium, enough to reduce perhaps one or two percent of the uranium trichloride, need be added to assure greater than 90 percent zirconium reduction and transfer to the metal phase. Only a few tenths of a percent plutonium would be reduced if the plutonium titration did not overlap the uranium titration too closely. It should be pointed out, however, that a process must achieve high uranium recovery as well as high plutonium recovery if enriched uranium is utilized in the fuel.

The concept discussed above was tested in an experiment, MA-FL-4, carried out as a flowsheet demonstration. It was assumed that the fuel would be dissolved by zinc chloride oxidation in the presence of a molten chloride salt and a liquid metal solvent, with noble elements, such as niobium, molybdenum, technetium, ruthenium, rhodium, and palladium, remaining as metals either dissolved or precipitated in the metal phase and the elements of Groups IA, IIA, and IIIA together with uranium, plutonium, and zirconium oxidized into the salt phase. Zirconium would then be transferred to the metal phase by titration with magnesium metal and would be removed along with the noble metals by phase separation.

A relatively low temperature, 550 C, and a lithium chloride-potassium chloride eutectic mixture containing one weight percent lithium fluoride were selected to minimize volatilization of zirconium

[4]Chiotti, P., and Parry, S. J. S., Separation of Various Components from Uranium by Oxidation-Reduction Reactions in a Liquid KCl-LiCl/Zinc System, IS-286 (1961).

tetrachloride. Fluoride was added to the salt to avoid the difficulties previously found by this and other investigators (see ANL-6379, page 58) in obtaining salt samples free of metal drops. Cadmium rather than zinc was selected as the metal solvent because of the greater solubility of uranium in cadmium than in zinc at 500 C, thus allowing an analytical check on the amount of uranium reduced into the metal phase during magnesium reduction. This also allowed observation, by analysis, of the buildup of zinc in the metal phase which resulted from the reduction of zinc chloride. Pieces of cadmium-5.04 w/o magnesium alloy were added as the reductant, since the equivalent amounts of pure magnesium were inconveniently small. A description of the experiment follows.

Neutron-irradiated zirconium (1.71 g) was dissolved in 712 g of cadmium under 306 g of lithium chloride-potassium chloride eutectic containing 3.2 g of lithium fluoride. The charge was contained in a Morganite recrystallized alumina crucible equipped with alumina thermocouple wells and a tantalum stirrer. A Type 304 stainless steel perforated basket containing 95.7 g of uranium-1.1 w/o plutonium alloy was next lowered into the salt phase, and preweighed amounts of zinc chloride sticks were added stepwise. A total of 102 g of zinc chloride, about 15 percent more than was required in order to oxidize all of the uranium and plutonium to trichlorides and all of the zirconium to tetrachloride, was used. The chlorides of zinc, zirconium, uranium, and plutonium were next reduced by stepwise additions of 115 g of cadmium-5.04 w/o magnesium alloy. The entire experiment was performed at 547 to 556 C in an argon atmosphere. Samples of salt and metal phases were taken by pressurizing the liquids through tantalum filters press-fitted into tantalum tubes. The analytical results of Experiment MA-FL-4 are given in Table 7.

Table 7

ANALYTICAL RESULTS OF EXPERIMENT MA-FL-4

Conditions: Morganite Al_2O_3 crucible and thermowells; tantalum stirrer; argon atmosphere; liquid samples pressurized through tantalum frits into tantalum tubes

Temperature: 547 to 556 C

Procedure:
I. 1.71 g neutron-irradiated Zr dissolved in 712 g Cd, 306 g LiCl-KCl eutectic 3.2 g LiF
II. 95.7 g U-1.1 w/o Pu alloy suspended in salt phase within SS 304 basket, and $ZnCl_2$ added stepwise
III. Cd-5.04 w/o Mg alloy added stepwise

Procedure	Sample	Hr at Temp	Salt Phase (w/o) U	Pu	Zr	Zn	Mg	Metal Phase (w/o) U	Pu	Zr	Zn	Mg
I. Zirconium Dissolution	1	2.5	-	-	0.00032	-	-	-	-	0.210	-	-
II. Oxidation $ZnCl_2$ Addition (g)												
34.3	2	3.5	5.0	0.053	0.165	2.25	-	0.0003	3×10^{-6}	0.077	0.69	-
33.9	3	2	7.1	0.077	0.317	4.72	-	0.0047	5×10^{-5}	0.0004	1.32	-
17.1	4	18	19.7	0.219	0.248	0.51	-	0.0080	0.00010	0.0002	3.8	-
8.5	5	2	19.8	0.206	0.278	0.89	-	0.13	0.0015	0.0005	5.3	-
8.5	6	1.5	19.9	0.212	0.270	1.56	-	0.087	0.00097	0.0003	6.0	-
III. Reduction Cd-5 w/o Mg Addition (g)												
28.9	7	18	19.7	0.222	0.255	0.74	0.29	0.062	0.00071	0.0003	5.5	-
29.1	8	1.5	19.9	0.217	0.209	0.03	0.54	0.078	0.00091	0.0012	6.2	-
14.3	9	1.2	19.8	0.230	0.0055	0.01	0.53	0.43	0.0044	0.0091	5.8	-
14.4	10	2	18.8	0.223	0.0044	-	0.78	0.48	0.0029	0.0104	5.1	-
14.2	11	1	17.9	0.223	0.0038	-	0.99	1.03	0.0060	0.0113	5.3	-
14.5	12	6	17.0	0.216	0.0039	-	1.16	1.55	0.0096	0.0112	5.4	~0.01

The data for Sample 1 in Table 7 show that zirconium distribution favors the cadmium phase almost completely in the absence of an oxidant. After zinc chloride is added, zirconium is oxidized into the salt phase. A material balance calculation (not given) showed that about 20 to 30 percent of the original zirconium was unaccounted for in Samples 2 to 6. The absence of any significant trend in the material balance data, however, suggests that zirconium was not being lost by volatilization of zirconium tetrachloride.

Dissolution of the uranium-1.1 w/o plutonium alloy (Samples 2 and 3) proceeded slowly. The alloy was held in the upper part of the salt phase, and the stirrer was positioned and rotated so as not to mix in the cadmium phase. Sample 4, which was taken after the mixture remained overnight with little stirring, indicates that the uranium-plutonium alloy was completely dissolved. Further additions of zinc chloride merely increased the zinc chloride concentration in the salt phase (deduced from analysis of Samples 5 and 6).

The first two additions of cadmium-5.04 w/o magnesium were each intended to reduce about half of the excess zinc chloride. The data for Samples 7 and 8 in Table 7 show such a decrease in the zinc chloride concentration but also reveal reduction of small fractions of zirconium chloride. The next magnesium addition (see data for Sample 9) caused almost all the zirconium to disappear from the salt phase without a corresponding increase in the metal phase concentration. A possible explanation for this result is the precipitation of an iron-zirconium-zinc intermetallic compound.[5] The nickel content of the metal phase* indicates that sufficient iron to precipitate the zirconium was introduced through corrosive attack by the salt phase of the stainless steel basket used to suspend the uranium-plutonium alloy. Further additions of cadmium-5.04 w/o magnesium (see data for Samples 10, 11, and 12) had little or no effect on zirconium concentration in either the salt phase or the metal phase.

The reduction of uranium and plutonium chlorides can best be followed by examination of the metal phase concentrations in Table 7. The data for Sample 9 show that small but appreciable amounts of both uranium and plutonium are reduced to metal at the point of complete reduction of zinc and zirconium chlorides. Further additions of reductant (see data for Samples 10, 11, and 12) cause more uranium and plutonium to appear in the metal phase, the uranium being preferentially reduced.

The reduction data in Table 7, together with material balance estimates, were used to plot the titration curves shown in Figure 9.

---

[5] Johnson, I., private communication.

*Approximately 0.035 percent nickel was found in the metal phase of Sample 7.

Despite the overlap that occurs during titration, it is evident that a titration technique can effectively separate zirconium from uranium and plutonium. However, critical control of the magnesium addition must be exercised to avoid serious losses of uranium and plutonium. Potentiometric methods employing indicator electrodes might provide such control.

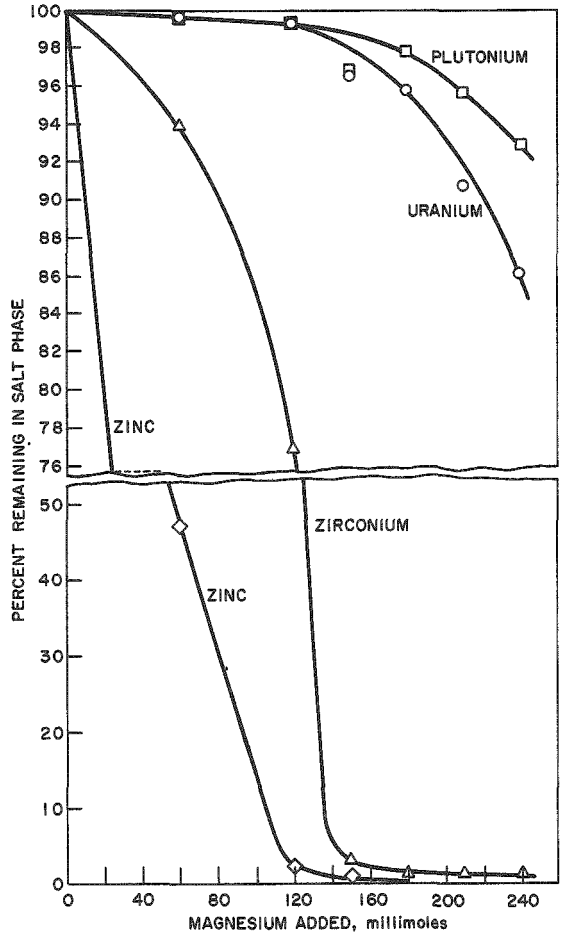

Figure 9

TITRATION OF THE CHLORIDES OF PLUTONIUM, URANIUM, ZIRCONIUM, AND ZINC WITH MAGNESIUM METAL

Experiment MA-FL-4
(millimoles in salt phase)

Pu	4.2
U	400
Zr	14
Zn	114

Salt phase: ~475 g (see Sample 6, Table 7)
Metal phase: ~700 g (see Sample 6, Table 7)
Temperature: 550 C

It is also interesting to note that during reduction (see data from Samples 7-12), the plutonium-uranium separation factors, defined as

$$\frac{(\text{w/o Pu in salt})/(\text{w/o Pu in metal})}{(\text{w/o U in salt})/(\text{w/o U in metal})} ,$$

vary between 1.0 and 2.3. These values are in good agreement with those calculated from previous distribution experiments (see ANL-5959, page 131) at 470 C in the systems (1) lithium chloride-potassium chloride eutectic/cadmium-1.7 w/o uranium-0.2 w/o magnesium and (2) lithium chloride-potassium chloride eutectic/cadmium-1.7 w/o uranium-2 w/o magnesium. The separation factors for the latter experiments are 3.1 and 1.7,

respectively. Similar distribution experiments (see ANL-5896, page 137) with a Dow-230 flux and zinc solvent at 742 C gave plutonium-uranium separation factors of about 100. The disparity in separation factors found in zinc and cadmium is most likely explained by a relatively greater increase in activity coefficient of uranium as compared with that of plutonium when cadmium is used rather than zinc as solvent. Thus, if magnesium reduction in the present experiment had been done with a zinc solvent, the amounts of plutonium reduced relative to uranium reduced would have been considerably smaller. Coreduction and coprecipitation by calcium-zinc alloy of the uranium trichloride and plutonium trichloride contained in the final salt phase from this experiment are described below.

(3) Coreduction of Uranium Trichloride and Plutonium Trichloride by Calcium-Zinc Alloy

(M. Ader, J. T. Feeney)

In one of the schemes proposed for processing uranium-plutonium-fissium alloy fuels from fast reactors, the uranium, plutonium, and fission product elements of Groups IA, IIA, and IIIA are oxidized into a molten halide flux and subsequently reduced by a calcium-rich zinc solution. The reduction is expected to leave the uranium and plutonium coprecipitated as the metals and therefore separable from the Group IA, IIA, and IIIA metals which are soluble in calcium-zinc solution. The feasibility of separating cerium from uranium and from uranium-plutonium in calcium-zinc solutions has been demonstrated previously (see ANL-6379, p. 71, and ANL-6543, p. 51).

A preliminary test of the concept of simultaneously co-reducing and coprecipitating uranium and plutonium was made at a uranium-to-plutonium ratio of about 80. Three hundred sixty grams of the final salt phase from Experiment MA-FL-4 (see Table 7) were mechanically separated from the accompanying cadmium phase at room temperature in a nitrogen atmosphere and used for the present experiment. The salt phase was reheated in a tantalum crucible in an argon atmosphere and sampled at 550 and 650 C to redetermine the uranium, plutonium, and magnesium concentrations. (Zirconium, because of its low concentration, was ignored.) The salt mixture was next cooled to room temperature, and 152 g of calcium and 78 g of zinc were added with the intention of reaching a concentration of about 61 w/o calcium in the metal phase after reduction. The salt-metal mixture was heated and stirred. At 530, 646, and 731 C, samples of both phases were taken for analysis by pressurizing the liquids through tantalum filters into tantalum tubes. Sampling of the metal phase at 430 C was abandoned after several unsuccessful attempts. There were definite indications that a portion of the salt phase had solidified at this temperature. In addition, it was noticed that segregation of salt and metal solutions was poor at both 430 and 530 C, which may be attributable to the small difference in their densities.

The analytical results are given in Table 8. The data for Samples 13 and 14 show that the uranium, plutonium, and magnesium concentrations of the starting salt mixture were about the same as at the end of Experiment MA-FL-4. The salt-phase data for Samples 15, 16, and 17 show that the uranium trichloride, plutonium trichloride, and magnesium chloride were completely reduced by calcium. However, the calcium concentrations found in the salt phase, i.e., 13 to 15 percent, are about 7 percent higher than those calculated to result from the reduction of uranium trichloride, plutonium trichloride, and magnesium chloride. This excess calcium concentration in the flux resulted from the reduction of roughly 20 percent of the lithium chloride and 7 percent of the potassium chloride by the calcium metal. The reduction of these alkali metal chlorides emphasizes the strength of calcium as a reductant in zinc solution and the need for investigating more stable salt solvents, e.g., those containing calcium chloride. From the standpoint of processing, however, some reduction of the salt solvent is tolerable if the reduced metal is soluble in calcium-zinc solution, since the latter is considered a waste solution.

Table 8

COREDUCTION AND COPRECIPITATION OF URANIUM AND PLUTONIUM FROM SALT SOLUTION BY CALCIUM-ZINC SOLUTION

Conditions: Tantalum crucible, thermowell, and stirrer; argon atmosphere; liquid samples pressurized through tantalum frits into tantalum tubes

Temperature: As indicated below

Procedure: I. 360 g of salt mixture from Expt. MA-FL-4[a] sampled and cooled to room temperature
II. 152 g of calcium and 78 g of zinc added to salt mixture, followed by heating and stirring

			Salt Phase (w/o)				Metal Phase (w/o)						
Sample	Temp (C)	Hr at Temp	U	Pu	Mg	Ca	U	Pu	Mg	Ca	Zn	Li[b]	K[b]
I. Sampling													
13	550	1	16.8	0.203	1.15	-	-	-	-	-	-	-	-
14	651	0.5	17.0	0.211	1.10	-	-	-	-	-	-	-	-
II. Calcium Reduction													
15[c]	530	19	5×10^{-4}	1×10^{-6}	<0.001	13	5×10^{-3}	0.0049	1.2	30	21	4	30
16	646	3.2	6×10^{-4}	4×10^{-6}	<0.001	15	6×10^{-4}	0.0195	2.4	51	39	2	4
17	731	15	5×10^{-4}	4×10^{-6}	<0.001	15	3×10^{-4}	0.0222	2.2	46	38	2	1

[a]Original composition of salt: 99 w/o LiCl-KCl eutectic-1 w/o LiF. At end of Experiment MA-FL-4 (see Table 7), the salt contained 17 w/o uranium, 0.216 w/o plutonium, and 1.16 w/o magnesium.

[b]Spectrographic analysis, factor-of-two accuracy.

[c]Metal phase believed to be contaminated with salt phase.

Analysis of the metal sample taken at 530 C (Sample 15) shows probable contamination by the salt phase, for comparison of the analysis with analyses of the next two metal samples (Samples 16 and 17) shows low calcium, magnesium, and zinc concentrations and high lithium and potassium concentrations for Sample 15. Thus, only the samples taken at 646 and 713 C are valid for examining the coprecipitation behavior of uranium and plutonium.

By assuming that the uranium and plutonium not present in the metal phase (Samples 16 and 17) were precipitated, it can be calculated that essentially 100 percent of the starting uranium and about 95 percent of the starting plutonium were precipitated at 646 and 731 C. The plutonium data are believed to represent coprecipitation, rather than solubility behavior. At these temperatures, the plutonium solubilities in zinc solutions containing about 50 w/o calcium are believed to be considerably greater than those found - of the order of tenths, rather than of hundredths, of a percent. It should be pointed out, however, that the coprecipitation behavior of plutonium may have been influenced by the presence of lithium and potassium in the metal phase.

Although only 95 percent of the plutonium was coprecipitated, this result is encouraging and further exploration of the scheme advanced above for separating uranium-plutonium from Group IA, IIA, and IIIA elements is warranted. Coprecipitation behavior is likely to be influenced by the precise manner in which the precipitation is carried out, e.g., by the temperature and rate of calcium addition, and conditions may be found which will result in coprecipitation of 99 percent or more of the plutonium with uranium.

e. Recovery of Plutonium from EBR-II Blanket Material (I. O. Winsch, T. F. Cannon, P. J. Mack)

The blanket material of the EBR-II reactor will be processed to recover the plutonium when the plutonium concentration reaches about one percent. Pyrometallurgical processes with liquid metal solvents are to be used for the separation of plutonium from uranium. In particular, the separation of plutonium from uranium is based on the high solubility of plutonium in magnesium-rich zinc alloys and the contrasting low solubility of uranium in them.

(1) Blanket Process Demonstration Run

A sixth blanket process demonstration run* has been completed and is summarized in Table 9. This run was made in accordance with the usual procedure of dissolving the blanket material in a 12 to 15 w/o magnesium-zinc alloy to produce an approximately 13 w/o uranium solution, precipitating the uranium from solution by adding magnesium to produce a 50 w/o concentration, cooling to reduce the uranium solubility as much as possible, and then separating the supernatant phase containing the soluble plutonium from the precipitated uranium.

After the separation of the supernatant, no further process steps were carried out in this and preceding demonstration runs. In the

*The results of previous blanket processing runs are reported in ANL-6379, p. 76; ANL-6413, p. 56; ANL-6477, p. 47; ANL-6569, p. 43; and ANL-6596, p. 66.

final process step, for which equipment is now being designed and installed, the bulk of the magnesium and zinc will be evaporated from the transferred supernatant to produce a plutonium product concentrate suitable for incorporation into a core fuel cycle for replenishment of the fissionable material.

Table 9

SUMMARY OF BLANKET PROCESS DEMONSTRATION RUN 6

2930 g Zinc
440 g Magnesium
501 g Uranium
5.32 g Plutonium

Dissolution at 800 C

Time (hr)	U Conc (w/o)	% of Theoretical U Concentration	Pu Conc (w/o)	% of Theoretical Pu Concentration
4	12.4	95.8	0.138	100
8	12.9	100.0	0.137	100

2490 g Magnesium

Uranium Precipitation at 800 C Followed by Cooling to 400 C

Temp (C)	Concentration in Mg-Zn Solution (w/o) U	Concentration in Mg-Zn Solution (w/o) Pu	% of Theoretical Pu Concentration
770	0.31	0.09	100
582	0.11	0.089	99
415	0.035	0.089	99

Phase Separation at 430 C

5200 g Mg-Zn-U-Pu
90% of Supernatant

Concentration in Transferred Supernatant (w/o) U	Concentration in Transferred Supernatant (w/o) Pu[a]	% in Transferred Supernatant of Total Pu Present
0.047 (2.44 g)	0.0905 (4.70 g)	90.0

490 g Uranium
0.453 g Plutonium
620 g Magnesium-Zinc

127 g Magnesium
2644 g Zinc

Dissolution at 810 C

Time (hr)	U Conc (w/o)	% of Theoretical U Concentration	Pu Conc (w/o)	% of Theoretical Pu Concentration
8	12.5	95	0.0129	105

[a]The total plutonium in the supernatant was 4.70 g of a possible 5.21 g or 90 percent of that available. This is the theoretical recovery since the percentage of supernatant removal was also 90. A plutonium separation factor of 181 was realized.

The phase separation actually achieved in this run was 90 percent (see Table 9), which for this scale of operation is considered to be a reasonably good separation. In the five previous runs at the same scale of operation, phase separation efficiencies of 70, 87, 72, 97, and 92 percent had been realized. Although the scale of these runs was small (500 g of uranium), it was hoped that a 95 percent phase separation of the plutonium product solution from the precipitated uranium could be achieved. A 95 percent phase separation would result in a corresponding 95 percent plutonium recovery in this step and might be sufficient to satisfy the economic requirements of the process. Under reasonable reactor operating conditions, the value of the unrecovered plutonium would

be very low (0.05 mill/kwh*). If greater plutonium recoveries are desired, the uranium precipitate may be washed with additional 50 w/o magnesium-zinc alloy. Phase separation work on large-scale runs (one-half full-plant scale) has given reasonably good assurance that 95 percent phase separations can be achieved on a plant scale (see Table 10).

Table 10

PHASE SEPARATION OF MAGNESIUM-ZINC SUPERNATANT SOLUTIONS FROM PRECIPITATED URANIUM METAL

Scale: 45 kg of 50 w/o magnesium-zinc and 4 kg of uranium

One hour was allowed for settling of the uranium precipitate.

Run No.	Phase Transfer Temp (C)	Uranium Concentration (w/o)			Percent of Supernatant Phase Transferred	Percent of Total Uranium Transferred
		Solubility at Transfer Temp[a]	Transferred Phase[b]	Precipitated Phase		
1	420	0.027	0.03	53.5	92.8	0.33
2[c]	415	0.062	0.062	45.5	89.5	0.63
3	430	0.068	0.068	57.6	94.0	0.72
4	475	0.085	0.090	84.0	99.0	1.01
5	450	0.075	0.094	82.5	98.0	1.02
6[c,d]	450	0.045	0.050	42.3	90.5	0.63
7[d]	450	0.048	0.056	57.0	94.9	0.74
8[d]	450	0.056	0.058	59.4	95.0	0.74
9[d]	450	0.058	0.060	58.5	95.0	0.77
10[d]	455	0.070	0.066	60.0	95.0	0.75

[a]Filtered samples of melt before transfer.

[b]Grab samples of transferred magnesium-zinc phase.

[c]Incomplete decomposition of uranium-zinc intermetallic.

[d]Because of the physical carryover of uranium experienced in Runs 4 and 5, a flat metal shield or disk was placed about 1/16 in. from the tube opening (see further details in ANL-6543, p. 58).

The plutonium concentration in the transferred phase, 0.0905 percent, is the theoretical concentration, indicating no loss of plutonium either on transfer or by coprecipitation with uranium. The uranium concentration of the transferred supernatant (0.047 w/o) is just slightly higher than the uranium solubility. This indicates a slight physical carryover of precipitated uranium, which possibly resulted from loss of the transfer line shield (described in ANL-6543, p. 58). A plutonium separation factor of 181 obtained in this run may be compared with values of 80, 169, 157, and 231 in previous runs. The overall uranium material balance in this run was 96 percent, and the plutonium material balance was 99.5 percent.

No further blanket process demonstration runs at this scale of operation and of this type are planned. The demonstration runs have shown: (1) theoretical recovery of plutonium to be possible, i.e., recovery equivalent to the percent removal of product phase, (2) adequate

*Calculation based on a 2 percent burnup of fuel, a one percent buildup of plutonium in the blanket, and approximately equal core and blanket processing rates.

separation of uranium from plutonium, and (3) good uranium and plutonium material balances. Additional blanket demonstration runs will be made with lightly irradiated blanket material to determine the behavior of iodine and fission products in the process.

(2) Separation of Magnesium-Zinc Supernatent Solutions

Ten phase-separation runs have been completed in a study of the separation of the magnesium-zinc supernatant from the precipitated uranium phase at one-half plant scale (about 45 kg of 50 w/o magnesium-zinc and 4 kg of uranium). A cross-sectional view of the apparatus used in these runs is shown in Figure 10 and a photograph of the assembled apparatus is shown in Figure 11.

Figure 10

CROSS SECTION OF EQUIPMENT FOR SEPARATION OF SUPERNATANT LIQUID METAL PHASE FROM PRECIPITATED URANIUM METAL

(Fig. 11 is a photograph of equipment)

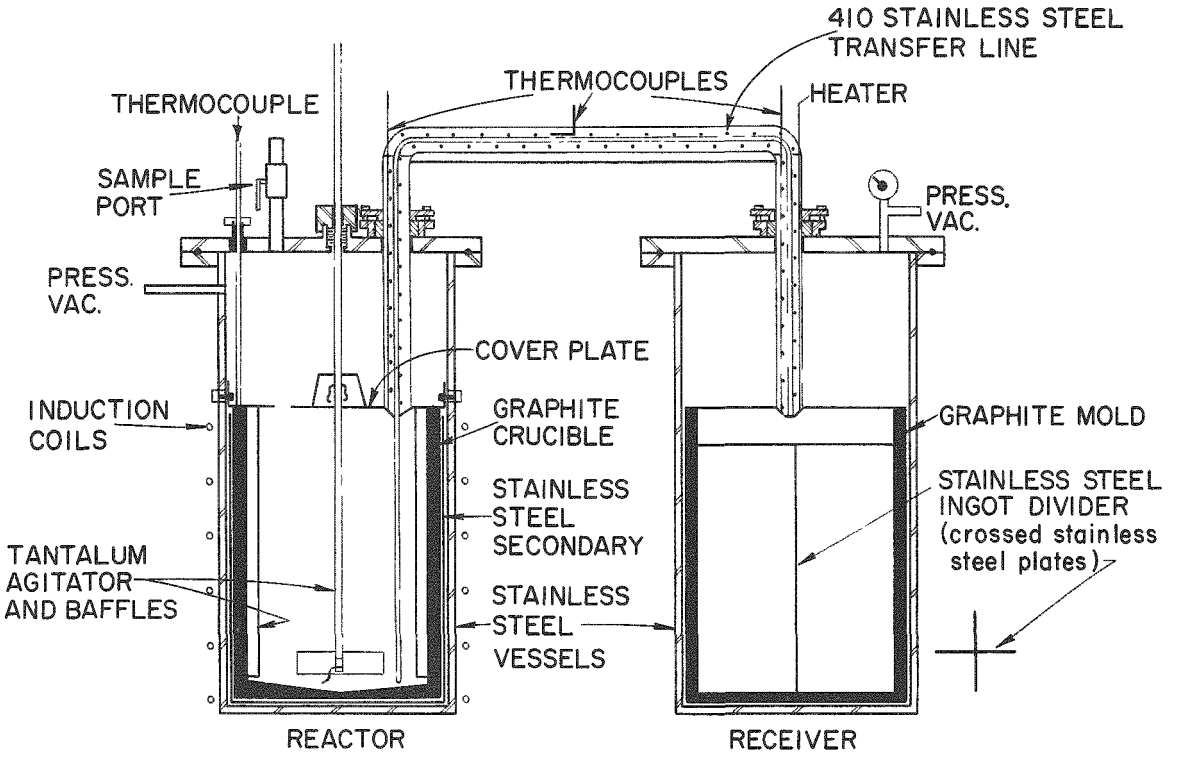

Figure 11

EQUIPMENT FOR SEPARATION OF SUPERNATANT LIQUID METAL PHASE FROM PRECIPITATED URANIUM METAL

(Cross-sectional view shown in Fig. 10)

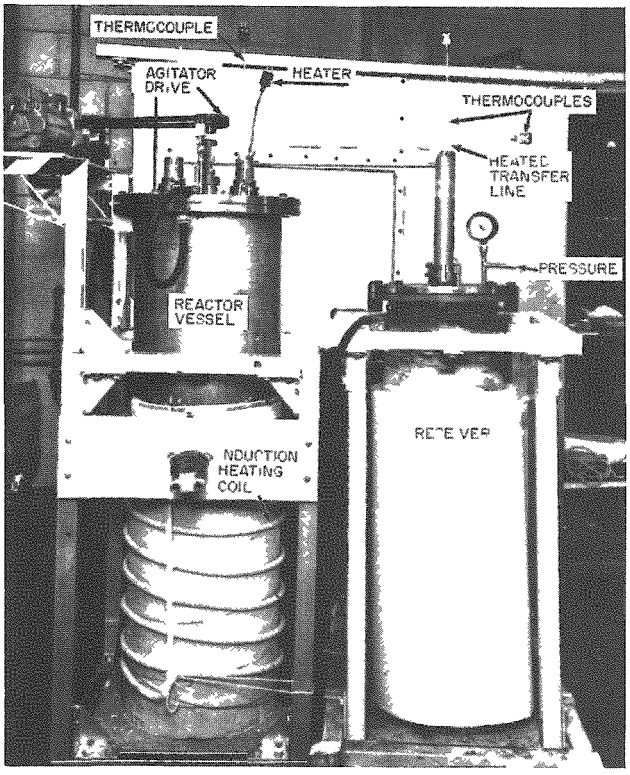

108-5434

In these runs, uranium was initially dissolved in a 12 w/o magnesium-zinc solution by heating to 800 C in a graphite crucible. After the melt was cooled to room temperature, thereby not only solidifying the alloy but also precipitating uranium as a uranium-zinc intermetallic compound (U_2Zn_{17})*, a sufficient amount of solid magnesium was added to make a 50 w/o magnesium-zinc alloy. This charge was heated to 800 C to produce a molten alloy and agitated for 4 hr, during which uranium metal precipitated. In one run complete decomposition of the intermetallic compound did not occur. Additional precipitation of uranium was effected upon cooling the melt to the transfer temperature of 415 to 475 C. The magnesium-zinc phase was pressure-transferred to the graphite crucible contained in the receiver after about a one-hour settling time at the transfer temperature. The pressure differential required for these transfers was about 11 to 12 psi. The elevation of solution in these transfers was probably greater than would be required in a plant.

With one exception, the percentage of the supernatant phase transferred was above 90 percent, and in many runs was 95 percent or greater (see Table 10). In Runs 4 and 5, phase transfer efficiencies were 99 and 98 percent, but these were achieved at the expense of some physical carryover of precipitated uranium metal. After this physical carryover was experienced, a small metal shield was placed over the transfer tube opening at a distance of about $\frac{1}{16}$ in. from the tube end (see ANL-6543, p. 58). In subsequent runs, there was very little or no physical carryover of uranium metal.

---

*In plant operation cooling to room temperature would not be a process step. Magnesium would simply be added to the solution at 800 C to bring the magnesium concentration up to 50 w/o.

A typical heel containing precipitated uranium in the residual magnesium-zinc alloy is shown in Figure 12. Such heels, which are about one-quarter to one inch thick, are brittle and can be broken into smaller pieces. Both in the blanket process and in the skull reclamation process (in which a similar uranium product is obtained), the brittleness of heels may be of importance in the sizing of retorting crucibles or in providing flexibility by allowing the use of less than an entire heel.

Figure 12

HEEL CONTAINING PRECIPITATED URANIUM AND RESIDUAL MAGNESIUM-ZINC ALLOY AFTER REMOVAL OF THE BULK OF THE SUPERNATANT LIQUID METAL PHASE

(Heel is about one-quarter to one inch thick)

108-5437

f. Materials and Equipment Evaluation
(P. A. Nelson)

Materials studies are in progress to evaluate the compatibility of various materials with liquid metal and flux systems of the types contemplated for reprocessing reactor fuels. The main objective of these studies is the selection of materials for EBR-II processing equipment, but data of more general interest are also being accumulated. Work is reported below on the corrosion of tungsten and tungsten alloys by molten metal-flux systems, on the attack of ceramic containers by molten metal-flux systems, and on the attack of stainless steels by zinc vapor.

(1) Corrosion of Tungsten and Tungsten Alloys by Molten Metal-Flux Systems (M. Kyle, M. Deerwester)

Further data are now available for runs, previously reported in ANL-6596, p. 70, to test the corrosion resistance of tungsten and tungsten alloys to the systems and conditions of the noble metal extraction step of the skull reclamation process. In this step a molten chloride flux containing suspended skull oxide is contacted with liquid zinc at 800 C. In the corrosion tests, the corrosion specimens were fabricated into agitator blades and rotated in the corroding media.

Sintered tungsten and rolled tungsten sheet performed well, with no apparent change in size or weight (see Table 11). Metallographic examination has also shown no significant corrosion and no change in structure of sintered tungsten (see Figure 13). An apparent increase in strength and ductility of tungsten after exposure, probably attributable to surface effects, is shown by the data in Table 11. Under the conditions employed in testing these samples for rupture stress, tungsten is normally notch sensitive. Any condition which would tend to smooth the surface would increase its apparent rupture strength.

Table 11

CORROSION OF TUNGSTEN AND MOLYBDENUM-30 w/o TUNGSTEN ALLOY EXPOSED TO SALT-METAL SYSTEM OF THE NOBLE METAL EXTRACTION STEP

Samples were exposed as agitator blades fastened to a tungsten shaft (see ANL-6596, p. 70)

Sample Size: 0.090 x 0.090 x 1.5 in.

Conditions:
- Time: Run 1 - 500 hr; Run 2 - 400 hr
- Temperature: 800 C
- Metal Phase: 1350 g zinc
- Salt Phase: 425 g of composition (m/o): 46.6 LiCl, 46.6 $MgCl_2$, 4.8 MgF_2, and 2.0 $ZnCl_2$
- Agitation: 460 rpm
- Crucible: Alumina containing four 1/4-in. tungsten baffles

	Sintered and Rolled Tungsten Sheet		Pressed and Sintered Tungsten		Molybdenum-30 Percent Tungsten Alloy	
	Run 1	Run 2	Run 1	Run 2	Run 1	Run 2
Weight Change (percent)	[a]	-0.020	-0.22	+0.078	[a]	-3.8
Thickness Change (mils)	0.000	0.000	0.000	0.000	0.000	0.000
Modulus of Rupture (psi)[b]						
Before Corrosion	111,000	111,000	50,000	50,000	209,000[c]	209,000[c]
After Corrosion	150,000	139,000	71,000	62,000	173,000[c]	176,000[c]
Deflection at Rupture (mils)[d]						
Before Corrosion	5	5	3	3	133	133
After Corrosion	7	9	4	4	187	120
Depth of Attack (mils)	<1	<1	<1	<1	6-8	4-7

[a] Value not determined.

[b] Calculated value (see ANL-6543, pp. 65 and 66, for method of calculation).

[c] Value should be used for comparison purposes only. The formula used does not strictly apply in this instance because of plastic deformation of the sample.

[d] Deflection of center of sample at rupture with an effective sample length of 1.25 in.

Figure 13

CORROSION OF PRESSED AND SINTERED TUNGSTEN EXPOSED TO CONDITIONS OF NOBLE METAL-EXTRACTION STEP OF THE SKULL RECLAMATION PROCESS

(see conditions in Table 11, Run 1)

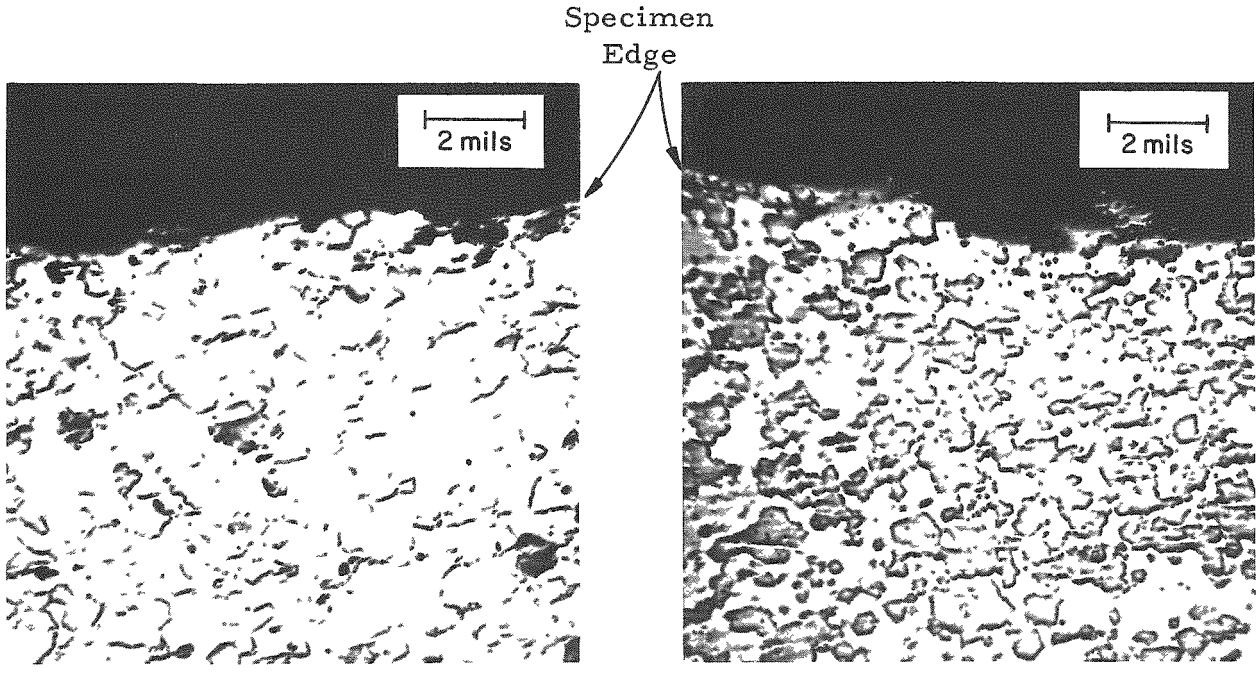

The molybdenum-30 percent tungsten alloy was attacked somewhat by the noble metal-extraction conditions (see Table 11). The weight loss noted was equivalent to approximately 5 percent of the molybdenum content of the alloy. Metallographic examination of the samples indicated that a leaching type of attack had occurred (see Figure 14). Normal to the direction of swaging of the sample, the depth of attack was about 2 to 4 mils in 500 hr. Along the direction of swaging (attack from the ends of the sample), the attack was more severe and less uniform, varying from about 3 to 8 mils. The greater depth of attack parallel to the direction of swaging seems to indicate that attack is along the grain boundaries, although intergranular attack was not apparent under metallographic examination.

Results of bend tests of the molybdenum-tungsten samples showed a decrease in strength after exposure. This is understandable in view of the observed extent of attack. The variation of bend deflection is probably also due to surface effects. It should be noted that the molybdenum-30 percent tungsten alloy is significantly more ductile than tungsten.

Figure 14

CORROSION OF MOLYBDENUM-30 PERCENT TUNGSTEN ALLOY EXPOSED TO NOBLE METAL EXTRACTION STEP OF THE SKULL RECLAMATION PROCESS

(see conditions in Table 11, Run 1)

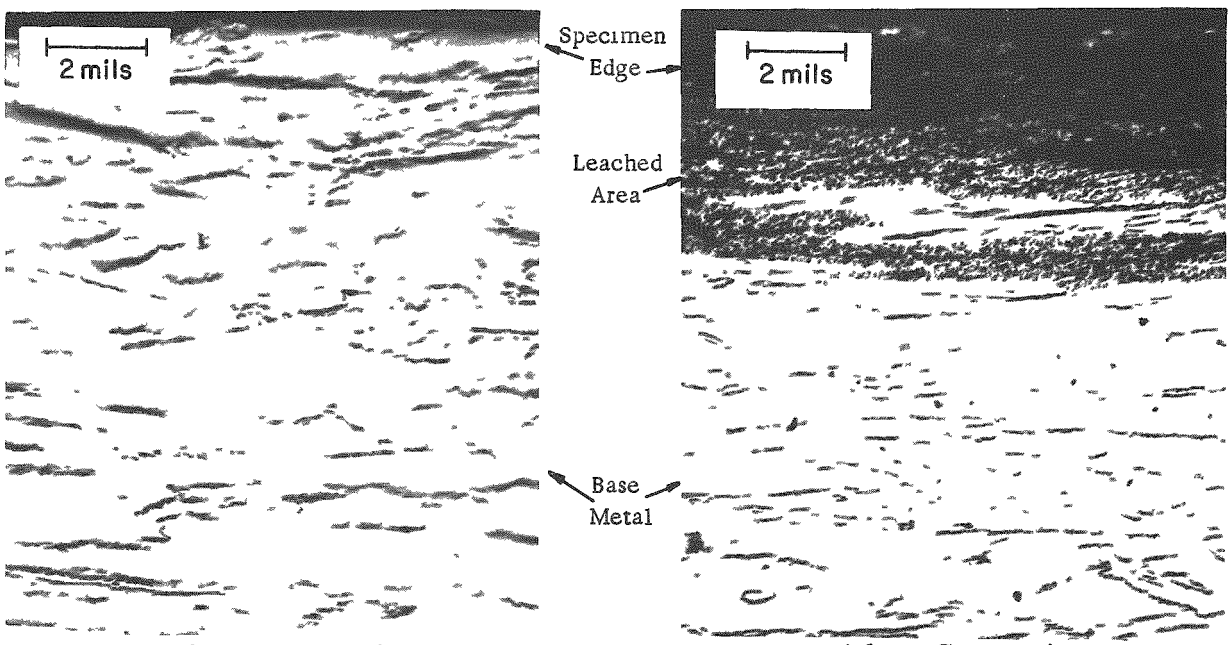

A molybdenum-30 percent tungsten alloy agitator exposed to conditions of noble metal extraction for 500 hr and to reduction conditions for an additional 500 hr (see ANL-6596, p. 73) underwent greater attack, by pitting, than did specimens of the alloy in the runs reported above.

Although attacked to a slight extent, the molybdenum-30 percent tungsten alloy is considered the best material for applications, such as agitators and transfer lines, because of its machinability. However, tungsten appears to be the best material for crucibles because of its superior corrosion resistance and relatively low cost.

(2) Containment of Molten Zinc-Magnesium-Flux Systems in Ceramic Vessels
(P. A. Nelson, G. A. Bennett, L. F. Dorsey)

Consideration is being given to the use of ceramic vessels fabricated of stable oxides, such as alumina and magnesia, because of the possibility that they can be more easily fabricated in large sizes and at lower cost than can tungsten and beryllia crucibles. The

problems of obtaining vessels with the necessary thermal shock resistance and impermeability to metal and flux systems were discussed and some approaches to these problems were outlined in the last summary report, ANL-6596, p. 75. Also of concern if ceramic oxide crucibles were used would be contamination of the metal phase as a result of reduction of alumina or other oxides by magnesium contained in the metal charge. Tests made with alumina and beryllia crucibles are described below.

In a series of experiments, a ram-molded alumina crucible* and two types of dense, slip-cast, high-fired alumina crucibles,** which were considered to be representative of commercially available types of alumina, were tested as containers for zinc-magnesium solutions. The experiments were conducted at 800 C for periods of 24, 45, or 48 hr, with agitation of the molten materials at 230 rpm (see Table 12). A zinc-50 w/o magnesium alloy was charged into the ram-molded crucible in an experiment that simulated the conditions of the uranium precipitation step of the

Table 12

INTERACTION OF ALUMINA CONTAINMENT CRUCIBLES WITH ZINC-MAGNESIUM-URANIUM-FLUX SYSTEMS AT 800 C

Agitation: 230 rpm

Type of Crucible	Charge Composition (w/o)			Flux[a] Present	Time at Temp (hr)	Aluminum Pickup in Metal Phase (w/o)[b]	Final Condition of Crucible
	Zinc	Magnesium	Uranium				
Ram-molded alumina[c]	50	50	0	No	48	0.10	Walls penetrated by melt
Slip-cast alumina[d]	89.5	10	0.5	Yes	24	0.02	Crucible cracked
Slip-cast alumina[d]	89.5	10	0.5	Yes	45	0.02	Crucible cracked
Slip-cast, recryst. alumina[e]	89.5	10	0.5	Yes	48	0.01	Crucible cracked

[a] Flux composition (m/o): 47.5 $CaCl_2$, 47.5 $MgCl_2$, and 5 MgF_2.

[b] The aluminum pickup also represents the final aluminum concentration since the initial metal charges contained less than 10 ppm aluminum.

[c] Alundum (Norton Co.): 99.0 percent Al_2O_3, 0.58 percent SiO_2.

[d] Cast alumina (Coors Porcelain Co.): 99.0 percent Al_2O_3, 0.8 percent SiO_2, and trace percentages of CaO, MgO, and TiO_2.

[e] Morganite recrystallized alumina: 99.7 percent Al_2O_3.

*An Alundum crucible manufactured by the Norton Co., having a nominal composition of 99.0 percent aluminum oxide and 0.58 percent silicon oxide.

**The two types are: (1) A cast alumina crucible manufactured by the Coors Porcelain Co., having a nominal composition of 99.0 percent alumina, 0.8 percent silica, and traces of calcia, magnesia, and titania. (2) Morganite recrystallized alumina (99.7 percent aluminum oxide).

skull reclamation process. A zinc-10 w/o magnesium-0.5 w/o uranium alloy and a 47.5 m/o calcium chloride-47.5 m/o magnesium chloride-5 m/o magnesium fluoride flux (flux-to-metal weight ratio = 0.4) were charged into the slip-cast crucibles in tests that simulated the conditions in the skull oxide reduction step of the skull reclamation process.

All crucibles failed as container materials (as shown in Table 12), either by cracking or by penetration of the walls by flux and metal. Cracking of the high density slip-cast crucibles was more severe than in the longer (500-hr) experiments with similar crucibles in which corrosion specimens were tested in a zinc-flux medium which did not contain magnesium (see Table 11 of this report). Therefore, it is possible that the cracking of these crucibles was associated with attack by the magnesium.

Aluminum contamination of the metal phase was slight (100-200 ppm), except in the case of the ram-molded (Alundum) crucible, for which the aluminum concentration in the metal phase reached 0.10 percent. This may have resulted from the high apparent porosity (19 percent) of the ram-molded crucible or from the higher magnesium concentration used in this run (50 w/o as compared with 10 w/o in the other runs). It is not believed that uranium would be precipitated by the small aluminum contamination. Analytical results which might confirm this are not complete.

A similar experiment was made with a thixotropically cast beryllia crucible supplied by Brush Beryllium Co. In manufacture, this crucible had been washed several times with a beryllia slip (a dilute slurry of beryllium oxide) to increase the density to approximately 2.55 g/cc (83 percent of theoretical). A zinc-50 percent magnesium solution was held in this crucible at 800 C for 48 hr. Although beryllium pickup by the melt was slight (approximately 200 ppm maximum), hairline cracks and slight leakage of the metal through the bottom of the crucible occurred. The metal penetration probably did not occur until after a period of several hours, for this same crucible subsequently performed satisfactorily in a short-term demonstration of the intermetallic decomposition and retorting steps of the skull reclamation process, for which the conditions were similar to those in the above experiment.

(3) Corrosion of Anodized Beryllium by Molten Metal-Flux Systems
(M. Kyle, M. Deerwester)

Beryllia has shown promise as a container material for zinc and zinc-magnesium systems, especially for the precipitation and retorting steps of the skull reclamation process. Anodized beryllium (that is, beryllium metal coated with a beryllium oxide coating by an anodization process) has also been considered for this application because beryllium metal possesses greater strength and density than does beryllia.

Initial testing of the anodized beryllium was done by thermal cycling to determine if repeated temperature changes would cause cracking or breaking away of the thin (approximately 1-mil) anodized layer. After 15 temperature cycles between room temperature and 850 C in an argon atmosphere, the coating broke away from the base metal at the edges of the specimens (which were $\frac{3}{8}$-in.-dia, $1\frac{3}{4}$-in.-long, right circular cylinders with a $\frac{1}{32}$-in. radius on all edges). Despite the breaking away of the coating at the relatively sharp edges, most of the coating appeared to be unaffected.

Additional runs were made to test the corrosion resistance of new specimens of the anodized beryllium to zinc-magnesium, to halide flux, and to combined systems. Conditions employed and results obtained are presented in Table 13. Portions of the anodized coating were

Table 13

CORROSION OF ANODIZED BERYLLIUM BY ZINC-MAGNESIUM-FLUX SYSTEMS

Conditions:	Test:	Static
	Time:	100 hr
	Temperature:	800 C
	Specimens:	Beryllium, right circular cylinders, $\frac{3}{8}$-in. dia x $1\frac{3}{4}$-in. long with a $\frac{1}{32}$-in. radius on all edges, with 1-mil anodized coating.
Corrosion Capsule:		1-in.-dia x 2-in.-long; tantalum
Flux Composition:		46.6 m/o LiCl 46.6 m/o $MgCl_2$ 2.0 m/o $ZnCl_2$ 4.8 m/o MgF_2
Metal Composition:		95 w/o Zn 5 w/o Mg

Metal Present	Flux Present	Depth of Penetration (mils)	Remarks
Yes	No	10	Coating broke away; Be-metal reaction.
No	Yes	25	Coating broke away.
Yes	Yes	25	Coating broke away; Be-metal reaction.

broken or destroyed on all specimens by exposure to the zinc-magnesium and/or halide flux systems. The anodized coating may have provided some protection in areas where it did not break away, as evidenced by the fact that only slight corrosion took place along some surfaces (see Figure 15). The beryllium substrate was attacked by the zinc-magnesium metal and the flux by a reaction which removed the solid metal in gross amounts. It is concluded that the anodized coatings will not adequately protect beryllium from attack at fuel-processing temperatures by the zinc-magnesium solutions or halide fluxes used.

Figure 15

ANODIZED BERYLLIUM AFTER EXPOSURE TO ZINC-5 PERCENT MAGNESIUM AND HALIDE FLUX FOR 100 HOURS AT 800 C

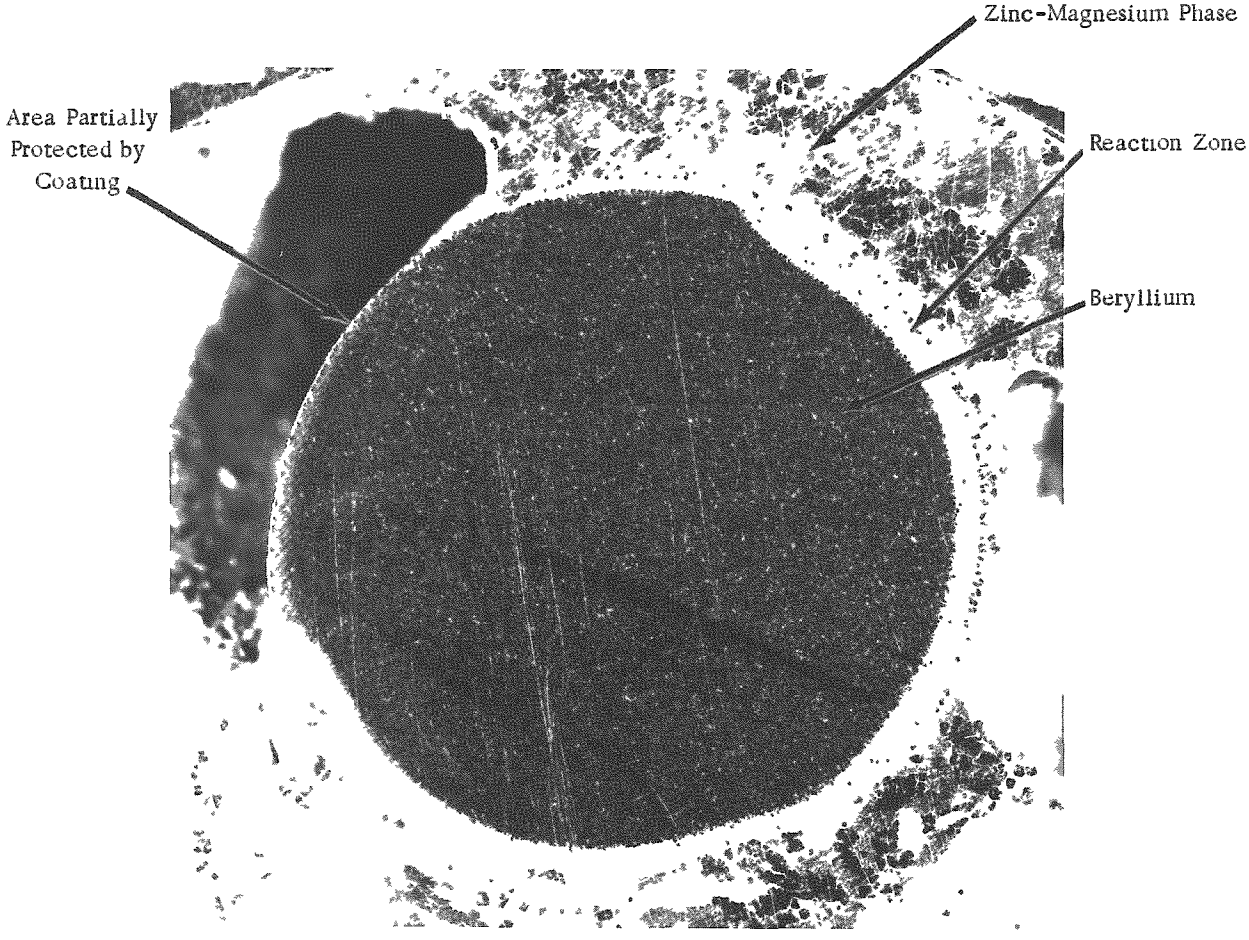

(4) Corrosion of Stainless Steels by Zinc Vapor
(G. A. Bennett, L. F. Dorsey)

In experimental work with zinc systems, the container vessels are nearly always housed in stainless steel equipment, principally

to permit maintenance of an inert atmosphere and operation at desired pressures. It has often been observed that stainless steel (usually Type 304) suffers little attack by zinc vapor, but is severely attacked by liquid zinc in areas where condensation of zinc occurs. Because stainless steel may be considered for equipment which would be exposed to attack by zinc vapor only, the extent of attack of several stainless steels by zinc vapor was determined. In 500-hr exposures to zinc vapor at 900 C, two austenitic 300 series stainless steels (Types 304 and 347) suffered severe attack. Loss of nickel from these steels indicates the probable formation of low-melting phases. Good corrosion resistance to attack by zinc vapor was exhibited by a 400 series stainless steel, Type 405, a ferritic steel. Another 400 series stainless steel, Type 440C, a martensitic steel, also exhibited good corrosion resistance, although suffering some loss in weight.

Experimental Equipment and Procedure

The procedure consisted of exposing stainless steel coupons to static zinc vapor for 500 hr at a temperature above the dew point of the zinc vapor. The apparatus, shown in Figure 16, consisted of a $11\frac{3}{4}$-in.-long, closed tantalum tube, jacketed in Type 304 stainless steel to prevent oxidation of the tantalum. In the bottom of the tube, a zinc-10 w/o magnesium alloy charge, maintained at a temperature of about 740 C, was the source of zinc vapor.

Figure 16

CORROSION APPARATUS FOR EXPOSURE OF STAINLESS STEEL COUPONS TO ZINC VAPOR

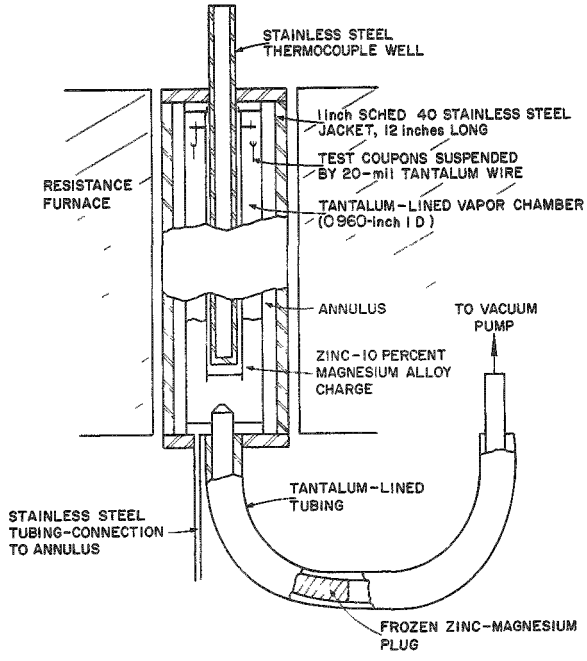

Four stainless steel coupons of various compositions were suspended in the vapor space in the upper part of the tantalum tube. Through proper positioning of the tube in the furnace, this space was maintained at 890 to 900 C in order to prevent vapor condensation. At the conclusion of the run, condensation of zinc vapor on the steel coupons was prevented by first cooling the lower end of the chamber. Thermocouples in a thermowell extending axially nearly the full length of the tantalum tube allowed temperature measurement over most of the tube length. A complete temperature profile was taken each 24 hr.

Magnesium was added to the zinc to a concentration of 10 w/o (alloy prepared before charging) to decrease the corrosiveness of zinc to tantalum (see ANL-6287, pp. 74 to 76) and to approximate conditions of vapor attack in the skull reclamation and blanket processes. The vapor in equilibrium with zinc-10 percent magnesium at 740 C would contain less than one percent magnesium (see ANL-5996, pp. 77 to 82), and it was assumed that this slight amount would not appreciably affect the attack of zinc vapor on the steels which were tested. The attack of liquid zinc on stainless steels is only slightly reduced, if at all, by the presence of one percent magnesium, but is more substantially reduced at higher magnesium concentrations (see ANL-6477, pp. 65 to 67).

No leaks in the apparatus could be detected with a helium mass spectrometer leak detector. The annulus between the tantalum tube and stainless steel shell was alternately evacuated and filled with argon before finally being pressurized with argon to a pressure of 20 in. of water for the duration of the run. The inner tantalum chamber was evacuated to the limit of a mechanical vacuum pump (about 50 μ pressure) and sealed off under vacuum by melting the zinc-magnesium alloy and allowing it to flow into the small ($\frac{1}{4}$-in.-diameter) outlet tantalum tube shown in Figure 16, where it was allowed to freeze. This freeze seal, which was expected to be effective because zinc wets tantalum well, was backed up by a mechanical vacuum pump. Examination of the freeze seal at the conclusion of the run showed that it had effectively closed the outlet line.

The four types of stainless steel tested were as follows:

Type	Nominal Composition (%)[6]
304 (austenitic)	Fe; 18-20 Cr; 8-12 Ni; 0.08 max. C; 2 max. Mn; 1 max. Si; 0.045 max. P; 0.03 max. S
347 (austenitic)	Fe; 17-19 Cr; 9-13 Ni; Cb + Ta (10 x C conc. min.); 0.08 max. C; 2 max. Mn; 1 max.Si; 0.045 max. P; 0.03 max. S
405 (ferritic)	Fe; 11.5-14.5 Cr; 0.1 to 0.3 Al; 0.08 max. C; 1 max. Mn; 1 max. Si; 0.04 max. P; 0.03 max. S
440C (martensitic)	Fe; 16-18 Cr; 0.95 to 1.20 C; up to 0.75 Mo; 1 max. Mn; 1 max. Si; 0.06 max. P; 0.03 max. S

The coupons were initially 1 in. long, $\frac{5}{16}$ in. wide, and 50 mils thick, and weighed about 2 g each. One side of each coupon was machined to a 32-microinch surface finish.

Results and Discussion

"Before and after" photomicrographs of the steels are shown in Figure 17. Types 304 and 347 stainless steels were severely attacked. The photomicrographs show much grain growth to have occurred

[6] "Working Data" Carpenter Stainless and Heat Resisting Steels, The Carpenter Steel Co., Reading, Pa.

Figure 17

PHOTOMICROGRAPHS OF FOUR TYPES OF STAINLESS STEEL BEFORE AND AFTER EXPOSURE TO ZINC VAPOR

(All coupons were exposed at 900 C to zinc vapor for 500 hr. Apparatus is shown on Figure 16. Weight and dimensional changes of coupons are given in Figure 18.)

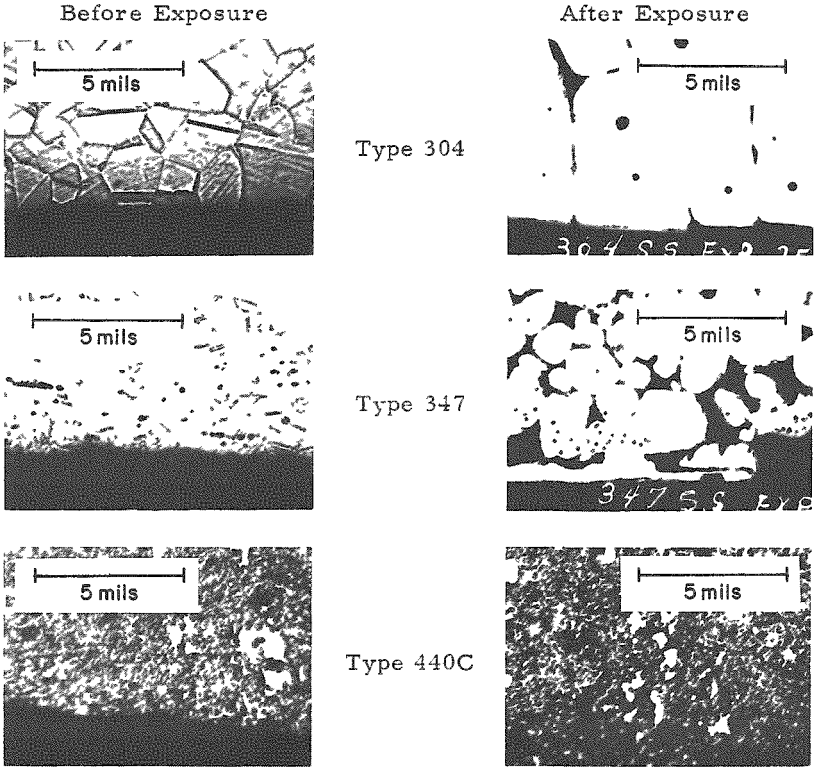

Before Exposure

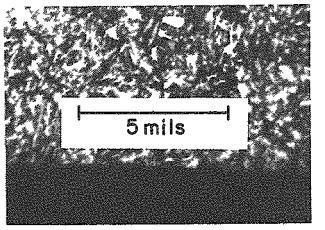

Type 405

After Exposure

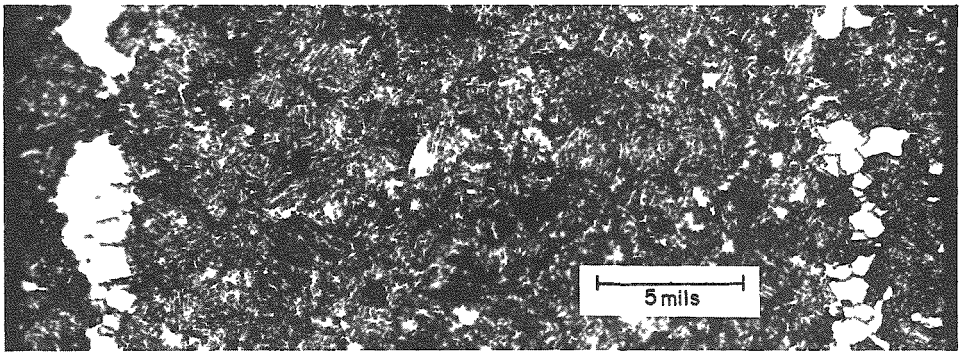

Type 405

in these two steels and show large voids between the grains. The occurrence of these voids is attributed to leaching of nickel, which forms low-melting solutions with zinc.

Type 405 stainless steel was relatively unattacked, but one row of large grains was formed about $3\frac{1}{2}$ mils in from each side of the sample. These are believed to represent partial transformation from an alpha phase (ferritic) to a gamma phase (austenitic structure). Examination of the iron-chromium phase diagram[7] shows this transformation to be reasonable at the exposure temperature of 900 C. Confirmation of the gamma-phase transformation is being sought by means of microhardness and X-ray measurements.

Type 440C stainless steel also appeared to be relatively unaffected by exposure to zinc vapor as determined by metallographic examination. The photomicrographs indicate a surface penetration of about 2 mils; no other effects are discernible.

Figure 18

WEIGHT AND DIMENSIONAL CHANGES OF STAINLESS STEEL COUPONS AFTER EXPOSURE TO ZINC VAPOR AT 900 C

Original coupons were 1 in. long, 5/16 in. wide, 50 mils thick, and weighed about 2 g.

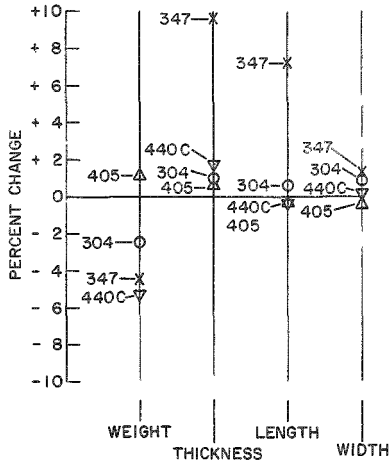

Weight and dimensional changes of the steel coupons are shown in Figure 18. Large changes occurred in the dimensions and weights of Types 304, 347, and the 440C steels. By comparison, the changes in Type 405 were small. Despite these results, which were obtained in long-duration tests at a high temperature, all of the steels could probably be used in experimental apparatus where the exposures to zinc vapor are relatively short. However, the Type 405 stainless steel appears definitely superior to the others in withstanding corrosive attack by zinc vapor. Both of the 400 series steels (Types 405 and 440C) offer better corrosion resistance to zinc vapor than do the 300 series steels, which suffer attack by nickel leaching.

g. Supporting Chemical Investigations
(R. K. Steunenberg)

Liquid metals and molten salts are being used extensively in the development of pyrometallurgical processes for EBR-II fuel.

---

[7] Hansen, M., and Anderko, K., Constitution of Binary Alloys, McGraw-Hill Book Co., Inc., New York, N. Y. (1958).

Fundamental chemical studies of these materials are needed to supply data for process use and to gain a fuller understanding of the principles involved. Work on this program during the quarter has been devoted principally to the reactions of uranium oxides in molten chloride solvents, and to a redetermination of the calcium-zinc phase diagram.

(1) Reactions of Uranium Oxides in Molten Chloride Media
(M. D. Adams, D. A. Wenz)

In previous reactor fuel-processing studies, the effectiveness of uranium oxide reduction by magnesium-zinc alloys was found to depend markedly upon the composition of molten salts used as fluxes (see ANL-6287, p. 51). Magnesium chloride proved to be a particularly beneficial flux constituent. The reactions of uranium oxides in molten chloride media have been investigated further in an effort to interpret these results.

It was reported previously (see ANL-6569, p. 54) that a soluble uranium (V) species, believed to be UO_2^+ ion, is formed upon the addition of the higher uranium oxides to molten chloride salts. The absorption spectrum of this species in the visible and near-infrared regions differs decidedly from the spectra of uranium (III) chloride, uranium (IV) chloride, and uranyl (VI) chloride (see Figure 19). More recent observations have shown that the same uranium (V) spectrum is observed when uranyl (VI) chloride is added to molten chloride solvents at elevated temperatures. This result is attributed to the thermal decomposition of uranyl chloride via the reaction

$$UO_2Cl_2 \text{ (solution)} \rightleftarrows UO_2Cl \text{ (solution)} + \tfrac{1}{2} Cl_2 \quad . \qquad (1)$$

Figure 19

ABSORPTION SPECTRA OF VARIOUS URANIUM SPECIES IN MOLTEN CHLORIDE SOLVENTS

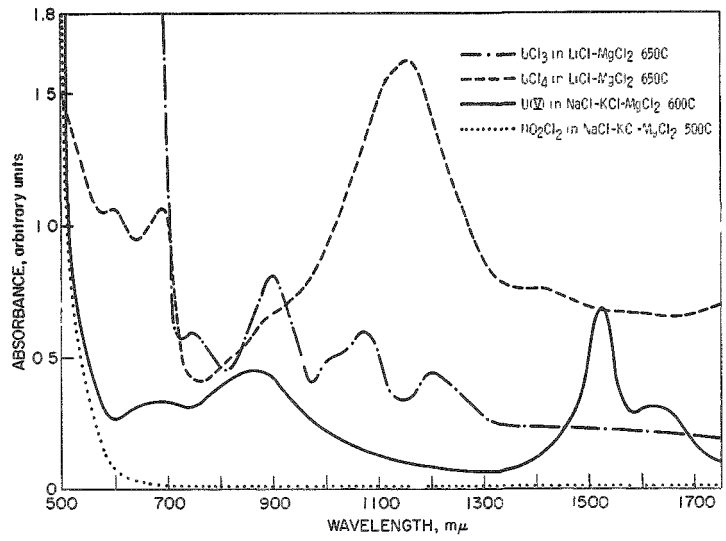

Several experimental results tend to support Reaction 1, which is written as an equilibrium. The behavior of uranyl (VI) chloride at various temperatures in equimolar lithium chloride-potassium chloride and in the sodium chloride-potassium chloride-magnesium chloride eutectic was examined by spectrophotometric methods. The spectra of uranyl (VI) chloride added to both solvents were measured at 500, 600, 700, and 800 C in sealed quartz cells. In both systems the absorbance attributed to uranium (V) increased progressively with increasing temperature. The increases in the absorbances in the ternary eutectic salt, which were somewhat larger than in the binary salt, are presented in Figure 20. At constant temperature the spectra did not change with time. These results are believed to reflect the temperature dependence of Reaction 1.

Figure 20

EFFECT OF TEMPERATURE ON THERMAL DECOMPOSITION OF URANYL CHLORIDE

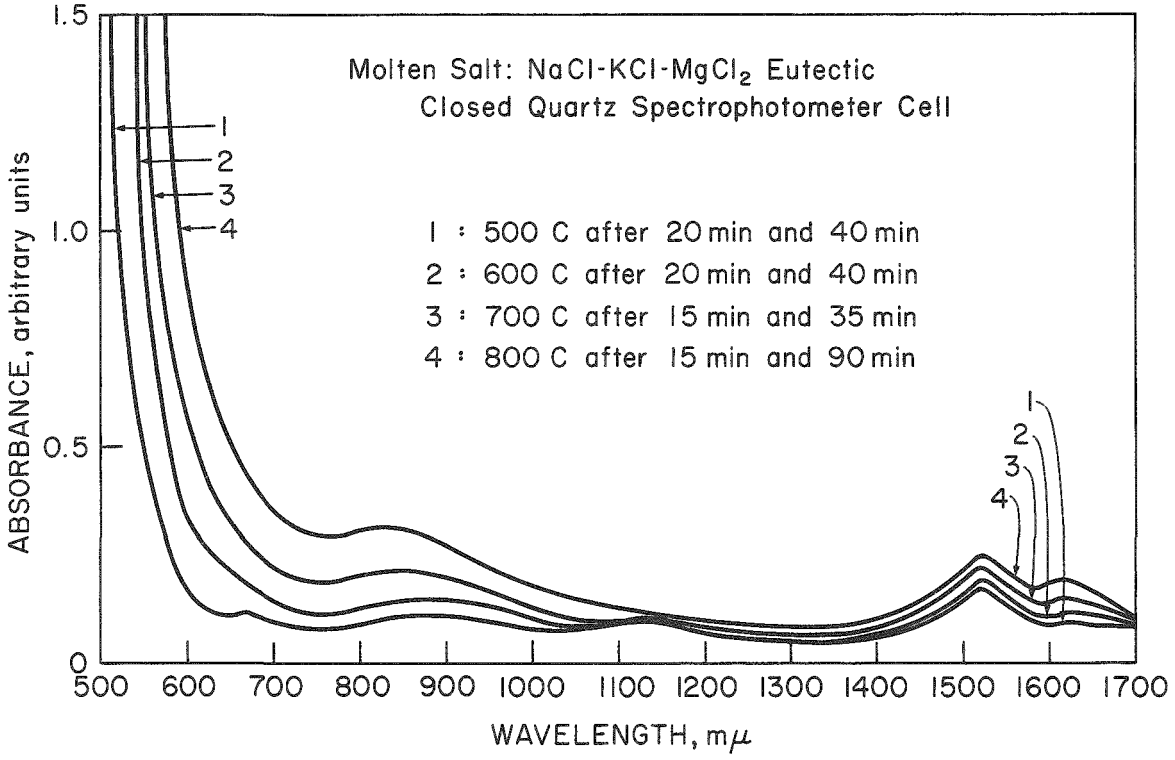

108-5914

A further indication of the reversibility of Reaction 1 was obtained from an exploratory experiment in which the absorbance was measured as the chlorine pressure over the molten chlorides was varied (see Figure 21). When chlorine evolved by the decomposition reaction was first removed by evacuating the cell, a continuous increase in the

absorbance of the uranium (V) spectrum was evident. Conversely, when chlorine at a pressure of 500 mm was later added to the cell, the uranium (V) spectrum almost disappeared. The family of curves presented in Figure 21 shows an isosbestic point* at about 590 mμ, which implies the presence of two absorbing species with a constant total concentration. The two species are probably UO_2^{++} and UO_2^{+} ions.

Figure 21

EFFECT OF CHLORINE REMOVAL ON THERMAL DECOMPOSITION OF URANYL CHLORIDE

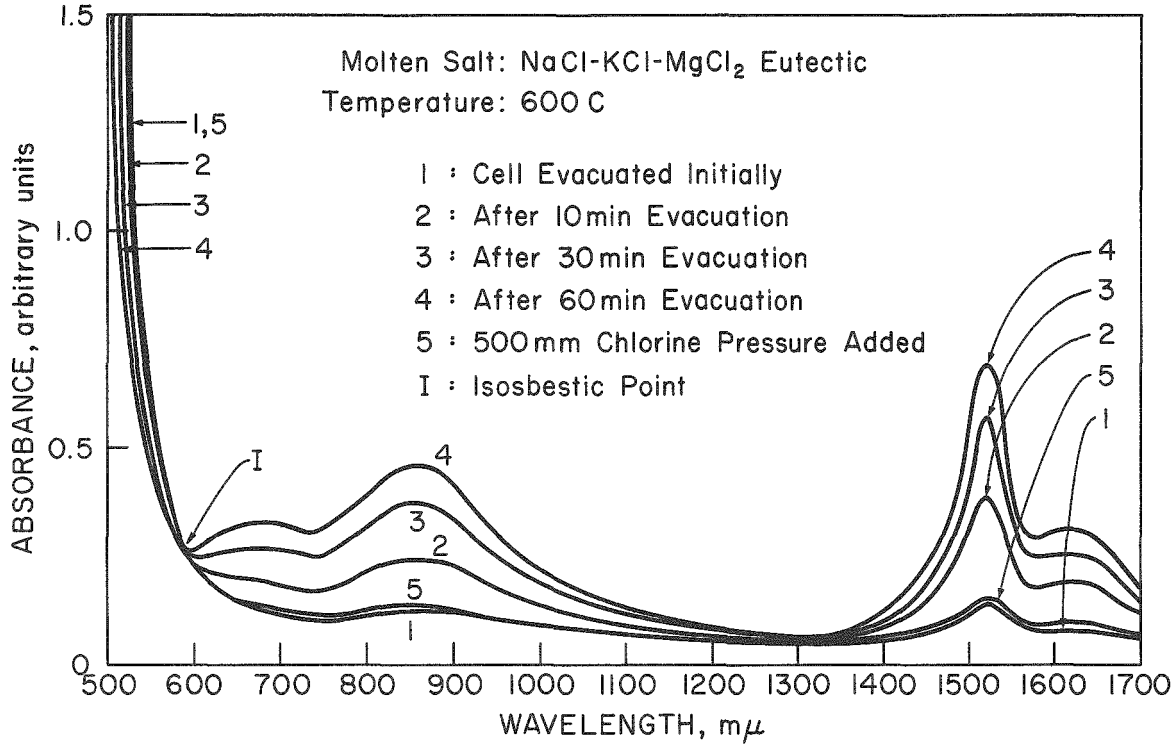

108-5913

Future experimental work on this problem is expected to include molar absorptivity determinations for the uranium (V) spectrum. Provisions are also being made to prove the stoichiometry of Reaction 1 by measuring the amount of chlorine evolution associated with increases in the uranium (V) absorbance. Equilibrium constants will then be determined by varying the chlorine pressure over the salt.

---

*Isosbestic point: It frequently happens that species existing in chemical equilibrium have overlapping optical absorption bands, so that their curves of molar absorptivity vs wave length intersect at a particular wavelength. This point of intersection is called the isosbestic point.

(2) Phase Diagram of the System Calcium-Zinc

(A. F. Messing, M. D. Adams)

Liquid calcium-zinc alloys are being considered as media for the separation of uranium and plutonium from rare earth fission products (see ANL-6596, p. 58). During the course of investigations, the presently accepted phase diagram for the calcium-zinc system[8] was found to be in error. A redetermination of the major features of the diagram was therefore undertaken, by means of differential thermal analysis primarily. Supplemental information was obtained from X-ray diffraction data from the solid phases, and from vapor pressure-composition isotherms determined by effusion techniques.

Previous thermal analysis studies of the calcium-zinc system[9] indicated the occurrence of five compounds: Ca_4Zn, Ca_2Zn_3, $CaZn_4$, $CaZn_{10}$, and possibly CaZn. Further investigations by microscopic methods[10] showed the occurrence of compounds Ca_5Zn_2, Ca_2Zn_3, $CaZn_4$, and $CaZn_{10}$. More recent X-ray and microscopic results have indicated that the compounds in the zinc-rich region of the system are $CaZn_2$ instead of Ca_2Zn_3,[11,12] $CaZn_5$ instead of $CaZn_4$,[11,13] and $CaZn_{13}$ instead of $CaZn_{10}$.[11,12,14] Hansen and Anderko[8] present a composite phase diagram which is based on the data of Donski[9] and Paris,[10] and is supplemented by the more recent work.[11-14]

The zinc and calcium used in the experimental determinations were purified separately by sublimation under reduced pressure and collection on a cold finger. A helium atmosphere was used in all of the operations until the calcium-zinc samples were prepared for chemical analysis after the thermal analysis determinations.

Emission spectrographic analysis of the zinc showed no impurities in concentrations above the limits of detection. Emission spectrographic and chemical analyses showed less than 0.1 w/o total barium and strontium in the purified calcium. No other metallic impurities were present in concentrations greater than 80 ppm. The nitrogen content of the calcium was 24 ppm, and the hydrogen content 200 ppm.

---

[8]Hansen, M., and Anderko, K., Constitution of Binary Alloys, 2nd ed., McGraw-Hill Book Company, Inc., New York (1958), p. 65.

[9]Donski, L., Z. Anorg. Chem. 57, 185 (1908).

[10]Paris, R., Publ. Sci. Tech. Min. Air (France) 45, 41 (1934).

[11]Haucke, W., Z. Anorg. Chem. 244, 17 (1940).

[12]Wieting, J., Naturwissenschaften 48, 401 (1961).

[13]Nowotny, H., Z. Metallk. 34, 247 (1942).

[14]Ketelaar, J. A. A., J. Chem. Phys. 5, 668 (1937).

The differential thermal analysis apparatus was a modified version of a unit designed by Boersma.[15] The samples were contained in small tantalum crucibles, and a helium atmosphere was maintained in the system at a small positive pressure. Aluminum oxide and sodium chloride were used as reference samples. The equipment was calibrated with sodium chloride (m.p. 800.4 C), sodium molybdate (m.p. 687 C) and zinc (m.p. 419.5 C). The precision of the measurements was ± 2 C, and the accuracy was estimated to be within ± 5C.

Each sample of calcium-zinc alloy was prepared by weighing the components into the tantalum crucibles. Both open and sealed crucibles were used, and identical results were obtained. Each sample was cycled through the temperature range of interest at least twice, and at the conclusion of the thermal analysis measurements, certain samples were selected for X-ray diffraction studies.* The redetermined phase diagram of the system is presented in Figure 22.

Figure 22

CALCIUM-ZINC PHASE DIAGRAM

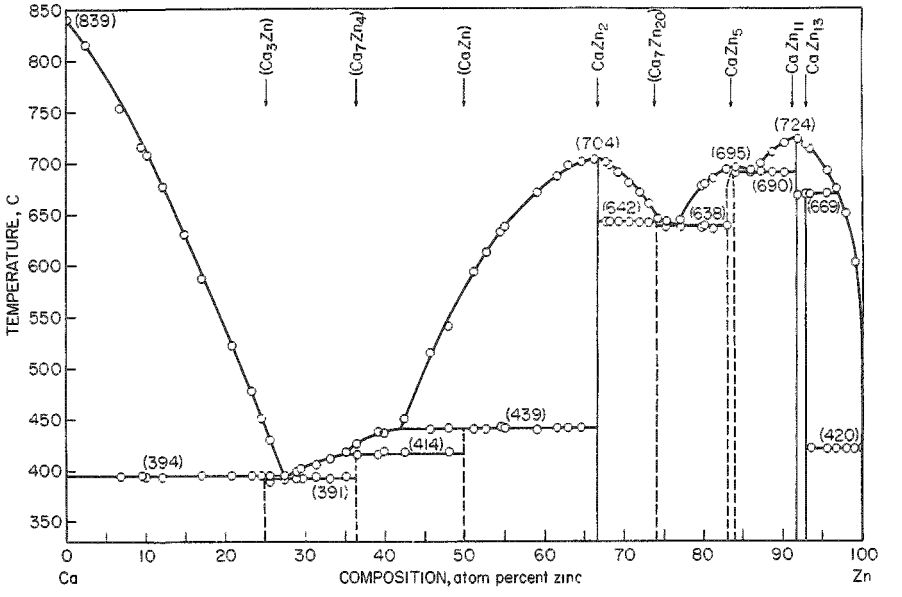

108-5563

In 100 percent calcium and at very low zinc concentrations (<5 a/o), calcium transitions were found in the solid. Increases in the temperatures of these transitions associated with the presence of small amounts of hydrogen in the calcium were consistent with the

---

[15] Boersma, S. L., J. Am. Ceram. Soc. 38, 381 (1955).

*X-ray diffraction data provided by R. V. Schablaske and B. S. Tani.

observations of Peterson and Fattore.[16] At higher zinc concentrations, however, the presence of hydrogen in small concentrations appeared to have no effect on the results.

In the region from zero to 50 a/o zinc, the X-ray patterns of the alloy samples were ill-defined. Furthermore, the vapor pressure of the system in this composition region is too low to obtain reliable effusion measurements. With the thermal analysis and X-ray results available, however, it was possible to distinguish three compounds. At about 25 a/o zinc, evidence was found for a compound melting incongruently at 394 C and having the probable composition Ca_3Zn. A second compound at 35 to 37 a/o zinc and having the probable composition Ca_7Zn_4 melts incongruently at 414 C. The lowest-temperature eutectic in the system, at 27.4 a/o zinc and 391 C, falls between these two compounds. In the region of 49 to 51 a/o zinc, a compound indicated by these as well as earlier studies to be CaZn[9,13] melts incongruently at 439 C.

The composition region from 50 to 100 a/o zinc was at first believed to have been well defined by previous work. The compounds $CaZn_2$, $CaZn_5$, and $CaZn_{13}$ were confirmed by comparing X-ray patterns from powder compacts of these compositions with published information.[11,12,14] However, $CaZn_5$, which melts at 695 C, exists not as a line compound, but over a narrow composition range. Also, $CaZn_{13}$ melts incongruently at 669 C, rather than congruently as previously reported.[8] The melting point of $CaZn_2$ was found to be 704 C instead of 688 C.

Two new compounds were found in the zinc-rich region: One has the composition $CaZn_{11}$ and melts congruently at 724 C; the other has the probable composition Ca_7Zn_{20}. Comparison of the X-ray pattern for $CaZn_{11}$ with those reported in the literature for similar compounds[17] indicates a body-centered tetragonal structure. This is very likely the compound listed as $CaZn_{10}$ by Donski[9] and Paris.[10] The second compound, believed to be Ca_7Zn_{20}, appears at about 74 a/o zinc, and the X-ray data indicate 26 to 28 atoms per unit cell. This compound melts incongruently at 642 C.

The effusion measurements,* which were successful above about 50 atom percent zinc, were in general agreement with the diagram in Figure 22. The compounds $CaZn_2$, $CaZn_5$, $CaZn_{11}$, and $CaZn_{13}$ were confirmed. No break was observed in the vapor pressure-composition isotherms for the compound Ca_7Zn_{20}. This observation does not necessarily disprove the existence of the compound, however, since similar free energies of formation for Ca_7Zn_{20} and $CaZn_5$ could account for this result.

---

[16]Peterson, D. T., and Fattore, V. G., J. Phys. Chem. 65, 2062 (1961).

[17]Sanderson, M. J., and Baenziger, N. C., Acta Cryst. 6, 627 (1953).

*Effusion measurements performed by E. Veleckis.

Two eutectics were found in the zinc-rich portion of the diagram, one between Ca_7Zn_{20} and $CaZn_5$ at 76.4 a/o zinc and 638 C, and the other between $CaZn_5$ and $CaZn_{11}$ at 86.4 a/o zinc and 690 C.

h. Supporting Engineering Studies
(L. Burris, Jr.)

Engineering studies of liquid metal systems are in progress, principally in the areas of distillation, heat transfer, and mass transfer.

(1) Metal-distillation Studies

(a) Performance of Large-scale Cadmium-distillation Unit
(J. F. Lenc, P. A. Nelson, and J. Arntzen)

Operation of the large-scale cadmium-distillation unit (for description see ANL-6379, p. 95) was continued during the past quarter to gain additional operating data and to evaluate the performance of the various components of the unit. This unit has a feed tank capacity of 750 kg of cadmium and is capable of distilling about 100 kg of cadmium per hour.

In a previously reported cadmium-distillation run (see ANL-6569, p. 57, Run 25), considerable entrainment of liquid cadmium (estimated to be about 15 percent) was suspected because of an unexpectedly high apparent rate of distillation. Attempts have subsequently been made to determine the extent of entrainment of liquid cadmium through use of tin, a nonvolatile solute, at a nominal one percent concentration in the cadmium in the distillation crucible (see ANL-6596, p. 79). The extent of entrainment was determined from tin analyses of the distillate.

The extent of entrainment was measured in six runs in which the apparent rate of evaporation was varied from 25 to 90 kg/hr (see Table 14). Only at a distillation rate of 90 kg/hr (Run 32) did entrainment of liquid cadmium in cadmium vapor (5 to 8 percent of the cadmium collected) begin to approach the 15 percent estimated for Run 25 (apparent distillation rate of 102 kg/hr). No consistent pattern of entrainment is evident at lower distillation rates. It is possible that bumping begins to occur as high distillation rates are approached (above about 85 kg of cadmium per hour) and causes the large entrainment values that were observed or estimated in Runs 25 and 32.

It has been observed, as expected, that power efficiencies increase as the distillation rate increases. Also a high entrainment rate, as experienced in Run 32, would be expected to increase the apparent power efficiency. (The apparently high power efficiency in Run 25 is the basis for assuming that considerable entrainment occurred in that

run.) The low power efficiency actually found in Run 32 is, therefore, anomalous and presently not understood.

Table 14

ENTRAINMENT OF CADMIUM IN LARGE-SCALE DISTILLATION UNIT

(The unit was previously described in ANL-6379, p. 95. All distillations were conducted at near 30 mm of pressure and at corresponding temperatures between 553 and 562 C. About 200 kg of cadmium was distilled in each run.)

Run No.	Power (kw) Input	Power (kw) Calcd from Rate of Distillation	Power (kw) Calc Loss	Apparent Rate of Distillation (kg/hr)	Apparent Power Efficiency (%)	Liquid Entrainment (% of Cd Collected)[a]
25	35	26.8	8.2	102	77	-[b]
26	20	9.6	10.4	36.7	48	2.5
27	22.5	11.1	11.4	42.8	50	1.5
28	18	6.7	11.3	25.4	37	0.1-0.8
30	30	18.2	11.8	69.5	61	0.4
31	35	22.7	12.3	86.5	65	0.8
32	40	23.7	16.3	90.0	59	5.0-8.0

[a]Tin was present as a monitor at a nominal one percent concentration in the cadmium in the distillation crucible. The extent of entrainment was determined by analysis of the distillate for tin.

[b]No tin was present in this run. The extent of entrainment was estimated to be about 15 percent from a comparison of the power efficiency with that of other similar runs.

Although not significant from a power efficiency standpoint, the entrainments observed in Runs 26 through 31 would be excessive if the objective of the distillation were either the recovery of a nonvolatile solvent or purification of the material being distilled. Therefore, design and testing of one or more deentrainment devices in the large-scale cadmium-distillation unit is planned.

(b) Study of Mechanisms of Liquid Metal Boiling and Entrainment

(J. Wolkoff, L. F. Dorsey)

The boiling and entrainment phenomena in aqueous systems have been studied extensively and continue to provide fertile areas for fundamental investigations. Comparable studies with liquid metals are relatively scarce even though liquid metal systems have become technically important in recent years as heat transfer agents and as solvents for

pyrometallurgical processes. The nature and magnitude of the boiling and entrainment phenomena in liquid metal systems may differ significantly from those in aqueous systems as the physical properties (e.g., thermal conductivity and surface tension) known to affect these phenomena differ for the two types of systems.

Vaporization from a vapor-liquid interface without formation of vapor bubbles (here called nonturbulent vaporization) is being studied with mercury in glass equipment. Vapor formed under these conditions should be free of entrained droplets of liquid which are encountered in normal boiling (where vapor bubbles form below the surface, rise, and break through the liquid surface, creating liquid droplets). Although nonturbulent vaporization can take place at low heat fluxes with most liquids, it should be possible to achieve high rates of nonturbulent vaporization at correspondingly high heat fluxes with many liquid metals. This possibility arises from the good thermal conductivity of metals and from the relatively high density of many metals. A high density causes the boiling temperature to increase rapidly with increased distance from the liquid metal surface. In addition, other factors, such as surface tension and bubble nucleation tendencies, are also important.

Additional studies have been made with the glass boiling loop (see Figure 23). In these and previous studies, the mercury pools of two contrasting geometries were heated by resistance or induction

Figure 23

SHALLOW-POOL MERCURY BOILING LOOP

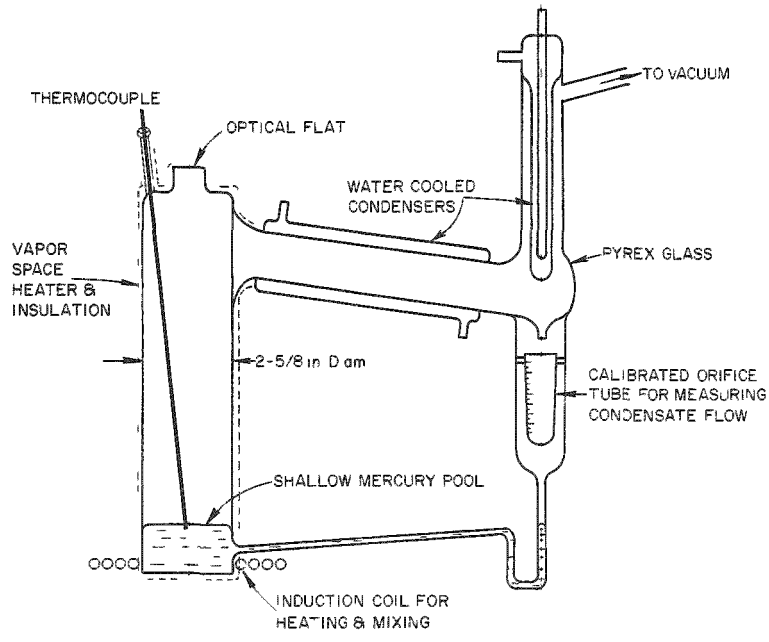

heating. The runs consisted of vaporizing, condensing, and returning the mercury to the pool by gravity in a closed-loop system. The recirculation rate was measured by means of a calibrated tube with a small orifice through which the condensate passed.

The first mercury pool used was relatively shallow ($1\frac{7}{8}$ in. deep and $2\frac{5}{8}$ in. in diameter). The maximum nonturbulent vaporization rate achieved by resistance heaters before onset of bumping was 55,000 Btu/(hr)(sq ft), as was previously reported in ANL-6569, p. 59. This rate is equivalent to the vaporization of 2.1 lb-moles of mercury per hour per sq ft. This shallow-pool geometry is not conducive to heat transfer to the surface by natural convection.

With a geometry more conducive to natural convection (a 1-in.-diameter by $8\frac{1}{2}$-in.-deep pool heated by cylindrical resistance heaters), nonturbulent vaporization rates of about 110,000 Btu/(hr)(sq ft) were achieved (see ANL-6596, p. 80).

In recent runs it was found that the rate of nonturbulent vaporization from a shallow pool could be increased considerably by stirring the mercury during vaporization to increase the rate of heat transfer to the mercury surface. A flat, four-turn induction coil of 3-in. inner diameter (see Figure 23) operating at a frequency of 10 kc provided both the heat and the mixing power to a $1\frac{1}{8}$-in.-deep pool of mercury. The system pressure was low (1 to 10 mm Hg), and the temperature of the mercury just beneath the boiling surface was 177 C. Under these conditions, nonturbulent vaporization rates as high as 103,000 Btu/(hr)(sq ft) were attainable.

When the boiling rate was further increased, some vapor bubbles began to form within the pool. The liquid droplets which formed as the vapor bubbles emerged were visible. However, even at vaporization rates as great as 167,000 Btu/(hr)(sq ft), the rate of droplet formation was low and most of the mercury vaporized nonturbulently. The changeover from nonturbulent boiling to turbulent boiling under these conditions was gradual.

Other methods of improving the heat flow within the liquid metal pool will be studied. Methods are also being devised for measuring the degree of entrainment occurring in the two boiling regimes (nonturbulent boiling and turbulent boiling).

(2) Mass Transfer in Agitated Metal Systems

(R. D. Pierce and S. A. Miller*)

The influence of agitation on the rate of solution of small metal cylinders in a liquid metal solvent is being investigated. In

*Consultant and summer professor from Rochester University.

the current experiments, small uranium cylinders are being dissolved at 500 C in cadmium contained at a depth of 5 in. in a 5-in.-ID flat-bottom cylindrical Type 304 stainless steel tank equipped with four vertical 0.5-in.-wall baffles which extend to 0.5 in. above the tank bottom. The agitator (Type 304 stainless steel) is a two-blade, 45-degree-pitched paddle rotated to deflect downward and located coaxially within the tank; its lower edge is 1.25 in. above the tank bottom. The paddle is 2.5 in. long (tip to tip) and 0.625 in. wide (measured in the plane of the blade). The uranium right cylinders (which were of two sizes, 7 mm in diameter and 7 mm long, and 4 mm in diameter and 4 mm long) were cut from cast uranium rods so that crystal orientation would be random and were wetted with zinc prior to use to insure an oxide-free surface for dissolution.

In each experiment, the agitator speed was first adjusted to the desired value, and then the uranium cylinders were quickly added to the solute-free cadmium and a timer simultaneously started. Samples of the solution were withdrawn through graphite filters into Pyrex sample tubes at appropriate time intervals and subsequently were analyzed for uranium concentration. From the resulting data, solution rate coefficients were calculated for each desired time interval.

After an equal-scale simulation model of glass cylinders in water was observed and appropriate density corrections were made, it was concluded that at stirring speeds below about 450 rpm the 7-mm uranium cylinders would not be suspended in cadmium but that suspension would be complete above about 1100 rpm. The corresponding values for 4-mm cylinders are 390 rpm and 1100 rpm.

Solution rate coefficients obtained to date are presented in Figure 24, in which the integrated mean solution rate coefficient k_m, expressed as gram-atoms solute/(min)(sq cm of interfacial area)(g solute/g solvent), is plotted against the agitator speed. It is hoped that ultimately the data can be correlated by dimensionless groups to provide greater utility for scale-up or for application to other systems.

The data in Figure 24 show two regimes of solution rates for the 7-mm cylinders. In one regime of slow solution rates at stirring rates of 400 rpm and below, the cylinders are not suspended but may be in motion on the bottom of the tank. In the other regime of appreciably faster solution rates at stirring rates above about 500 rpm, suspension of cylinders begins, with the degree of suspension increasing with stirring speed. Presumably, there is a transition region between these regimes. In both regimes, the rate of solution increases with stirrer speed.

Most of the runs were made with charges of seventy 7-mm by 7-mm cylinders, but a few runs were made with different numbers of cylinders in order to investigate the effect of particle population. Little

effect of particle population was found in runs made with 35, 114, and 100 cylinders. The solution rates for the 4-mm cylinders (388 cylinders per run) were slightly higher than those for the 7-mm cylinders.

Figure 24

SOLUTION RATE COEFFICIENTS AT 500 C FOR SMALL URANIUM CYLINDERS IN AGITATED CADMIUM

5-in. ID, Cylindrical Baffled Tank
5-in. Liquid Level
$2\frac{1}{2}$-in.-long, 45°-pitched Paddle,
$\frac{5}{8}$-in. Face, Deflecting Downward

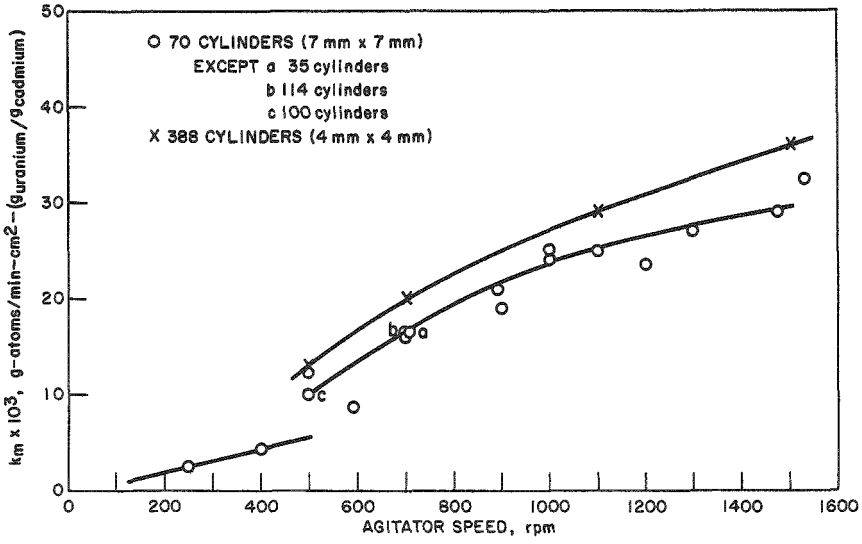

A few more runs are planned with the 4-mm and 7-mm cylinders. Then the program will be concluded by making a few runs with 9-mm cylinders.

4. Reactor Materials
(R. K. Steunenberg)

Pyrometallurgical procedures offer considerable promise as simple, economical methods for producing materials suitable as nuclear fuel. One method of synthesizing refractory compounds of interest as high-performance reactor fuels is by adding carbon, silicon, or other elements to liquid metal solutions of the actinide metals. The product precipitates from solution and is recovered by suitable phase-separation and retorting techniques. Other methods for the preparation of refractory compounds, such as carbides and sulfides, are also being investigated. An effective procedure for the preparation of metallic fuel materials is the direct reduction of actinide oxides, chlorides, or fluorides from a molten halide flux by liquid metal solutions containing magnesium.

The work during the past quarter has been concentrated mainly on the preparation of uranium sulfide, the construction of a high-integrity drybox to be used for the preparation of uranium carbide and plutonium carbide, the production of thorium metal directly from the oxide, and the direct reduction of uranium ore concentrates to the metal.

a. Preparation of Uranium and Plutonium Sulfides
(S. Vogler, J. A. Trischan)

Among the refractory compounds of uranium and plutonium which show promise as high-performance reactor fuels, the oxides and carbides have been investigated the most extensively. Sulfides also appear to fulfill the necessary requirements,[18] and they are receiving increasing attention as candidate materials. The thermodynamic properties of uranium monosulfide have been determined recently by the effusion technique.[19] Preparative methods and metallurgical properties[20] and the thermoelectric characteristics[21] (see also ANL-6569, p. 158) of uranium monosulfide have also been investigated. In view of the importance of these materials as potential reactor fuels, preparative methods for uranium monosulfide are being examined. A subsequent objective will be to extend the techniques to the synthesis of plutonium monosulfide.

Uranium monosulfide can be prepared by the direct combination of powdered uranium and sulfur, but the reaction is strongly exothermic and can become violent.[21] The preparative method used by Eastman and coworkers,[22] chosen for our initial work because it is simple and has been amply demonstrated, consists of three steps: (1) bulk uranium is hydrided and dehydrided several times to produce a finely divided, reactive uranium metal powder, (2) the uranium powder is heated with the stoichiometric quantity of hydrogen sulfide required to form uranium monosulfide, and (3) the reaction mass, consisting of unreacted uranium metal and higher uranium sulfides, is ground, sieved, and heated in vacuum to about 2000 C to form homogeneous uranium monosulfide.

---

[18] Loch, L. O., Engle, G. B., Snyder, M. J., and Duckworth, W. H., Survey of Refractory Uranium Compounds, BMI-1124 (1956).

[19] Cater, E. D., The Vaporization, Thermodynamics and Phase Behavior of Uranium Monosulfide, ANL-6140 (1960).

[20] Shalek, P. D., Fabrication and Properties of US and ThS Bodies, Trans. Am. Nucl. Soc. 5 (1), 244 (1962).

[21] Blankenship, W. P., Preparation and Preliminary Thermoelectric Evaluation of Uranium Chalcogenides, WCAP-1866 (Oct 1961).

[22] Eastman, E. D., Brewer, L., Bromley, L. A., Gilles, P. W., and Lofgren, N. A., J. Am. Chem. Soc. 72, 4019 (1950).

The necessary equipment for carrying out these steps has been constructed in such a way that the equipment can later be used for the preparation of plutonium sulfides with minimum modification. A few preliminary preparations of uranium monosulfide have been performed in order to test the apparatus and techniques.

b. Reduction of Thorium Dioxide
(A. V. Hariharan,* J. B. Knighton, J. W. Walsh)

Attempts are being made to develop a practical method for the direct reduction of thorium dioxide to the metal by means of the liquid metal-flux technique. The thorium dioxide, suspended in a molten halide flux of the proper composition, is reduced by a liquid magnesium-zinc alloy. Results have been reported previously (see ANL-6477, p. 40; ANL-6569, p. 66; ANL-6596, p. 91) on the effects of flux composition, temperature, and mixing rate of the flux and metal phases on the reduction reaction. In the laboratory-scale equipment used for these experiments, a reaction time of about 4 hr was necessary to achieve complete reduction of the oxide at a temperature of 800 C and a mixing rate of 800 rpm. In these experiments, the final thorium concentration in the metal phase upon complete reduction was 1.0 w/o, and the flux was composed of 75 m/o calcium chloride, 15 m/o magnesium chloride, and 10 m/o calcium fluoride.

During the past quarter the effects of the following variables on the reduction reaction have been investigated: (1) agitation of the flux-metal system, (2) calcination of the thorium dioxide, (3) the final thorium concentration in the metal phase, (4) magnesium concentration in the metal phase, and (5) the quantity of flux used. The solubility of thorium metal in zinc-magnesium solutions was also determined in the composition range of interest.

Agitation

Results presented in the previous quarterly report (ANL-6596, p. 91) showed that efficient mixing is required in order to achieve satisfactory reduction rates. The earlier data at 200, 400, 600, and 800 rpm have been extended to include a reduction rate curve at 1000 rpm (see Figure 25). It is clear that the time required for complete reduction is decreased considerably by increasing the mixing rate to at least 1000 rpm in the laboratory-scale equipment used for the experiments. Although these data are unlikely to be directly applicable in scaling up the process, they indicate that efficient mixing will be a primary consideration in equipment on a larger scale.

---

*Affiliate, International Institute of Nuclear Science and Engineering.

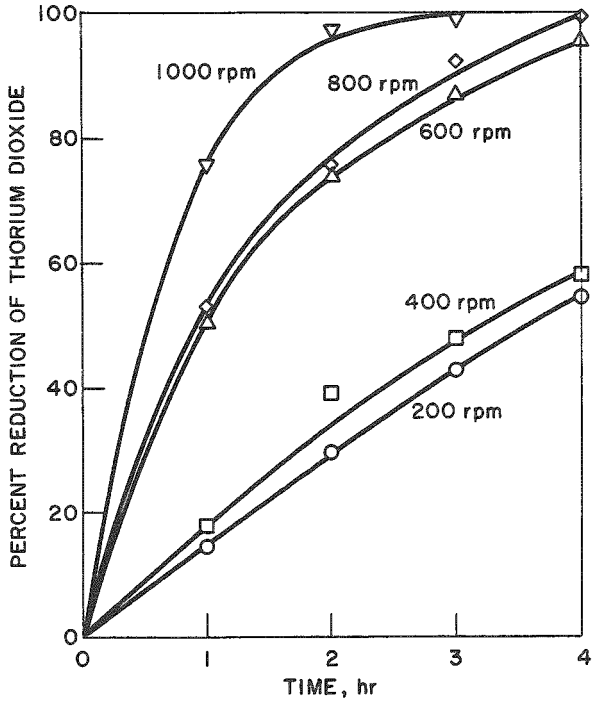

Figure 25
EFFECT OF MIXING RATE ON THE REDUCTION OF THORIUM DIOXIDE

Conditions

Zinc	570 g	600 g alloy
Magnesium	30 g	
Flux:	300 g (75 m/o $CaCl_2$-15 m/o $MgCl_2$-10 m/o CaF_2)	
ThO_2:	6.83 g (to give a 1 w/o alloy on complete reduction)	
Temp:	750 C	
Crucible:	tantalum	
Agitator:	tantalum paddle 1 1/2 in. wide x 3/4 in. high x 50 mils thick; located 1/8 to 9/16 in. from bottom of crucible.	
Atmosphere:	argon	

Calcination of Thorium Dioxide

It is likely that either calcined or uncalcined thorium dioxide could be used as a feed material for this process. The calcined material is obtained by heating thorium oxalate to 1000 C; the uncalcined material is prepared by heating the oxalate to 350 C. It was considered possible that some sintering occurs at 1000 C, with a resulting decrease in the surface area available for reaction. Reduction rates for the two types of thorium dioxide were measured under the following conditions:

Zinc:	570 g	Temp:	800 C
Magnesium:	30 g	Mixing Rate:	800 rpm
Flux:	300 g (75 m/o $CaCl_2$-15 m/o $MgCl_2$-10 m/o CaF_2)	Apparatus:	tantalum
		Atmosphere:	argon
ThO_2:	6.83 g (calcined and uncalcined)		

Although the uncalcined thorium dioxide appeared to react somewhat faster in the initial stages of the reduction, a 4-hr period was required for 100 percent reduction of both types of thorium dioxide.

Final Thorium Concentration in the Metal Phase

In all of the previous experiments, the quantity of thorium dioxide added to the system was adjusted to yield a thorium metal

concentration of 1.0 w/o in the metal phase on complete reduction. Additional experiments have now been performed in which the final thorium concentrations in the metal phase were increased to about 3, 5, 7, and 9 w/o. These experiments utilized 600 g of zinc-5 w/o magnesium, plus the additional amount of magnesium required to reduce each loading of thorium dioxide. The temperature was 800 C and the mixing rate was 800 rpm. After a 4-hr reaction period, the entire flux phase was analyzed for thorium dioxide to determine the extent of reduction.

One consequence of the higher thorium loadings in the system was that higher concentrations of magnesium chloride were needed in the flux to achieve complete reduction of the thorium dioxide. The interrelationship of the thorium loading and the flux composition is shown in Figure 26.

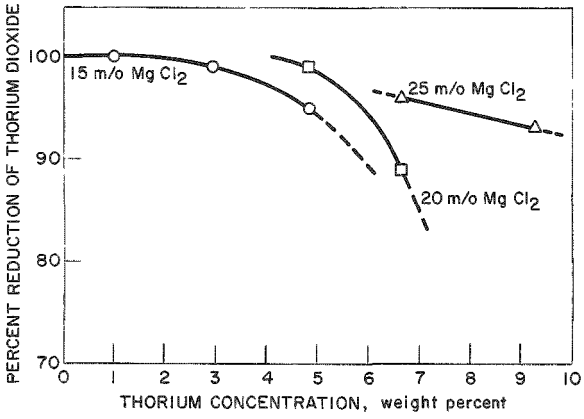

Figure 26

EFFECT OF FLUX COMPOSITION AND THORIUM CONCENTRATION ON THORIUM DIOXIDE REDUCTION

Conditions

Zinc-50 w/o magnesium (at end of reduction): 600 g
Flux: 300 g ($CaCl_2$-$MgCl_2$-10 m/o CaF_2)
Temp: 800 C
Mixing rate: 800 rpm
Time: 4 hr.
Atmosphere: argon

The effect of the magnesium chloride concentration in the flux on the reduction of thorium dioxide to produce 9.1 w/o thorium in zinc-10 w/o magnesium was investigated. The results of varying the magnesium chloride concentration in a calcium chloride-magnesium chloride-5.0 m/o calcium fluoride flux are shown below:

Magnesium Chloride in Flux, m/o	Percent Reduction of Thorium Dioxide
30.0	94
35.0	96
47.5	99

In these experiments the reaction mixture was raised to a temperature of 850 C after a 4-hr reduction period at 800 C and the mixture was poured into a mold. By using the zinc-10 w/o magnesium alloy and pouring at 850 C, pouring yields as high as 95 percent were possible. In a batch-type process, the 5 percent heel remaining in the crucible would become

a part of the charge for the following batch. To achieve final thorium concentrations in the region of 9 w/o, magnesium chloride concentrations of about 47.5 to 50 m/o are needed in the flux.

Magnesium Concentration in the Metal Phase

The effect of magnesium concentration in the metal phase on the reduction of thorium dioxide is illustrated in Figure 27. A distinct maximum in the curve shows that the optimum magnesium concentration lies in the range of 5 to 10 w/o for the two systems used. The marked decrease in the extent of thorium dioxide reduction above 10 w/o magnesium is attributed to the increasing activity of thorium in the liquid metal solvent.

Figure 27

EFFECT OF MAGNESIUM CONCENTRATION IN METAL ON THE EXTENT OF REDUCTION OF THORIUM DIOXIDE

Conditions

Zinc, Magnesium } 600 g at end of reduction (concentration varied)

Flux: 300 g (composition as given in key)

ThO_2: 68.27 g (to give a 10 w/o alloy on 100% reduction)

Crucible: Tantalum (baffled)

Stirrer: Tantalum

Atmosphere: Argon

Reduction at 800 C for 4 hr, with liquid metal-flux phases mixed at 800 rpm; equilibrated at 850 C before pouring

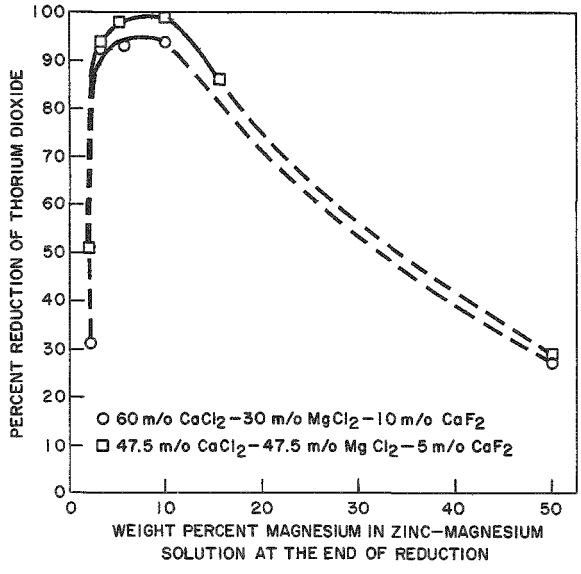

Quantity of Flux

Figure 28 shows the effect of variations in the quantity of flux on the percent reduction of thorium dioxide and pouring yields. In these experiments 600 g of zinc-10 w/o magnesium plus the amount of magnesium required to reduce the 68.3-g charge of thorium dioxide was used with a flux consisting of 47.5 m/o calcium chloride, 47.5 m/o magnesium chloride, and 5.0 m/o calcium fluoride. The extent of reduction after 4 hr decreased only slightly as the amount of flux was decreased. Beyond the range covered in these experiments, however, it is suspected that there might be a critical amount of flux below which the reduction drops off sharply. Also shown on Figure 28 is the percentage of the final thorium-magnesium-zinc alloy that was recovered by pouring. In general, better pours of the metal product were obtained when smaller quantities of flux were used.

Figure 28

EFFECT OF THE AMOUNT OF FLUX ON THE EXTENT OF REDUCTION OF THORIUM DIOXIDE AND ON POURING YIELDS

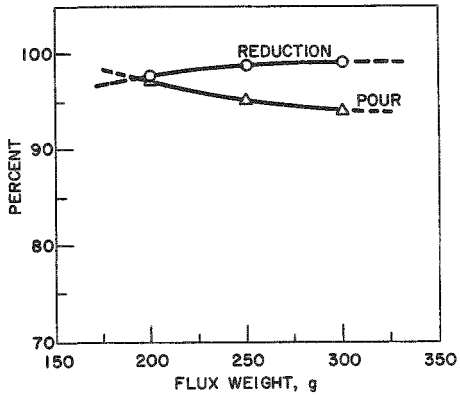

Conditions

Zinc-10 w/o magnesium (at end of reduction): 600 g

Flux: 47.5 m/o $CaCl_2$-47.5 m/o $MgCl_2$-5 m/o CaF_2

ThO_2: 68.3 g (to give 10 w/o alloy on complete reduction)

Temp: 800 C

Mixing rate: 800 rpm

Time: 4 hr

Atmosphere: argon

Mixture heated to 850 C and poured.

Solubility of Thorium in Zinc-Magnesium Solutions

In the study of thorium loadings that can be accommodated in zinc-magnesium solution, the solubility of thorium is of interest. For the solubility determinations, thorium metal sponge was dissolved in the zinc-magnesium solution. Samples were taken after equilibrating the solution at 850, 800, and 750 C for 30 to 45 min; then the composition of the solution was changed by the addition of zinc. The liquid metal samples were withdrawn into tantalum tubes equipped with filters. After cooling, the solidified samples were dissolved and analyzed for thorium and magnesium.

The solubility data are presented in Figure 29, in which thorium solubility at 750, 800, and 850 C is plotted against magnesium concentration. The results show that thorium solubility increases by a

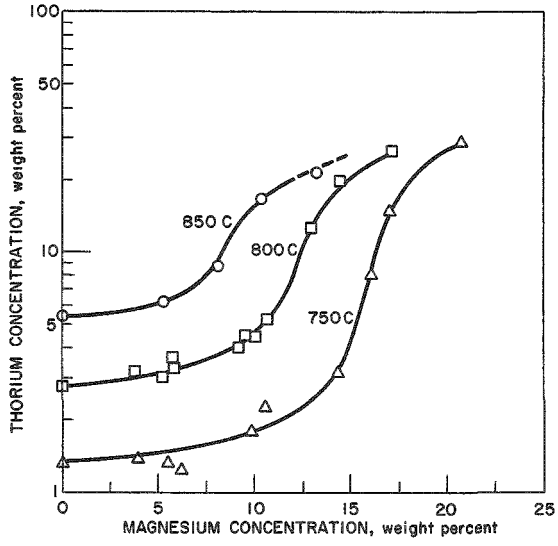

Figure 29

SOLUBILITY OF THORIUM IN ZINC-MAGNESIUM SOLUTIONS

factor of about two with a temperature increase of about 50 degrees in the range from 750 to 850 C, and that it increases markedly with magnesium concentration in the region of 5 to 15 w/o.

The data obtained thus far on the reduction of thorium dioxide indicate that suitable conditions for the laboratory-scale equipment used in the studies are as follows:

Reduction Temperature:	800 C
Mixing Rate:	800 rpm
Atmosphere:	argon
Final Magnesium Concentration in Metal Phase:	10 w/o
Flux Composition:	47.5 to 50 m/o $MgCl_2$; 5 to 10 m/o CaF_2; balance, $CaCl_2$
Reduction Time:	4 hr
Pouring Temperature:	850 C

Future work is expected to consist mainly of a few laboratory-scale demonstration experiments to evaluate the yields and the purity of the thorium metal product.

c. Direct Reduction of Uranium Ore Concentrates (R. B. Subramanyam,* J. B. Knighton)

The reduction of uranium oxides to the metal by zinc-magnesium alloy in the presence of molten halide flux constitutes one of the steps used in the recovery process for melt refining skulls. The successful demonstration of the method in skull processing has led to its consideration for the direct production of uranium metal from ore concentrates, thereby bypassing a number of chemical conversion steps. A process of this type, in addition to reducing the uranium oxides efficiently, must be capable of removing the gangue elements to the extent required for a product of satisfactory purity.

Two preliminary experiments were performed in which a typical uranium ore concentrate was reduced in an alumina crucible by zinc-5 w/o magnesium in an air atmosphere at 750 C. The flux consisted of 47.5 m/o magnesium chloride, 47.5 m/o calcium chloride, and 5.0 m/o magnesium fluoride. The results were generally encouraging, but they showed that silicon, which is present in the ore concentrate to the extent of about 1.1 w/o, is coreduced with the uranium. Several exploratory

*Affiliate, International Institute of Nuclear Science and Engineering.

experiments have therefore been performed in an effort to arrive at a simple, economical pretreatment step for the removal of silica from the ore concentrate. All of the experiments involved the addition of fluorinating agents to volatilize the silicon as the tetrafluoride.

Fusion with Sodium Carbonate and Calcium or Magnesium Fluoride

One of the methods evaluated for removing silicon from uranium ore concentrate prior to reduction involved the use of sodium carbonate (m.p. 850 C) as a flux, and either calcium fluoride or magnesium fluoride as a source of fluorine. In experiments in which beach sand was used in place of ore concentrate, fusions were conducted at 900 C for periods of 0.5, 1.0, 1.5, 2.0, and 3.0 hr, with 100 percent excess sodium carbonate and 100 percent excess calcium fluoride. After the treatment, the solid mixture was leached with a boiling nitric acid-hydrochloric acid solution to dissolve constituents other than any silica which might remain. In all instances, complete removal of the silica was achieved, both with the calcium fluoride mixture and with the magnesium fluoride mixture.

Uranium Tetrafluoride Treatment

A second method of silica removal involves roasting the ore concentrate at 900 C with uranium tetrafluoride. Again, beach sand was used to simplify the experiments. The experimental results, shown in Table 15, indicate that 100 percent silica removal is effected by roasting the material with 100 percent excess uranium tetrafluoride for 3 hr.

Table 15

REACTION OF URANIUM TETRAFLUORIDE WITH SILICA

Silicon Dioxide:	1 g beach sand
Atmosphere:	air
Crucible:	platinum
Uranium Tetrafluoride:	10.4 g (100% excess)
Temperature:	900 C

Time (hr)	Percent Silica Removed
1	94.4
2	98.1
3	100.0
4	100.0

Ammonium Bifluoride Treatment

Ammonium bifluoride also appears to be a convenient source of fluorine for the removal of silica from ore concentrates. The ammonium bifluoride and ore concentrate are simply heated together, volatilizing silicon tetrafluoride and the excess ammonium bifluoride. In preliminary experiments with 50 percent excess ammonium bifluoride (based on the amount of silica present), 77 percent of the silica present was removed from beach sand, compared with 71 percent removal for the ore concentrate. The temperature of the mixture was raised from 25 C to 500 C over a 2-hr period; then it was maintained at 500 C for one hour. In similar experiments with 100 percent excess ammonium bifluoride, the silica removals were 78 percent for beach sand and 74 percent for the ore concentrate.

Experiments were conducted at various temperatures with beach sand to determine the conditions of maximum silica removal, using 100 percent excess ammonium bifluoride. The results, presented in Figure 30, indicate that nearly complete volatilization of the silica is effected in 3 hr at a temperature of about 140 C.

Figure 30

REMOVAL OF SILICON DIOXIDE BY AMMONIUM BIFLUORIDE FUSION

Conditions

Temperature:	as indicated
Atmosphere:	air
Crucible:	platinum
Silicon Dioxide:	1 g beach sand
Ammonium Bifluoride:	3.8 g (100% excess)
Time:	as indicated

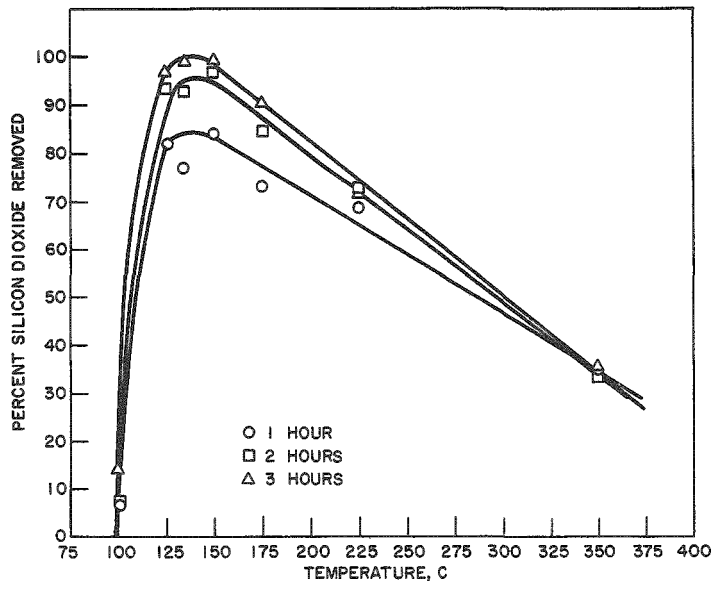

All of the fluoride treatments were effective in converting beach sand to volatile silicon tetrafluoride. The ammonium bifluoride treatment, however, appears to be the most convenient and effective method for the removal of silicon from the ore concentrate.

Attention is presently being directed to techniques for the separation of certain other gangue elements, such as vanadium and molybdenum, which would be expected to accompany the uranium product through the oxide-reduction procedure.

B. Fuel-processing Facilities for EBR-II

(J. H. Schraidt, M. Levenson, L. F. Coleman)

A direct-cycle fuel-reprocessing plant based on pyrometallurgical procedures was designed and is being constructed as part of the Experimental Breeder Reactor No. II (EBR-II) Project. Melt refining, liquid metal extraction, and processes involving fractional crystallization from liquid metal systems are being examined for the recovery and purification of EBR-II fuels. Based on these studies, process equipment is being designed and tested.

1. Status of Fuel Cycle Facility

a. Building and Building Services

(E. J. Petkus, M. A. Slawecki, H. L. Stethers)

(1) Construction

Work on the installation of equipment and correction of fabrication and construction deficiencies, which is being done by the J. F. Pritchard Company under a cost-plus-fixed-fee contract (see ANL-6543, p. 77), is nearing completion.

A shielding plug supplied by the original construction contractor, Diversified Builders, to seal the 7-ft-square hatch in the roof of the Argon Cell has been welded into place. Leaks have been found in the plug. Corrective measures to eliminate these leaks are being investigated. A new plug may be required if these leaks cannot be satisfactorily repaired.

(2) Radiographing of Air Cell and Argon Cell Shielding

An initial radiographing* of the Air Cell and Argon Cell shielding has been completed. Several deficiencies in the shielding have been found. Radiation leakage of a substantial nature was detected in two places, one below the Air Cell sample transfer port, and the other

*More than 700 readings were taken to check the 11,000 sq ft of shielding.

above the large shielding door leading to the Air Cell. Radiation leakage of a less serious nature was found below one of the shielding windows in the Argon Cell. A detailed analysis of the radiographic data is being made to evaluate the integrity and adequacy of the process cell shielding and to ascertain the need for additional radiographing. Diversified Builders, Inc., the original construction contractor, has been advised of these shielding deficiencies and has been requested to propose suitable corrective measures.

(3) Emergency Electrical Power

Electrical power for the Fuel Cycle Facility process and service equipment is provided by three electrical feeder lines from the EBR-II-site power plant. One feeder line supplies power to a 480-v distribution panel and to a 600-amp distribution system (busway) that encircles the Air Cell and Argon Cell on the service floor. Power for most of the process equipment located in the cells is supplied from this source. The other two feeders supply power to two sections of a motor control center.* One feeder supplies the normal section and one the emergency section of the motor-control center. The equipment operated from the emergency section, such as instrument power, suspect exhaust fans, and radiation-monitoring equipment, is of a critical nature. To provide for continuous operation of critical equipment in case of an electrical power failure, a diesel generator and required switch-gear have been installed on the service floor of the Fuel Cycle Facility (see ANL-6477, p. 76; ANL-6543, p. 78). The diesel generator starts automatically when a power interruption occurs. The generator is connected to the Fuel Cycle Facility emergency system by means of an automatic transfer switch which is activated as soon as the generator output voltage is sufficient to service the feeder. From interruption of power to transfer of load to the diesel generator requires 11 sec. This period can be shortened by reducing the time delays in the automatic transfer switch. The diesel generator goes from standstill to full speed in less than 5 sec.

b. Argon Cell and Air Cell Cranes
(J. Graae, W. Voss, R. Vree)

One 5-ton crane has been installed in the Air Cell and two cranes have been installed in the Argon Cell. The design of the Air Cell crane bridge differs from the design of the Argon Cell crane bridges in that the movement of the bridge in the Air Cell is rectilinear, whereas the movement of each bridge in the Argon Cell is radial about a center pivot. The trolleys for these cranes are, however, identical in design and are interchangeable.

---

*A motor control center is an assembly of cubicles in an enclosed structure, each cubicle being a complete unit containing equipment required for control and protection of one motor or one power subfeeder.

Difficulties were encountered with the crane gears and the electrical equipment in the operation of these cranes (see ANL-6596, p. 93). The status of the measures to correct these difficulties is as follows:

1) The supports for the bus bars on the three crane bridges have been redesigned and are being ordered.

2) The sliding electrical collector assemblies on the three crane trolleys have been redesigned and detail drawings are being made.

3) New drive units for the crane bridges, in which Master worm-gear motor units* will be used, are being developed. Separate power-supply leads to the solenoid clutches on the bridge drive units are also planned. In the presently installed units, each solenoid is connected to two of the power-supply leads for each motor. Thus, when the motor is started, the solenoid is energized, and the clutch engages as the motor turns. When the power to the motor is cut off, the solenoid becomes de-energized, and the clutch disengages. This makes accurate positioning of the bridges difficult. Therefore, by connecting the solenoid to a separate power supply, the solenoid can be kept energized while the crane is in use. This change, made on crane No. 2 in the Argon Cell, has greatly facilitated close positioning of the bridge.

After 10 hr of additional operation, a bridge drive gear reducer unit on one of the Argon Cell cranes has again failed. This same bridge drive unit had failed previously after 5 hr of operation and had been reconditioned by replacing the ring gears which had been worn out (see ANL-6596, p. 94). The failure of the gear reducer unit is attributed to the high starting torque of the motor, which exceeds the rated torque of the gear reducer. The bridge drive unit is being repaired by the manufacturer.

c. Air Cell and Argon Cell Manipulators
(J. Graae, E. Petkus, W. Voss, R. Vree)

(1) Electromechanical Manipulators

There are two electromechanical manipulators in the Air Cell and six in the Argon Cell. The designs are basically the same except that the movement of the bridge in the Air Cell is rectilinear whereas the movement of the bridge in the Argon Cell is radial about a center pivot. Alternate bridges in the Argon Cell are at two different elevations** to permit partial overlap of adjacent bridges. The carriages of the manipulators are interchangeable with each other, although three of them are especially adapted to the low bridges in the Argon Cell.

*A product of the Master Electric Co., Dayton, Ohio.

**Three bridges are 11 ft 8 in. above the cell floor; the other three bridges are 13 ft 5 in above the cell floor.

All bridge and carriage drive units for the manipulators have been checked for interchangeability and dimensional alignment with special templates (see ANL-6596, p. 95). Of the sixteen drive units, six did not meet these requirements and corrective measures are being made. Otherwise, the manipulators operate satisfactorily and are being used for the remote installation of equipment in the cells.

(2) Master-Slave Manipulators

Two sleeves, which will permit installation of a pair of sealed-type master-slave manipulators* in the existing wall penetrations in the Argon Cell have been fabricated. The sleeves and the manipulators are being installed.

Nine pairs of slave end mounts for the general-purpose master-slave manipulators (Model B)** are to be modified to insure proper low-friction motion in the high-radiation field. The grease in the bearings will be replaced with a radiation-resistant grease (NRRG-159†) and the bearing shaft will be coated with molybdenum disulfide. The NRRG-159 grease should provide low-friction lubrication for about 2 yr. When the grease becomes thickened due to radiation damage, the molybdenum disulfide should provide adequate lubrication, although the friction will be greater than that with fresh grease.

d. Cell Viewing and Lighting
(T. W. Eckels, J. Graae)

(1) Shielding Windows

The final inspection of all the Fuel Cycle Facility shielding windows was made by representatives of Argonne National Laboratory and of Pittsburgh Plate Glass Company. The light transmittance of the windows, tested with a light source (illuminant A††), was determined to be from 15 to 17 percent, which exceeds the guarantee of 9 percent. Clarity of view and resolution of detail are exceptionally good.

---

*Model A, manufactured by Central Research Laboratories, Inc., Red Wing, Minnesota.

**Model B, manufactured by Central Research Laboratories, Inc., Red Wing, Minnesota.

†A radiation-resistant grease, a product of Standard Oil Company of California.

††Illuminant A is light of color temperature 2848 K as defined by the International Commission on Illumination (CIE).

(2) Shielding Window Shutters

Fifteen additional steel shutters for the shielding windows and shutter drive units to move these shutters have been ordered. When these are installed, each of the 31 shielding windows in the process cells will be provided with a shutter. These shutters will be used to protect the windows from radiation damage when the windows are not in use. In the current design of the shutter drive units, chattering of the motor drive gear on the shutter gear rack occurs when the shutter reaches the end of its travel because of the high stalling torque of the drive motor. The use of a slip clutch on the motor drive shaft is being investigated to eliminate the problem of the chattering.

(3) Wide-angle Viewers

Four wide-angle viewers have been installed in existing sleeves in the roof and wall of the Argon Cell to view locations within the cell not readily visible through the Argon Cell shielding windows (see ANL-6569, p. 75). Two variable-power spotting telescopes which were modified for use with the wide-angle viewers have been delivered to the Facility. The viewing capabilities and quality of image of the wide-angle viewers are reported to be excellent.

(4) Periscope for Air Cell

The installation of the Kollmorgen periscope for use in the wall of the Air Cell has been completed (see ANL-6287, p. 84). The horizontal leg of the periscope was modified to permit a double offset in the optical path and to incorporate more effective internal, annular lead shielding. A hemispherical, nonbrowning-glass protective dome to avoid radioactive contamination of the periscope was installed on the hot side of the cell.

e. Cell Transfer Locks
(G. Bernstein, A. Chilenskas, J. Graae, J. Ludlow, E Petkus)

Material transfers in and out of the Argon Cell will be through transfer locks (see ANL-6569, p. 70; ANL-6596, p. 97). Two small transfer locks penetrate the wall between the Air Cell and Argon Cell, and a large transfer lock penetrates the floor of the Argon Cell and connects to the Air Cell through a Transfer Cell.

(1) Large Transfer Lock

The large transfer lock, which is basically a cylinder (6 ft in diameter and 8 ft long), is composed of three major sections. The upper section (see Figure 31) consists of a 41-in.-long spool piece to which

is attached a counterbalanced hinged lid. The middle section is imbedded in the 4-ft-thick concrete cell floor. The bottom section of the lock is a steel platform which can be elevated by a hydraulic ram and seals to the lower flange of the center lock section.

Figure 31

LARGE TRANSFER LOCK IN ARGON CELL:
UPPER SECTION

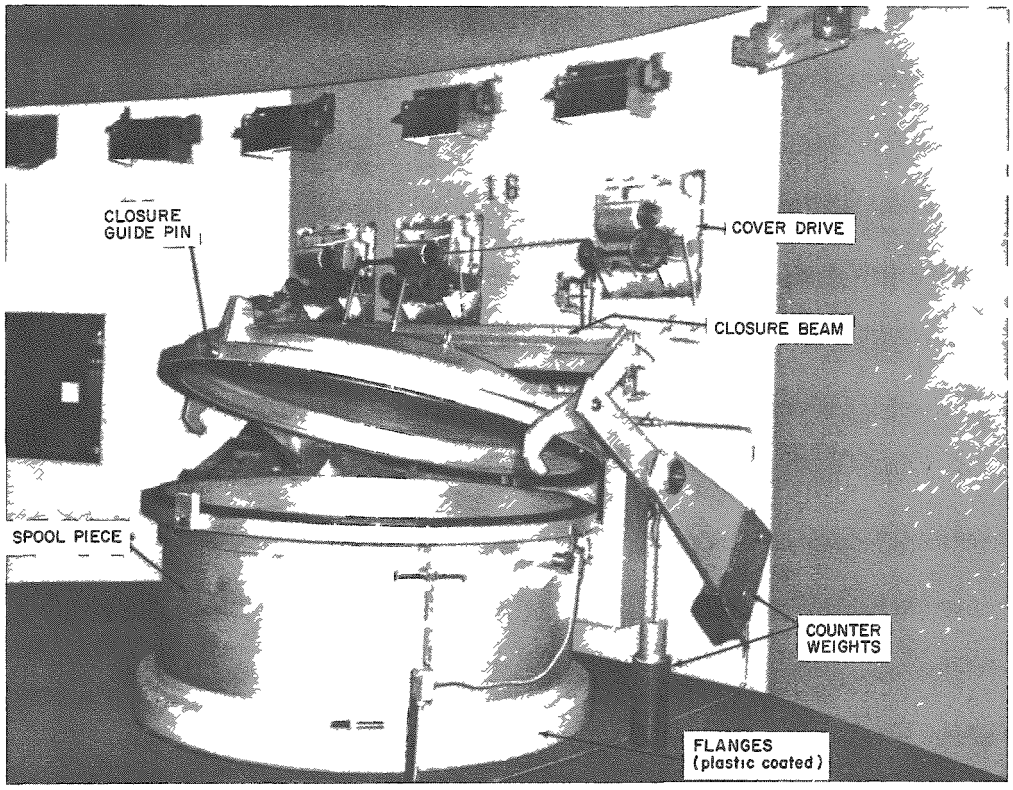

In the original installation of the lock, the upper (spool piece) section was bolted to the middle embedded section with a soft steel gasket between the flanges of the sections. This seal leaked continuously. Efforts to reduce the leakage by additional tightening of the flange bolts were unsuccessful. This leakage problem has been satisfactorily solved by welding a steel band on the inside circumference of the transfer lock at the original gasket seal level between the two sections. The weld area of the steel band was tested with helium and was found to be free of leaks. With this new method of sealing between the two sections, the spool piece is now not remotely removable. The bolted flange construction of the original design made this possible. However, the remote removal and replacement of the spool piece would have been a major operational undertaking and would have necessitated the shutdown of the

entire Argon Cell and the opening of the roof hatch. Therefore, the welding of a steel band to make the seal between the two sections was accepted as a compromise in order to get the Argon Cell into operating condition as soon as possible.

(2) Transfer Cell

Corrective work on the Transfer Cell equipment (see ANL-6596, p. 97) is almost completed. Limit switches for the transfer lock have been installed and changes in the wiring have been made. The drive units for lifting the hinged lid of the large transfer lock were installed and are in operating condition. The controls for the Transfer Cell cart and for the hydraulic rams have been integrated into the transfer lock control system. The system is operating satisfactorily. However, the hydraulic rams require additional ballast in order for them to be able to lower. A new motor brake must also be installed on the cart drive. An operating procedure for the Transfer Cell has been written. All future transfers of large items into or from the Argon Cell will be made using the Transfer Cell and will be carried out completely by remote control operations.

Figure 32

SMALL TRANSFER LOCK END ASSEMBLY

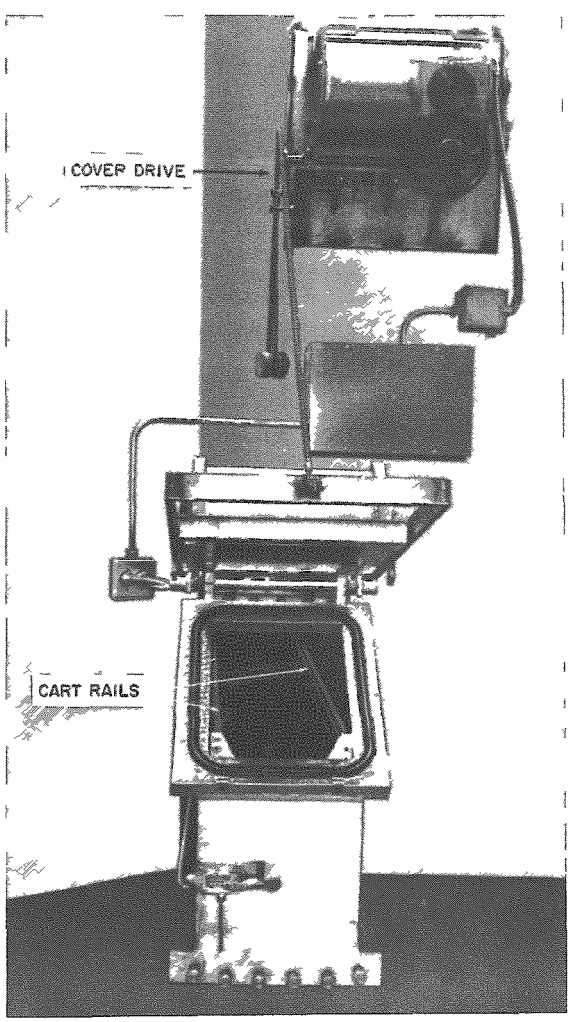

(3) Small Transfer Locks

The two small horizontal transfer locks between the Air Cell and the Argon Cell will accept small carts containing items 20 in. high and $9\frac{3}{16}$ in. in diameter for transfer. A cart or series of carts moves between cells on inclined rails mounted in the transfer lock. The carts are gravity operated and one lock is provided for each direction of travel. The end assembly of one of the small transfer locks is shown in Figure 32.

The installation of the drive units for opening the covers on the small transfer locks and of the associated limit switches has been completed. Remote operation of the

transfer locks has been demonstrated and an operating procedure is being written. During the radiographing of the shielding of the Air Cell and Argon Cell, the small transfer locks were used for between cell transfers of the radioactive sodium sources used in the survey. The transfer locks will continue to be used routinely for the remote transfer of all small items into and from the Argon Cell.

(4) Transfer Lock Vacuum Systems

Since both the large transfer lock and the small transfer lock systems connect the Argon Cell directly to the Air Cell, and since the pressure in the Argon Cell is negative compared with the pressure in the Air Cell, it is necessary to insure isolation between the cells. This is accomplished by the use of interlock switches which permit only one of the transfer locks to be opened at any given time. This system is integrated with a vacuum and venting system which insures that the atmosphere in a given lock is appropriate for the direction of transfer. The vacuum valves (Saunders type) do not seal sufficiently well to permit proper atmosphere control. New diaphragms have been purchased, and an attempt is being made to polish the valve weirs in order to provide proper closure. If proper closure is not obtained, new valves will have to be installed. Leakage will not prevent the use of the vacuum valves until an inert atmosphere is introduced into the Argon Cell.

(5) Air Cell Hatch Cover

A new hatch cover has been designed for the opening in the Air Cell floor. The hinged cover will be opened by an electric motor drive that is remotely operated. Since the hatch cover (7 ft square) occupies a large portion of the floor area, the load-carrying capacity of the new cover has been designed for 5 tons to permit its use as a temporary storage station for material or equipment.

f. Installation of Process Equipment

Two injection-casting furnaces which were designed and tested by the Argonne National Laboratory Metallurgy Division have been installed in the Argon Cell under their supervision. These furnaces will be used to injection-cast pins from reconstituted fuel alloy.

Components of the furnaces were transferred into the Argon Cell by means of the cell transfer equipment and were remotely assembled by means of the operating manipulators controlled from the operating areas outside the process cells. Color motion pictures were taken within the Argon Cell of the remote installation of the injection-casting furnaces. These motion pictures will be used as a visual aid for training purposes and as information for future maintenance when access to the Argon Cell by personnel is no longer possible. Motion pictures were also made during the installation of the melt refining furnaces in the Argon Cell.

g. Miscellaneous Cell Service Equipment
(E. J. Petkus, M. A. Slawecki, H. L. Stethers)

Most of the pumps, valves, and similar service equipment necessary for the operation of processes in the cells is located in the subcell area under the Argon Cell and in the adjacent basement (see ANL-6596, p. 96). The installation of this equipment is complete. Operational testing of this equipment is in progress.

Fuel subassemblies, equipment, and other items are moved into and out of the Air Cell through an opening in the floor at the west end of the Air Cell. The maximum opening is 6 ft in diameter. Three 6-in.-thick steel slabs which fit within the floor opening are used for biological shielding. In the center of the shielding slabs are two concentric (6- and 24-in.-diameter) removable plugs. The transfer of large items which cannot be accommodated by the 24-in.-diameter plug involves the removal of the 6-ft-diameter steel slabs. Removing the 6-ft-diameter steel shielding slabs is time consuming and creates problems in providing adequate shielding to the space beneath the opening. In addition, equipment in the Air Cell may have to be moved in order to provide temporary storage space for the shielding slabs. Therefore, a 36-in.-diameter removable plug has been designed for these shielding slabs. The plug will be fabricated from the steel cut out of the existing 6-ft-diameter slabs. The weight of the 36-in.-diameter plug will be within the 5-ton load capacity of the Air Cell crane, so that the plug can be removed in one piece. The availability of a 36-in.-diameter plug will reduce the number of occasions when the full 6-ft-diameter opening will have to be used.

Two argon compressors, each rated 60 scfm at 120 psig, have been installed on the service floor outside the subcells. These compressors will be used to compress cell argon for use with pneumatic equipment located in the Argon Cell. The use of recirculated cell argon instead of cylinder argon in equipment such as cylinder operators and ring gauges * will provide substantial savings.

An isolation wall has been erected around the compressor area, and separate ventilation facilities for this enclosure have been installed. After the compressors were installed, they were tested by the vendor and they are now ready for operating service.

2. Development of Service Equipment

a. Interbuilding Fuel Transfer Coffins
(G. J. Bernstein, A. A. Chilenskas)

Fuel subassemblies containing spent or reconstituted fuel will be transferred between the Reactor Building and the Air Cell of the

*Fuel-pin diameters are determined by insertion of the pin into a ring gauge. Argon flowing into the ring gauge develops a back pressure when the pin is inserted, and the amount of back pressure indicates the fuel-pin diameter.

Fuel Cycle Facility in 20-ton, interbuilding fuel-transfer coffins. Two interbuilding coffins will be built (see ANL-6596, p. 98). One coffin, designed and fabricated by O. G. Kelley and Company of Boston, Massachusetts, was shipped to Idaho on October 29, 1962. Preliminary tests conducted at the fabricator's shops indicated that the specifications for heat-removal performance and leaktightness can be met. More detailed mechanical and heat removal performance tests will be made at the EBR-II site in Idaho.

The other coffin is being designed by the Chemical Engineering Division of the Argonne National Laboratory and is being built at Argonne. Fabrication of the coffin shell and internal piping is complete. The coffin shell is being prepared for lead filling. The motor and sealed blower which will be used to circulate the coolant gas through the fuel subassembly have been received. The results of preliminary tests show that the drive motor is overloaded when the blower is performing at rated output. This problem is being studied.

When a spent fuel subassembly is discharged from the EBR-II reactor, the subassembly will be coated with a thin film of sodium. Because of its pyrophoricity, this sodium must be removed before the subassembly is moved into the Air Cell. To accomplish this, a sodium-removal station is to be located in the enclosed passageway between the Reactor Building and the Fuel Cycle Facility. The design and layout of process equipment have been completed.

The process (see ANL-6596, p. 98) consists of converting the sodium to sodium oxide by the addition of a small amount of humidified air to the circulating argon in the transfer coffin and converting the oxide to sodium hydroxide by passing humidified air through the coffin. The sodium hydroxide will be removed by a water wash, and the coffin and subassembly will be dried by an air purge. The argon, air, and water vapor will be passed through a venturi scrubber unit and absolute filters before discharge to the suspect stack.

b. Materials Testing
(G. J. Bernstein, A. A. Chilenskas)

The suitability of oil-impregnated, sintered bronze sleeve bearings for use in high-intensity radiation areas of the Fuel Cycle Facility has been investigated. In this study, the bearings were lubricated with either a commercially available SAE-10 oil recommended by the bearing manufacturer or a radiation-resistant oil (NRRO-358*). The NRRO-358 was chosen because of its resistance to radiation damage and its similarity in absolute viscosity to SAE-10 oil. A lathe was modified to permit maintaining a precise alignment of the bearing and the shaft while testing the

*A product of Standard Oil Company of California.

sleeve bearings under radial load. The bearings* are supplied impregnated with an oil which was removed for these tests. The bearings were washed with trichloroethylene, dried, and then reimpregnated by being immersed in the test oil at 140 F for 3 hr. In order to increase the amount of oil absorbed by the bearings, the bearings were also subjected to several rough vacuum cycles while immersed in the oil and then allowed to remain in the oil overnight under a partial vacuum. The oil was not heated for the overnight immersion step. The vacuum treatment resulted in about a 50 percent increase in the weight of oil that was absorbed by the bearing.

Bearings impregnated with these test oils were wrapped in aluminum foil and were irradiated in an air-filled irradiation urn to a gamma-radiation level of 1×10^9 rad. Measurements of wear and bearing temperature were made while unirradiated and irradiated bearings were subjected to an axial load of 160 lb at a shaft speed of 310 rpm. Under these conditions, the axial load was about 50 percent of the manufacturer's maximum rating. The temperature of the bearing was continuously recorded.

An unirradiated, SAE-10 oil-impregnated bearing performed satisfactorily for 100 hr. At this time, the test was voluntarily terminated. Two irradiated, SAE-10 oil-impregnated bearings (irradiated to 1×10^9 rad) failed after run durations of about 34 hr each. Two unirradiated, NRRO-358 oil-impregnated bearings failed after run durations of about 20 hr each. Two irradiated NRRO-358 oil-impregnated bearings (irradiated to 1×10^9 rad) failed after run durations of 2 and 20 hr, respectively.

During operation, the temperature of each bearing normally fluctuated between room temperature and about 130 C, with gradual changes. Degradation of the bearing was always indicated by an abrupt temperature rise. For purposes of comparison, failure in these tests was considered to occur at the time the bearing temperature reached 170 C, for operation of the bearing after the bearing temperature had reached 170 C resulted in squeaking and rapid wear.

The results of these tests indicated that the performance of unirradiated, SAE-10 oil-impregnated bearings was much better than that of unirradiated or irradiated, NRRO-358 oil-impregnated bearings. The results also showed a marked deterioration in performance for irradiated, SAE-10 or NRRO-358 oil-impregnated bearings.

These exploratory tests have shown no specific desirable performance characteristics of oil-impregnated, sintered bronze sleeve bearings that would be subjected to high-intensity radiation which would

---

*Oilite bearings, a product of Amplex Division, Chrysler Corporation.

justify continued investigation. Further testing of these bearings has therefore been discontinued.

c. Miscellaneous Cell Service Equipment
(W. E. Miller, M. A. Slawecki)

(1) Storage Racks

Small items which are used in melt refining processing will be brought into the Argon Cell in batches. These items will be stored on racks (see ANL-6569, p. 71) that will be mounted on the outside walls between the shielding windows. A prototype rack was built at Argonne for testing of the design in the Argon Cell in Idaho. Based on the in-cell tests, a final design for the rack was completed, and eight racks were ordered.

(2) Heaters for Solder Pots (Fusible Metal Seals)

A prototype clamp-on-type solder pot heater has been built and is being tested for melting of the fusible metal in solder pots that are used to obtain a leaktight seal for the gas and vacuum tubing connections between service feed throughs and process equipment.

3. Development of Process Equipment

a. Skull Oxidation Equipment
(W. E. Miller, M. A. Slawecki, H. Stethers)

After the melt refining step is carried out, a skull remains in the zirconia crucible. This skull contains significant quantities of fissionable material which will be recovered by means of the skull reclamation process. In order to remove the skull from the crucible, the skull will be oxidized to a powder and the powder transferred to an oxide-storage container. Equipment for the skull oxidation step and for the transfer of the oxide powder is being developed.

The prototype skull oxidation furnace has been operated for some 590 hr (see ANL-6596, p. 102). During this period, about 48 kg of skull material and uranium-fissium alloy scrap has been oxidized. This is equivalent to oxidizing about 95 skulls from plant-scale melt refining runs of 95 percent yield.

During the operating period, several runs were made to determine if the skull oxidation furnace could also be used to oxidize massive pieces (9 to 10 kg) of alloy scrap (uranium-5 w/o fissium and uranium-0.35 w/o fissium). Stainless steel containers were used to hold each 9- to 10-kg piece of alloy scrap while being oxidized in the skull

oxidation furnace. At 10- to 12-hr intervals, the oxidation of the alloy scrap was interrupted, and the oxidized alloy scrap (about 1 kg) was poured off. The residual, unoxidized alloy scrap was then returned to the skull oxidation furnace for further oxidation.

In each of two runs, 9.6- and 8.5-kg massive pieces of uranium-5 w/o fissium were used. About 83 percent of the charge in each run was oxidized to uranium oxide (U_3O_8) in runs of 100- and 74-hr duration, respectively. In one run, a 9.5-kg massive piece of uranium-0.35 w/o fissium was used. Ninety-five percent of the charge in this run was oxidized. The gain in weight of the oxidized alloy scrap was used to calculate the percent of uranium in the alloy scrap which had been oxidized. It was assumed that the product formed was U_3O_8. These runs have shown that the skull oxidation furnace could be used to oxidize massive pieces of uranium-fissium alloy scrap. The greatest amount of oxidation was shown with the uranium-0.35 w/o fissium alloy scrap.

The skull oxidation furnace, an oxygen-removal unit, and associated gas-control equipment will be combined into an integrated operating unit and tested at Argonne. Installation of the valves, piping, and instruments for the gas-control system is essentially complete. Fabrication of the panelboard for the gas-control system has started. Fabrication of the remotely rechargeable oxygen-removal unit, which uses a heated copper bed to remove oxygen from the gas discharged from the oxidation furnace, is essentially complete.

b. Skull-oxide Processing Equipment
(G. J. Bernstein, W. E. Miller)

The first model of the skull-oxide processing furnace was installed in the EBR-II mockup area at Argonne. A 30-kw high-frequency (10,000 cycles/sec) motor-generator unit is being used to furnish the power to the skull-oxide processing furnace. The coupling of the power from the motor generator to the induction coil of the furnace was satisfactory. With this power-supply system, about 4 hr were required to heat an empty 20-gal. graphite crucible to 800 C. This is a rather long heatup time. A shorter heatup time is not possible because of the small power-supply unit being used. However, this long heatup time is not expected to be a problem in future development work with the skull-oxide processing furnace.

c. Collection of Metal Vapors
(W. E. Miller)

The product from the precipitation step of the skull reclamation process is uranium coated with magnesium-zinc. Distillation is a convenient means of removing the magnesium-zinc coating from the

uranium. If possible, the melt refining furnace will be adapted for this distillation. The main problem in this approach is the design of a condenser to collect the distillate.

In previously reported magnesium-zinc distillation runs (see ANL-6596, p. 102) made with a graphite condenser which rested directly on the gasketed lip of the crucible, the condenser and crucible were found at the end of each run to be bonded at the gasket. The bond was formed by deposition of distilled metal at the gasket surfaces. Such bonding would hinder remote disassembly of the equipment. A new design with a graphite condenser and a separate graphite distillate collector has been tested in the melt refining furnace. This new design (see Figures 33 and 34) eliminates the need for a gasket between the condenser and the crucible, and is more adaptable to the remote disassembly of the condenser from the crucible. In this new design, the condensed magnesium-zinc vapors are collected in the graphite collector which rests directly on the lip of the graphite crucible. The condenser fits over the graphite collector and rests on the stepped portion of the crucible, that is, below the lip of the crucible. The collector will be discarded after each run. The condenser and the crucible, however, would be used for more than one run.

Figure 33

DISTILLATION CONDENSER AND COLLECTOR FOR MELT REFINING FURNACE

Crucible: 6 3/8 in. in OD by 9 in. high
Condenser: 6 3/8 in. in OD by 19 in. high

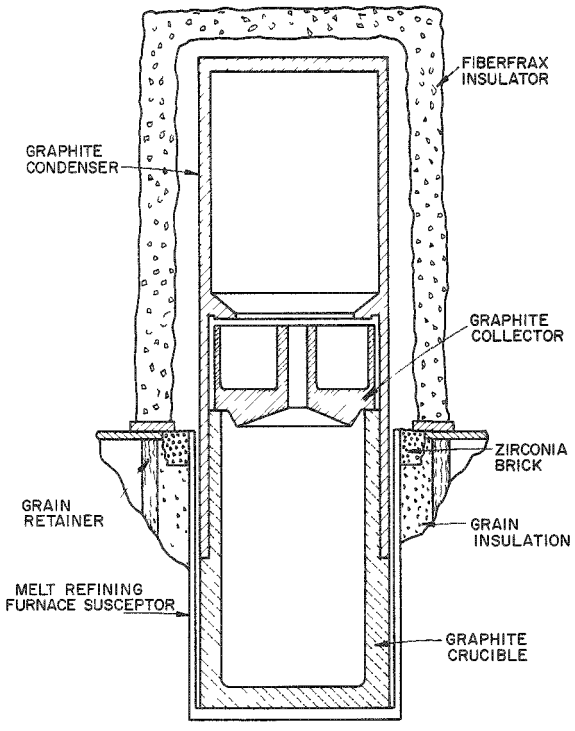

Figure 34

DISTILLATE COLLECTORS USED IN MELT REFINING FURNACE RUNS

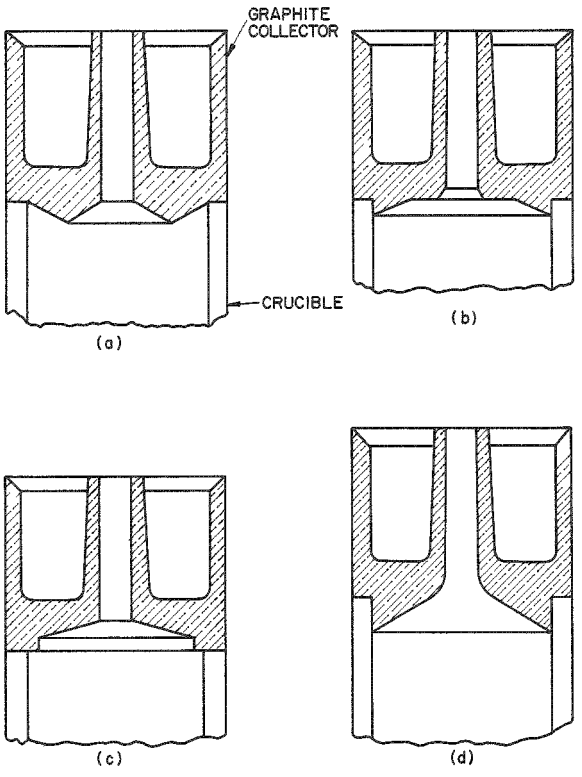

The results of a series of magnesium-zinc distillation runs made with the new design are summarized in Table 16. Four collector designs which differed from each other only in the shape of the bottom of the collector (see Figure 34) were evaluated in these runs. A new collector was used in each of the six runs. The shape of the bottom of the collector was found to be important for the distillation of the final trace amounts of magnesium-zinc alloy from the crucible and for preventing the formation of a magnesium-zinc bond between the collector and the crucible, which would make their separation by remote handling difficult. In some runs, it was not possible to distill all the magnesium-zinc from the crucible. Even prolonged heating after a distillation run was apparently thought to be complete, as indicated by termination of the temperature arrest, was not helpful. On cooling down at the end of some of the runs, drops of distilled magnesium-zinc alloy that were clinging to the bottom of the collector solidified and bridged the junction formed by the collector and the crucible. In Runs 5104 and 5105, such bridging made it difficult to remove the collectors (see Figures 34a and 34c) from the crucibles. In Runs 5103, 5107, and 5108, however, there was no bridging, and the collectors (see Figures 34b and 34d) could be readily separated from the crucibles.

Table 16

RESULTS OF MAGNESIUM-ZINC DISTILLATIONS

Charge: 1 kg of 50 w/o magnesium-zinc
Pressure: Atmospheric (Argon blanket)
Temperature Arrest: 1030 to 1090 C
Power input: 14 kw

Run No.	Duration of Temp Arrest	Percent Charge Distilled	Percent Distillate Found in Collector	Percent Distillate Found on Condenser Surfaces	Percent Distillate Found on Fiberfrax Insulator	Percent Distillate Unaccounted For
5100	1 hr 50 min	97.5	83.0	7.1	8.9	1.0
5103	1 hr 25 min	97.6	85.2	6.2	8.2	0.4
5104	2 hr 15 min	96.3	84.0	0.3	11.0	4.7
5105	2 hr 25 min	99.4	59.5	0.2	22.9	17.4
5107	2 hr 25 min	99.7	74.1	9.1	12.5	4.3
5108	2 hr 45 min	98.7	81.8	6.1	2.8	9.3

In Runs 5100, 5103, 5104, and 5105, the same condenser and crucible were used for all the experiments. Continued reuse of the same condenser, however, resulted in some buildup of metal on the condenser wall immediately adjacent to the collector. In Runs 5107 and 5108 the same condenser and crucible were used; however, a different Fiberfrax insulator was used in each of the runs. The use of different insulators could account for the slight difference in distillation times noted for these two runs. This effect is being investigated further.

The inconsistencies in the amounts of metal which escape from the condenser enclosure (sum of the last two columns on the right in Table 16) cannot be explained at this time. It is believed that the amount of magnesium-zinc vapor which escapes (see Table 16) should be less in future experiments when component parts of the condenser made with a more impervious graphite become available. Type CS graphite was used as the material of construction in the condenser design studied in this current investigation. Liquids and vapors readily diffuse through Type CS graphite.

d. Inductive Heating and Mixing
(A. A. Chilenskas)

The skull reclamation process requires the heating and mixing of metal-salt systems at temperatures up to 800 C. Although conventional mixing and heating methods have been found satisfactory for the demonstration of the process on a small scale, the use of low-frequency inductive power to provide both heating and mixing is being investigated. Appreciable simplification of plant equipment is anticipated if inductive heating and mixing should prove feasible.

An experiment (IM-10) was performed in which a 24.2-lb charge of magnesium was melted and mixed inductively in a graphite crucible which was heated by a 17-turn, water-cooled coil. The geometry and the charge data for this run are shown on Figure 35. This experiment was conducted in a closed furnace with argon used as the blanket gas. (This furnace is described in ANL-6596, p. 104).

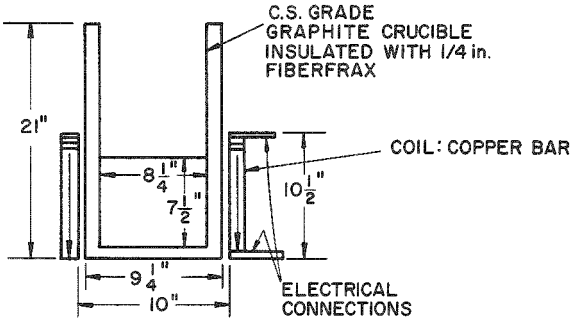

Figure 35

APPARATUS FOR INDUCTIVE MIXING OF MAGNESIUM RUN IM-10

Charge: Magnesium, 24.2 lb

Coil: Copper bar, 1/2 in. x 1 in., 17 total turns, water-cooled.

Power: 60 cycle

Observation of the melt surface through the furnace window showed that the molten charge underwent vigorous agitation at modest power inputs. At a power input of 4.5 kw to the coil,* the lift** was estimated to

*This is estimated from the measured power input to the primary of the transformer. A 10 percent loss is assumed for the transformer and leads to the coil.

**An index of the vigor of agitation is the height to which the molten metal charge surface rises with reference to its edge. This rise is referred to as "lift."

be between 2 and 3 in. At a power input of 8.1 kw, the agitation became vigorous enough to throw magnesium out of the crucible. It was not possible to see the surface of the molten charge clearly enough to estimate the lift at this power input because of the condensed fumes which had accumulated on the furnace window.

A comparison of Run IM-10 with Run IM-8,* in which the molten charge was zinc, shows that the lift obtained with magnesium was about three to four times that obtained with zinc for the same power input of 4.5 kw. This behavior is consistent with the expected performance in that the thrust developed (for similar geometries) is directly proportional to the power delivered to the charge and that the lift is directly proportional to the thrust and inversely proportional to the density of the liquid metal. This suggests that, as the proportion of magnesium increases in zinc-magnesium mixtures, an increase in the vigor of agitation should result.

An experiment (IM-12) has been completed in which 40 lb of magnesium-zinc (50 w/o) was mixed with 14.4 lb of flux (47.5 w/o $CaCl_2$, 47.5 w/o $MgCl_2$, 5 w/o MgF_2). The molten metal charge was about 7 in. deep by 9 in. in diameter, while the molten salt was about 3 in. deep. With a power input of about 8.5 kw to the coil, the metal charge was observed to break through the salt layer on top of the charge and cause very vigorous agitation of the salt.

A run (IM-11) has been completed in which 66 percent reduction of a skull oxide charge of 2.7 lb was obtained. The charge was heated and mixed inductively at a temperature of 800 C for about 2 hr prior to sampling. The charge consisted of 54.6 lb of zinc, 9 lb of magnesium, 2.6 lb of Dow 230 flux,** and 6.2 lb of flux consisting of 47.5 w/o $CaCl_2$, 47.5 w/o $MgCl_2$, and 5 w/o MgF_2. The geometry of the system was as shown for Run IM-10 (see Figure 35) except that the metal charge height was 7 in. and the salt height was 2.2 in. The fume-control system for the furnace (see ANL-6596, p. 104) did keep the furnace atmosphere clean so that at the operating temperature of 800 C the charge could be observed through the furnace window. The molten metal phase was seen to break through the molten salt layer and to agitate it vigorously.

An experiment (Run IM-13, Part I) has been completed in which a new coil was tested for power delivery to a zinc charge. The coil consists of 32 turns of $\frac{3}{8}$ in. x 1 in. bar stock and has an 11-in.-ID. Electrical taps were copper welded on turns 17 and 24 for testing with different

*Run IM-8 gave a lift of $\frac{3}{4}$ in. for a power input of 4.5 kw to the coil (see ANL-6596, p. 105). The same coil was used for IM-8 and IM-10 and the crucibles differed only slightly in their inside diameters.

**A flux manufactured by the Dow Chemical Company. The flux contains 55 percent KCl, 34 percent $MgCl_2$, 9 percent $BaCl_2$, and 2 percent CaF_2.

effective number of coil turns. The zinc charge of 129 lb was contained in a graphite crucible. The charge diameter was $9\frac{1}{2}$ in. and its height was $7\frac{1}{2}$ in. The coil was electrically connected at the bottom and at the 24th turn for an active coil height of $10\frac{1}{2}$ in. For a power input of 10.8 kw to the coil and with the melt at 450 C, the developed thrust lifted the center of the zinc about 1.7 in. higher than its edge. For a power input of 16.2 kw, the lift was about 2.5 in. This represents the largest thrust developed for a zinc system thus far. Further increases in power input are limited by the present power-supply system. Most of the components for a larger power-supply system have been received, and its installation will begin shortly.

C. Chemistry of Liquid Metals
(I. Johnson and H. M. Feder)

The chemistry of liquid metal systems is being investigated to provide basic concepts and data for the design of methods for the reprocessing of reactor fuels. The results of these studies also provide ideas and data for the formulation and testing of theories of liquid metal solutions.

1. Solubilities in Liquid Metals

Of prime importance in the practical design of fuel-reprocessing methods are the solubilities of the metals whose separations are being attempted. These solubilities need to be known as a function of both temperature and solvent composition. Since the solubility and temperature coefficient of solubility of a metallic phase in a liquid metal solvent are dependent on the interatomic forces operative in the solution, systematic studies may lead to greater insight into the nature of these forces and their variation with the basic properties of the solute and solvent atoms. For such fundamental studies, it is necessary to know the constitution of the solid phase in equilibrium with the saturated liquid phase.

Zinc-Technetium System
(M. G. Chasanov and P. D. Hunt)

The solubility of technetium in liquid zinc was determined by taking filtered samples of the saturated solution. The charge consisted of 90 g of high-purity zinc (99.999 percent) and 0.4 g technetium-99. The technetium, obtained as a powder from Oak Ridge National Laboratory, had been arc-melted to remove volatile impurities. Spectrographic analysis of the product showed that sodium at a concentration of 0.1 percent was the principal impurity.

The experimental data are given in Table 17 and shown in Figure 36. The best fit to the solubility data was obtained by the following empirical equations:

$$\text{(428 to 527 C) } \log \text{ (atom percent technetium)} = 6.431 - 7159\ T^{-1} \quad ;$$

$$\text{(552 to 758 C) } \log \text{ (atom percent technetium)} = 9.431 - 15690\ T^{-1} + 4.979 \times 10^{6}\ T^{-2} \quad .$$

The relative standard deviations for these equations are 5 and 8 percent, respectively. These data indicate a peritectic at about 544 C.

Table 17

SOLUBILITY OF TECHNETIUM IN LIQUID ZINC

Temp (C)	Technetium (a/o)	Temp (C)	Technetium (a/o)
428[a]	4×10^{-4}	630	$1.5_6 \times 10^{-2}$
470	$1.3_2 \times 10^{-3}$	662	$1.9_5 \times 10^{-2}$
507	$1.8_5 \times 10^{-3}$	684	$2.6_9 \times 10^{-2}$
527	$3.0_1 \times 10^{-3}$	718	$4.4_4 \times 10^{-2}$
552	$5.1_4 \times 10^{-3}$	734	$5.5_3 \times 10^{-2}$
580	$6.7_4 \times 10^{-3}$	758	$7.7_9 \times 10^{-2}$
601	$1.0_3 \times 10^{-2}$		

[a]Datum not used in computing solubility equation.

Figure 36

SOLUBILITY OF TECHNETIUM IN LIQUID ZINC

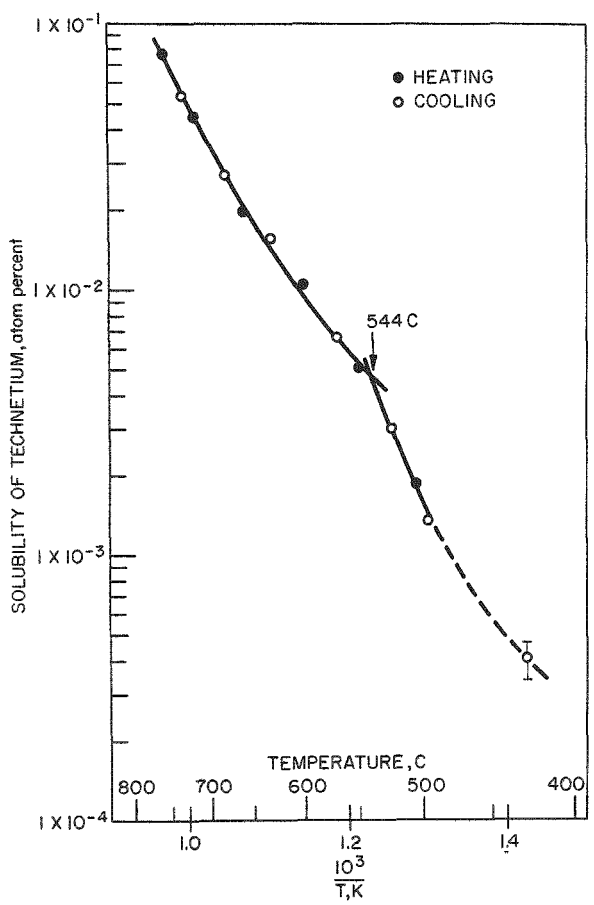

Differential thermal analysis of a zinc-about 3 a/o technetium alloy yielded arrests on heating at 417, 540, and 953 C. The arrest at 417 C corresponds to the melting point of zinc. The arrest at 540 C is a peritectic transformation, which is in good agreement with the peritectic transition indicated at 544 C by the solubility data. Metallographic examination indicates that the arrest at 953 C is also associated with a peritectic transition.

X-ray analysis of these alloys showed the presence of at least two intermetallic compounds in this system. These compounds have the approximate compositions of $TcZn_6$ and $TcZn_{15}$. The characterization of these compounds has not yet been completed.

In a previous report (ANL-6029, p. 47), the solubilities of several metals of the second transition series in liquid zinc at

600 C were plotted against the atomic numbers of the elements in this series. The resulting graph suggested that a minimum solubility would occur at the position of technetium. Data obtained in the present experiments verify this prediction.

Zinc-Tantalum System

(M. G. Chasanov, R. Schablaske,* P. D. Hunt, and B. S. Tani*)

Zinc-tantalum alloys were prepared by heating mixtures of the component metals in a rocking furnace and also by powder metallurgical methods. The interaction between these metals is very sluggish, and samples heated for periods as long as two months gave evidence that equilibrium had not been attained. X-ray diffraction analyses of these alloys indicated the existence of at least five intermetallic compounds in the system. A Laves phase constitutes one of these phases; the other intermetallic compounds have not yet been characterized.

Thermal analysis of zinc-tantalum alloys gave the arrests reported in Table 18. These arrests were obtained on heating the samples at about one to two C per minute. Essentially the same arrests were observed in differential thermal analysis of a 13 a/o tantalum alloy.[23] It appears that a number of the intermediate phases in this system decompose peritectically.

Table 18

THERMAL ANALYSIS OF ZINC-TANTALUM ALLOYS

Thermal Arrests Observed on Heating	
7.4 a/o Ta (C)	60 a/o Ta (C)
420[a]	-
610	600
-	670
700	700
755	760

[a]Melting point of zinc.

Zinc-Tungsten System

(M. G. Chasanov and P. D. Hunt)

It has been reported previously (see ANL-6243, p. 4) that tungsten is inert to attack by molten zinc. Henmann[24] indicated that intermetallic compounds may exist in this system. To investigate the possible occurrence of intermediate phases in this system, a series of alloys was prepared by powder metallurgical techniques. Pellets, $\frac{1}{4}$ in. in diameter, were prepared by compacting 99.95 percent tungsten powder and 98.8 percent zinc powder. The compacts, which had the following nominal compositions: WZn_{20}, WZn_{10}, WZn_5, $WZn_{2.5}$, WZn, and $W_{1.5}Zn$, were heated at about 430 C for 2 weeks in ampoules containing helium. Metallographic examination of the specimens showed that the metals

*Members of the X-ray Diffraction and Spectroscopy Group.

[23]Martin, A. E., private communication.

[24]Henmann, T., Z. Metallkunde 39, 51 (1948).

had not reacted. This was confirmed by X-ray diffraction studies,[25] which showed that elemental tungsten and zinc accounted for the patterns obtained with the compacts.

These compacts were then reheated to 650 C for 31 days. Metallographic examination showed no interaction and the X-ray patterns were again that of tungsten and zinc. Thus, no evidence for the existence of intermediate phases in the zinc-tungsten system was found.

Figure 37

THE SOLUBILITY OF URANIUM IN ZINC-MAGNESIUM MELTS IN THE TEMPERATURE AND COMPOSITION RANGE IN WHICH THE EQUILIBRIUM SOLID PHASE IS URANIUM

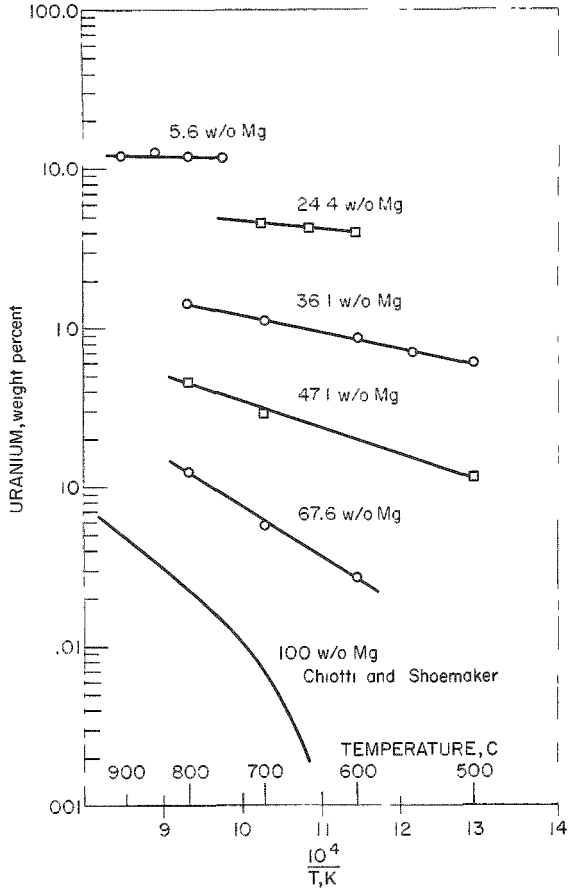

The Zinc-Magnesium-Uranium System

(A. E. Martin and C. Wach)

Additional solubility experiments were carried out with the zinc-magnesium-uranium system at magnesium levels of about 47.1 and 67.6 w/o. At these relatively high magnesium contents, all of the data obtained were in the temperature range where the equilibrium solid phase was elemental uranium. In previous studies (see ANL-6543, pp. 93 to 94; ANL-6477, pp. 93 to 94), uranium was the equilibrium solid phase only for data obtained at relatively high temperatures.

All of the solubility data obtained in experiments in which uranium was the equilibrium solid phase are plotted in Figure 37 together with similar data from the literature[26] about the magnesium-uranium system. From the figure it may be deduced that the temperature coefficient of solubility increases with increasing magnesium content, and that the uranium solubility decreases with increasing magnesium content at a given temperature. Thus, in the range in which the primary crystallizing phase is uranium, the solubility relationships are relatively simple. However, as indicated in a previous report (ANL-6477, pp. 93 to 94), the solubility relationships are more complicated in composition and temperature regions where other solid phases are in equilibrium with the melt.

[25] Schablaske, R., and Homa, M., private communication.

[26] Chiotti, P., and Shoemaker, H. E., Ind. and Eng. Chem. 50, 137-140 (1958).

A ternary intermetallic phase has been observed in the zinc-magnesium-uranium system. Crystals of the ternary phase have been isolated from ingots by electrolytic etching. Chemical analyses of samples recovered from two ingots were as follows:

	Uranium (w/o)	Zinc (w/o)	Magnesium (w/o)
Ingot No. 1	22.83	64.14	10.06
Ingot No. 2	23.0	65.7	10.12
Average	22.9	64.9	10.09

This average composition of the ternary phase corresponds to the empirical formula $UZn_{10.3}Mg_{4.3}$. X-ray diffraction examination* indicated that this phase has a hexagonal lattice with parameters a = 14.58 Å and c = 8.68 Å. Thermal analysis and metallographic examinations have shown that the primary crystallization field of this ternary phase in the ternary diagram is bounded by the fields of uranium, $MgZn_2$, and the delta phase (U_2Zn_{17}). This ternary phase does not have a maximum melting point but, instead, decomposes peritectically on heating. The peritectic temperatures range from 400 to about 570 C. This phase cannot form on cooling from melts containing more than 41 percent magnesium. The ternary phase has most commonly been observed as a peritectic reaction layer on delta-phase crystals.

2. Thermodynamic Studies

Thermodynamic functions for key elements in liquid metal solvents and for the more important solid intermetallic phases are being measured by two methods. The use of galvanic cells has proved to be especially useful for the measurement of activities in liquid metal solutions as well as for the determination of the free energy of formation of the equilibrium solid phase in solid-liquid, two-phase regions. On the other hand, for systems composed of several well-defined intermetallic phases, measurement of the decomposition pressure by the recording effusion balance is proving to be very useful. The two methods supplement each other.

Studies of the plutonium-zinc system are underway by means of the galvanic cell method. The effusion method is being used to study systematically the light rare earth metal-zinc and -cadmium systems. The results for the neodymium-zinc system are presented below.

*The X-ray diffraction studies were performed by R Schablaske and B. S. Tani of the X-ray Diffraction and Spectroscopy Group.

Zinc-Neodymium System (Effusion Studies)
(E. Veleckis and E. Van Deventer)

No literature information is available pertaining to the phase relationships in the zinc-neodymium system. The behavior of the system is generally expected to be similar to that of other light rare earth-zinc systems. Recent effusion studies, however, have indicated that significant variations may occur among the rare earths in their ability to form compounds with zinc. In the present report, the effusion results for the zinc-neodymium system are presented, and a comparison of the data with those available for other light rare earth-zinc systems is made.

Figure 38
ZINC-NEODYMIUM SYSTEM. ISOTHERM AT 531 C

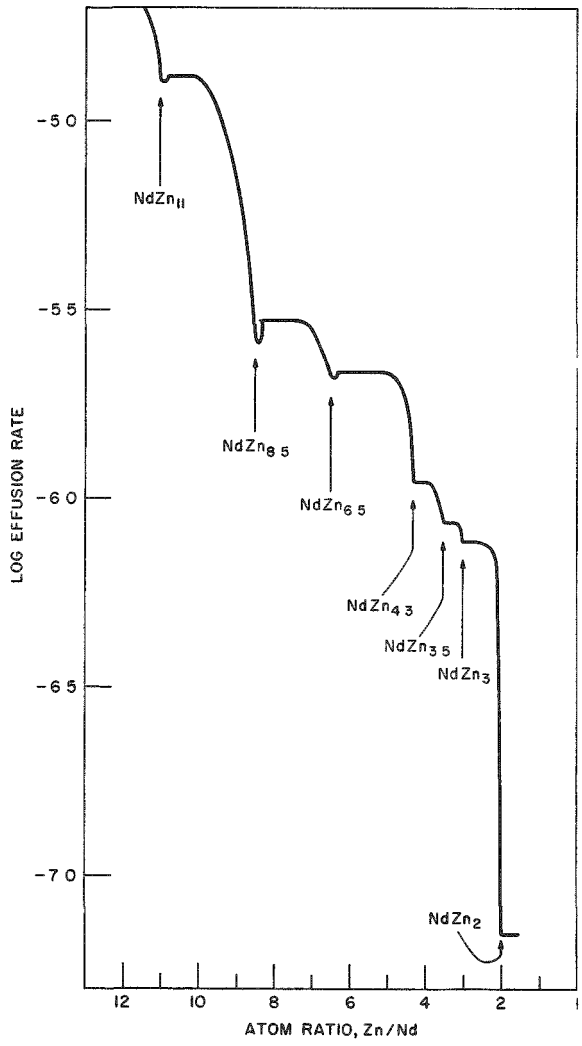

A typical effusion isotherm at 531 C is shown in Figure 38, in which the logarithm of the effusion rate (g/sec) is plotted against the zinc: neodymium atom ratio. The curve is comprised of a series of descending steps, of which the horizontal portions correspond to the heterogeneous phase fields. The points at which the horizontal portions of the curve intersect the descending portions correspond to the compositions of the intermetallic compounds. The figure shows that at 531 C the following phases succeed one another: $NdZn_{11}$, $NdZn_{8.5}$, $NdZn_{6.5}$, $NdZn_{4.3}$, $NdZn_{3.5}$, $NdZn_3$, and $NdZn_2$.

This effusion experiment was made with a zinc-neodymium alloy that was not heated above 500 C during its preparation. Experiments made with samples that were exposed to higher temperatures (e.g., samples heated for 2 hr at 900 C followed by a 14-day annealing period at 500 C) failed to yield $NdZn_{11}$. Instead, a phase with a wide composition range which extended from $NdZn_{8.5}$ to $NdZn_{12}$ was formed. X-ray diffraction analysis showed that this phase is analogous to a phase observed in the zinc-uranium system.[27] Apparently, the zinc-neodymium system undergoes a solid-state

[27] Veleckis, E., Rosen, C. L., and Feder, H. M., J. Phys Chem. 65, 2127 (1961).

transformation above 500 C. Although the conversion of $NdZn_{11}$ to $NdZn_{8.5-12}$ is readily accomplished, the reverse process appears to be very sluggish and could not be achieved even after prolonged annealing at 500 C of alloys which had been exposed to higher temperatures.

A summary of the intermetallic phases found in the lanthanum-, cerium-, praseodymium- and neodymium-zinc systems is shown in Table 19. Previous effusion data for the lanthanum-zinc system (see ANL-6596, p. 114) and revised data* for the cerium-zinc and praseodymium-zinc systems are incorporated in the table. X-ray diffraction analysis has shown that a total of twelve different phase types exist in these systems. In Table 19, the phases belonging to a particular type are listed in the horizontal rows. Common to all four systems are the types MZn, MZn_2, $MZn_{\sim 7}$, $MZn_{8.5}$, and MZn_{11}. The phases MZn_4 and MZn_{13} are peculiar to lanthanum, $MZn_{8.5-12}$ occurs only with neodymium, and only cerium, praseodymium, and neodymium exhibit MZn_3, $MZn_{3.6}$, and $MZn_{4.3}$. The $MZn_{5.25}$ phase occurs with lanthanum, cerium, and probably with praseodymium, but not with

Table 19

INTERMETALLIC PHASES FOUND IN SOME LIGHT RARE EARTH-ZINC SYSTEMS

La	Ce	Pr	Nd
$LaZn_{13}$	-	-	-
-	-	-	$(NdZn_{8.5-12})$
$(LaZn_{11})$[a]	$CeZn_{11}$	$PrZn_{11}$	$NdZn_{11}$
$LaZn_{8.5}$	$CeZn_{8.5}$	$PrZn_{8.5}$	$NdZn_{8.5}$
$LaZn_{7.25}$	$CeZn_7$	$PrZn_7$	$NdZn_{6.5}$
$LaZn_{5.25}$	$CeZn_{5.25}$	$(PrZn_{5.25})$	-
-	$CeZn_{4.4}$	$PrZn_{4.3}$	$NdZn_{4.3}$
$LaZn_4$	-	-	-
-	$CeZn_{3.6}$	$PrZn_{3.6}$	$NdZn_{3.5}$
-	$(CeZn_3)$	$PrZn_3$	$NdZn_3$
$LaZn_2$	$CeZn_2$	$PrZn_2$	$NdZn_2$
LaZn	CeZn	PrZn	(NdZn)

[a] Parentheses represent partial identification.

*Recent re-runs of the cerium-zinc and praseodymium-zinc systems with smaller effusion crucible orifices (0.008-in. dia as compared with 0.016-in. dia) have necessitated revision of some of the results of previous effusion studies (see ANL-6333, p. 116; ANL-6413, p. 96).

neodymium. The phases MZn, $MZn_{5.25}$, $MZn_{8.5}$, $MZn_{8.5-12}$, MZn_{11}, and MZn_{13} are of known structural type. The remaining phases exhibited distinguishable diffraction patterns, but were not structurally identified. Small variations in the stoichiometry of the $MZn_{4.3}$ and $MZn_{3.6}$ phase types are attributed to the experimental errors. The significant changes observed for the $MZn_{\sim 7}$ type, however, are outside the error limits and may indicate a solubility range.

3. Magnetic Studies of Intermetallic Compounds
(F. Cafasso and D. Gruen*)

The magnetic susceptibilities of a series of isomorphous and magnetically dilute intermetallic compounds AB_{11} where A is either a rare earth or actinide element and B is cadmium, are being measured in a joint effort of the Chemical Engineering and Chemistry Divisions. Measurements with the systems $CeCd_{11}$, $NdCd_{11}$ and UCd_{11} were reported earlier.** Preliminary measurements on the $ThCd_{11}$ system are reported below.

An ingot of $ThCd_{11}$ was prepared by melting the pure metals in the indicated proportion together. Examination by X-ray powder methods showed this preparation to be $ThCd_{11}$. A section of this ingot was powdered and used for the magnetic measurements.

Preliminary measurements were made at both room temperature and 77.2 K. The data collected at maximum field strength are given below for both temperatures. A small negative force was measured on a $ThCd_{11}$ sample which was contained in a quartz ampoule and which in turn was enclosed in a copper capsule. When the corrections for the quartz and copper containers were made, a small positive force of about 0.2 mg resulted. The magnitude of this force did not change significantly with temperature.

Temp (K)	Measured Force on Sample and Containment Materials (mg)	Quartz Correction (mg)	Copper Capsule Correction (mg)	Corrected Force on Sample (mg)	Gram Susceptibility $g\chi_{ThCd_{11}} \times 10^6$
295.2	-0.162	-0.182	-0.184	0.204	0.40
77.2	-0.127	-0.182	-0.169	0.224	0.44

*Cooperating Chemist - Chemistry Division.

**Measurements may be found for the $CeCd_{11}$ system in ANL-6287, p. 118, for the $NdCd_{11}$ system in ANL-6333, p. 118, and for the UCd_{11} system in ANL-6596, p. 114.

The susceptibility of $ThCd_{11}$ appears to be reasonably temperature independent. Magnetic behavior of this type is indicative of a system with no unpaired spins. The small positive force which was measured is no doubt associated with the weak temperature-independent paramagnetism of the conduction electrons in this alloy system. When a correction for the diamagnetism of cadmium in the alloy is made, the susceptibility of thorium in $ThCd_{11}$ is calculated to be 0.54×10^{-6} emu/g. This value is in fair agreement with the value of 0.42×10^{-6} emu/g which has been reported for the susceptibility of thorium metal at room temperature.

II. FUEL CYCLE APPLICATIONS OF VOLATILITY AND FLUIDIZATION TECHNIQUES*

The development of a Direct Fluorination Volatility Process for the recovery of uranium and plutonium from irradiated nuclear reactor fuels was continued. In this process, uranium and plutonium dioxides are fluorinated to produce hexafluoride products, which are then decontaminated by volatility techniques.

Laboratory studies have been concerned with the development of a fluorination scheme whereby optimum removals of uranium and plutonium from the inert solids can be achieved. This phase of the investigation is economically important, since the inert solids will be discarded as waste.

In the development of the Direct Fluorination process, current emphasis is placed on the evaluation of a two-zone process technique as a means of avoiding caking tendencies. In this scheme, a mixture of oxygen and nitrogen is introduced into the lower reaction zone formed by the uranium dioxide pellet bed, and fluorine is introduced into the upper zone which consists of a fluidized bed of alumina grain. The alumina, which also fills the voids of the pellet bed, is fluidized by the mixture of oxygen and nitrogen. This mixture is introduced into the system at the bottom of the pellet zone, while fluorine is introduced at the top of the pellet zone. Uranium oxide (U_3O_8) fines are formed in the lower zone and transported into the upper zone, where they are removed by fluorination.

Additional studies of a fluidization-volatility scheme for reprocessing enriched uranium-zirconium alloy fuels were carried out. This processing scheme involves first a direct hydrochlorination (or chlorination) reaction while the alloy is submerged in an inert fluid-bed medium (currently Norton Type RR Alundum). This step produces volatile zirconium tetrachloride and permits ready separation of the uranium from the bulk alloying material. A subsequent fluorination step to volatilize the uranium as the hexafluoride provides the means of product recovery.

Studies of a fluid-bed pyrohydrolysis reaction of zirconium tetrachloride with steam were continued. The tetrachloride, which is produced during the chlorination of uranium-zirconium alloy fuels, is converted to the solid dioxide, a form which is more convenient for ultimate waste disposal.

Additional studies were made of the conversion of uranium hexafluoride to high-density uranium dioxide by the simultaneous reaction of the hexafluoride with steam and hydrogen.

Supporting studies are also underway to obtain design data and to clarify fluidization mechanisms involved in particular equipment configurations used in the Direct Fluorination Process.

*A summary of this section is given on pages 19 to 25.

A. Laboratory Investigations of Fluoride Volatility Processes (J. Fischer)

1. Fluorination of Plutonium-Uranium Oxides (R. L. Jarry, T. D. Baker, J. J. Stockbar)

In the Direct Fluorination Volatility Process,[28] declad uranium dioxide fuel will be fluorinated in a fluidized Alundum bed to convert the uranium and plutonium to their respective hexafluorides. In the procedure as now conceived, a typical charge to the fluid bed fluorinator contains 100 kg of uranium, 0.4 kg of plutonium, about one kg of fission product elements, and 30 kg of Alundum as the inert fluidized solid. The laboratory work has been directed toward devising a fluorination scheme to achieve the removal of uranium and plutonium as hexafluorides from synthetic mixtures, the compositions of which are similar to those of the charge which will be used in the fluid-bed fluorinator. After fluorination, the solids remaining in the fluorinator will be discarded as waste.

Work outlined in previous quarterly reports (see ANL-6379, pp. 137-145; ANL-6413, pp. 110-115; ANL-6477, pp. 106-113; ANL-6543, pp. 108-114; ANL-6569, pp. 93-99) has led to the conclusion that Alundum is a satisfactory inert material for use in the fluidized bed. This conclusion is based on the fact that uranium and plutonium can both be rather completely volatilized by fluorination. In addition, the work has shown that the fluorination is best carried out in two stages with low fluorine content (10 v/o) and relatively low temperature (450 C) initially, followed by a higher fluorine content (50-75 v/o) and a higher temperature (550 C). The use of this procedure has resulted in removal of essentially all of the uranium and about 99 percent of the plutonium from the mixtures of uranium dioxide-plutonium dioxide containing fission product oxides with Alundum.

Experimental work with a two-stage procedure in which the uranium dioxide-plutonium dioxide solid solution was oxidized prior to fluorination is described below. Oxidation of the solid solution of plutonium dioxide in uranium dioxide results in a mixture of plutonium dioxide in uranosic oxide (U_3O_8). The uranosic oxide is in the form of a free-flowing powder which has a surface area of 6.2 m^2/g.

Oxidation of uranium dioxide fuel prior to fluorination can serve two other purposes. First, since the spent uranium dioxide reactor fuel may contain cracked pellets and fragments of pellets, the oxidation, in addition to allowing less severe fluorination conditions, serves to produce a uniform feed for the fluidized bed fluorinator. Secondly, the oxidation step

---

[28] Jonke, A. A., Fischer, J., and Mecham, W., Fluoride Volatility Processing of Low Enriched Fuels, Trans. Am. Nuclear Soc., 4 (2), 184-185 (1961).

may also be employed as a means of initiating the separation of the uranium and plutonium oxides from stainless steel cladding as considered by Atomics International.[29]

Solid solutions of plutonium dioxide in uranium dioxide, which contained about 0.4 w/o plutonium and about 0.8 w/o of fission product element oxides, were used in experiments. The preparation of the first mixture, designated Batch IV, was described in a previous report (see ANL-6569, p. 97).* The uranium dioxide-plutonium dioxide mixture was fabricated into pellets, $\frac{1}{4}$ in. in diameter and $\frac{1}{4}$ in. long, and sintered at about 1700 C by J. Handwerk of the Metallurgy Division.

A second mixture, Batch V, was prepared by the coprecipitation of ammonium diuranate and plutonium hydroxide, followed by reduction at 1000 C. This method of preparation of a solid solution of plutonium dioxide in uranium dioxide was described in a previous report (see ANL-6379, p. 139). A portion of the mixture of ten fission product element oxides used for Batch IV was blended with the solid solution powder. The relative quantities of these fission product element oxides in the mixture were given in a previous report (see ANL-6477, p. 110).

The fluorine used in these experiments was about 99 percent pure. The oxygen and nitrogen used were passed through Molecular Sieves to remove water.

The horizontal tubular reactor and associated apparatus used in the experiments have been described previously (ANL-6145, p. 101). The uranium dioxide-plutonium dioxide solid solution was placed in a nickel boat in the horizontal tubular reactor, heated to 450 C, and a gas containing 20 v/o oxygen in nitrogen was passed over the sample for a period of 3 hr. Following the oxidation period, the nickel boat containing the oxidized mixture was removed from the reactor. After adding the proper amount of 60 mesh Alundum to the mixture, the boat was returned to the reactor for the fluorination cycle. Upon completion of the fluorination reaction, the entire Alundum residue was submitted for uranium and plutonium analyses.

Table 20 summarizes the results obtained for various combinations of fluorination time, temperature, and gas mixture. In some cases, the items listed are average values for several experiments. The complete data are listed in Tables 21, 22, and 23. Fluorination of the oxidized mixture of Batch V with Alundum for 2 hr at 450 C, by 10 v/o fluorine, resulted in the removal of about 84 percent of the plutonium originally present in the

---

[29] Guon, J., et al., Low Decontamination Reprocessing Studies on Irradiated Uranium Dioxide Reactor Fuels, NAA-SR-7136 (Dec 15, 1961).

*Prepared by the addition of UO_2 and FP III mixture (which contains the following oxides: BaO, ZrO_2, La_2O_3, CeO_2, Y_2O_3, Nd_2O_3, Sm_2O_3, Pr_6O_{11}, Eu_2O_3, and Gd_2O_3) to the UO_2-PuO_2 solid solution containing about 4 w/o Pu. Analyses of Batch IV gave 89 percent U and 0.33 percent Pu.

solid mixture (see Item 2, Table 20, and Experiments 178 and 182, Table 21). The enhanced reactivity of the oxidized uranium dioxide-plutonium dioxide solid solution is made evident when the results given in Item 2, Table 20 are compared with the results given in Item 1, Table 20 (Experiment 187, Table 21). The latter results were obtained in an experiment in which the uranium dioxide-plutonium dioxide solid solution was not oxidized prior to fluorination. In this experiment, only 31 percent of the original plutonium was removed from the solid mixture.

Table 20

SUMMARY OF RESULTS OF FLUORINATIONS OF OXIDIZED URANIUM DIOXIDE-PLUTONIUM DIOXIDE MIXED WITH ALUNDUM INERT SOLIDS

Oxidation Conditions: 450 C; 3 hr; 20 v/o O_2, 80 v/o N_2
Gas Flow Rate: 800 ml/min (linear velocity of gas: 5 ft/sec)
System Pressure: one atm

Item No.	Temp (C)	Time (hr)	Fluorinating Gas Mixture			Percent Original Pu Removed
			v/o F_2	v/o O_2	v/o N_2	
1[a]	450	2	10	25	65	31
2[b]	450	2	10	25	65	84[c]
3[d]	450	2	10	25	65	
	550	5	75	25		98.6[c]
4[e]	450	10	10	25	65	
	550	10	75	25		99.4[c]
5[d]	500	1	10	25	65	
	500	5	100			97.2
6[d]	450	1	10	25	65	
	450	4	100			90.4
7[d]	550	1	10	25	65	
	550	4	100			96.0

[a]The $(U\text{-}Pu)O_2$, Batch V, used in this experiment was not oxidized prior to fluorination. The complete data are given in Table 21, Experiment 187.

[b]The complete data for the two experiments averaged in this item and for others carried out for longer periods of time are listed in Table 21.

[c]These values are averages for several experiments.

[d]Complete data for these runs are given in Table 22.

[e]Complete data for the seven experiments averaged here are contained in Table 23.

Table 21

SINGLE-STEP FLUORINATION OF OXIDIZED URANIUM DIOXIDE-PLUTONIUM DIOXIDE MIXED WITH ALUNDUM INERT SOLIDS

Initial Solid Mixture for Each Experiment:

3.42 g $(U\text{-}Pu)O_2$, Batch V,[a] which contains 2965 mg U, 10.9 mg Pu, and approximately 30 mg fission product oxides; this was mixed with 0.90 g Al_2O_3, 60 mesh

Reaction Conditions:
(1) Oxidation; 450 C; 3 hr; 20 v/o O_2, 80 v/o N_2
(2) Fluorination; 450 C; 10 v/o F_2, 25 v/o O_2, 65 v/o N_2

Gas Flow Rate: 800 ml/min (linear velocity of gas: 5 ft/sec)

System Pressure: one atm

Exp. No.	Time (hr)	Residue					Percent of Original Pu Removed
		Wt U (mg)	Wt Pu (mg)	U (w/o)	Pu (w/o)	wt (g)[b]	
178	2	0.08	2.54	0.008	0.27	0.945	77
182	2	0.12	1.12	0.013	0.12	0.930	90
						average	84
187[c]	2	32	7.5	3.14	0.741	1.01	31
181	4	0.06	1.14	0.006	0.12	0.955	90
180	6	0.07	0.43	0.008	0.10	0.930	92
183	8	0.08	1.30	0.009	0.14	0.930	87

[a] $(U\text{-}Pu)O_2$ Batch V. Prepared by the coprecipitation of ammonium diuranate and plutonium hydroxide followed by reduction at 1000 C to form a solid solution of PuO_2 in UO_2. To this solid solution a mixture of ten fission product element oxides, designated FP III, was added (FP III contains BaO, ZrO_2, La_2O_3, CeO_2, Y_2O_3, Nd_2O_3, Sm_2O_3, Pr_6O_{11}, Eu_2O_3, and Gd_2O_3). One gram of Batch V contains 3.2 mg Pu, 867 mg U, and about 10 mg of fission product elements.

[b] The theoretical weight of the residue would be 0.93 g. In those cases where the residue weights were greater than 0.93 g, the increase in weight is attributed to the presence of NiF_2.

[c] The $(U\text{-}Pu)O_2$ used in this run was not oxidized.

Table 22

EFFECT OF TEMPERATURE, TIME, AND GAS COMPOSITION ON TWO-STEP FLUORINATION OF OXIDIZED URANIUM DIOXIDE-PLUTONIUM DIOXIDE MIXED WITH ALUNDUM

Initial Solid Mixture for Each Experiment:
3.42 g of $(U\text{-}Pu)O_2$, Batch V,[a] which contains 10.9 mg Pu, 2956 mg U, and approximately 30 mg of fission product elements; this was mixed with 0.90 g Al_2O_3, 60 mesh

Oxidation Conditions: 450 C; 3 hr; 20 v/o O_2, 80 v/o N_2

Gas Flow Rate: 800 ml/min (linear velocity of gas: 5 ft/sec)

System Pressure: one atm

Exp. No.	Time (hr)	Temp (C)	Fluorinating Gas Mixture			Residue			Percent of Original Pu Removed
			v/o F_2	v/o O_2	v/o N_2	Wt Pu (mg)	Pu (w/o)	Wt[b] (g)	
184	2	450	10	25	65	0.16	0.016	0.98	98.6
	5	550	75	25					
185	2	450	10	25	65	0.18	0.019	0.97	98.3
	5	550	75	25					
189	2	450	10	25	65	0.09	0.009	1.00	99.2
	5	550	75	25					
190	2	450	10	25	65	0.17	0.018	0.97	98.4
	5	550	75	25				Average value	98.6 ± 0.3
188	1	450	10	25	65	1.04	0.11	0.95	90.4
	4	450	100						
186	1	550	10	25	65	0.44	0.045	0.98	96.0
	4	550	100						
191	1	500	10	25	65	0.31	0.032	0.96	97.2
	5	500	100						

[a]See footnote (a) Table 21.

[b]See footnote (b) Table 21.

Table 23

TWO-STEP FLUORINATION OF OXIDIZED URANIUM DIOXIDE-PLUTONIUM DIOXIDE MIXED WITH ALUNDUM

Reaction Conditions:

Oxidation: 450 C; 3 hr; 20 v/o O_2, 80 v/o N_2

Fluorination: 450 C; 10 hr; 10 v/o F_2, 25 v/o O_2, 65 v/o N_2
550 C; 10 hr; 75 v/o F_2, 25 v/o O_2

Gas Flow Rate: 800 ml/min (linear velocity of gas 5: ft/sec)

System Pressure: one atm

		Initial Solid Mixture			Residue			
Exp No.	$(U-Pu)O_2$ [a] Batch No.	Wt $(U-Pu)O_2$ (g)	Wt Pu (mg)	Wt Al_2O_3 (g)	Wt (g)	Pu (w/o)	Wt Pu (mg)	Percent of Original Pu Removed
171	IV	2.830	8.17	0.850	0.900	0.006	0.05	99.4
172[b]	IV	2.915	9.45	0.870	0.895	0.008	0.07	99.3
173	IV	2.795	9.08	0.840	0.895	0.007	0.06	99.3
174	V	3,420	10.9	0.900	0.855	0.009	0.08	99.3
175	IV	3.280	10.6	0.865	0.945	0.006	0.06	99.4
176	IV	2.905	9.45	0.870	0.915	0.006	0.05	99.5
177[c]	IV	2.790	9.07	0.825	0.830	0.003	0.02	99.8

[a](1) $(U-Pu)O_2$ Batch IV. In the form of $\frac{1}{4}$ in. by $\frac{1}{4}$ in. pellets. Original mixture prepared by the addition of UO_2 and FP III mixture [see footnote (a) Table 21] to a $(U-Pu)O_2$ mixture containing about 4 w/o Pu. One gram of Batch IV contains 3.25 mg Pu, 890 mg U, and about 10 mg of fission product elements.

(2) For preparation of $(U-Pu)O_2$ Batch V, see footnote (a) Table 21.

[b]Fluorination conditions:
1st period 450 C; 15 hr; 10 v/o F_2, 25 v/o O_2, 65 v/o N_2
2nd period 650 C; 5 hr; 75 v/o F_2, 25 v/o O_2

[c]The 60 mesh Alundum used in this experiment contained 0.26 percent Fe, 0.35 percent Ni, and 0.33 percent Cr as chlorides which were formed during the chlorination of stainless steel.

Item 3, Table 20, gives the average value 98.6 percent for the removal of plutonium based on four experiments (Experiments 184, 185, 189, and 190, Table 22) in which two fluorination periods were used. In the first period, fluorination was carried out for 2 hr at 450 C with 10 v/o fluorine; in the second period, fluorination was carried out for 5 hr at 550 C with 75 v/o fluorine. The average removal, 98.6 percent, can be compared with the best value of 98.7 percent obtained in previously reported experiments (see ANL-6569, p. 95, Table 22, Item 5), in which a nonoxidized solid solution of uranium dioxide-plutonium dioxide was fluorinated for 10 hr at 450 C with 10 v/o fluorine, followed by a 5-hr fluorination period in which 75 v/o fluorine was used. Increasing each of the two fluorination periods to 10 hr, the first period at 450 C and the second at 550 C, resulted in an average removal of 99.4 percent plutonium (see Item 4, Table 20, and Experiments 171 to 177, Table 23).

In one experiment (see Item 5, Table 20), two fluorination periods at 500 C were carried out: the first for one hour with 10 v/o fluorine, and the second for 5 hr with 100 percent fluorine. This run resulted in a 97.2 percent removal of plutonium from the solid mixture.

In two other experiments (see Items 6 and 7, Table 20), each of the two fluorination periods were again carried out at the same temperature. The temperature in one experiment was 450 C and in the other was 550 C. A removal of 90.4 percent plutonium was obtained in the experiment at 450 C and a removal of 96.0 percent was obtained in the experiment at 550 C.

From the data given in this and previous reports (ANL-6145, p. 100; ANL-6379, p. 137; ANL-6413, p. 110; ANL-6477, p. 106; ANL-6543, p. 108; ANL-6569, p. 93) on the fluorination of uranium dioxide-plutonium dioxide solid solutions mixed with an inert solid, several observations can be made regarding the optimum conditions for the removal of plutonium. Of the materials tested, Alundum (refractory grain alumina) was found to be the best material for use as an inert solid in the fluorinations, since its use resulted in the lowest retention of plutonium on the solid residues. In the initial portion of the fluorination process, in which most of the uranium is removed from the solid mixture, a low temperature (450 C) and a low concentration of fluorine (10 v/o) were found to be desirable. However, a higher temperature (550 C) and a higher fluorine concentration (75 v/o) were found to be desirable for the effective removal of plutonium in the latter portion of the fluorination process. A two-step procedure, in which the uranium dioxide-plutonium dioxide is first oxidized and then fluorinated in two stages, one at 450 C and the other at 550 C, was found to yield plutonium removals of 99 percent or better.

The work on the static-bed fluorinations of materials of interest to the Direct Fluorination Volatility Process is being terminated. Future work will be concerned with laboratory-scale fluid-bed operations.

2. Fluid-bed Fluorination of Plutonium-Uranium Dioxide

(G. Manevy,* R. L. Jarry, A. V. Hariharan,** J. Riha, J. J. Stockbar)

In the conceptual flowsheet of the Direct Fluorination Volatility Process, plutonium and uranium are removed from spent oxide fuels as plutonium hexafluoride and uranium hexafluoride by fluorination at 450 to 550 C. This process will employ a fluid-bed reactor for the fluorination step. The laboratory work on process development (described in the previous section) has been concerned mainly with studies of plutonium removal from mixtures of alumina, uranium dioxide, plutonium dioxide, and fission product element oxides, by fluorination in static beds at 450 C to 550 C. These studies have indicated that the removal of plutonium from the Alundum bed increased when mixtures containing uranium dioxide-plutonium dioxide solid solutions were oxidized to uranosic oxide-plutonium dioxide mixtures prior to fluorination.

Laboratory development work is now being directed toward the study of fluid-bed fluorinations. The procedure will consist of oxidizing uranium dioxide to produce powdered uranosic oxide, and then feeding the powder into the fluidized bed contained in a $1\frac{1}{2}$-in.-diameter fluorination reactor. The uranosic oxide powder will be fed into the fluorination reactor either by gas transport or by a mechanical feeding device. Initially, the experiments will be made with uranium oxides. Work with plutonium-containing material will be started after the apparatus has been tested and the experimental conditions have been defined. A two-zone oxidation-fluorination reactor for the study of the overall process will be constructed when sufficient data on the fluorination step become available.

Preliminary results of tests on the gas distribution in the $1\frac{1}{2}$-in. fluidized-bed reactor and on the feeding of uranosic oxide powder into the fluidized bed reactor indicated that satisfactory fluidization of the solids and distribution of the gas were obtained when the fluidizing gas and uranosic oxide entered the bed through an annular inlet. A double-cone gas distributor, shown in Figure 39, was developed for this work. The annular inlet was provided by the interposition of metal spacers between the bottom surface of the double-cone gas distributor and the conical bottom of the reactor. These spacers held the double-cone $\frac{1}{16}$ in. away from the conical bottom, and the fluidizing gas containing the U_3O_8 powder passed into the bed through the slots between eight metal spacers. Fluorine entered the gas distributor by means of a central tube and then passed into the bed through eight holes drilled in the upper part of the distributor, as shown in Figure 39. With this system, 20g of powder, having an average particle diameter of 6μ, could be fed in one minute into a 5-in.-high, 60 mesh Alundum bed. The flow rate of the fluidizing gas was approximately 0.5 ft^3/min measured at room temperature.

---

*Appointee from Atomic Energy Commission - France.

**Affiliate, International Institute of Nuclear Science and Engineering.

It was necessary to devise a means for feeding uranosic oxide powder into the fluidizing gas line. A vibratory powder feeder, shown in Figure 40, was tested. The body of the feeder, containing the uranosic oxide, was a hollow cylinder with a conical bottom. A conical plug was vibrated by means of a rod which passed through a bellows on the cover of the container. The eccentric attached to the shaft of a variable-speed motor moved the rod up and down to give a vibrating motion to the plug. The powder, released by the vibrating plug, dropped down into the gas stream and was then injected into the fluidized bed, as shown in Figure 39. Tests of this feeder showed that it could be used in the range between 2 and 20 g/min, with 6-μ-diameter uranosic oxide powder.

Figure 39

GAS DISTRIBUTOR FOR ONE AND ONE-HALF-INCH FLUIDIZED BED REACTOR

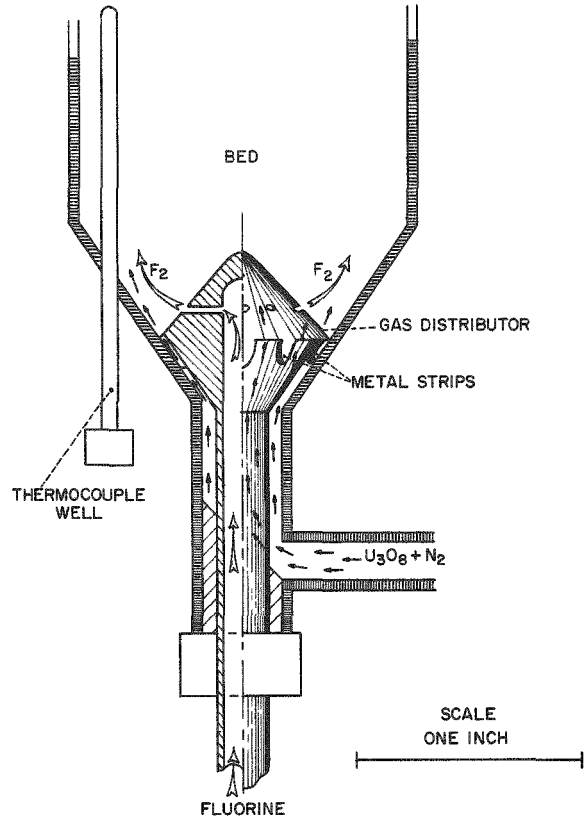

108-6288

Figure 40

VIBRATORY POWDER FEEDER FOR FLUIDIZED BED REACTOR

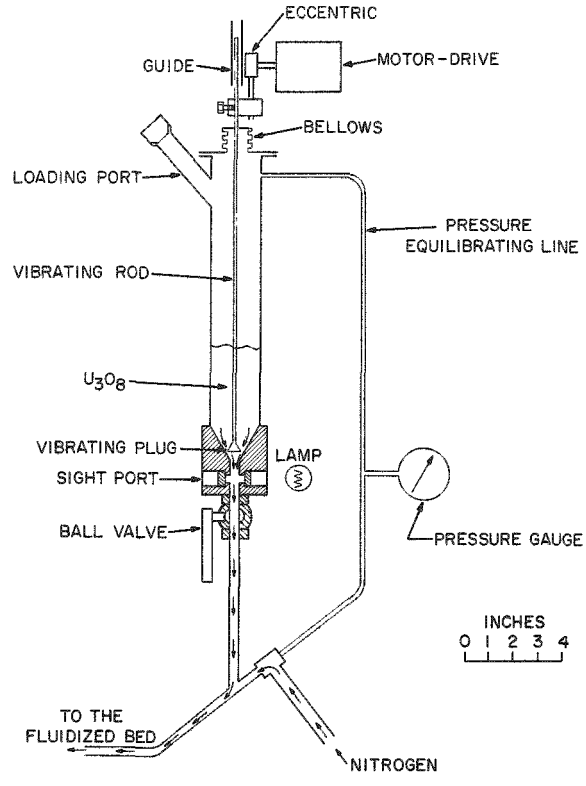

108-6287

B. Engineering-scale Investigation of Fluoride Volatility Processes (A. A. Jonke)

1. Direct Fluorination of Uranium Dioxide Fuel (W. J. Mecham, J. D. Gabor, L. Anastasia, J. Wehrle, R. Kinzler, and A. Rashinskas)

Development of the Direct Fluorination Process applied to uranium dioxide fuel has continued. In this process, the uranium and plutonium dioxides from discharged reactor fuel are reacted with fluorine directly to produce hexafluoride products, which are then decontaminated by volatility techniques. The reaction is carried out in a fluidized bed in which pellets (or pellet fragments) of uranium dioxide form a packed bed, with fluidization provided by means of inert solid (alumina grain) in the space above and in the voids of the pellet bed. The fluidization aids in the heat transfer and in the mixing of solid fines formed as intermediates or residues in the system. Engineering-scale studies thus far have been directed toward process optimization of the primary fluorination of uranium dioxide pellets. The major objectives of these studies have been to demonstrate short-time (less than 20 hr) batch fluorination and satisfactory fluorine utilization efficiency (greater than 75 percent) under practical operating conditions.

Early results (see ANL-6379, p. 161) showed that reaction control could be obtained when fluidization of the alumina is maintained. The total surface area of uranium solids reacting to form hexafluoride was found to be governed largely by the amount of intermediate uranium compounds present in the system. The intermediates, UO_2F_2 and U_3O_8, which are highly reactive, appear mostly as fine particles (~20 μ in diameter) of high specific surface area (see ANL-6477, p. 137). Accordingly, for pellet beds in which low fluorine efficiencies are obtained, the introduction of oxygen along with fluorine (one-zone system) has been shown to be capable of increasing both the reactivity of the system and the fluorine utilization (see ANL-6379, p. 162).

A 4.4-kg batch of pellets (6-in. initial pellet depth) has been completely fluorinated in a satisfactory manner in about 6 hr at 500 C; a gas recycle system was used to furnish oxygen and to minimize fluorine loss. This production rate is equivalent to about 41 lb UF_6/(hr)(sq ft of reactor cross section). Continuous feeding of pellets was also carried out successfully for nominal 6-in. pellet beds at 500 C with inlet oxygen concentration controlled at the 5 percent level (see Table 28, ANL-6596). Runs with deeper pellet beds (18-in.-deep initial batch charges) were, however, found to be subject to caking; and satisfactory fluorinations were carried out only at lower production rates, about 17 lb UF_6/(hr)(sq ft reactor cross-sectional area), as is shown in Table 28, ANL-6569. The most promising results with pellet beds of more than 6-in. depth were obtained with a two-zone reaction scheme (e.g., Run UOF-61, Table 29, ANL-6596).

In the two-zone operation, a mixture of oxygen and nitrogen is introduced at the bottom of the lower reaction zone of uranium dioxide pellets, and fluorine is introduced into an upper zone of fluidized alumina just above the uranium dioxide pellets. The alumina, which also fills the voids of the pellet bed, is fluidized by the mixture of oxygen and nitrogen. Uranium oxide (U_3O_8) fines are formed in the lower zone and transported into the upper zone, where they are removed by fluorination. One possible advantage of this scheme is that caking due to solids formation by the reaction of uranium hexafluoride with uranium oxides may be reduced. Another anticipated advantage is that the quality of fluidization in the upper zone will be improved by the absence of uranium dioxide pellets. Also, in the two-zone operation, only the oxidation reaction (ΔH = -26 kcal/gram mole uranium at 25 C) takes place in the pellet bed, while fluorination of the fines (ΔH = -231 kcal/gram mole uranium at 25 C) takes place in the upper, unhindered fluidized bed of Alundum. The more favorable heat removal obtained thereby should reduce the possibilities of sintering and of caking.

In the initial two-zone batch run (UOF-61, Table 29, ANL-6596) carried out previously with a 12-in. pellet bed at 500 C, good fluidization quality was achieved. The superficial gas rate in the pellet zone was 1.2 ft/sec (based on reactor cross-sectional area), and the oxygen concentration was 4 to 8 percent. Fluorine concentration in the upper zone was varied from 5 to 13 percent. The overall uranium hexafluoride production rate was 33 lb uranium hexafluoride/(hr)(sq ft), and overall fluorine utilization efficiency was 61 percent. In a subsequent run, UOF-62, the superficial gas velocity was lowered in order to determine the effect on fines elutriation from the upper zone of fluidized alumina. In this run, fluidization quality was poorer than that obtained during UOF-61, and the run was terminated before completion in order to examine the condition of the bed. A small portion of the alumina was caked. Of the 8.8 kg of pellets charged, the residue was found to consist of 0.50 kg of unreacted pellets and 0.89 kg of uranium intermediate fines. The caking and the accumulation of fines are believed to have been caused by a combination of rapid oxidation rates and nonuniform fines transport from the pellet zone. Absence of caking in Run UOF-61 (made under generally similar conditions) may have been due to the slightly higher gas rates used in that run. A summary and discussion of these earlier results was presented in the previous quarterly report, ANL-6596, pp. 135 to 146.

In the present period, continued emphasis has been placed upon evaluation of the two-zone oxidation-fluorination approach for batch fluorinations in a single vessel. However, because of the fines accumulation in the pellet zone and the poor fluidization quality during Run UOF-62, attention was directed to methods of reducing oxidation rates and improving fines transport from the pellet zone. Two methods of achieving a controlled reduction in oxidation rates in the pellet zone were tested:

1. use of back-diffusion to supply oxygen to the top of the lower reaction zone (i.e., the top of the pellet zone);

2. use of a lower temperature in the lower reaction zone than in the upper reaction zone.

In addition, preliminary tests were made in a glass mock-up column to study the effect of gas pulsing as a means of enhancing transport of oxide fines from the lower to the upper zone.

Oxygen Back-Diffusion

If only the topmost layer of pellets in the lower zone were exposed to oxygen, the overall rate of oxidation would be lowered and the oxides formed would be more directly transported to the upper zone. A test of this scheme was carried out in a 3-in.-diameter nickel reactor at 500 C. A 6-in.-deep charge of uranium dioxide was covered by a 24-in. bed of alumina grain. Nitrogen was the fluidization gas (0.8 cfm at 25 C and 1 atm). Oxygen was introduced through a $\frac{1}{4}$-in.-diameter tube just above the pellets at a rate sufficient to give a total gas composition of 25 m/o oxygen. Samples of the fluidized bed taken initially and after one hour gave uranium analyses of 0.21 and 0.16 w/o, respectively. It was concluded that oxidation was negligible under these conditions, and the back-diffusion approach was abandoned.

Reduction of Temperature in the Lower Reaction Zone

Although 500 C appears to be a satisfactory fluorination temperature, oxidation of uranium dioxide may be better controlled at lower temperatures. It appeared possible that the baffling effect of pellets in the lower zone would serve to restrict the axial movement of solids to an extent that a temperature gradient could be established in the lower zone; that is, the topmost pellets would be at a relatively high temperature because of their contact with the 500 C fluidized bed in the upper zone, while the pellets at lower elevations could be kept at lower temperatures by cooling the bottom of the reactor. Since the oxidation reaction has a rather high temperature coefficient, such a temperature gradient would be expected to have the desirable effect of limiting the oxidation to the topmost pellets only. A thermal gradient test was performed with a 12-in. pellet bed with 6 in. of fluidized Alundum below the bed and a 24-in. bed of Alundum above the pellets. Heat was supplied to the reactor wall adjacent to and above the pellets. Water-cooled coils attached to the bottom flange removed heat from the column in the lower portion of the reactor. The temperatures obtained are shown below:

Pellet Bed Height (in.)	Temperature (C)
0 (bottom)	170
4	310
8	370
12 (top)	410

Run UOF-63, which was performed with a longitudinal temperature gradient in the pellet bed, is described in a following section.

Gas-pulsing of Fluidized Packed Beds

Another method under consideration for the improved mixing and transport of fines from the pellet bed is pulsing of the gas flow introduced at the bottom of the pellet bed. Since a number of variables require consideration in a pulsed system, a brief experimental program was undertaken with a 3-in.-diameter Lucite-glass column in order to determine the effect of gas pulsing on a bed of $\frac{1}{2}$-in. uranium dioxide pellets and fluidized alumina. The effect of pulse frequency, pulse duration, and pressure on movement of the nonfluidized pellets and the fluidized phase was noted. The pulsing, of 0.1-sec duration and of frequencies ranging from 20 to 200 pulses per minute, was obtained from a gas supply independent of the fluidization gas supply and was controlled by an air-operated valve, a solenoid, and an electric timer. Nitrogen was used as both the fluidizing and pulsing gas in these tests.

Visual observations on the effectiveness of the pulse have been made at manifold pressures from 5 to 20 psig and fluidization velocities up to 1.5 ft/sec with 6- and 12-in. beds of pellets. Greater effectiveness of the pulse on solids movement was observed for higher manifold pressures (up to 20 psig) and for lower rates of the (uninterrupted) fluidizing gas flow. At the higher manifold pressures, momentary expansion of the pellet bed was noted. Possibly, this method could be applied to fluidized packed beds to promote solids mixing.

Two-zone Reactor Operation with Lowered Oxidation Temperature

In the initial two-zone oxidation-fluorination with longitudinal temperature gradients in the pellet bed (UOF-63), 91 percent of the uranium dioxide in a 12-in. bed of pellets reacted in 13.8 hr with an overall fluorine efficiency of 49 percent. Oxygen concentrations of 18 and 31 percent in nitrogen were passed through the pellets at a total gas flow of 1.1 cfm (25 C and 1 atm). In the fluorination zone, the total gas flow was 1.3 cfm. The gas contained 15 percent fluorine. The Alundum bed extended from 6 in. below to 24 in. (under static conditions) above the pellet bed.

With the fluid bed held at 525 to 550 C, a temperature gradient was obtained through the pellet bed such that the upper layer of pellets was initially at 400 C while the bottom of the pellet bed was at about 140 C. As the run continued, the top and bottom temperature of the pellet bed each increased about 100 C. Thus, in this run, pellet oxidation was carried out at a lower temperature than in previous (one- and two-zone) runs, and a higher concentration of oxygen in the fluidizing gas could be passed

through the pellets without excessive oxide fines production. The fact that oxidation occurred preferentially at the top of the pellet bed may also have been favorable. Internal pellet bed temperatures were monitored and recorded by means of a multipoint thermocouple assembly and recorder.

A plot of the temperatures at various elevations in the pellet bed and in the fluidized bed is shown in Figure 41. As the uppermost pellets were reacted, the relatively cool pellet bed surrounding a given thermocouple gradually was replaced by the heated fluid bed. This is indicated in Figure 41 as an overall increase in temperature at thermocouple positions 3, 4, and 5. The drop in temperature at the 5-hr mark resulted from a decrease in gas flow, which was caused by an obstruction in the off-gas scrubber system. This effect would not occur in a normal run.

Figure 41

BED TEMPERATURES DURING RUN UOF-63 - A TWO-ZONE OXIDATION-FLUORINATION OF URANIUM DIOXIDE PELLETS WITH A TEMPERATURE GRADIENT THROUGH THE PELLET ZONE

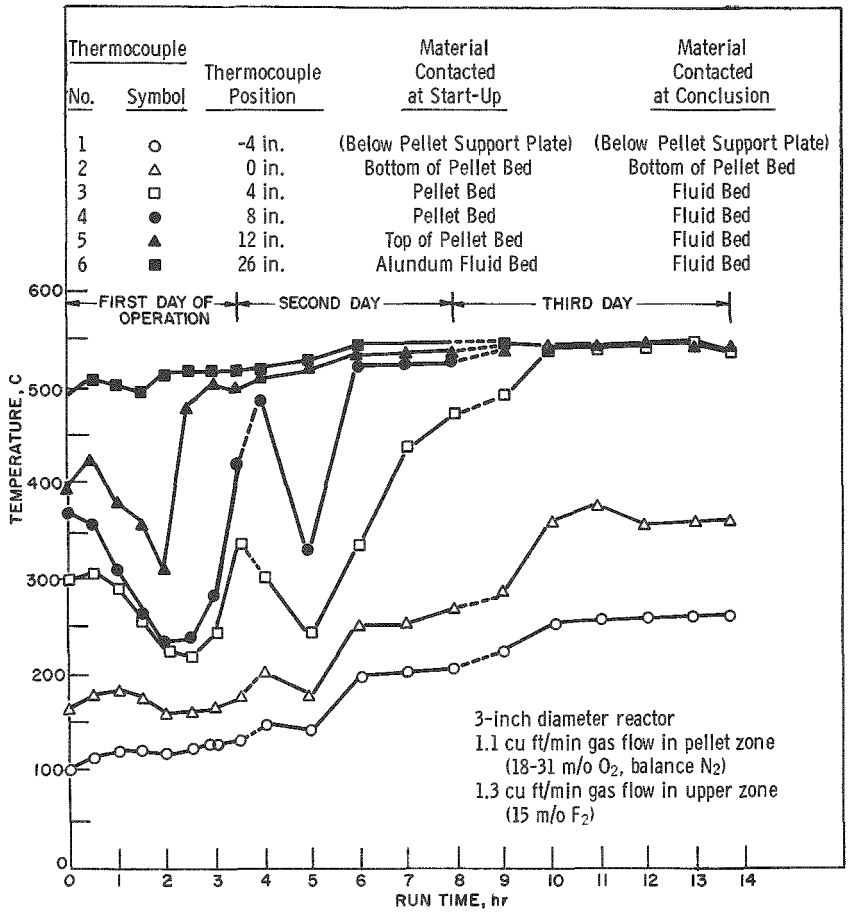

The temperature at the bottom of the pellet bed did not reach 400 C because of the heat loss through the bottom flange, which was not heated. This low temperature is believed to account for unreacted pellets which remained at the end of the run. Since water cooling of the flange was found not to be necessary to establish the thermal gradient through the pellets, the cooling coils were replaced by calrod heaters so that the lower section of the pellet bed can be heated to high temperatures when required.

The uranium hexafluoride production rates for Run UOF-63 are plotted in Figure 42. The production rates during each day of operation were quite uniform. Also, it was observed that external vibration of the column did not materially increase production rates. In these respects, the performance of the present run was superior to that of runs with oxidation at higher temperatures.

Figure 42

URANIUM HEXAFLUORIDE PRODUCTION RATES DURING RUN UOF-63 - A TWO-ZONE OXIDATION-FLUORINATION OF URANIUM DIOXIDE PELLETS, WITH A TEMPERATURE GRADIENT THROUGH THE PELLET BED

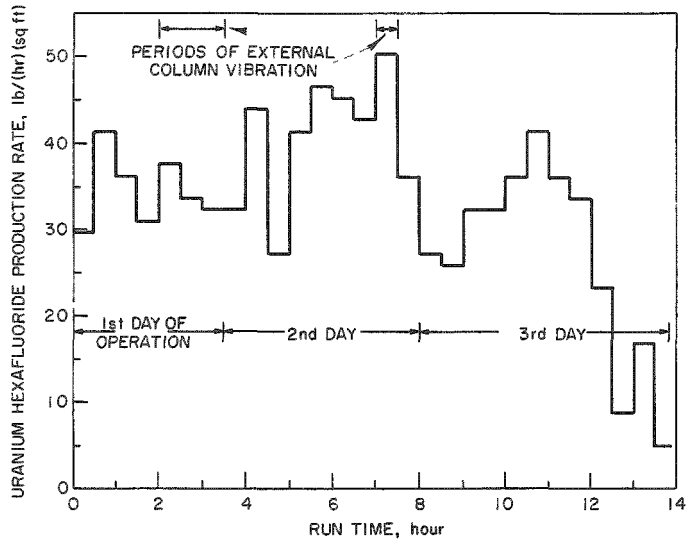

Operating conditions and average production rates for Run UOF-63 are shown in Table 24. Also shown in the table are the apparent steady-state fluorine utilization efficiencies for each period of operation. These efficiencies averaged about 55 percent during the first 12 hr of the run, while the overall fluorine efficiency for the entire run (13.8 hr) was about 49 percent.

The average production of uranium hexafluoride increased from about 34 to about 44 lb UF_6/(hr)(sq ft reactor cross section) when the oxygen content of the gas stream passed through the pellets was increased from

18 to 31 percent. As the weight of the pellet bed decreased, however, the production rate dropped to 36 lb UF_6/(hr)(sq ft). This rate could be improved by raising the temperature of the bottom of the column near the end of the run.

Table 24

CONDITIONS AND RESULTS FOR RUN UOF-63, A TWO-ZONE OXIDATION-FLUORINATION OF URANIUM DIOXIDE PELLETS WITH A THERMAL GRADIENT THROUGH THE PELLET ZONE

Overall Fluorine Efficiency: 49%
Total Processing Time: 13.8 hr
Temperature: Fluid Bed: 525 C
Upper Layer of Pellets: ≥400 C

Process Time (hr)	Gas Flow: Pellet Zone Total (cfm)	Gas Flow: Pellet Zone O_2 [a] (%)	Gas Flow: Fluorination Zone Total (cfm)	Gas Flow: Fluorination Zone F_2 (%)	Average Fluorine Utilization Efficiency[b] (%)	Average UF_6 Production Rate [lb/(hr)(sq ft)]
0-3.5	1.1	18	1.3	14	54	34
3.5-8	1.1	31	1.3	16	57	44
8-12	1.1	31	1.3	15	55	36
12-13.8	1.1	31	1.3	15	23	15

[a] Remainder - nitrogen.

[b] Fluorine Efficiency $= 100\left[\frac{3\ (\text{mole } UF_6 \text{ produced/hr})}{(\text{mole } F_2 \text{ fed/hr})}\right]$

In Run UOF-63, an excess of fluorine (approximately 2 times stoichiometric for the uranium hexafluoride produced) was used to ensure complete reaction of the fines and thus eliminate the possibility of fines buildup on the column filters (see ANL-6596, p. 141, Figure 53). Because conditions in the upper zone are favorable to high fluorination rates, it is believed that fluorine efficiency could be increased by matching fluorine input more closely to the rate of collection of uranium hexafluoride product than was done in this run.

The uranium material balance for Run UOF-63 was 98.5 percent. Of the initial charge of 8.8 kg of pellets, 211 g was not oxidized during the run. One hundred and fifty-eight g of uranosic oxide fines were recovered from the Alundum bed. Inspection showed no indications of cake formation in the bed and no fines buildup on the column filters. These facts, as well as the uniform uranium hexafluoride production rates,

indicate that the rates of fines formation, elutriation, and fluorination were approximately matched during the run.

A second run (UOF-64) was carried out to obtain information concerning (1) the reproducibility of the results obtained in Run UOF-63, (2) the feasibility of programming fluorine input to the uranium hexafluoride collection rate to improve fluorine utilization efficiency, and (3) the effectiveness of heating the bottom of the reactor column near the end of the run in order to achieve complete fluorination of the uranium dioxide charge.

For this run, the bottom flange was provided with a calrod heater so that the bottom of the column could be heated to reactor temperature (~500 C) near the end of the run; the heater was used for about 3.5 hr.

Uranium hexafluoride collection rates and the operating conditions and results for Run UOF-64 are shown in Figure 43 and Table 25, respectively. The temperature gradient through the pellet bed and the pellet bed temperature profiles were similar to those for Run UOF-63.

Figure 43

URANIUM HEXAFLUORIDE PRODUCTION RATES DURING RUN UOF-64 - A TWO-ZONE OXIDATION-FLUORINATION OF URANIUM DIOXIDE PELLETS, WITH A TEMPERATURE GRADIENT THROUGH THE PELLET BED

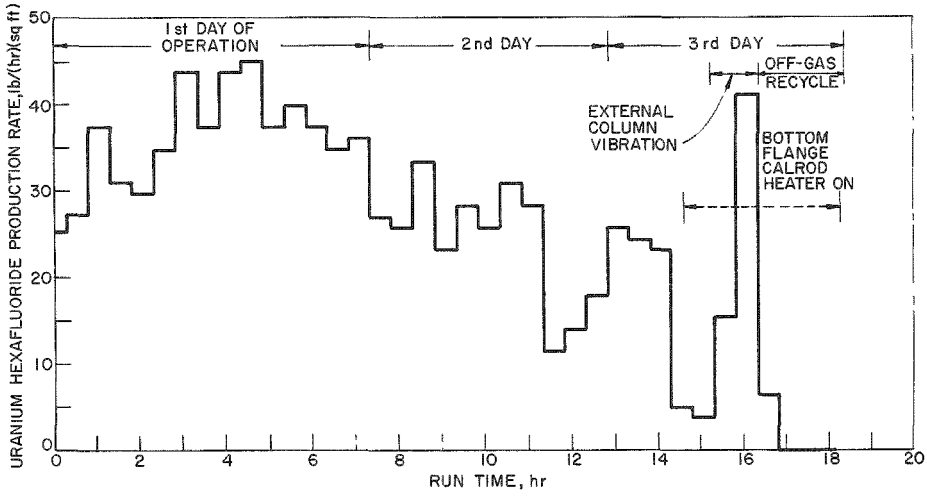

In the period from 2 to 7.3 hr (see Table 25), the uranium hexafluoride collection rate of 39 lb UF_6/(hr)(sq ft) was comparable with rates obtained during UOF-63; however, since fluorine input was programmed to the hexafluoride collection rate, the fluorine utilization efficiency (78 percent) was much higher than in the corresponding period of UOF-63. After this period

of operation at high fluorine efficiency, the run was interrupted to allow inspection of the column disengaging section and porous metal filters. No buildup of fines was in evidence, and it appears that fines transported from the oxidation zone were completely fluorinated with a moderate excess of fluorine (about 20 percent in excess of the stoichiometric amount).

Table 25

OPERATING CONDITIONS AND RESULTS FOR RUN UOF-64, A TWO-ZONE OXIDATION-FLUORINATION OF URANIUM DIOXIDE PELLETS, WITH A THERMAL GRADIENT THROUGH THE PELLET ZONE

Overall Fluorine Efficiency: 53%
Total Processing Time: 18.3 hr
Temperatures: Fluid Bed ≤525 C
Upper Layer of Pellets ≥400 C

Process Time (hr)	Gas Flow: Pellet Zone Total (cfm)	Gas Flow: Pellet Zone O_2[a] (%)	Gas Flow: Fluidized Upper Zone Total (cfm)	Gas Flow: Fluidized Upper Zone F_2 (%)	Average Fluorine Utilization Efficiency[b] (%)	Average UF_6 Production Rate [lb/(hr)(sq ft)]
0-2	1.2	26	1.3	11.7	54	30
2-7.3	1.2	26	1.4	11.2[c]	78	39
7.3-11.8	1.2	26	1.3	10.5	53	26
11.8-13.8	1.2	26	1.3	10.4	38	21
13.8-16.3	1.2	26	1.3	8.5	29	11

[a] Remainder - nitrogen.

[b] Fluorine efficiency $= 100\left[\frac{3(\text{mole } UF_6 \text{ produced/hr})}{(\text{mole } F_2 \text{ fed/hr})}\right]$

[c] Average for period, i.e., fluorine input was programmed to UF_6 collection rate.

In the second period of the run, when the fluorine input was kept constant (7.3 to 11.8 hr, Table 25), the fluorine utilization efficiency obtained, 53 percent, was comparable with the efficiencies obtained during Run UOF-63; the hexafluoride collection rate of 26 lb UF_6/(hr)(sq ft) was somewhat lower than those in the previous run. After 13.8 hr of operation, 85 percent of the pellet charge had been collected as the hexafluoride in Run UOF-64; this should be compared with 91 percent reaction after a similar period of time in Run UOF-63. Thus, overall uranium hexafluoride production rates were similar for these runs.

The final 4.5 hr of operation in UOF-64 was required in order to complete fluorination of the remaining pellets. During this period, use of external column vibration produced a short period of increased hexafluoride collection rate (see Figure 43). Off-gas recycle through the reactor was used for the last hour of operation.

The alumina removed from the column after Run UOF-64 was free-flowing and contained no pellet residue. No uranium fines were seen in the alumina. A chemical analysis of the alumina showed it to contain 0.055 w/o of uranium. Since the weight of uranium charged was about equal to the weight of alumina charged, only about 0.05 percent of the uranium remained in the bed residue at the end of the run. In addition, inspection showed that no buildup of fines occurred in the upper sections of the column. The condition of the final bed, together with pressure drop and temperature measurements taken during the run, indicates that no caking had occurred.

In summary, it appears that the major objectives, short processing time and freedom from caking, can be achieved in two-zone operation by maintaining a temperature gradient of 140 to 400 C in the oxidation zone and a temperature of 500 C in the fluorination zone. During substantial periods of operation, fluorine efficiencies were about 80 percent. Further refinement of operation may yield satisfactory overall fluorine utilization efficiencies with a once-through gas flow system rather than a more complicated recycle system.

2. Design and Construction of Engineering-scale Plutonium Handling Facility
(G. J. Vogel, E. L. Carls, W. J. Mecham, W. A. Murphy, J. Wehrle, and L. Marek)

Construction activities are continuing on the High-Alpha Engineering-scale Facility designed to study various steps of the Direct Fluorination Process as applied to uranium-plutonium oxide reactor fuels. Details of the room layout together with a general description of the equipment to be installed have been presented in a previous report (see ANL-6569, p. 110).

The structural changes of the room and process cell have been completed, together with the installation of the glove boxes and various services to the operating and cell areas. Most of the equipment and accessories concerned with the fluorination step of the process have been fabricated and delivered. Present emphasis is being placed on four major activities:

a. Ventilation, Electrical, and Miscellaneous Room Modifications

Design details are being worked out for the provision of room and alpha box ventilation and for electrical and air connections from the panel board to the alpha boxes. This installation also involves a refrigeration system, elevator lifts to give personnel access to the upper levels of the alpha boxes, and fire-detection equipment.

b. Equipment Layout

Work has begun on equipment layout in the large alpha box. A one-eighth-scale model (see ANL-6569, p. 112, Figure 34) together with full-scale wooden mockups of various pieces of equipment are used as engineering aids in determining optimum equipment placement.

c. Separations Equipment

Design has begun on equipment concerned with the separations step of the process, namely, a distillation column where uranium and plutonium hexafluorides will be separated from fission product elements, and a plutonium hexafluoride decomposer where plutonium will be separated from uranium hexafluoride.

d. Efficiency and Capacity Tests of Uranium Hexafluoride Condensers

Efficiency and capacity tests of the condensers (to be used for collection of uranium and plutonium hexafluorides prior to the separations step) were started. After the tests have been completed, these units will be mounted in the alpha enclosure. The results of the tests to date are described below.

The new condensers are basically similar to that now used in the fluidized-bed pilot plant. This condenser is 10 ft long, 3 in. in diameter, and contains an internal finned tube through which the coolant is circulated. The capacity of this condenser, i.e., the amount of solid uranium hexafluoride that can be condensed before a solid plug forms to block gas flow, is approximately 25 lb, and the overall collection efficiency is approximately 96 percent. These results were obtained in process operation with a coolant temperature of -40 C. The tests with the new condensers were concerned with increasing the capacity while achieving a high collection efficiency.

The new condenser design, which is shown in Figure 44, was fabricated from 4-in.-diameter Monel tubing. It is U-shaped in order to avoid the need for an expansion joint in the finned coolant tube. This shape

Figure 44

URANIUM HEXAFLUORIDE CONDENSER

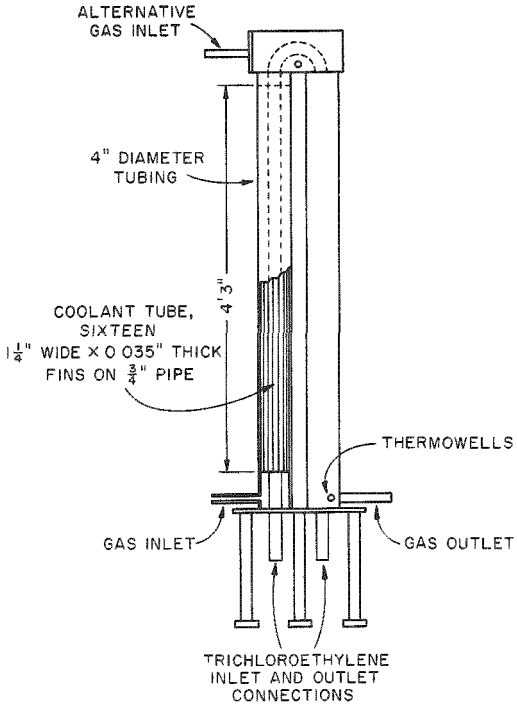

also provides complete drainage of trichloroethylene coolant from the internal finned tube, as heating of the condenser to 300 C may be required to fluorinate any plutonium tetrafluoride deposited by radiation decomposition of plutonium hexafluoride. Each leg of the fin tube unit through which the coolant flows is a $\frac{3}{4}$-in.-diameter pipe to which 16 longitudinal fins are welded. Four heating coils, Variac-controlled, are wrapped around each leg; one coil covers the entire length of the leg, and the other three are wrapped over the first coil, one each around the bottom, middle, and top to provide close regulation of the condenser wall temperature.

Test Equipment and Procedure

The flow diagram for the capacity test system is shown in Figure 45. A mixture of nitrogen and uranium

Figure 45

SYSTEM FOR DETERMINATION OF URANIUM HEXAFLUORIDE CAPACITY OF CONDENSER

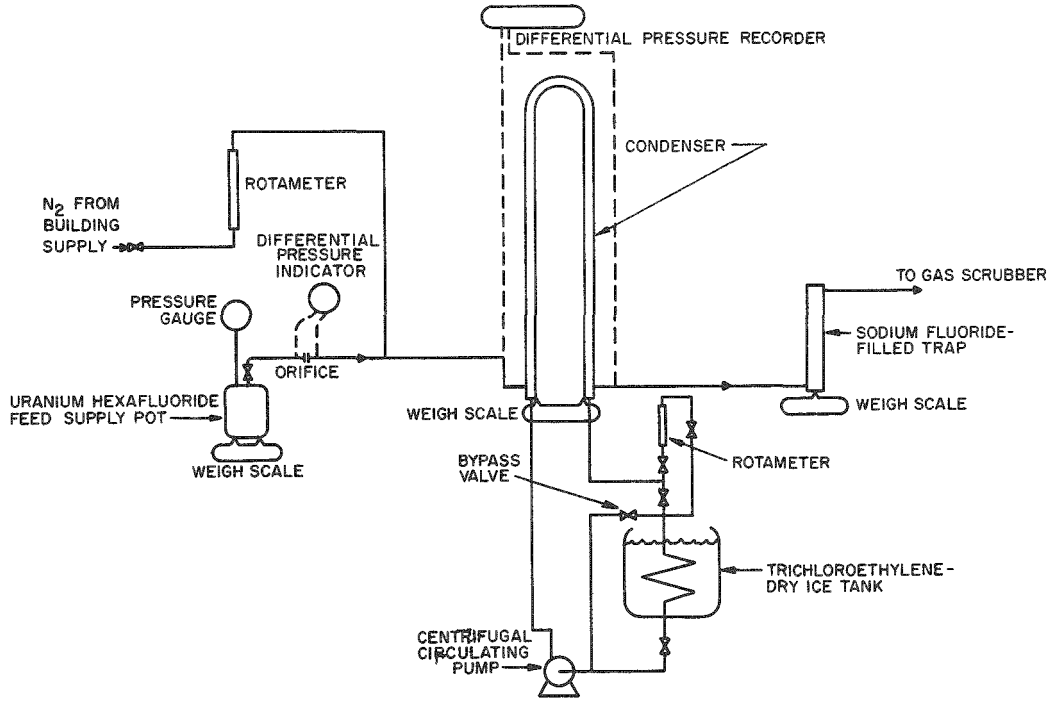

hexafluoride passes through the condenser, where most of the uranium hexafluoride desublimes. The condenser effluent then passes through a sodium fluoride bed on which is fixed any remaining hexafluoride. The condenser and the uranium hexafluoride feed pot are each weighed on beam scales capable of being read to the nearest $\frac{1}{2}$ oz; the trap filled with sodium fluoride is weighed on a beam balance capable of being read to the nearest gram. The trichloroethylene circulating through the condenser coolant tube is cooled by being passed through a coil immersed in a trichloroethylene-dry ice slush bath. The coolant can be partially bypassed to vary coolant temperatures.

The uranium hexafluoride used in these tests was produced by fluorination of uranium dioxide in the fluidized-bed pilot plant. Nitrogen of low water content (3 to 15 ppm) was taken from the building supply system. Sodium fluoride pellets (of $\frac{1}{8}$-in. diameter by $\frac{1}{8}$-in. long) were prepared by heating sodium bifluoride pellets at about 450 C while the pellets were swept with nitrogen.

The system was brought to temperature equilibrium at the selected condenser wall temperature and coolant temperature with nitrogen flowing through the unit. The uranium hexafluoride was vaporized into the nitrogen stream; the weight readings of the heated feed pot, the condenser, and the sodium fluoride bed each were taken at hourly intervals. The procedure was to terminate the run when the pressure drop across the condenser reached 2 psi, or when the collection efficiency dropped below about 90 percent, as indicated by the weight readings of the condenser and the still pot.

All capacity tests were made at flowrates that will be encountered in the pilot plant, i.e., about 1 cfm nitrogen and approximately 3 lb of uranium hexafluoride per hour. A series of runs was made at different condenser wall temperatures and coolant temperatures. These two variables were thought to influence the condenser capacity most. In each of these tests, the wall temperature was held within ten degrees of the specified temperature.

Results

In Table 26 are presented data from the preliminary tests of condenser capacity. The condenser efficiency was determined by comparing the amount of uranium hexafluoride sorbed on the sodium fluoride with the amount fed to the condenser. The data in Table 26 indicate that the best results for both high capacity and good efficiency (above 99 percent for capacities up to 50 lb uranium hexafluoride) were obtained with a coolant temperature of -75 C and with a condenser wall temperature of about 50 C. It is possible that lower coolant temperatures might lead to higher efficiencies; however, with the present cooling system, temperatures lower than -75 C could not be obtained. In a test made with the condenser wall

temperature at 100 C and the coolant at -75 C, condenser capacity was greater but the collection efficiency was somewhat lower. This can be seen from Figure 46.

Table 26

CAPACITY AND COLLECTION EFFICIENCY OF URANIUM HEXAFLUORIDE CONDENSER

Flow Conditions: 3 lb UF_6/hr; 1.0 cfm N_2

Condenser Wall Temperature (C)	Condenser Performance at Coolant Temperature	
	-75 C	-30 C
100	No plugging; low efficiency (<90%) after 77 lb UF_6 collected	No test made
50	Good efficiency; plugged at 67 lb UF_6 collected	Low efficiency immediately
Unheated, <0	Good efficiency; plugged at 16 lb UF_6 collected	Plugged at 32 lb UF_6 collected

Figure 46

CONDENSER COLLECTION EFFICIENCY AT CONDENSER WALL TEMPERATURES OF 50 AND 100 C

Conditions

Flowrates: N_2, 1 cfm; UF_6, 45 oz/hr

Coolant Temperature: -75 C

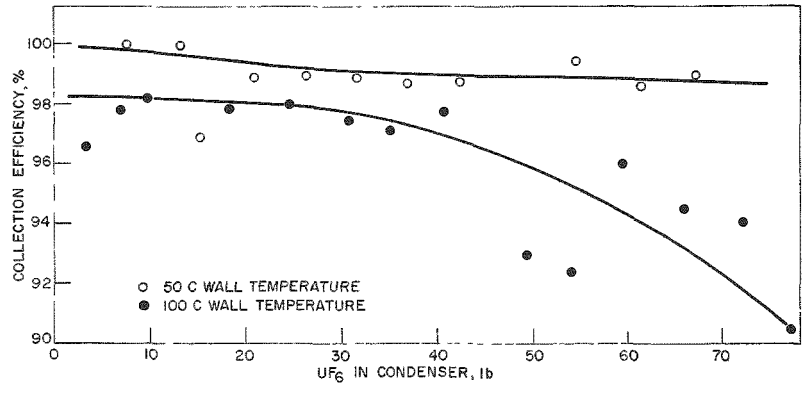

Increasing the coolant temperature was found to have an adverse effect. For example, with a coolant temperature of -30 C and a wall temperature of 50 C, a collection efficiency of only 80 percent was obtained during a 2-hr run. This approach was discontinued after two tests.

The capacity data in Table 26 do not necessarily reflect the maximum amount of uranium hexafluoride that can be collected in the condenser, since the runs were arbitrarily terminated, as mentioned above, when a pressure drop of 2 psi across the condenser was noted, or when the collection efficiency dropped below 90 percent. Generally, near the end of a run, the pressure drop did not increase smoothly, but varied in a wave pattern.

Subsequent tests will be made of condenser operation with the coolant at -75 C and the wall temperature at 50 C. Gas flow rate (contact time) and uranium hexafluoride concentration in the gas mixture will be varied in these tests to observe the effect of these variables on the collection efficiency.

3. Axial Heat Transfer in Fluidized Packed Beds

(J. D. Gabor and B. E. Stangeland*)

Supporting studies are being made in order to obtain design data and to clarify the fluidization mechanisms involved in the particular equipment configurations used in the Direct Fluorination Process. In this process, inert fluidized particles of alumina are used as an aid to the removal of heat from the highly exothermic reaction of uranium dioxide pellets with fluorine. While the pellets themselves are too massive to be fluidized, the alumina particles are fluidized in the voids of the pellet bed. This configuration has been termed a fluidized packed bed.

Studies have been made previously of the radial thermal conductivities by Bayens (see ANL-6333, p. 178) and by Ziegler (see ANL-6413, p. 128). Bayens studied the thermal conductivities for systems consisting of pellet beds with a fluidized medium in the pellet voids. Effective thermal conductivities along the radius were found to be 0.8 Btu/(hr)(sq ft)(F/ft) in nonfluidized case and 5 to 10 Btu/(hr)(sq ft)(F/ft) in the fluidized case. Ziegler, using different packing materials and different sizes of fluidizing material, found the radial coefficients to lie within the range of 2 to 30 Btu/(hr)(sq ft)(F/ft). These values are considerably lower than those for a pure fluidized system containing no packing material. Lewis et al.[30] found that the radial conductivities in fluidized systems (without packing) ranged from 200 to 500 Btu/(hr)(sq ft)(F/ft). They also found that the longitudinal conductivity in the same system ranged from 2000 to 25,000 Btu/(hr)(sq ft)(F/ft). The radial conductivity measured by Lewis was never found to be greater than 2 percent of the longitudinal conductivity.

* Student Aide from the University of Illinois.

30 Lewis, W. K., et al., "Heat Transfer and Solids Mixing in Beds of Fluidized Solids," AIChE Symposium on Fluidization: Part II, Dec. 2-7, 1961, New York.

In the present study, axial heat transfer in a fluidized packed bed was studied as a function of the size and composition of fluidized material, gas velocity, and packing shape. Two types of packing were used in these studies, $\frac{3}{8}$ x $\frac{3}{8}$-in. brass cylinders and $\frac{1}{2}$-in. steel spheres. Three types of fluidized material were used: 70 mesh glass beads, 120 mesh glass beads, and 60-140 mesh alumina grain. Size distributions of these fluidizing particles are given in Table 27. Air was used as the fluidizing gas in these studies.

Table 27

SIZE DISTRIBUTIONS OF FLUIDIZING PARTICLES

Material	Screen Size	Weight Percent
70 mesh glass beads	+40 mesh	53.8
	+100 -40	45.8
	+120 -100	0.2
	+140 -120	0.1
	-140	0.1
120 mesh glass beads	+40	0.3
	+100 -40	1.4
	+120 -100	94.2
	+140 -120	3.6
	+170 -140	0.4
	-170	0.1
60-140 mesh alumina	+40	0.1
	+100 -40	66.6
	+120 -100	20.3
	+140 -120	12.5
	-140	0.5

The apparatus used for studying longitudinal heat transfer in a fluidized packed bed is shown in Figure 47. It consisted of a 40-in. length of 3.75-in.-ID stainless steel tubing. A brass flange was silver brazed to the bottom of the tube to support the bottom plate. A sintered stainless steel disc ($\frac{1}{8}$ in. in thickness) was fastened to the bottom of the tube to serve as a gas-distributor plate. Air was supplied to the column through the bottom of a hollowed-out disc of 1-in.-thick Lucite, bolted to the brass flange and supported the sintered disc. A set of three high-temperature Neoprene gaskets sealed the outer edges of the sintered disc.

Heat was introduced and removed internally in this system. A 300-w heating element was suspended about 2 in. above the sintered plate by its insulated lead wires. Heat was removed by a $\frac{1}{4}$-in. cooling coil of

Figure 47

COLUMN USED FOR LONGITUDINAL HEAT TRANSFER STUDIES OF FLUIDIZED PACKED BEDS

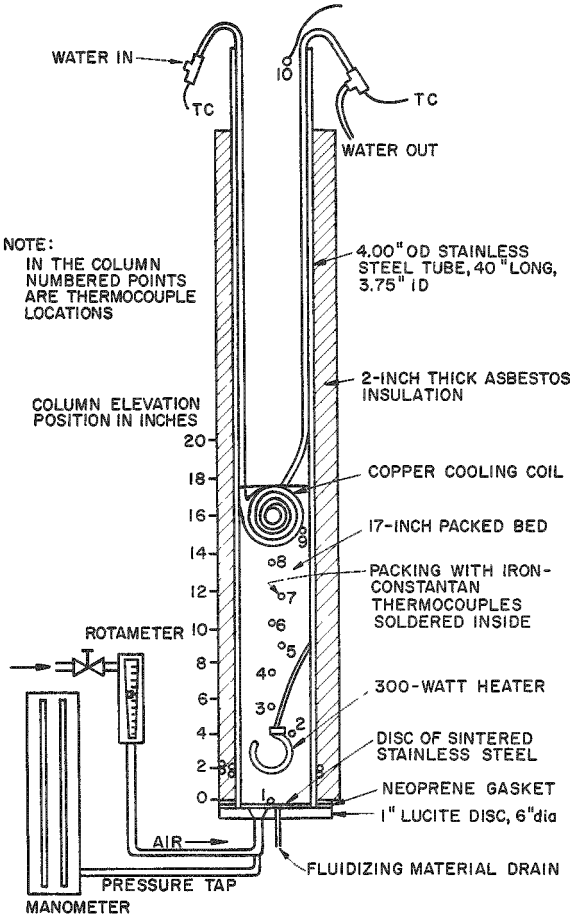

copper, suspended 14 to 17 in. above the plate. The entire column was insulated with 2-in.-thick asbestos to minimize heat losses to the ambient air.

Temperature probes were mounted along the axis of the bed to determine temperature profiles. Each probe was made by drilling a hole in either a $\frac{3}{8}$ x $\frac{3}{8}$-in. brass cylinder or a $\frac{1}{2}$-in. steel sphere, and soft soldering the end of an iron-constantan thermocouple inside the hole. The thermocouples were connected to a 12-point temperature recorder having a range from 0 to 200 C. Thermocouples were also mounted in the inlets and outlets of the water-cooled coils to determine the heat flux in the column.

A typical longitudinal temperature profile for a run is shown in Figure 48. The discrepancy of the point at about a 10-in. column height is attributed to local differences in the void structure of the bed. The amounts of heat transported to the

Figure 48

TYPICAL LONGITUDINAL TEMPERATURE PROFILE IN FLUIDIZED PACKED BED

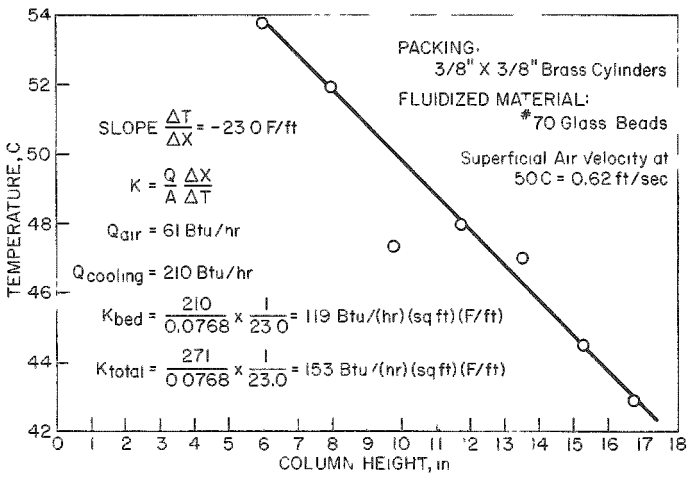

cooling water, $Q_{cooling}$, and to the air, Q_{air}, were determined from the fluid flow rates, their heat capacities, and their change in temperature.

Values of the thermal conductivity k_A were calculated on the basis of Fourier's Law

$$q = -k_A A \frac{dT}{dX} \qquad (1)$$

with $q = Q_{cooling}$, A = 0.0768 sq ft, and dT/dX = the slopes of the temperature gradients. The usage of $Q_{cooling}$ follows from defining the heat-transfer coefficient to describe only the heat carried by the fluidized particles. Values of k_A as a function of fluidization gas velocity are plotted in Figures 49 and 50, and are discussed below.

Figure 49

AXIAL THERMAL CONDUCTIVITY AS A FUNCTION OF SUPERFICIAL AIR VELOCITY FOR DIFFERENT FLUIDIZING MATERIALS

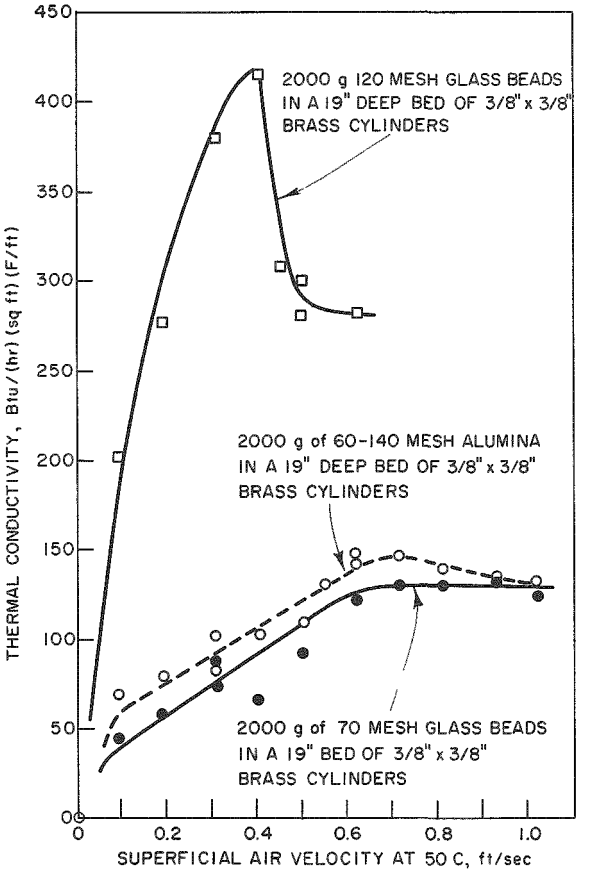

Figure 50

AXIAL THERMAL CONDUCTIVITY AS A FUNCTION OF SUPERFICIAL GAS VELOCITY FOR DIFFERENT SHAPES OF PACKING MATERIAL

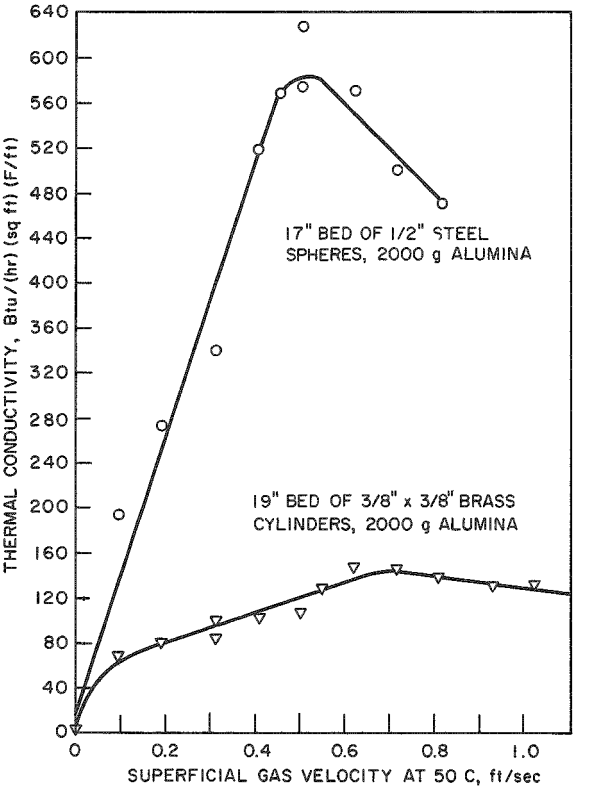

If the thermal conductivity is defined to include heat carried by the particles and by the air stream, the sum of $Q_{cooling}$ and Q_{air} would have to be used in Equation 1 to determine an appropriate thermal

conductivity. Heat transfer to the air stream became significant at higher velocities. At about 1 ft/sec, the air carried about 40 percent as much heat as the water. If $Q_{cooling}$ plus Q_{air} were used to calculate k_A, a plot of k_A versus gas velocity would be approximately linear instead of having a maximum as do the curves in Figures 49 and 50.

The curves in Figures 49 and 50, which were calculated with the use of $Q_{cooling}$ alone, have a maximum for gas flow between 0.4 and 0.7 ft/sec because of the interaction of two effects. The thermal conductivity of a fluidized packed bed depends both on the degree of motion (i.e., mixing) of the particles and on their density in the gas stream. As the gas velocity increases, the particle motion increases, increasing the rate of heat transport. At the same time, increasing the velocity expands the bed of particles and decreases the particle density in the gas stream. This decrease in density has the opposite effect on thermal conductivity of the increased particle motion, and the conductivity attains a maximum.

Figure 49 shows that the thermal conductivity is strongly dependent on the particle size of the fluidized material. The particle size distributions, which are tabulated in Table 27, show that the 70 mesh glass beads are roughly twice the size of the 120 mesh glass beads. The mean mesh sizes of these two fractions are about 70 and 120 mesh, respectively. The thermal conductivity values for the 70 mesh beads are only about one-third those determined for the 120 mesh beads. The 60-140 mesh alumina and the 70 mesh glass beads (which are about the same size) had about the same thermal conductivity values.

Figure 50 shows the strong dependence of thermal conductivity on the packing shape, which in turn affects the shapes and sizes of voids. Spheres pack more uniformly and have a greater void space than do cylinders. Greater void space increases the freedom of motion of the fluidized particles and results in a higher thermal conductivity for a bed of spheres. Thermal conductivities of the $\frac{1}{2}$-in. steel spheres and the $\frac{3}{8}$-in. brass cylinders differ by a factor of four.

In the present investigation, values of the longitudinal thermal conductivities in fluidized packed beds as high as 600 Btu/(hr)(sq ft)(F/ft) were obtained. These values appear to be higher by at least a factor of 10 than the radial heat transfer coefficients obtained with similar systems in previous investigations.

4. Process Studies on the Recovery of Uranium from Enriched Uranium-Zirconium Alloy Fuels
(N. Levitz)

Studies were continued on the development of fluidization and volatility techniques for the recovery of uranium from highly enriched alloy

fuels. Current work is on zirconium-based fuel, although direct application of the process to other fuels, such as those containing aluminum, is believed feasible.

The basic process steps include an initial hydrochlorination step, to effect a separation of the alloying material from the uranium, and a fluorination step, to effect conversion of the uranium to the volatile hexafluoride for ready collection. The latter step also provides separation of the uranium from many minor (less volatile) constituents of the fuel.

Hydrochlorination is conducted with the alloy submerged in an inert fluidized bed (Norton Alundum) which serves as a heat-transfer medium for the exothermic gas-metal reaction. For uranium-zirconium alloy, separation of zirconium from uranium is achieved by a hydrochlorination reaction conducted at a temperature above the sublimation point (331 C at 14.7 psia) of zirconium tetrachloride. The uranium remains associated with the bed as particulate chlorides (primarily the trichloride) and is subsequently fluorinated to the volatile hexafluoride.

Particulate solids which are entrained by the gases leaving the fluidized bed are retained in the system by a high-temperature filter consisting of a fixed bed of granular material similar to that used in the fluidized bed. In most of the work to date, a down-flow bed filter has been used, although an up-flow type and the two types of filter beds in series have also been tested (see ANL-6413, pp. 137 to 140, and ANL-6477, pp. 145 to 147). The zirconium tetrachloride is condensed in an air-cooled Pyrex glass pipe condenser, and the remaining gases are treated in an aqueous scrub tower and finally exhausted.

Process reactions are being evaluated on the basis of: (a) uranium losses through the filter during hydrochlorination, (b) uranium retained by the inert solids in the fluid bed and filter beds after fluorination, (c) percent of total uranium collected as the hexafluoride product, and (d) overall uranium material balances. A high-recovery (about 99 percent) process is desired. Work to date has shown that good filtration, that is, uranium particulate solids losses of about 0.2 percent or less of the total uranium charged, is achieved with fixed-bed filtration (see ANL-6413, pp. 137 to 140) and that retention of uranium by the inert solids after fluorination can be reduced to less than one percent of the uranium charged by the use of a two-step fluorination procedure. The first fluorination is carried out at a relatively low temperature, about 350 C. (In previous work, this step was carried out at 400 C; however, in recent work it was found that equally satisfactory results could be obtained at 350 C.) The second fluorination is carried out at about 500 C (see ANL-6569, pp. 113 to 118, and ANL-6596, pp. 146 to 153).

In previous investigations of the effect of various chlorinating steps on uranium behavior (ANL-6596, p. 149), there appeared to be a

slight time advantage in using a 4:1 mixture of hydrogen chloride and phosgene, followed by a phosgene treatment instead of a sequence involving hydrogen chloride followed by phosgene or hydrogen chloride alone. The slight advantage of the mixed reactants was negated, however, because uranium losses through the down-flow filter were prohibitively high, about five percent compared with about 0.2 percent or less for the other chlorinating sequences evaluated. The high losses may have resulted from the formation of uranium chlorides more volatile than the trichloride when a hydrogen chloride-phosgene mixture was employed.

In current studies, reported below, the effect on uranium behavior of reaction sequences involving a hydrofluorination step between the chlorination and fluorination steps is being investigated.

In addition to studies of the main process reaction, which are being conducted in a $1\frac{1}{2}$-in.-diameter fluid-bed unit, studies are in progress in a 6-in.-diameter unit on the conversion of zirconium tetrachloride to zirconium dioxide by hydrolysis in a fluid bed. This conversion is economically important because of the greater ease of storage of the zirconium dioxide. In these fluid-bed hydrolysis studies, the range of operating conditions has been broadened in an attempt to discover the limits of satisfactory operation.

The main process steps (the hydrogen chloride-fluorine cycle and the fluid-bed hydrolysis of zirconium tetrachloride to the dioxide) will be demonstrated in an integrated pilot-plant facility now being installed. Inactive zirconium-uranium alloy (20 to 30 kg of alloy per charge, the amount being limited by the geometry of the charge with respect to column dimensions) and possibly tracer experiments will be used.

It is also planned to install a $1\frac{1}{2}$-in.-diameter unit for high-activity work. This unit will be used to establish fission product distribution for each step of the process and to ascertain whether irradiation affects the behavior (recovery) of uranium.

a. Chlorination and Fluorination Reaction Studies of Uranium-Zirconium Alloy Fuels and Evaluation of Fixed-bed Filters (D. Ramaswami, K. Turner, C. Schoffstoll, and D. Goeser)

Studies of the chlorination and fluorination steps of a fluid-bed volatility process proposed for the recovery of highly enriched uranium from low uranium-zirconium alloy fuel are in progress. The experimental work is being carried out in a prefluorinated $1\frac{1}{2}$-in.-diameter nickel (Nickel 200) reactor containing a fluidized bed of granular prefluorinated Alundum (Norton Co.). In series with the reactor is a $1\frac{1}{2}$-in.-diameter nickel filter section containing a fixed bed of Alundum grain. Downstream from the filter unit, the effluent gases are cooled to condense the volatile products, and the remaining gases are then treated and exhausted. Details

of the apparatus and the experimental procedure were reported previously (see ANL-6569, pp. 113 to 118).

In current experiments, the objectives were to determine: 1) the effect of a hydrofluorination step between the hydrochlorination and fluorination steps, 2) the overall effects of a reaction sequence in which several batches of alloy are hydrochlorinated in succession after which the accumulated uranium is recovered by a single fluorination (Run 32), and 3) optimum conditions for each step in a reaction cycle (by monitoring a key component during each reaction). Continuous "on stream" gas analysis (with Gow-Mac thermal conductivity cells) and/or analysis of the solids for key components are used to follow the course of the reactions. The reactant sequence and process conditions for the two current runs are summarized in Table 28.

Table 28

SEQUENCE USED FOR REACTING URANIUM-ZIRCONIUM ALLOY FUEL IN THE 1½-INCH-DIAMETER FLUID BED REACTOR (RUNS 31 AND 32)

(see Table 29 for other run conditions)

Run No.	Reactant[a] Type	Reactant[a] Quantity (x Stoichiometric)	Temperature (C) Fluid Bed	Temperature (C) Filter Bed	Time (hr)	Remarks
31	HCl	3[b]	400 ± 25	400	5	
	$COCl_2$	2[b]	400	370	1	
	HF	73[c]	400	370	2	
	F_2	60[d]	400	400	2	
	F_2	60[d]	500	500	2	
32	HCl	0.67[b]	400 ± 25	400	4.0	Hydrochlorination of first batch of alloy.
	HCl	0.33[b]	400 ± 25	400	4.2	Hydrochlorination of residue from first batch of alloy plus the second batch.
	HCl	2[b]	400 ± 25	400	13.1	Hydrochlorination of residue from previous batches plus the third batch.
	$COCl_2$	0.5[b]	350	350	1	
	HF	40[c]	350	350	2	
	F_2	20[d]	350	350	2	
	F_2	24[d]	500	500	2	

[a]Nitrogen used as diluent in all cases.

[b]Stoichiometric amount based on the total zirconium in the charge.

[c]Stoichiometric amount required to convert initial uranium in the charge into uranium tetrafluoride.

[d]Stoichiometric amount required to convert initial uranium in the charge into uranium hexafluoride.

In the two runs, a hydrochlorination step was followed by treatment of the system (both fluid and static beds) with phosgene, hydrogen fluoride, and fluorine. Subsequent work (to be reported completely next quarter) in which the phosgene step was omitted showed equally good uranium recovery, and it now appears that hydrogen chloride alone is required for the chlorination step.

Each batch of alloy charged consisted of 240 g of 5.1 w/o uranium-zirconium alloy chips. The reaction bed consisted of 320 g of -40 +60 mesh, Norton Type RR Alundum. The down-flow filter bed consisted of a layer of -40 +60 mesh Norton Type RR Alundum sandwiched between layers of coarser material, -14 +20 mesh Norton Type 38 Alundum (see Table 29).

Table 29

URANIUM MATERIAL BALANCES (RUNS 31 AND 32)

Equipment:	$1\frac{1}{2}$-in.-diameter fluidized bed unit with $1\frac{1}{2}$-in.-diameter downflow filter section
Fuel Charge:	5.1 w/o U-Zr alloy chips ($\frac{1}{8}$- to $\frac{1}{4}$-in. size); 240 g for Run 31, three batches of 240 g each for Run 32
Reaction Bed:	320 g of Alundum,[a] Type RR, -40 +60 mesh
Down-Flow Filter Bed:	Run 31 180 g of Alundum,[a] Type RR, -40 +60 mesh 140 g of Alundum,[a] Type 38, -14 +20 mesh
	Run 32 120 g of Alundum,[a] Type RR, -40 +60 mesh 200 g of Alundum,[a] Type 38, -14 +20 mesh

Superficial Velocity of Gas in the Fluidized Bed: 0.7 ft/sec

Uranium Disposition	Percent of Initial Uranium	
	Run 31	Run 32
I. Uranium in		
1. UF_6 Product Cold Traps	93.6	98.2
2. Samples of Bed Material (total for all steps)	5.6	0.7
3. Fluorine Disposal Tower	0.3	0.5
Total uranium recoverable by fluorination	99.5	99.4
II. Uranium Retained by Alundum in		
1. Fluid Bed, -40 +60 mesh	0.7	0.13
2. Fluid Bed, -60 mesh		0.01
3. Filter Bed, +20 mesh	0.2	0.21
4. Filter Bed, -20 mesh	0.1	0.08
Total uranium retained by Alundum	1.0	0.43
III. Uranium Lost to Gas Streams		
1. $ZrCl_4$ Condenser		
a. During hydrochlorination	0.4	0.25
b. During phosgene treatment		0.01
2. Scrub Tower		
a. During hydrochlorination	4×10^{-4}	2.4×10^{-2}
b. During phosgene treatment	6×10^{-7}	1.8×10^{-3}
c. During hydrofluorination	1×10^{-5}	1.3×10^{-3}
Total uranium lost to all gas streams	0.4	0.29

[a]Manufactured by Norton Company.

Only one batch of alloy was processed during Run 31, whereas three batches of alloy were processed in Run 32. In the latter run, the second and third batches were charged before hydrochlorination of the preceding batch was completed. Thus, operation for longer periods of time under conditions of high reaction rates and high efficiencies was achieved, as is discussed in later paragraphs. During all of the hydrochlorination periods, the temperature in the bed adjacent to the alloy charge was maintained at 400 ± 25 C; however, measurements with a thermocouple in actual contact with the alloy chips indicated that temperatures of over 500 C were reached. The remainder of the system (fluid bed, filter bed, and connecting piping) was maintained at the specified operating temperatures.

Uranium Material Balances. The results for Runs 31 and 32 are summarized as uranium material balances in Table 29. The total amount of uranium accounted for corresponds to 101 percent and 100.1 percent of the initial charges for Runs 31 and 32, respectively.

The uranium losses consist of material which passed through the down-flow filter and was lost to the gas streams, and the quantity of uranium retained by the Alundum after fluorination. Uranium losses through the filter were equal to about 0.4 and 0.3 percent of the initial charge in the two runs. Most of this loss was incurred during the hydrochlorination period; only a very small loss was sustained during the relatively short (1-hr) phosgene period. A factor that may have contributed to low losses during the phosgene treatment was the maintenance of somewhat lower temperatures in the filter, 350 to 370 C, instead of 400 C; thereby the tendency for the formation of volatile species of uranium chlorides was lessened. Negligible loss of uranium was sustained during hydrofluorination, as expected; also, no other marked effects of this step were noted as is discussed in following paragraphs.

Total retention (by both the fluid bed and the filter bed) of uranium was equal to about 1.0 percent of the initial uranium for the single-charge run (Run 31) and about 0.43 percent for the multiple-charge run (Run 32). For Run 32, this value corresponds to a uranium concentration in the Alundum of 0.02 w/o. The total uranium considered recoverable (that is, the sum of the uranium collected in the uranium hexafluoride product cold traps, the uranium which passed through the cold traps and was found in the fluorine disposal tower, and the uranium in the solid samples submitted for analysis) was over 99 percent of the initial uranium for both runs.

Chloride Associated with the Fluidized-bed Residues. In an attempt to learn the chemical form of the uranium present in the fluidized bed after hydrochlorination, both uranium and chloride contents of the fluidized bed were determined. The analyses showed a chloride-to-uranium mole ratio of 3.0 after hydrochlorination, indicating that uranium is present principally as the trichloride and confirming that very little chloride is

associated with either the Alundum grain or residual zirconium. Further, the mole ratio of chlorine to uranium for this material increased to 3.7 during the treatment with phosgene, indicating that higher chlorides were being formed.

Effect of Hydrofluorination on the Chloride Content of the Cold Traps. It was reported previously (see ANL-6596, p. 151) that during the initial part of chlorination, the chlorine associated with the bed (more specifically, with the uranium in the bed) was converted, at least in part, to chlorine trifluoride during the fluorination step. The chlorine trifluoride condensed in the cold traps used for the collection of product uranium hexafluoride and may have been the source of difficulties encountered during hydrolysis of the cold traps. It may be desirable to eliminate the chlorine associated with the bed before fluorination and cold-trapping are performed. A hydrofluorination step interposed between hydro chlorination and fluorination is expected to achieve this.

Results of analysis of bed samples taken during hydrofluorination in the current runs (see Table 31 and Figure 55) showed that the major fraction of the chlorine was released to the scrub tower; nevertheless, a small amount of chloride was still found in the cold traps after the fluorination step. The chlorine levels in the uranium hexafluoride collection traps from Runs 31 and 32, expressed as mole ratios of Cl_2 to U, were 0.02 and 0.01, respectively. These values are very similar to those obtained in experiments that did not use a hydrofluorination step (e.g., Run 26, Table 34, ANL-6596, p. 152, in which only hydrogen chloride and fluorine were used, while Run 28, Table 34, ANL-6596, p. 152, included a separate phosgene treatment after hydrochlorination). These results show no apparent benefits of a hydrofluorination step.

Analysis of the Hydrochlorination Step. In the reprocessing of uranium-zirconium alloys by the fluidization and volatility technique, the hydrochlorination step is the critical reaction in that this step requires the longest process time. Knowledge of the hydrochlorination rate and gas composition is essential to the design and successful operation of (1) the pyrohydrolysis reactor for converting zirconium tetrachloride to the more easily stored oxide and (2) the proposed monitoring system (a control signal from the thermal conductivity cells) for the recycle of hydrogen chloride. Since knowledge of the progress of hydrochlorination as a function of time may lead to improvements, data on this step are now being obtained with thermal conductivity cells by measuring the amount of hydrogen produced during reaction of the alloy (see ANL-6569, p. 117). In Run 32, the concentration of hydrogen in the exit gases was recorded continuously during the 21.3 hr of hydrochlorination. These data have been used in calculating the efficiency of hydrogen chloride utilization and the alloy reaction rate as is described below.

The utilization efficiency E has been defined as

$$E = \frac{\text{HCl reacted}}{\text{HCl input}} \times 100 \quad .$$

The hydrochlorination rate or alloy reaction rate has been tentatively defined as the mass of fuel reacted per unit time. It has been calculated from the amount of hydrogen evolved, assuming the reaction

$$Zr + 4\,HCl \rightarrow ZrCl_4 + 2H_2 \quad .$$

This calculation disregards the presence of the other elements in the Zircaloy charge.

The observed values of the hydrogen chloride utilization efficiency, the alloy reaction rate, and the inlet concentration of hydrogen chloride are reported in Table 30 and are plotted in Figures 51 and 52. The maximum observed value of the efficiency was 80 percent. The maximum hydrochlorination rate was about 50 g/hr, approximately twice that achieved in earlier work. These observed values may be in error by ±10 percent. The concentration of hydrogen chloride in the inlet nitrogen stream was limited to about 20 m/o during the first half of the hydrochlorination period, whereas up to 95 m/o hydrogen chloride was fed during the later portion of the run. This relatively low limit for the first half of the run was necessary because the cooling system (a $\frac{1}{4}$-in. coil wrapped on the reactor; dry air as coolant) was unable to remove the additional heat produced at higher rates of reaction while maintaining the desired bed temperature of 400 C. The cooling system is now being improved.

Relatively long periods of operation under steady-state conditions were achieved in Run 32. For example, during the middle three hours of hydrochlorination of the first alloy charge, the efficiency of utilization of hydrogen chloride was about 70 percent, the alloy reaction rate was about 34 g/hr, and the inlet hydrogen chloride concentration was about 16 m/o. During this portion of the run, no external heat was supplied and the heat of reaction was sufficient to maintain the desired temperature of 400 C in the fluidized bed.

From the data obtained by analysis of the off-gas for hydrogen, it was determined that, when the second charge of alloy was added, about 50 percent of the first charge had reacted, and that when the third charge was added, about 37 percent of the first two charges had reacted. After the second charge was added, a peculiarity in operation was noted. The reaction zone, as indicated by temperature measurements in the bed, shifted to the upper portion of the bed. This was apparently due to trapping of some of the alloy chips in the upper region of the bed, possibly in the space between the solids sampler tube, the thermocouples, and the column wall. It became necessary to operate at somewhat lower rates than had been achieved in the first portion of the run. This condition was atypical, and corrective measures are being taken to prevent it from reoccurring.

Table 30

HYDROCHLORINATION OF THREE BATCHES OF URANIUM-ZIRCONIUM ALLOY CHIPS (RUN 32)

Equipment:	$1\frac{1}{2}$-in.-diameter fluidized bed unit with $1\frac{1}{2}$-in.-diameter down-flow filter section.
Fuel Charge:	1st Batch = 240.3 g; 2nd Batch = 240.2 g; 3rd Batch = 240 g of 5.1 w/o U-Zr alloy chip ($\frac{1}{8}$ - $\frac{1}{4}$-in. size).
Reaction Bed:	320 g of Alundum, -40 +60 Mesh (Norton Company, Type RR)
Down-flow Filter Bed:	120 g of Alundum, -40 +60 Mesh (Norton Company, Type RR) 200 g of Alundum, -14 +20 Mesh (Norton Company, Type 38)
Hydrochlorination Temperature:	400 ± 25 C
Diluent Gas:	Nitrogen
Volume Flow Rate of Gas:	15 cfh (70 F, 1 atm)

Run Time (hr)	Mole Percent HCl in Feed	Efficiency of HCl Utilization (%)	Rate of Hydrochlorination (g/hr)
0		First Batch of Fuel Charged	
0.33	6	65	15.9
0.66	7	74	14.3
1.0	15	75	36.1
2.0	17	69	33.4
3.0	17	69	33.4
4.0	95	7	18.0
4.03		Second Batch of Fuel Charged[a]	
4.36	7	60	14.9
4.69	7	60	14.9
5.03	8	58	14.3
6.03	3	30	4.2
7.03	6	60	14.9
8.03	8	73	26.5
8.19		Third Batch of Fuel Charged[b]	
8.52	5	70	10.6
8.85	5	74	11.1
9.19	8	30	8.5
10.19	8	70	17.0
11.19	11	63	23.3
12.19	15	80	33.4
13.19	25	51	41.9
14.19	26	56	38.7
15.19	22	41	29.7
16.19	36	32	38.2
17.19	85	9	20.7
18.19	85	12	49.5
19.19	95	5	12.2
20.19	95	3	7.4
21.0	95	<0.4	<0.8

[a]About 50 percent of the first charge had been reacted when the second batch of fuel was charged.

[b]A total of about 37 percent of the first two charges had been reacted when the final batch of fuel was charged.

Figure 51

HYDROCHLORINATION OF THREE BATCHES OF URANIUM-ZIRCONIUM ALLOY CHIPS. EFFICIENCY OF HCl UTILIZATION AND CONCENTRATION OF HCl IN THE FEED GAS DURING RUN 32

(see Table 30 for operating conditions)

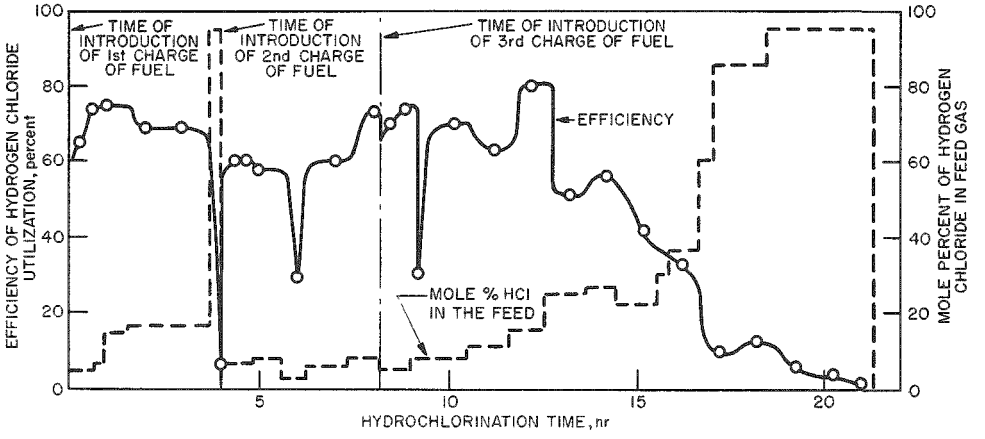

Figure 52

HYDROCHLORINATION OF THREE BATCHES OF URANIUM-ZIRCONIUM ALLOY CHIPS. RATE OF HYDROCHLORINATION OF ALLOY VERSUS TIME DURING RUN 32

(see Table 30 for operating conditions)

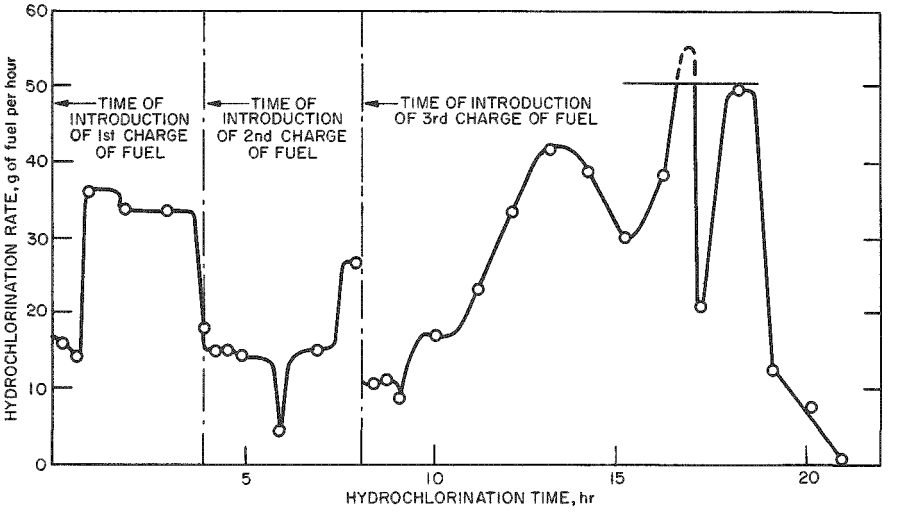

Hydrochlorination was stopped in Run 32 when hydrogen could no longer be detected in the off-gas. At this time, the total quantity of hydrogen chloride which had been fed was about three times the stoichiometric amount. The overall average rate of alloy reacted was about 34 g/hr for the 21.3 hr of hydrochlorination. The gas-monitoring system (in-line thermal conductivity cells) for following the progress of hydrochlorination operated satisfactorily and should prove very valuable in future work. Fluctuations in the data, such as those in Figures 51 and 52, are expected, since currently control of the reaction system is manual.

Discussion of the Hydrochlorination Reaction. The entire hydrochlorination period for a single charge of fuel may be divided into two parts, viz., a constant-rate period and a falling-rate period (see Figure 53).

Figure 53

ALTERNATIVE SCHEMES FOR MULTI-BATCH HYDROCHLORINATIONS

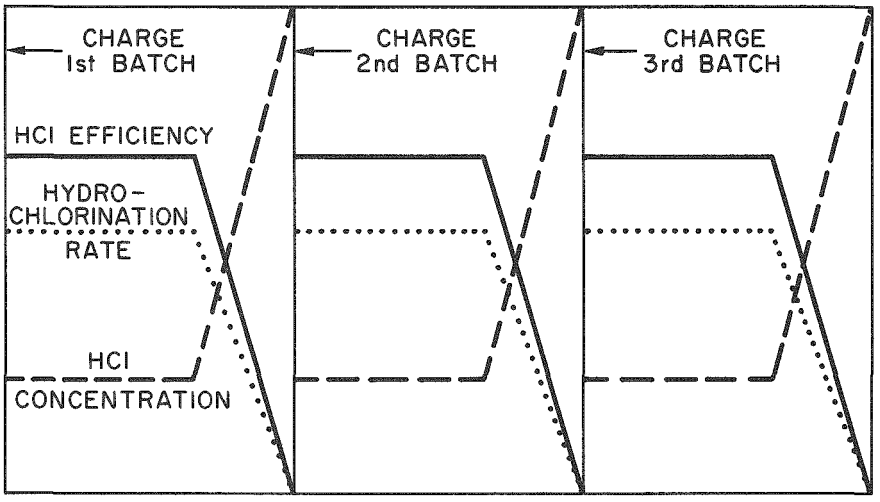

(a) COMPLETE HYDROCHLORINATION WITH EACH BATCH

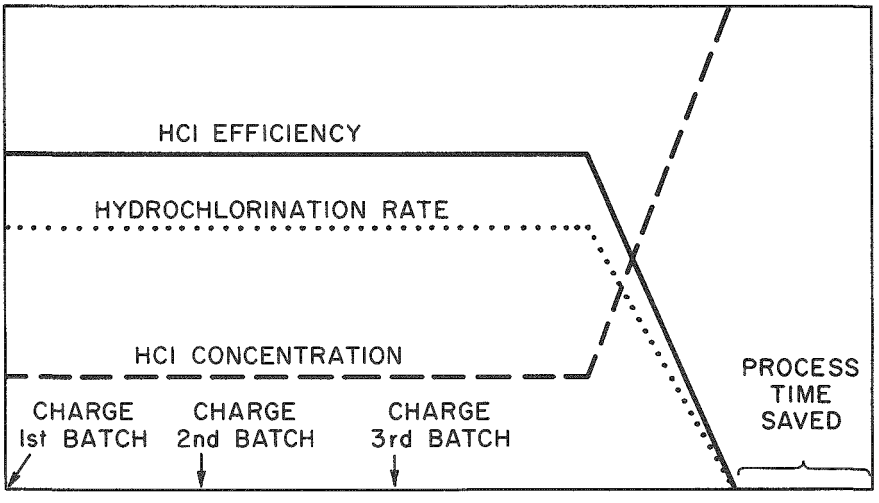

(b) IDEAL MULTI-BATCH HYDROCHLORINATION

During the constant-rate period, the reaction in the fluidized bed is self-sustaining, i.e., the heat produced by the hydrochlorination is equal to the sum of the heat losses to the surroundings and the heat removed by the gas streams. External heating may not be needed to maintain the fluidized bed at temperature. Steady state may be attained with respect to the concentration and flow rate of gas streams. Efficiency of hydrogen chloride utilization is constant.

During the falling-rate period, the reaction in the fluidized bed is not self-sustaining, i.e., the temperature of the fluidized bed has to be maintained by one or more of the following: (1) by increasing the concentration of hydrogen chloride in the inlet gas stream, (2) by stopping the circulation of cooling gas, and/or (3) by supplying heat from external heaters.

During the falling-rate period, both the reaction rate and the efficiency of hydrogen chloride utilization decrease rapidly. If multiple charges of fuel are being hydrochlorinated, knowledge of the time of transition from a constant-rate period to a falling-rate period allows a fresh batch to be charged soon after the constant-rate period for the preceding batch has ended (see Figure 53). By performing most of the hydrochlorination during the constant-rate period, the overall efficiency of hydrogen chloride utilization can be greatly improved, and, if a once-through system is used for the reactants, much less hydrogen chloride is required. In plant practice, the number of successive charges that may be hydrochlorinated may be limited because of heat generation by fission products and/or the accumulation of uranium (criticality considerations) in the fluidized bed.

In Run 32, charging of the second and third batches of fuel soon after completion of the constant-rate period for the preceding batch was attempted. Because the feed gases were controlled manually, this was not achieved (see Figure 52). It is believed, however, that the overall hydrochlorination time could have been reduced with proper control of the system.

Selection of Optimum Process Conditions. The duration of any reaction sequence contributes directly or indirectly to processing costs as well as equipment costs; therefore, it is highly desirable to lower overall processing time. In work to learn the optimum conditions for each of the steps in the current process scheme, the concentration of a key component was followed during the course of each reaction.

The first component studied was zirconium. The change in zirconium content of the bed during the phosgene treatment period was determined. Similarly, the change in the chloride content of the bed during hydrofluorination was determined, as well as the change in uranium content of the bed during fluorination. Samples of the fluidized bed were taken every half hour during each of the steps.

During the 2-hr hydrofluorination of the fluidized bed at 400 C (Run 31), reduction of the concentration of chloride (possibly present as uranium tetrachloride from reaction of the trichloride with phosgene) from 0.47 to 0.015 w/o was achieved (see Table 31 and Figure 55). The analytical data for both runs are summarized in Table 31 and are shown plotted against time on Figures 54, 55, and 56.

Table 31

CHANGE IN CONCENTRATION OF KEY COMPONENTS IN THE FLUIDIZED BED DURING CHLORINATION WITH PHOSGENE, HYDROFLUORINATION, AND FLUORINATION (RUNS 31 AND 32)

Equipment:	$1\frac{1}{2}$-in.-diameter fluidized bed unit with $1\frac{1}{2}$-in-diameter down-flow filter section
Fuel Charge:	240 g of 5.1 w/o U-Zr alloy chips during Run 31; 720.5 g of 5.1 w/o U-Zr alloy chips during Run 32 (charged in three equal-sized batches)
Reaction Bed:	320 g of Alundum -40 +60 mesh (Norton Company, Type RR)
Hydrochlorination Temperature:	400 ± 25 C, Quantity of HCl fed was 3 times the stoichiometric amount
Temperature of Phosgene Step:	Run 31, 400 C; Run 32, 350 C
Hydrofluorination Temperature:	Run 31, 400 C; Run 32, 350 C
Fluorination Temperature:	Run 31, 400 and 500 C; Run 32, 350 and 500 C

Time (hr)	$COCl_2$ Step[a] (w/o Zr in Alundum)		HF Step[b] (w/o Cl^- in Alundum)		F_2 Step[c] (w/o U in Alundum)	
	Run 31	Run 32	Run 31	Run 32	Run 31	Run 32
0	0.12	0.13	0.47	0.8	1.14	1.57
0.5	0.09	0.02	0.026[d]	0.05	0.29	0.08
1.0	0.02	0.02	0.015[d]	0.03	0.11	0.07
1.5	-	-	0.015[d]	-	0.07	0.05
2.0	-	-	0.015	0.03	0.07	0.06
2.5	-	-	-	-	0.06[e]	0.05[e]
3.0	-	-	-	-	0.05[e]	0.04[e]
3.5	-	-	-	-	0.05[e]	0.02[e]
4.0	-	-	-	-	0.05[e]	0.02[e]

[a]Concentration of phosgene in the feed gas stream was 60 m/o.

[b]Maximum concentration of hydrogen fluoride in the feed gas stream was 50 m/o.

[c]Maximum concentration of fluorine in the feed stream was 50 m/o for all of Run 31 and for the first 2 hr of Run 32. Thereafter, the concentration was increased to 90 m/o in Run 32.

[d]Interpolated from a smooth curve drawn through experimental values at 0, 0.67, 1.17, 1.67, and 2.00 hr.

[e]Temperature of the fluidized bed was 500 C for the second half of each run.

Figure 54

EFFECT OF PHOSGENE TREATMENT TIME ON ZIRCONIUM CONTENT OF THE FLUIDIZED BED (RUNS 31 AND 32)

60 m/o $COCl_2$ in the gas stream

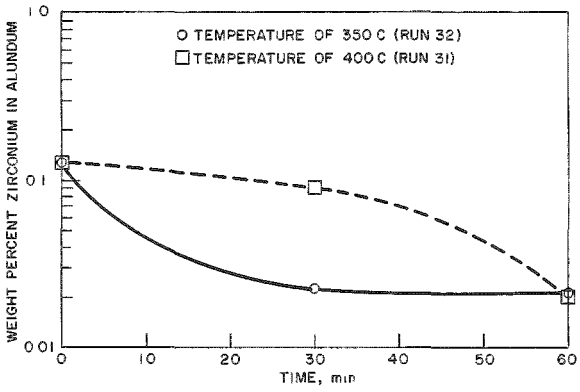

Figure 55

HYDROFLUORINATION OF RESIDUES FROM CHLORINATION STEP - EFFECT OF TREATMENT TIME ON CHLORIDE CONTENT OF THE FLUIDIZED BED (RUNS 31 AND 32)

50 m/o hydrogen fluoride in the gas stream

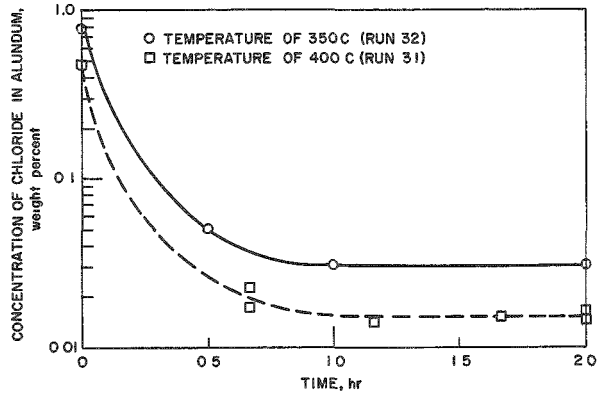

Figure 56

FLUORINATION OF RESIDUES FROM HYDROFLUORINATION STEP - EFFECT OF TREATMENT TIME ON URANIUM CONCENTRATION IN THE FLUIDIZED BED (RUNS 31 AND 32)

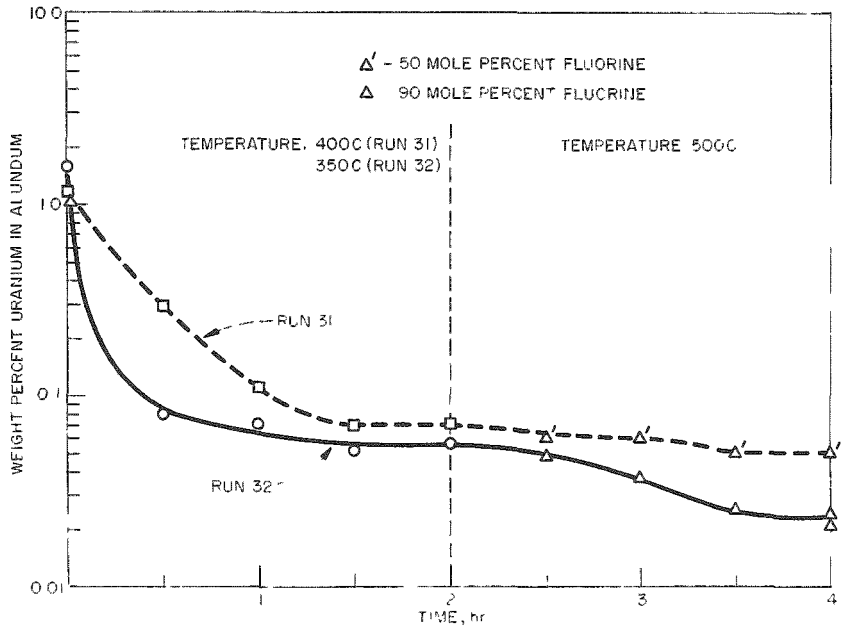

The weight percent of zirconium in the fluidized bed decreased from 0.12 to 0.02 during one hour of chlorination with phosgene at 400 C, and from 0.13 to 0.02 in about one-half hour at 350 C (see Figure 54 and Table 31). The rate of removal of zirconium from Alundum at the

lower temperature of 350 C appeared to be quite different from that at the higher temperature of 400 C (see Figure 54), indicating possible differences in chlorination rates at the two temperature levels for the various zirconium compounds present in the fluidized bed.

During the 2-hr hydrofluorination of the fluidized bed at 400 C (Run 31), the amount of chloride in the fluidized bed (possibly as uranium tetrachloride from reaction of the trichloride with phosgene) was reduced from 0.47 to 0.015 w/o (see Table 31 and Figure 55). The chloride concentration in the bed reached the apparent equilibrium value of 0.015 in about one hour. During the hydrofluorination at 350 C, an equilibrium chloride concentration of about 0.03 w/o was reached in a similar period. In the latter case, the initial chloride value was 0.8 w/o. From these data it may be concluded that hydrofluorination at either 400 C or 350 C for one hour would be sufficient to lower the chloride content of the fluidized bed sufficiently so that further removal of chlorine during fluorination would be negligible. Residual chloride values in the bed after fluorination have been in the region of 0.01 w/o.

During fluorination of the fluidized bed after hydrofluorination in Run 31, the concentration of uranium in Alundum decreased from 1.14 to 0.07 w/o during the first 2 hr at 400 C, and from 0.07 to 0.05 w/o during the subsequent 2 hr at 500 C (see Table 31 and Figure 56). During the fluorination at 350 C in Run 32, the concentration of uranium in the fluidized bed decreased from 1.57 to 0.07 w/o during the first hour and did not decrease significantly during the second hour (see Figure 56 and Table 31). With continued fluorination at 500 C, using 90 m/o instead of 50 m/o fluorine concentration, the concentration of uranium reached an equilibrium value of 0.02 w/o within an additional 2 hr. Prolonged fluorination at this temperature did not achieve additional uranium removal. From these data it may be concluded that the optimum fluorination conditions are one hour at 350 C and 2 hr at 500 C with a gas composition of 90 m/o fluorine. Also, since similar residual uranium values were achieved in previous work (see ANL-6569, p. 116) which did not involve a hydrofluorination step, it is believed that this step is not a factor in uranium removal and can be eliminated.

The optimum process conditions for the reactant sequence hydrogen chloride-phosgene-hydrogen fluoride-fluorine may now be summarized (see Table 32). A total reaction time of 10 hr is indicated.

Table 32

SUMMARY OF PROCESS CONDITIONS FOR ACHIEVING HIGH URANIUM RECOVERY FROM ZIRCONIUM-URANIUM ALLOY

Reactant			Temperature (C)		
Type	Mole Percent	Quantity without Reactant Recycle (x stoichiometric)	Fluid Bed	Filter Bed	Time (hr)
HCl	As needed	3[a]	400	400	5
$COCl_2$	60	2[a]	350	350	1
HF	50	30[b]	350	350	1
F_2	90	30[c]	350	350	1
F_2	90	30[c]	500	500	2

[a]Stoichiometric amount based on the initial zirconium in the charge.

[b]Stoichiometric amount required to convert the uranium in the initial charge into uranium tetrafluoride.

[c]Stoichiometric amount required to convert the uranium in the initial charge in the form of UCl_3 into UF_6.

Simplification of the cycle by complete elimination of the phosgene and hydrogen fluoride steps may be possible (subsequent work to be reported in the next quarterly has indeed shown this to be the case). This is suggested by the significant additional uranium removal that was achieved upon refluorination (carried out this quarter) at a higher temperature (500 C instead of 350 C) of a ground sample from a bed which had been used for five complete hydrochlorination and fluorination cycles (see Runs 18 to 22, pp. 149 to 150, ANL-6543). The residual uranium and zirconium contents of the bed material had apparently reached equilibrium values of about 1.3 percent zirconium and about 0.1 percent uranium, corresponding to 0.43 percent and 0.64 percent of the total initial charge, respectively. After refluorination of the sample in a tube furnace at 500 C for 2 hr with 90 m/o fluorine, analysis showed a residual uranium content in the bed of 0.024 w/o, corresponding to about 0.15 percent of the total initial uranium charge. Unexpectedly, the zirconium content of the bed was also reduced, the final concentration being 0.56 w/o. Although this material is not typical, since it was ground prior to further processing (refluorination), the magnitude of the improvement is believed significant. This experiment also tends to confirm the fact that the two-step fluorination, a period at a moderate temperature (350 C) followed by a period at a higher temperature (500 C), is beneficial regardless of the reaction cycle in use.

Pressure Buildup across the Down-flow Filter. The problem of undesirable buildup of pressure across the down-flow filter during hydrochlorination and fluorination has been noted in previous studies

(see ANL-6543, p. 150; ANL-6569, pp. 115 and 117; ANL-6596, p. 150). This pressure buildup has been attributed to the resistance to gas flow caused by the deposition and subsequent reaction (fluorination) of a layer of fine particulate solids on the top surface of the down-flow filter bed. These solids were believed to be principally nickel chloride formed during hydrochlorination as a result of corrosion of the primary reactor when the temperature of the reactor walls was appreciably above 400 C (temperatures up to 550 C were used). Of the two types of Alundum tried in the fluid bed, Type RR and Type 38, the latter apparently exhibits a greater attrition rate and the resulting fines also are believed to have contributed to pressure buildup.

This problem of pressure buildup has been of some concern but, as a result of several changes in the system, as listed below, good operation has been achieved in current work. These changes included: a) maintaining the temperature at the zone adjacent to the alloy charge at about 400 ± 25 C during hydrochlorination to reduce corrosion; (b) installation of an auxiliary settling chamber (similar in dimensions to the down-flow filter section) between the fluid-bed reactor and the filter section, and c) the use of narrow and coarser size fractions of Alundum as filter material, thus providing larger void spaces.

The filter is comprised of a layer of -40 +60 mesh, Type RR Alundum sandwiched between layers of -14 + 20 mesh, Type 38 Alundum. The total height of the bed is about 6 in. The distribution of these materials in layers in previous and current beds is shown below:

Previous Beds	Current Beds (Runs 31 and 32)
50 g -14 +20	170 g -14 +20
220 g -14 +60	120 g -40 +60
50 g -14 +20	30 g -14 +20

The total amount of material has remained constant at about 320 g.

In the current work, no sustained pressure buildup was noted; however, pressure measurements across the filter bed reflect the flow of zirconium tetrachloride and of uranium hexafluoride through the bed, as these gases have relatively high viscosities compared with the other components of the gas stream, namely, nitrogen, hydrogen, fluorine, and hydrogen chloride.

Future Work. Studies in which phosgene and hydrogen fluoride steps are omitted are being resumed to obtain data for the comparison of various reaction schemes. More accurate "on stream" gas-analysis equipment is being installed to get additional data on the progress

of hydrochlorination and fluorination. These changes are expected to help in the process scale-up work (see ANL-6543, p. 153). The unit is being simplified by removal of the auxiliary settling chamber. This modification will permit further evaluation of the filter bed alone.

Among the planned activities in this program are a) experiments with long, narrow plate sections of alloy rather than chips to determine how fuel shape may affect the operation, b) work with alloy containing simulated fission products to determine whether overall uranium retention is affected by the presence of minor amounts of other elements, and c) preliminary work on the recovery of uranium from uranium-aluminum alloy.

b. Fluid-bed Hydrolysis of Zirconium Tetrachloride
(K. S. Sutherland, D. J. Raue)

The processing of uranium-zirconium alloys by hydrochlorination produces relatively large amounts of waste zirconium tetrachloride. This material is in the form of vapor which may be condensed or treated for waste disposal. To convert this vapor to a form which is more easily stored, it is proposed that it be hydrolyzed by steam to the solid zirconium dioxide. The hydrolysis reaction is being studied in a fluidized bed with the aim of determining the optimum reaction conditions for the process. Previous work (see ANL-6569, p. 118, and ANL-6596, p. 154) has demonstrated the feasibility of the process at zirconium tetrachloride feed rates in the region of 2 kg/hr for a variety of reaction conditions.

In recent efforts the range of operating conditions has been broadened in an attempt to discover the limits of satisfactory operation. Also, since this operation is being incorporated into the pilot plant (see ANL-6543, p. 153), conditions approaching those contemplated for the pilot plant are being simulated in the current studies by including hydrogen chloride as a major component of the feed gas.

The equipment employed is similar to that previously described (see ANL-6569, pp. 118 to 119), the only changes being the elimination of the carrier gas preheater and the addition of an air vibrator fixed to the zirconium tetrachloride-feed hopper. The preheater is not needed since it has been found that the resistance furnace used for vaporizing the zirconium tetrachloride has sufficient capacity to heat the carrier gas to the required temperature. Removal of the preheater has eliminated the possibility of prematurely subliming some zirconium tetrachloride upstream from the furnace, thereby avoiding a condition that has resulted in feed-line blockages. The added air vibrator was necessary to prevent solids holdup in the hopper. More uniform feed rates have thereby been achieved.

Operating conditions for the nine runs covered by this report are given in Table 33. Major variations in conditions were:

a) the use of a small particle size for the starting bed material in Run CO-37 (120 mesh Alundum as compared with 60 mesh and 90 mesh Alundum used previously);

b) the use of a higher bed temperature in Run CO-38 (500 C as compared with a previous maximum of 450 C);

c) the addition of hydrogen chloride as a major component of the feed gas in Runs CO-41, 43, and 44; and

d) the use of sand instead of Alundum as a starting bed material in Runs CO-42 to CO-44.

Also, an initial bed weight of 20 kg was employed in all current runs, since determinations of bulk densities showed that the amount of material used in previous runs, 16 kg, was giving a fluidized bed depth of just over 18 in., whereas a depth of about 24 in. was considered advisable to provide adequate residence time. The steam enters the reaction vessel nearly 12 in. above the bed-support plate.

Table 33

FLUID-BED HYDROLYSIS OF ZIRCONIUM TETRACHLORIDE RUN CONDITIONS AND RESULTS

Equipment: 6-in.-diameter fluidized-bed reactor
Initial Bed Weight: 20 kg
Blowback Pressure: 80 psig

Run No.	Run Duration (hr)	$ZrCl_4$ Feed Rate (kg/hr)	Steam Rate (x stoich)	Bed Temp (C)	Initial Bed Material	Carrier Gas Flow Rate		Increase in Pressure Drop (in. Hg)
						N_2 (cfm)	HCl (cfm)	
CO-36	4.5	1.8	3.5	350	90 mesh Alundum	2.65	-	0.4
CO-37	4.5	1.7	3.7	350	120 mesh Alundum	2.3	-	0.3
CO-38	4.75	1.7	3.7	500	90 mesh Alundum	2.65	-	1.5
CO-39	4.5	2.7	3.3	350	Alundum coated with zirconium dioxide	2.65	-	0.5
CO-40	4.75	3.2	3.1	350	Final bed from Run CO-39	2.65	-	0
CO-41	3.25	2.5	3.4	350	Final bed from Run CO-40	0.9	1.75	0
CO-42	3.5	2.3	3.7	350	Sand[b]	3.0	-	0.3
CO-43	3.25	2.5	3.3	350	Sand[b]	0.9	1.75	0
CO-44	11.5[a]	2.6	3.2	350	Sand[b]	0.9	1.75	0.5

[a]Combined time for operations conducted on two successive days with overnight shutdown.

[b]The sand was about 50 percent +60 mesh and about 50 percent -60 mesh (including about 5 to 10 percent -200 mesh).

Since the proposed pilot plant will be operated as a batch process, with the possible need to discard the hydrolysis bed after each batch, it may be necessary to employ a starting bed material that is

cheaper than the refractory-grade Alundum used until now. Accordingly, white sand, crushed to the desired size, has been examined as a starting bed material. The sand was about 50 percent +60 mesh and about 50 percent -60 mesh (including about 5 to 10 percent -200 mesh).

The zirconium tetrachloride feed rates given in Table 33 are no greater than those previously used. Whereas the earlier values were averages of rates which varied widely during the course of any one run, the current rates (obtained with the additional air vibrator attached to the feed hopper) are uniform values for entire runs. The feed rate of $3\frac{1}{4}$ kg/hr represents the maximum rate than can be achieved with the present equipment.

All of the runs reported here were completed satisfactorily, that is, there was no excessive pressure buildup at the exit gas filters (see last column of Table 33). The initial bed material for nearly all of these runs contained a significant proportion of fines (-200 mesh), and this fact, coupled with the inherent error of sieve analyses, has made it difficult to obtain accurate figures for fines production during the runs. It is probable that about 25 to 35 percent of the zirconium dioxide produced by the hydrolysis is in the form of particles smaller than 200 mesh, while the remainder is deposited on the bed material. A more accurate determination of the distribution of product oxide awaits complete chemical analyses of bed samples and a better method for determining the quantity of fines present. An elutriation technique is being considered for this latter purpose.

The variables that have been studied in this program to date are as follows:

1) zirconium tetrachloride feed rates of up to $3\frac{1}{4}$ kg/hr;
2) bed temperatures ranging from 250 to 500 C;
3) starting beds of zirconium dioxide, Alundum, and sand;
4) nominal starting bed average particle sizes of 60, 90, and 120 mesh;
5) run durations up to $11\frac{1}{2}$ hr.

Satisfactory operation of the column has been achieved within these ranges.

An important independent variable which is yet to be studied extensively is the steam feed rate (or steam excess). There are indications, however, that rates falling much below three times the required stoichiometric amount tend to result in filter blockage. Thus a steam-to-zirconium tetrachloride ratio of at least three will be maintained in future work.

Experimental effort will be devoted to operation at higher zirconium tetrachloride feed rates in an attempt to discover the maximum capacity of the 6-in.-diameter fluidized bed. A larger feed screw is being incorporated into the system to facilitate this work. Results of these studies will be of importance to the operation of the pilot plant, since the rate of production of zirconium tetrachloride in the new facility based on recent data from the $1\frac{1}{2}$-in.-column work may be as much as two or three times greater than the rates currently used in the hydrolysis experiments.

c. Installation of a Fluid-bed Volatility Pilot-plant Facility for Recovery of Uranium from Zirconium Alloy Fuels
(N. Levitz, J. Barghusen, J. Holmes)

All of the fabricated pieces of equipment and essentially all other items for the fluoride volatility pilot plant for the recovery of uranium from zirconium alloy fuels (see ANL-6543, p. 153) have been received from Central Shops and outside vendors. Installation of the equipment and the testing of equipment components is underway.

d. High-level Radiation Experiments on Uranium-Zirconium Alloy Fuel
(J. W. Loeding)

Plans have been initiated for a bench-scale, high-radiation-level study of the basic reaction steps of the fluid-bed volatility process for highly enriched uranium-zirconium alloy fuel. Highly irradiated, short-term-cooled alloy specimens will be used for this work. The purposes of this study will be to determine the following:

a) the fission product distribution in each step of the process and the decontamination factors which might be expected from the initial separation and collection of the uranium;

b) the effect of radiation on the process, i.e., on reaction rates, yields, etc.

c) short-term effects of radiation on the equipment or components of the system.

Also, experience will be gained in the design of remote handling operations associated with the process.

The equipment will include a $1\frac{1}{2}$-in.-diameter fluid-bed column, a fixed-bed filter unit, and associated items similar to those being used for the inactive alloy studies (see ANL-6569, p. 114). The proposed unit is to be installed in an existing cave in the Chemical Engineering Division facilities during the second half of 1963. Direct operation and maintenance with manipulators will be used.

C. Conversion of Uranium Hexafluoride to Uranium Dioxide; Preparation of High-density Particles

(I. Knudsen, N. Levitz, M. Jones)

Process development studies were continued on a direct fluid-bed method for preparing high-density uranium dioxide particles from uranium hexafluoride. The dense spheroidal product is intended for use in dispersions or packed fuel elements. The process involves the simultaneous reaction of the hexafluoride with steam and hydrogen in the range from 650 to 700 C. The work to date has been concerned with the effect on particle density of operational variables such as reactant concentration in the inlet (fluidizing) gas stream, bed temperature, and feed rate.

In previous work (see ANL-6569, pp. 121 to 124), particle density was found to vary as the concentration of steam in the reactant feed stream was varied. Highest particle densities (up to about 9.3 g/cc or about 85 percent of theoretical) were obtained at steam concentrations corresponding to the range 0.75 to 1.4 times the stoichiometric requirements.* Higher temperatures (700 C) resulted in uranium dioxide particles with even greater densities, up to 9.8 g/cc, which is equivalent to about 89 percent of theoretical (see ANL-6596, p. 159).

Current work investigated the effects of increased bed height and reduced hydrogen excess on particle density. Also, since coarse particles (+14 mesh) are apparently a desirable component of a uranium mixture if high compaction densities[31] are to be achieved, preliminary trials to test the feasibility of preparing particles in this size range were made.

The studies are being conducted in the 3-in.-diameter cone-bottom Monel column described previously (see ANL-6379, p. 183). The run procedure involves periods when hexafluoride, steam, and hydrogen are fed alternating with periods when cleanup of residual fluoride is carried out. In the cleanup period, only steam and hydrogen are fed. Product is removed semicontinuously (after each cleanup period) such that the bed weight remains approximately constant. Sufficient seed particles in the size range of about 160 μ in diameter are added to maintain the average bed particle size in the desired range, which is between 325 to 350 μ. When larger particles are desired, no seed particles are added.

Results

A deep-bed run has been performed in which the height of the bed above the hexafluoride feed nozzle was held constant by increasing the

---

*Based on the reaction $UF_6 + 2\ H_2O + H_2 \rightarrow UO_2 + 6\ HF$.

[31] DeHollander, W. R., Vibrational Compaction of Uranium Dioxide, GEAP-4032 (March 1962).

nozzle penetration into the bed from about 4 to 13 in. The uranium dioxide particles obtained at a steam rate of 1.15 times stoichiometric at 650 C with an 18-in.-deep bed (Run 66R, Table 34) had a density of 9.6 g/cc. This result compares favorably with densities of 9.3 g/cc obtained with 8- to 10-in.-deep beds at similar steam rates. In the latter half of this run, the quantity of hydrogen fed was reduced from 17 times to 3.8 times the stoichiometric requirements, with no apparent effect on the product density. However, the hydrogen excess appeared to have an effect on residual fluoride content. When less hydrogen was used, the average residual fluoride content of the product was higher, 650 ppm as compared to 380 ppm. The quantity of fine material (believed to be produced by gas-phase reaction) elutriated over into the filter chamber was about the same during both parts of the run, averaging about 14 w/o of the hexafluoride fed.

Table 34

PREPARATION OF HIGH-DENSITY URANIUM DIOXIDE PARTICLES FROM URANIUM HEXAFLUORIDE IN FLUIDIZED BEDS

Equipment: 3-in.-diameter Monel Column
Temperature: 650 C
UF_6 Rate: 25 g/min
UF_6 Feed on-time: 30 min/hr
Starting Bed Weight: 11 kg for Run 66 R; 6 to 8 kg for Run 66 S

Run No.	Reactants (x Stoich)[a] Steam	Hydrogen	Run Duration (hr)	Bed Height (in.)	Superficial Velocity (ft/sec)	UO_2 Density (g/cc) Tapped Bulk	Particle[b]
66 R	1.15	17.0	17	18	1.0	6.7	9.6
66 R	1.15	3.8	12	18	1.0	6.8	9.6
66 S	1.25	4.2	15	10 to 14	1.5 to 3.45	5.9	8.9

[a]Based on the reaction $UF_6 + 2H_2O + H_2 \rightarrow UO_2 + 6\ HF$.

[b]Mercury-displacement determinations.

Results of a preliminary run (Run 66S) having the objective of preparing particles up to 14 mesh are shown in Table 34. The sieve analyses of the starting bed and final bed for that run are shown below:

Mesh Size	Weight Percent of Given Mesh Size: Starting Bed	Final Bed
+16	0	2.2
-16 +18	0	4.0
-18 +20	4.4	18.2
-20 +40	86.0	72.6
-40 +60	9.6	1.2
-60 +100	0	1.5
-100	0	0.3
Average Weight Mean Particle Diameter, μ	620	704

Particle growth up to 16 mesh occurred during the 15 hr of operation (accumulated over a 3-day period). Because of the particle growth during the run, it was found necessary to increase the superficial velocity from 1.5 to 3.5 ft/sec to maintain fluidization; nitrogen was introduced when additional gas was required for maintaining fluidization. Essentially all of the -60 mesh material in the final bed appeared (from microscopic examination) to be segments of the deposited layer of the larger particles. The bulk of the larger particles were intact and spheroidal. The fines collected overhead in the separate filter chamber amounted to about 5 w/o of the hexafluoride fed. The density of the final bed and of the coarse (+18 mesh) fraction of the final bed was 8.9 g/cc. This value is somewhat lower than that originally expected, possibly because some difficulty was experienced in controlling the hexafluoride feed rate during portions of the run. The feed rate was low at times. As a consequence, the steam excess was high, which condition gives lower particle densities.

Further effort will be made to prepare large particles. At least three different size fractions are required for high compaction efficiencies in the preparation of packed fuel elements. A typical mixture would consist of about 60 percent coarse, 20 percent medium, and 20 percent fines. A particle diameter ratio of 64:8:1 for these fractions would be desirable with the coarse fraction consisting of particles of at least 14 mesh size.

In future runs, in order to avoid the high gas velocities needed for fluidizing the relatively coarse particles, the bed will not be fluidized except at frequent intervals when a gas pulse is superimposed on the normal gas stream. By the pulse method, it is hoped the bed can be sufficiently agitated to achieve mixing and prevent caking.

III. CALORIMETRY*

(W. N. Hubbard, H. M. Feder)

Thermodynamic data are lacking for many compounds of interest in high-temperature chemistry because of the experimental difficulties involved in making the necessary measurements. A program has been undertaken to determine some of these data.

The basic data needed are heats of formation at 25 C. Part of the program of the group consists of determinations of heats of formation by the method of oxygen bomb calorimetry. However, many of the compounds of interest are difficult to burn in oxygen and, consequently, cannot be studied by oxygen bomb calorimetry. To study compounds of interest that are not amenable to oxygen bomb calorimetry, the techniques of the bomb calorimetric method (a method which has been developed to a high degree of precision and accuracy) have been modified so that fluorine can be used as the oxidant.

The accumulation of basic heat of formation data for fluorides is a necessary preliminary adjunct to the general use of fluorine bomb calorimetry for the study of compounds and is a valuable program on its own merit. To date, heat of formation values have been published for boron trifluoride, molybdenum hexafluoride, and the tetrafluorides of titanium, zirconium, hafnium, and silicon. The heats of combustion in fluorine of three compounds, boron nitride, silicon dioxide, and zirconium diboride, have been determined by fluorine bomb calorimetry. The value obtained previously for the heat of formation of boron trifluoride was needed to obtain the heat of formation of boron nitride, while the value for silicon tetrafluoride was needed to obtain the heat of formation of silicon dioxide, and the values for boron trifluoride and zirconium tetrafluoride are needed for zirconium diboride.

The heats of formation at 25 C from oxygen or fluorine combustion calorimetry will be combined with values of the change in enthalpy, which will be measured by a high-temperature enthalpy calorimeter, to determine thermodynamic properties at high temperatures. A calorimetric system for measurements up to 1500 C has been designed and is now being assembled and tested.

A. Combustion of Uranium in Fluorine

(J. L. Settle)

The heat of formation of uranium hexafluoride has been of interest to the atomic energy program since the early days of the Manhattan Project

*A summary of this section is given on page 25.

when Long and Davidson[32] determined the heat of solution of uranium hexafluoride in water. From these measurements values of the heat of formation were calculated as follows: for the gas -505 ± 3 kcal/g; and for the crystal -516 ± 3 kcal/g. Recently, Russian workers[33] have made confirmatory measurements of the heat of solution of uranium hexafluoride. However, in a recent critical review of the thermodynamics of uranium compounds Rand and Kubaschewski[34] were unable to select a value for the heat of formation of crystalline uranium hexafluoride with any more certainty than -523 ± 6 kcal/mole.

Because of this large uncertainty and because of the need for an accurate value as a necessary auxiliary datum for anticipated determinations of the heats of formation of other uranium compounds by fluorine bomb calorimetry, a direct determination of the heat of formation of uranium hexafluoride was undertaken.

Initial measurements yielded a mean value for a series of three combustions of -521 ± 3 kcal/mole for the heat of formation of crystalline uranium hexafluoride (see ANL-6333, p. 125). In order to obtain more precise data, it was necessary to develop: (1) satisfactory combustion techniques to burn relatively large samples of uranium; (2) techniques to obtain more nearly complete combustions; and (3) suitable analytical procedures to define the complex mixture of products remaining after the combustion. The development of suitable combustion and analytical techniques has been discussed in ANL-6379, p. 129; ANL-6413, p. 102; ANL-6477, p. 163; and ANL-6543, p. 165.

A recent series of seven combustions of uranium in fluorine has given a value of -522.7 ± 0.48 kcal/mole for the heat of formation of crystalline uranium hexafluoride. Although the final result of the direct determination does not differ significantly from the "selected" value of Rand and Kubaschewski, the uncertainty is now one whole order of magnitude less.

A detailed report of the work and the techniques used is being prepared for publication. Only the results obtained will be given here. The combustion experiments are summarized in Table 35. The numbered entries in the table are: (1) the mass in vacuo of the uranium reacted, which was determined by subtracting the total mass of unburned metal recovered after combustion from the mass of sample originally introduced into the

---

[32] Long, F. A., and Davidson, N. R., The Chemistry of Uranium, J. J. Katz and E. Rabinowitch, Eds., McGraw-Hill Book Co., Inc., New York (1951), p. 412.

[33] Popov, M. M., Kostylev, F. A., and Karpova, T. F., Zhur. neorg. Kim., 2, 9 (1957), IGRL-T/CA 56.

[34] Rand, M. H., and Kubaschewski, O., British Atomic Energy Report AERE-R-3487 (1960).

Table 35

URANIUM COMBUSTIONS IN FLUORINE[a]

Uranium, g	2.49738[b]	2.30162[b]	2.28921[b]	2.58984[b]	1.84847[c]	2.73206[c]	2.30727[c]
Uranium recovered and weighed, g	0.86244	0.64858	0.61383	0.89210	0.42726	0.98046	0.71244
Uranium recovered in scrapings, g	0.01076	0.02064	0.01546	0.01662	0.01123	0.01010	0.01137
Mass of scrapings, g	0.02003	0.04235	0.03249	0.03633	0.02944	0.05703	0.02448
UF_3 formed, g	0.00518	0.01165	0.00839	0.01093	0.01090	0.01433	0.00451
UF_4 formed, g	0.00409	0.01006	0.00864	0.00878	0.00731	0.03260	0.00860
1. $\underline{m}'$, uranium reacted, g	1.62418	1.63240	1.65992	1.68112	1.40998	1.74150	1.58346
2. $\Delta\underline{t}_c$, deg	0.97669	0.97903	0.99640	1.00822	0.84394	1.04267	0.95086
3. ϵ(calor.)(-$\Delta\underline{t}_c$), cal	-3522.87	-3531.31	-3593.96	-3636.60	-3044.05	-3760.86	-3429.70
4. $\Delta\underline{E}_{contents}$, cal	-12.28	-12.31	-12.53	-12.69	-10.60	-13.12	-11.95
5. $\Delta\underline{E}_{ignition}$, cal	2.49	2.63	2.56	2.56	2.56	2.56	2.10
6. $\Delta\underline{E}_{gas}$, cal	-1.40	-1.41	-1.45	-1.47	-1.12	-1.53	-1.34
7. $\Delta\underline{E}_{impurities}$, cal	2.92	2.93	2.97	3.01	0.91	0.94	0.93
8. $\Delta\underline{E}_{prereaction}$, cal	-1.7	-1.7	-1.7	-1.7	-1.6	-1.7	-1.7
9. $\Delta\underline{E}_{UF_3\ formation}$, cal	-3.11	-7.00	-5.04	-6.57	-6.55	-8.61	-2.71
10. $\Delta\underline{E}_{UF_4\ formation}$, cal	-0.95	-2.33	-2.00	-2.03	-1.69	-7.54	-1.99
11. $\Delta\underline{E}_{sublimation\ UF_6}$, cal	-22.38	-22.38	-22.38	-22.38	-22.38	-22.38	-22.38
12. $\Delta\underline{E}^\circ_c/\underline{M}$, cal/g	-2191.43	-2188.73	-2188.97	-2187.75	-2187.63	-2189.06	-2190.61

Mean $\Delta\underline{E}^\circ_c/\underline{M}$ = -2189.17 cal/g

Std. dev. of mean = ±0.53 cal/g

[a]These results are to be considered tentative pending an independent check of the calculations.
[b]Rod 1 used.
[c]Rod 2 used.

bomb; (2) the temperature increase of the calorimetric system, corrected for heat exchange between the calorimeter and its surroundings; (3) the energy equivalent of the calorimetric system, multiplied by the corrected temperature increase; (4) the energy absorbed by the contents of the bomb during the hypothetical isothermal process at 25 C; (5) the measured electrical energy input for ignition of the fuse; (6) the net correction for the compression and decompression of the bomb gases to standard state conditions; (7) the net correction for impurities in the uranium sample; (8) the net correction for oxidation and fluorination of the sample before ignition; (9) and (10) the corrections for uranium trifluoride and uranium tetrafluoride formation; (11) the correction for the energy of sublimation of the uranium hexafluoride appearing in the gas phase; and (12) the energy change per gram of uranium for the reaction

$$U(c) + 3\ F_2(g) \rightarrow UF_6(c)$$

with the reactants and product in their respective standard states at 25 C. Item 12 is the sum of items 3 through 11 divided by the mass of uranium reacted.

Table 36 lists the derived data for the formation of both crystalline and gaseous uranium hexafluoride. The uncertainties given in the table are uncertainty intervals equal to twice the combined standard deviations arising from known sources.

Table 36

DERIVED DATA FOR THE FORMATION OF URANIUM HEXAFLUORIDE AT 25 C

The data are given in kcal/mole except for ΔSf° values, which are given in cal/(deg)(mole)

	Species	
	$UF_6(c)$	$UF_6(g)$
Energy of formation, ΔEf°	$-521.0_9 \pm 0.4_8$	$-509.8_1 \pm 0.4_8$
Enthalpy of formation, ΔHf°	$-522.8_7 \pm 0.4_8$	$-511.0_0 \pm 0.4_8$
Entropy of formation, ΔSf°	-102.9_0	-67.0_1
Gibbs energy of formation, ΔGf°	$-492.1_9 \pm 0.4_8$	$-491.0_2 \pm 0.4_8$

B. Combustion of Aluminum in Fluorine
(E. Rudzitis and R. Terry)

Techniques used for the calorimetric study of the combustion of aluminum in fluorine were described in the last quarterly report (ANL-6596, p. 171). Table 37 presents the impurity levels in the aluminum burned, and Table 38 presents the results of thirteen combustions carried

Table 37

IMPURITIES IN ALUMINUM

Impurity	Calculated[a] Levels (ppm)
AlF_3	500
Al_2O_3	720
CO_2	405
H_2O	270
N_2	50
SiO_2	30
Cu	30

[a]Based on elemental and spectrochemical analyses for F_2, O_2, C, H_2, N_2, Si, and Cu.

out over a period of several months. Because of ignition difficulties, a cadmium fuse wire was used in all but the first two runs. No CdF_2-AlF_3 interaction was observed either calorimetrically or from X-ray powder patterns.

Table 38

ALUMINUM COMBUSTIONS IN FLUORINE

1. $\underline{m}'$, g	0.27304	0.22444	0.22915	0.23277	0.29321	0.39984	0.38163	0.41936	0.41158	0.33584	0.21789	0.32619	0.27940
2. Δt_c, deg	1.00554	0.83033	0.85196	0.86935	1.08608	1.48483	1.41240	1.55315	1.52635	1.24384	0.80336	1.20700	1.03231
3. ϵ(calor.)(-Δt_c), cal	-3609.2	-2980.3	-3057.9	-3120.4	-3898.3	-5329.5	-5069.5	-5574.7	-5478.5	-4464.5	2883.3	4332.3	3705.3
4. $\Delta\underline{E}_{contents}$, cal	-7.1	-5.5	-5.5	-5.6	-6.9	-9.5	-9.8	-9.7	-10.5	-8.1	-6.9	-11.9	-10.3
5. $\Delta\underline{E}_{gas}$, cal	-0.5	-0.5	-0.5	-0.6	-0.7	-0.5	-0.8	-0.8	-0.8	-0.8	-0.4	-0.6	-0.7
6. $\Delta\underline{E}_{ignition}$, cal	0.3	0.4	0.3	0.2	0.2	0.1	0.1	0.1	0.1	0.2	0.3	0.1	0.3
7. $\Delta\underline{E}_{fuse}$, cal	-	-	15.5	10.1	5.9	10.0	8.1	8.1	7.9	8.2	8.9	4.56	10.4
8. $\Delta\underline{E}_{impurities}$, cal	10.4	10.4	41.4	51.8	47.7	66.9	55.5	28.8	37.2	34.5	24.3	26.7	26.0
9. $\Delta\underline{E}^\circ_c/\underline{M}$, cal/g	-13207	-13257	-13121	-13165	-13140	-13162	-13145	-13230	-13229	-13192	-13113	-13223	-13170

Mean $\Delta\underline{E}^\circ_c/\underline{M}$: -13181 cal/g

Std. dev. of mean = ±13 cal/g or 0.10 percent.

Items (1), (2), and (3) in Table 38 designate the mass of the metal burned, the corrected temperature rise of the calorimeter, and the total measured heat effect. Items (4) through (8) represent thermal corrections to the total heat effect: $\Delta\underline{E}_{contents}$ - heat capacity effect of the contents of the bomb, $\Delta\underline{E}_{gas}$ - standard state correction for fluorine gas, $\Delta\underline{E}_{ignition}$ - estimated electrical ignition energy, $\Delta\underline{E}_{fuse}$ - heat effect due to combustion of the cadmium fuse and $\Delta\underline{E}_{impurities}$ - impurity correction. The impurity correction is large mainly because of impurities in the support discs rather than impurities in the sample. The last item, $\Delta\underline{E}^\circ_c/\underline{M}$, the net energy evolved per gram of aluminum burned, has a mean value of -13181 cal/g. The standard deviation of the mean is ±13 cal/g or 0.10 percent.

The following thermodynamic constants were derived (in kcal/mole at 298.16 K): $\Delta\underline{Ef}^\circ$ = -355.6, $\Delta\underline{Hf}^\circ$ = -356.5, and $\Delta\underline{Gf}^\circ$ = -377.5. The entropy values for the standard free energy calculation were obtained from Bureau of Mines Bulletin 592.[35] An uncertainty interval of ±0.7 kcal/mole (twice the standard deviation) was applicable to all three constants.

Two recently reported ΔHf°_{298} values of -356.3[36] and -357.0[37] kcal/mole (±2 kcal) derived from the heat of the reaction Al + 1 1/2 PbF_2 = AlF_3 + 1 1/2 Pb are within the uncertainty interval of the present determination. At the 17th Annual Calorimetry Conference, August, 1962, a ΔHf°_{298} value of -358.2 kcal/mole ± 1.4 kcal/mole was reported by Domalski and Armstrong[38] of National Bureau of Standards. It was obtained by reacting a mixture of Teflon and aluminum powder with fluorine in a bomb calorimeter.

---

[35] Kelley, K. K., and King, E. G., U.S. Bureau of Mines Bulletin 592 (1961).

[36] Gross, P., Bull. Chem. Thermodynamics 2, 21 (1959).

[37] Kolesov, V. P., Martinov, A. M., and Skuratov, S. M., Bull. Chem. Thermodynamics, 4, 26 (1961).

[38] Domalski, E. S. and Armstrong, G. T., 17th Annual Calorimetry Conference, August 1962.

C. Combustion of Zirconium Diboride in Fluorine
(G. K. Johnson* and E. Greenberg)

A suitable technique for carrying out calorimetric combustions of zirconium diboride in fluorine has been developed and was discussed previously (see ANL-6596, p. 173). Calorimetric combustions and other experimental work have since been completed. Final calculations and the preparation of a manuscript for publication are currently in progress.

The combustion technique involves burning 200-300 mesh zirconium diboride powder on a relatively massive zirconium disc (1/4 in. thick and 2 in. in diameter). To insure reproducible spontaneous ignition of the sample, approximately 50 mg of sulfur was used as kindler under the zirconium diboride. The combustion reaction was carried out by means of the previously developed apparatus[39] for substances which ignite spontaneously when exposed to fluorine. The small amount of unburned zirconium diboride was determined by a calorimetric analytical procedure as described in ANL-6596, p. 173. A thermal correction was made for the small weight loss suffered by the zirconium disc during the combustion.

The solid combustion product was identified by X-ray diffraction analysis as beta (monoclinic) zirconium tetrafluoride. Infrared analysis confirmed that boron trifluoride and sulfur hexafluoride were the gaseous products of combustion.

Table 39 presents preliminary data for the combustion of zirconium diboride in fluorine. ϵ (calor.)$(-\Delta t_c)$ represents the total energy evolved

Table 39

ZIRCONIUM DIBORIDE COMBUSTIONS IN FLUORINE[a]

	Run 1	Run 3	Run 4	Run 5	Run 6	Run 7	Run 8	Run 9
1. m' (ZrB_2), g	0.63290	0.63669	0.63606	0.63729	0.63610	0.63950	0.63566	0.63463
2. Δt_c, deg	1.70048	1.65999	1.65660	1.66134	1.66982	1.66864	1.65466	1.65504
3. ϵ(calor.)$(-\Delta t_c)$, cal	5767	5730	5618	5634	5663	5659	5612	5613
4. m (sulfur), g	0.06891	0.04962	0.05063	0.05016	0.05526	0.05033	0.04920	0.05047
5. ΔE_{sulfur} cal	563	405	414	410	452	411	402	412
6. $m_{Zr\ loss}$, g	0.01505	0.00153	0.00163	0.00979	0.00068	0.00419	0.00109	0.00442
7. ΔE_{Zr}, cal	75	8	8	49	3	21	5	22
8. $\Delta E_{ZrB_2\ comb.}$, cal	-5129	-5217	-5196	-5175	-5208	-5227	-5205	-5179
9. $\Delta E_c/M$ (ZrB_2), cal/g	-8104	-8193	-8169	-8120	-8187	-8174	-8188	-8161

Mean $\Delta E_c/M$ (ZrB_2) = -8162 cal/g

Std. dev. of mean = ±12 cal/g or 0.15%

[a]Preliminary data.

*Resident Student Associate from the University of Wisconsin.

[39]Nuttall, R. L., Wise, S. S., and Hubbard, W. N., Rev. Sci. Inst. 32, 1402 (1961). See also ANL-6287, p. 126.

during the combustion. $\Delta\underline{E}_{sulfur}$ and $\Delta\underline{E}_{Zr}$ represent the corrections for the energy of combustion of the sulfur and the fluorination of the zirconium support disc. The net energy evolved per gram of ZrB_2 burned is given by $\Delta\underline{E}_c/\underline{M}(ZrB_2)$. The standard deviation of the mean of 0.15 percent is not unreasonable for this system. It should be noted that in runs 1 and 5, which showed the greatest deviation from the mean, there was a considerably greater attack of the zirconium disc which served as the sample support. Further evaluation of the results awaits completion of the detailed calculations, including corrections for the standard state.

D. Combustion of Ruthenium in Fluorine
(H. A. Porte and E. Greenberg)

A series of eight calorimetric combustions of ruthenium in fluorine has been completed. The sample arrangement and combustion technique were the same as that described[40] for the combustion of zirconium in fluorine.

Ruthenium was obtained from the International Nickel Company, Inc. in the form of 1/8-in.-diameter rod and 0.005-in.-thick foil. Because ruthenium wire was unavailable, 0.005-in.-diameter molybdenum wire was used as the fuse material.

A few additional calibration experiments will be run for the calorimetric system ANL-R1-Ni5 before the value of the heat of formation of ruthenium pentafluoride is calculated from the results of the ruthenium combustions.

E. Combustion of Niobium and Tantalum in Fluorine
(E. Greenberg and C. Natke)

The development of satisfactory combustion techniques for niobium and tantalum was reported in ANL-6333, p. 127. Analyses of high-purity samples of niobium and tantalum have been completed, and calorimetric combustions of tantalum in fluorine are in progress. Combustions of niobium in fluorine with the same system and by the same techniques will be carried out as soon as the tantalum experiments are completed.

F. High-temperature Enthalpy Calorimeter
(D. R. Fredrickson, R. L. Nuttall and R. Kleb)

A calorimetric system to measure changes in enthalpy up to 1500 C was described in ANL-6477, p. 164. This calorimetric system has been moved into the new laboratory, and assembly and testing of components has been accelerated. The components are the drop mechanism, furnace, gate,

[40]Greenberg, E., Settle, J. L., Feder, H. M., and Hubbard, W. N., J. Phys. Chem. 65, 1168 (1961).

and calorimeter. The drop mechanism and gate have been assembled apart from the system and are yet to be tested. The calorimeter components are complete but have not been assembled in the calorimeter shell. The furnace has been assembled and has been tested up to 800 C during the past quarter.

Work has been primarily directed toward the installation of controls for furnace temperature and toward heating of the furnace to check the performance of these controls. Figure 57 shows the molybdenum core of the furnace. Wells in the shields for platinum, platinum-10 percent rhodium thermocouples are shown. Not shown are a tungsten, rhenium thermocouple in the floating shield and a main shield-floating shield differential thermocouple. The furnace has three separate tantalum heater windings: the outer shield heater, bottom shield heater, and the main shield heater. Three power supplies of 200 w, 300 w, and 20 w, respectively, have been built for these heaters. The supplies consist of diode bridge rectifier circuits with filtering to provide a variable dc supply for the furnace heaters.

Absolute temperature control is obtained with the control thermocouple in the main shield. A diagram of the circuitry is shown in Figure 58. The difference between the control thermocouple voltage and the temperature-setting bucking voltage is amplified and recorded. A signal proportional to the deviation of the recorder from a set point is sent to the Leeds and Northrup Series 60 C.A.T. control unit, which produces an output current proportional (in the range 0-5 ma) to the input signal. This current is fed to a transisterized power controller which controls the power to the main shield heater. The control loops for the outer shield and the bottom shield are the same except in two respects: no recorders are used. (The circuitry of the C.A.T. control units is modified to accept input directly from the amplifier.) The power controller is a Barber Colman Series 620 silicon-controlled rectifier unit rather than the transistorized power controller used with the main shield.

As described above, the absolute control is with the main shield heater. The outer shield temperature then follows the main shield temperature and is controlled by the outer shield-main shield differential thermocouple. A bucking emf provides a 1 to 5 C temperature differential between shields. The bottom shield heater, in turn, is controlled by the outer shield-bottom shield differential thermocouple.

The furnace has been under control at three different temperatures: 584, 688, and 800 C, as indicated by the voltage of the main shield thermocouple. In each case over a period of about 16 hr, the main shield temperature variation was only a few tenths of a degree.

Figure 57

DROP CALORIMETER FURNACE

(Hot Body Only)

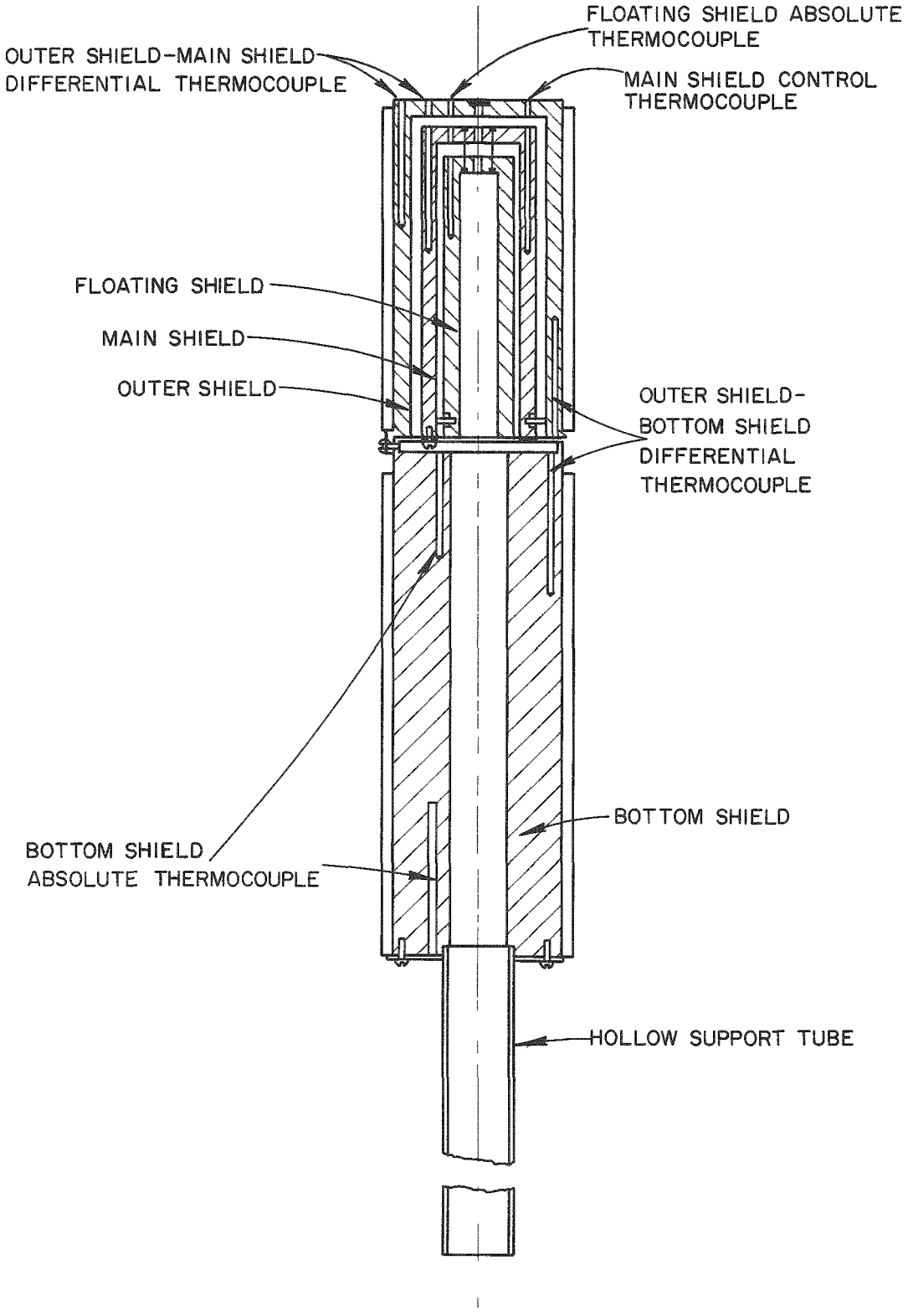

Figure 58

CONTROL CIRCUIT FOR MAIN SHIELD HEATER

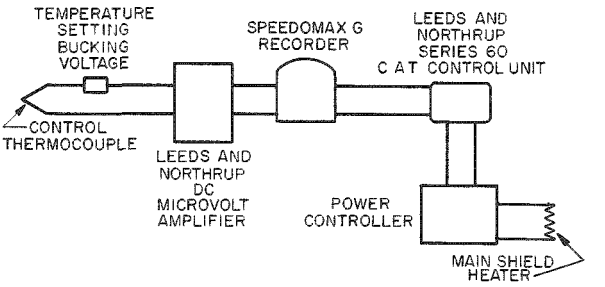

A gas-flooding system has also been connected to the furnace. This provides for flooding of the furnace with argon in case of accidental loss of the furnace vacuum. At the present time, a manual valve can be used for gas flooding. Paralleling the manually operated valve, a solenoid-operated valve is being installed. This valve will be connected to the control circuit of the thermocouple gauge.

IV. REACTOR SAFETY*

The oxidation, ignition, and combustion processes of metals and compounds used in nuclear technology are being studied to provide information to aid in minimizing the hazards associated with handling these materials.

An experimental program to determine the rates of reaction of molten reactor fuel and cladding metals with water is continuing. Methods currently being used to examine these reactions are the condenser-discharge and levitation methods in the laboratory and in-pile reactor transients in the TREAT reactor.

A. Metal Oxidation and Ignition Kinetics
(L. Baker)

1. Theory of Uranium Ignition
(L. Baker, J. D. Bingle)

Studies of the isothermal oxidation of uranium at temperatures above 300 C were reported previously (see ANL-6569, p. 136; ANL-6543, p. 168; and ANL-6413, p. 160). The purpose of these studies was to provide reaction rate data needed to develop a better understanding of previously reported ignition data. A simple relationship between isothermal oxidation rates and ignition temperature should exist if the ignitions are purely thermal in character. A thermal ignition is merely an accumulation of heat, in which the reacting system generates more heat than can be dissipated by heat-loss mechanisms, leading to a rapidly increasing temperature.

Calculations were reported in a previous quarterly (ANL-6569, p. 136) in which the rate laws found from isothermal studies of uranium oxidation at elevated temperatures were combined with a simple heat-transfer model. Specimen temperature-time curves were then computed for uranium specimens having specific surface areas of 0.5, 5, and 50 sq cm/g, subject to the condition that the ambient temperature increased uniformly at the rate of 10 degrees/min. The calculated temperature-time curves were compared with experimental temperature-time curves (which have previously been referred to as burning curves), and the ignition temperatures obtained graphically from both calculated and experimental burning curves were found to agree within 50 C.

It was evident from the computations that the unusual transition from an accelerating oxidation rate to a decelerating oxidation rate at 450 C (see ANL-6543, p. 170) plays an important role in the ignition process. The transition results in a sharp break in calculated ignition temperature as a function of specific surface area. Ignition temperatures obtained

*A summary of this section is given on pages 25 to 28.

from experimental burning-curve tests also show a sharp break as a function of specific surface area. Computations performed during this quarter were concentrated in the range of specific surface area between 2 and 10 sq cm/g where the break occurs in experimental ignition temperatures.

During the current series of calculations, it was discovered that a relatively minor error had been made in the earlier calculations for specific areas of 0.5, 5, and 50 sq cm/g (see ANL-6569, p. 138). These burning curves were, therefore, recalculated and are presented in Figure 59, along with curves calculated for specific areas of 2, 7, and 10 sq cm/g. It is evident from the figure that the break in ignition temperature occurs between specific areas of 5 sq cm/g (ignition temperature, 510 C) and 7 sq cm/g (ignition temperature, 388 C).

Figure 59

CALCULATED BURNING CURVES FOR ANL BASE URANIUM IN FLOWING OXYGEN USING RATE EQUATIONS DERIVED FROM EXPERIMENTAL DATA

(Specific area of samples and indicated ignition temperatures as shown)

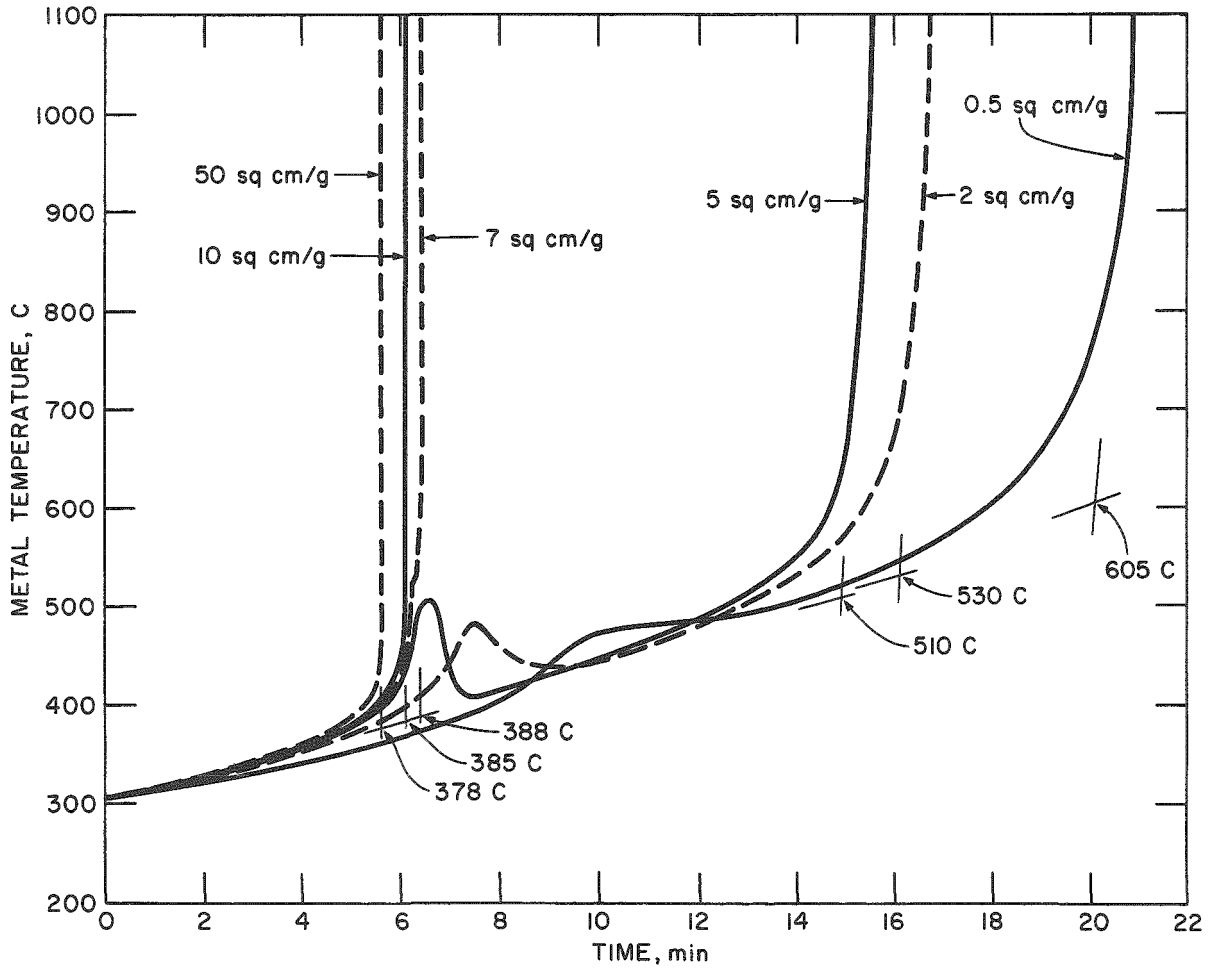

Experimental ignition temperatures for a variety of uranium specimens in oxygen are compared with calculated values in Figure 60. Experimental ignition temperatures undergo a sharp break at a specific area of about 2 sq cm/g, whereas the calculated ignition temperature break occurs near 6 sq cm/g. This difference is very likely a result of differences in the metallurgical character or the impurity content of the specimens, since the calculated ignition temperatures were determined from isothermal rate equations derived from data on β-quenched specimens in the form of 8.5-mm cubes, whereas the experimental ignition temperatures were obtained in experiments performed with a variety of foils, wires, and cubes from different sources. The extreme sensitivity of the oxidation reaction above 450 C to impurities and to the metallurgical character of specimens has been discussed in previous quarterlies (see, for example, ANL-6543, p. 174).

Figure 60

SPECIFIC AREA DEPENDENCE
OF URANIUM IGNITION

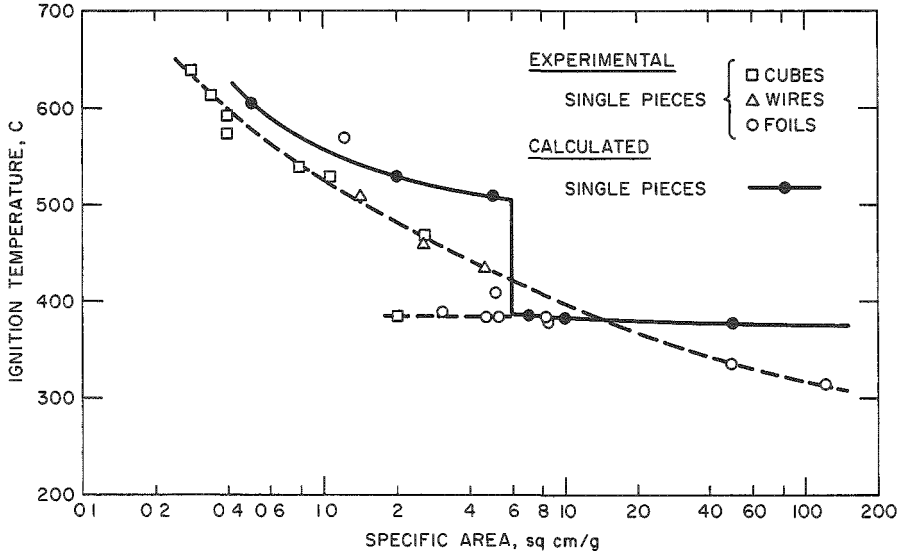

108-6103

Calculated ignition temperatures shown in Figure 60 are somewhat higher than experimental values. This could have resulted from the insulating character of the oxide. Thermal insulation of the metal by the oxide film would reduce heat losses and thereby increase sample self-heating and facilitate ignition. No corrections for the effect of the oxide film on the heat transfer were included in the calculations. The character of the oxide films produced is indicated by photographs (Figure 61) of nominal one-cm cube specimens of ANL uranium oxidized isothermally at 400 C or 625 C in oxygen. Oxide produced at 400 C formed fragile plates

of loosely compacted powder, while oxide produced at 625 C appeared to be of two types: a loose powdery material, and a rough but adherent coating on the cube.

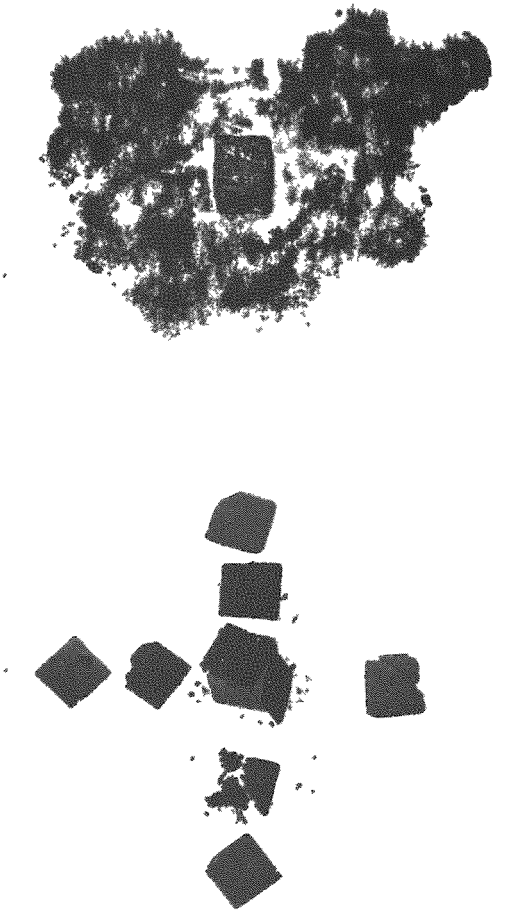

Figure 61

URANIUM OXIDE RESIDUES AFTER OXIDATION OF NOMINAL 1-cm CUBES AT 400 C AND 625 C IN OXYGEN

(Below: 400 C; Above: 625 C)

ANL-108-5613

The marked similarity of calculated and experimental ignition temperatures suggests that the mathematical ignition model takes into account the principal factors involved in the ignition process. The same mathematical model also described zirconium ignitions with reasonable accuracy (see ANL-6413, p. 152). It seems clear, therefore, that uranium and zirconium ignitions in air and oxygen are thermal in character and do not involve metal vaporization or unusual chemical reactions, such as the decomposition of surface peroxides, oxynitrates, and azides. A collection of postulated ignition mechanisms of this kind is available.[41]

A series of four publications are being prepared: the first describes isothermal oxidation studies of uranium and selected alloys in the temperature range from 300 to 625 C; the second describes experimental

[41] Zirconium Fire and Explosion Hazard Evaluation, TID-5365 (Aug 1956).

and theoretical studies of the ignition of pure uranium; the third describes ignition studies with 70 binary uranium alloys; and the fourth describes X-ray diffraction studies of oxides formed on uranium, which studies are discussed in the next section.

2. X-ray Diffraction Studies of Oxidized Uranium
(L. Leibowitz, J. D. Bingle, M. Homa)

As part of an investigation[42] of the kinetics of the oxidation of uranium, an examination was made of the oxidized metal surface by both X-ray and electron diffraction techniques. In that work, at 200 and 295 C, only UO_2 was found until almost all the metal was consumed. The uranium-oxygen system is a fairly complex one, however, and there is a notable lack of agreement among the various workers in this area.[43-46] Aronson et al.,[45] for example, hold that oxidation of UO_2 proceeds via a UO_{2+x} solid solution, while Blackburn et al.[46] maintain that oxidation of UO_2 is controlled by diffusion of oxygen through a U_3O_7 layer. Recent crystallographic work by Belbeoch, Piekarski, and Perio[47] and by Hoekstra, Santoro, and Siegel[48] has done much to clarify the situation. The latter authors have discussed in some detail the complications of identification and the sources of conflict in the earlier work. Because of these recent findings, it was decided to re-examine the oxidized surfaces of uranium by an X-ray diffractometer. All X-ray diffraction patterns were obtained with a G. E. XRD-5 diffractometer with Cu K_α radiation.

Cubes of uranium were oxidized at 100 and 200 C in the constant-pressure volumetric apparatus used previously (see ANL-5974, p. 41). At 300, 400, 500, and 600 C, samples were oxidized in the heat-sink apparatus described in ANL-6413, p. 160. At the higher temperatures, self-heating of the metal would ordinarily preclude isothermal oxidation. In the heat-sink apparatus, however, the uranium specimen is compressed between

---

[42] Leibowitz, L., Schnizlein, J. G., Bingle, J. D., and Vogel, R. C., J. Electrochem. Soc. 108, 1155 (1961).

[43] Alberman, K. B., and Anderson, J. S., J. Chem. Soc. 5303 (1949).

[44] Gronvold, F., J. Inorg. Nucl. Chem. 1, 357 (1955).

[45] Aronson, S., Roof, R. B., Jr., and Belle, J., J. Chem. Phys. 27, 137 (1957).

[46] Blackburn, P. E., Weissbart, J., and Gulbransen, E. A., J. Phys. Chem. 62, 902 (1958).

[47] Belbeoch, B., Piekarski, C. and Perio, P., J. Nuclear Materials 3, 60 (1961).

[48] Hoekstra, H. R., Santoro, A. and Siegel, S., J. Inorg. Nucl. Chem. 18, 166 (1961).

two massive stainless steel blocks which remove heat at a sufficient rate to maintain nearly isothermal conditions. All runs were carried out in pure oxygen at a pressure of about 200 mm.

Figure 62

X-RAY DIFFRACTOMETER TRACINGS OF THIN URANIUM OXIDE FILMS FORMED AT VARIOUS TEMPERATURES

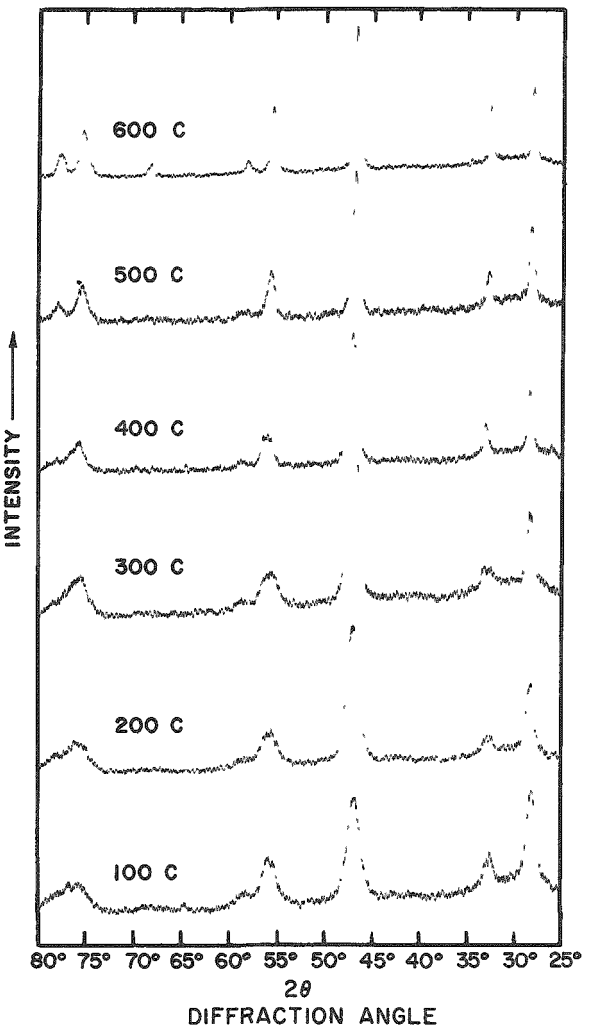

ANL-108-5769

In each run, when the desired amount of oxidation had occurred, the reactor was evacuated and the samples were allowed to cool in vacuum. Thin, adherent oxide films were formed after 400 to 1100 $\mu g\, O_2$/ sq cm was consumed; no evidence of flaking was observed.

In Figure 62 are shown sections of the diffraction patterns obtained from these samples. These are principally UO_2 patterns which, however, show some interesting details pertaining to the kinetics of uranium oxidation. A change in the character of the tracings occurs between 400 and 500 C: the diffraction maxima in the regions $2\theta = 55°$ and $2\theta = 75°$, which are broad and diffuse up to 400 C, are quite sharp at 500 and 600 C. The maximum in the region $2\theta = 33°$ shows a similar change between 300 and 400 C.

It is interesting in this respect to note that a change in the kinetics of oxidation of uranium occurs at 450 C (see ANL-6569, p. 136). Below that temperature, an accelerating oxidation rate was found, proportional to $(\text{time})^{5/4}$, whereas above 450 C a decelerating rate proportional to $(\text{time})^{5/6}$ holds. It is reasonable to ascribe this change in reaction kinetics to the changed character of the oxide.

Although some of the line broadening observed at low temperatures may be attributed to crystallite size being smaller than in the oxide formed at the higher temperature, not all of the changes in character of the diffraction patterns can be explained in this way. The splitting of the line in the region $2\theta = 55°$ for the oxide film prepared at 100 C, the

extreme broadening around 75°, and the indications of multiple peaks at 33° all indicate the presence of a phase higher than UO_2 at the lower temperatures. From the studies of UO_2 oxidation by Hoekstra, Santoro, and Siegel,[48] it is revealed that two cubic and three tetragonal phases may be present. The cubic phases are UO_2 and U_4O_9. The tetragonal phases and their c/a ratios are listed below:

	c/a
α-U_3O_7	0.989
β-U_3O_7	1.031
$UO_{2.3}$	1.016

Because these c/a values are so close to unity and because of the poor definition of the overlapping diffraction maxima, a clear distinction between these various possibilities was not possible.

The X-ray data are consistent with the uranium-oxygen phase diagram[48] if it is assumed that the molar ratio of oxygen to uranium in the oxide film is only slightly greater than 2. It is then likely that at 100 C we observe a two-phase UO_2 + α-U_3O_7 region and that at 200, 300, and 400 C a UO_{2+x} + U_4O_9 region exists, while at 500 and 600 C there is a single UO_{2+x} phase. Related X-ray studies of even thinner oxide films provided no evidence that the formation of the higher-oxide phases at low temperatures is related to the change from first- to second-stage oxidation,[42] as was once considered a possibility (see ANL-6543, p. 176).

In none of this work involving thin oxide films did we see evidence of the presence of U_3O_8. This is in contrast with the work of Loriers,[49] who reports that above 240 C a crystalline structure appears which is orthorhombic like U_3O_8. Since Loriers states that these layers scaled off readily, it is evident that he was working with fairly heavily oxidized uranium. Under those conditions, we also observe the formation of U_3O_8.

3. Plutonium-ignition Studies
(J. G. Schnizlein, D. F. Fischer)

Because of the increasing use of plutonium in the nuclear energy program, knowledge of its oxidation and ignition behavior is being acquired to allow safe handling. The facility and equipment used to perform the experiments safely have been described previously (see ANL-6413, p. 168). Samples of plutonium and its alloys used in our experiments were prepared at Hanford.*

---

[49] Loriers, J., Compt. rend. 234, 91 (1952).

*Preparations were under the supervision of P. G. Pallmer, T. Nelson, and O. J. Wick, General Electric Co., Hanford Atomic Products Division, Richland, Washington.

Burning curve ignitions* in oxygen and in air have been completed for all of the alloy cubes that have been received. The most recently acquired data and previously reported results (see ANL-6145, p. 142 and ANL-6543, p. 177) on cube and rod specimens are summarized in Table 40.

Table 40

IGNITION TEMPERATURES OF PLUTONIUM AND PLUTONIUM ALLOYS

(Burning curves on samples with specific area ~0.7 sq cm/g)

	Additive Content (a/o)		Ignition Temperature (C)	
Alloy	Nominal	Analyzed	In Oxygen	In Air
Pure Pu[a]			494[b], 512	508[b], 520
Ignition Temperatures Higher than Base Pu				
Al	2	3.4	576[c]	590[c], 588[c]
Cu	2	2.40	533, 546	555
Si	2	1.2[c]	540[b]	553[b]
Si	2	0.26	525	548
Si	1	0.28	537	548
Si	1/2	0.26	537[e]	544[e]
Ignition Temperatures Same as Base Pu				
Fe	2	1.8	515	548
Fe	2	1.95	520[e]	476[e], 485[e], 490
Zn	2	1.03	523	528
Zn	1	0.40	503	528
Mg	2	~0.2	512	520
Cr	2		498[e]	514[e]
Cr	2		507	512, 518
U	2		490	510, 513
Ce	2	0.5[d]	485	510
Ignition Temperatures Lower than Base Pu				
C	2		486	498
C	2	1.55	447[e], 455[e], 208[e,f]	459[g], 484[e,g]
Mn	2	2.7	477	499
Ni	2	1.26	489, 509	529
Ni	2	1.8	468	490
Co	2	1.8	462	474

[a]Base metal; total impurities 500 to 1000 ppm.
[b]Samples heavily oxidized prior to receipt.
[c]Specific area 10 to 20% higher than that of other samples.
[d]Estimated from density.
[e]Specific area 10 to 20% lower than that of other samples.
[f]This ignition temperature value was not reproduced in two other attempts.
[g]A marked self-heating was observed in the vicinity of 300 C.

*Samples heated in the oxidizing gas at a programmed rate of 10 C increase per min until ignition occurred.

Additives have little effect on the ignition temperature of plutonium. The greatest effects were found for aluminum, nickel, and cobalt. The ignition temperature of the 3.4 a/o aluminum-plutonium alloy was 60 degrees higher than that of the plutonium base metal. The 2.4 a/o copper-plutonium and the 1.2 a/o silicon-plutonium alloys ignited at a temperature 30 degrees higher than did the base metal. In contrast, the 1.8 a/o cobalt and 1.8 a/o nickel alloy ignition temperatures were 30 to 40 degrees lower than that of the plutonium base metal.

One carbon alloy, which was in the form of a cylinder, showed a marked self-heating in air in the vicinity of 300 C, at which the transition to the gamma phase would be expected. This same alloy in one of three experiments in oxygen ignited at 208 C. However, an alloy of similar carbon content in the form of a cube which was received at a later date showed no such peculiar behavior in either air or oxygen. It is suspected that the first samples of the alloy showing unique behavior may have had cracks or voids which were caused to open upon the transition from beta to gamma structure.

This completes the study of the effect of additives on the ignition behavior of large samples. As soon as foils of these alloys and pure plutonium are obtained, the effect of varied specific area will be determined.

B. Metal-Water Reactions
(L. Baker)

1. Studies of the Stainless Steel-Water Reaction by the Condenser-discharge Method
(L. Baker, Jr., R. Warchal)

The condenser-discharge experiment is an attempt to obtain fundamental rate data under experimental conditions similar to those that would be encountered during a serious accident in a nuclear reactor. Either a nuclear runaway or a sudden loss of coolant during operation of a water-cooled reactor could result in contact of very hot fuel and cladding metals with water or steam and might involve fine particles. The condenser-discharge experiment simulates the limiting case of a nuclear incident in that the heating time is very short and very fine metal particles are produced.

In the condenser-discharge experiment, metal wires are rapidly melted and dispersed in a water-filled cell by a surge current from a bank of condensers. The energy input to the wire is used to calculate the initial reaction temperature. The transient pressure measures the reaction rate, the amount of hydrogen generated gives the extent of reaction, and the particle size of the residue indicates the surface area exposed to reaction.

Analysis of results is based on one of the usual laws of metal oxidation (parabolic rate law) and on the laws of gaseous diffusion and heat transfer. In this way, an attempt is made to interpret experimental work as it proceeds.

The results of a series of runs with 30- and 60-mil-diameter stainless steel-316 wires in water at room temperature, at 100 C, and at 200 C were reported in the previous quarterly (ANL-6596, p. 186). A series of six runs with stainless steel-316 wires (30-mil diameter) in 315 C water (1500 psi pressure) has now been completed in the high-pressure reaction cell described in ANL-6231, p. 156. Results of the runs in 315 C water are given in Table 41.

Table 41

REACTION OF STAINLESS STEEL-316 WIRES IN WATER AT 315 C AND 1500 psi IN THE CONDENSER-DISCHARGE APPARATUS

30-mil wires, one inch long

The residue consisted of fine particles in each run.

Run No.	Calc Initial Metal Temp (C) and Physical State	Percent Reaction[a]	Run No.	Calc Initial Metal Temp (C) and Physical State	Percent Reaction[a]
348	2200, liquid	10.1	351	2800, liquid	21.8
347	2300, liquid	16.5	346	2900, liquid	31.6
350	2600, liquid	17.8	349	3500, liquid	34.2

[a]Based on reaction to Cr_2O_3, NiO, and FeO.

The percent of metal reacted in the individual runs in 315 C water, as well as curves representing the averages of previously reported results of experiments in room-temperature water and in water at 100 and 200 C, are plotted in Figure 63. Comparison shows that the extent of

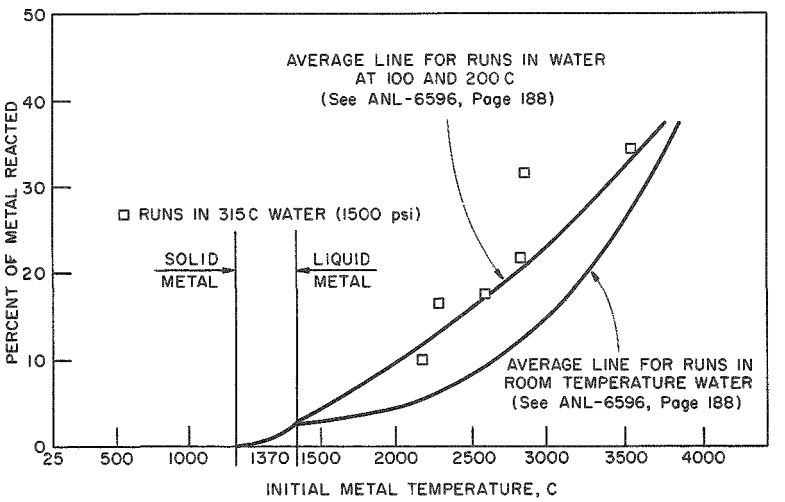

Figure 63

STAINLESS STEEL-WATER REACTION BY THE CONDENSER-DISCHARGE METHOD

(stainless steel-316)

metal-water reaction in 315 C water is nearly identical to that obtained in water at 100 and 200 C. In one run in 315 C water, a high result was obtained, possibly because of the formation of particles of significantly smaller average size than in other runs. Particle size measurements for the runs in 315 C water have not been completed.

The condenser-discharge experiment has shown that the high-temperature stainless steel-water reaction is independent of the water temperature over the range from 100 to 315 C (pressure range 15 to 1500 psi). The zirconium-water reaction was also found to be independent of water temperature and vapor pressure over the same range (see ANL-6548). These observations indicate strongly that the kinetics of the oxidation process for both metals are independent of pressure over a wide range.

2. Studies of the Aluminum-Water Reaction by the Levitation Melting Method
(R. E. Wilson, L. Mishler, C. Barnes)

The levitation method was developed to study the kinetics of reactions of molten metals with water vapor at high temperatures. This method, in which the sample is supported by means of a radiofrequency field and surrounded by a steam atmosphere, appears to be well suited to determine the nature of the reaction rate laws in the absence of contamination from crucibles or other supports. The results are to be used to help interpret data obtained from other metal-water studies.

This experimental technique has been applied to the study of the rate of reaction of steam with molten aluminum at temperatures above 1200 C. Results at 1200 C and below were reported by Mason and Martin (see ANL-6413, p. 179), who used the pressure pulse method.

a. Experimental Procedure

Heating was supplied by means of a 15-kw induction generator operating at about 250 kc. The power was supplied to the work coil by means of a step-down transformer to give a low-impedance output.

The work coil, shown in Figure 64, consists of one forward and one reverse turn. The opposing fields produce a null in the center, where a nominal 8-mm spherical sample may be held. The coil was made of $\frac{1}{4}$-in. copper tubing which was bent to shape and mounted on low-impedance leads. During the bending operation, the tubing was filled with Woods metal to prevent collapse of the tubing.

The work coil was brought into the Pyrex reaction cell through a 75/50 ground-glass ball joint, which was sealed to the leads of

the work coil by means of a quartz-filled epoxy resin, in order to make a vacuum-tight or pressure-tight seal. The remainder of the ball joint was filled with silicone rubber to limit the amount of steam condensation on the water-cooled leads, and also to prevent thermal shocks from cracking the epoxy seal. A close-up view of the coil with an aluminum sample being levitated at about 1600 C is shown in Figure 65.

Figure 64

LEVITATION COIL SHOWING VACUUM-STEAM SEALING SYSTEM

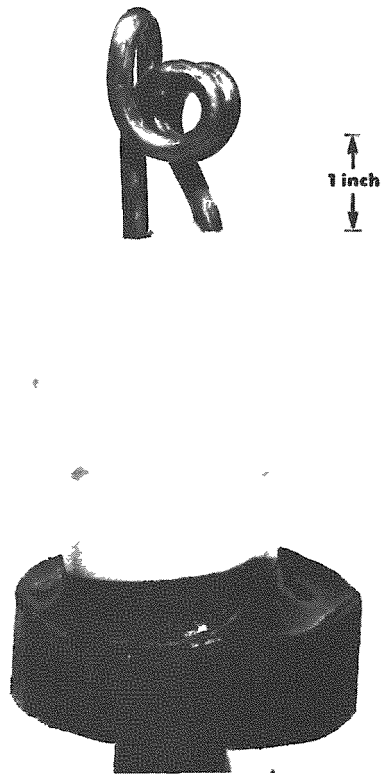

ANL-108-5785

Figure 65

MOLTEN DROP OF ALUMINUM SUSPENDED IN AIR AT 1600 C

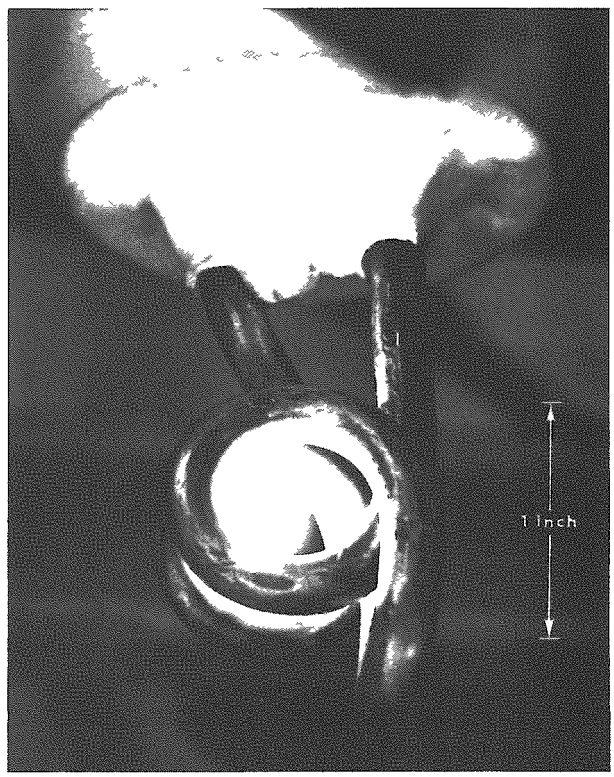

ANL-108-5783A

A small sheet of Teflon connected to a small magnet was used to support the specimen pellet before beginning a run. The sheet was rapidly removed as soon as the radiofrequency power was turned on. Once levitation was established, samples were rapidly heated to the test temperature. The temperature was measured by means of a commercial two-color optical pyrometer.* The use of this type of temperature sensor was dictated by the need for a noncontacting system and the lack of data for the emissivity values for molten metals. The output of the pyrometer, which

*Instrument Development Laboratories, Inc., Pyro-Eye.

was recorded on a potentiometric strip chart recorder, was also used to control the temperature of the aluminum sample by means of a motor-driven variable transformer controlling the output of the induction generator.

In this series of experiments, steam from the building supply was exhausted from the reaction vessel through a jet to prevent back-diffusion of air into the vessel. After exposure to the test conditions for a fixed period of time, the samples were cooled rapidly to room temperature and analyzed gravimetrically. The pellet of aluminum coated with oxide was weighed; the aluminum was then dissolved, according to the method of Pryor and Keir,[50] in an iodine-methyl alcohol solution, leaving only the oxide. From the starting weight, the weight of the reacted pellet, and the oxide weight, the amount of aluminum which had reacted with steam was calculated. Losses of oxide during the experiment did not interfere with the analysis. There was no indication that any loss of unreacted metal occurred.

b. Isothermal Oxidation Rates

The results of the experiments in which samples did not ignite are given in Table 42. The RMS (root mean square) errors are given for each value. A plot of the results given in Table 42 is shown in Figure 66. The lengths of the vertical lines are equal to the RMS errors. Where no lines are shown, the RMS error is less than the size of the point. It is evident from Figure 66 that the results at 1400, 1500, and 1600 C tend to follow a linear rate law, whereas the results at 1200 and 1300 C tend to follow a cubic rate law. Also shown in the figure are the results reported by Mason and Martin for the aluminum-steam reaction at 800, 1000, and 1200 C.

Table 42

EFFECT OF TEMPERATURE ON THE REACTION OF ALUMINUM AND STEAM

(8-mm spheres in levitation)

Reaction Time (min)	Aluminum Reacted (mg/sq cm ± RMS error) at Indicated Temperatures				
	1200 C	1300 C	1400 C	1500 C	1600 C
5	-	-	-	1.59 ± 0.11	3.9 ± 0.2
10	0.76 ± 0.65	1.37 ± 0.17	1.28 ± 0.33	3.19 ± 0.59	7.7 ± 0.2
15	-	-	2.19 ± 0.15	-	11.4 ± 2.2
20	-	-	-	5.37 ± 0.34	-
30	0.47 ± 0.15	1.95 ± 0.54	2.17 ± 0.08	7.2 ± 1.0	-
60	1.07 ± 0.26	1.90 ± 0.14	4.91 ± 0.31	15.7 ± 3.6	-
100	1.48 ± 0.07	2.58 ± 0.92	6.47 ± 0.40	16.0 ± 1.4	-

[50] Pryor, J. J., and Keir, D. S., J. Electrochem. Soc. 102, 370 (1955).

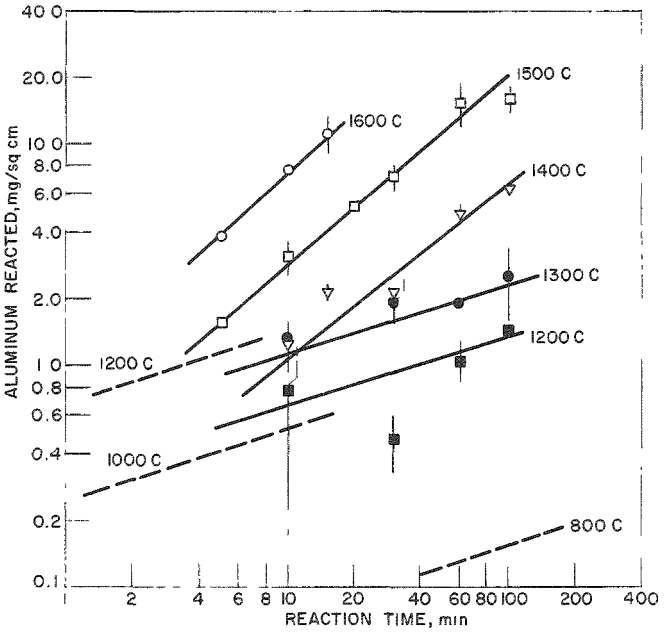

Figure 66

THE REACTION OF ALUMINUM WITH STEAM

(Data points and solid lines obtained by the levitation melting method. Dashed lines obtained by the pressure pulse method; see ANL-6413, p. 179).

ANL-108-6102

Reaction rates at 1200 C obtained by Mason and Martin with the pressure-pulse method were about twice those obtained by the levitation melting method at 1200 C. In the pressure-pulse method, molten aluminum was contained in alumina crucibles and was brought to temperature in vacuum or an inert environment. Steam was then brought into momentary contact with the molten metal and rapidly removed by a system of electrically activated valves. The amount of reaction was determined by an analysis of the quantity of hydrogen generated during the period of contact. The higher results obtained by the pressure-pulse method might have been due to reaction of aluminum with steam which diffused through the side and bottom of the slightly porous alumina crucibles. Additional reaction of steam may have occurred with small quantities of aluminum vaporized onto the upper portions of the crucibles or onto the walls of the reaction cell during sample heating. Results of both methods of studying the aluminum-steam reaction indicate that the cubic rate law is valid in the temperature region around 1200 C.

The possibility was studied that the differences in results obtained from the two methods were caused by an inaccurate method of determining the quantity of reaction. Two runs were therefore performed by the levitation method in which the quantity of aluminum reacted was determined gravimetrically and also by collecting the hydrogen generated by reaction. The value obtained gravimetrically was 2.29 ± 0.07 mg Al reacted per sq cm, whereas the value obtained from the hydrogen analyses was 2.32 ± 0.35 mg Al reacted per sq cm, based on the assumption that the reaction products were Al_2O_3 and H_2. Values found by the two methods agreed within the anticipated limits of error.

In Figure 67 is shown the variation of the linear rate constants with reciprocal temperature. The parameters of the Arrhenius equation,

$$k = Ae^{-E/RT} ,$$

where

k is the reaction rate constant, mg/(sq cm)(min)

A is the frequency factor, mg/(sq cm)(min)

E is the activation energy, cal/mole

R is the gas constant, 1.99 cal/(mole)(deg)

T is the temperature, K

were determined to be as follows:

$$A = 2.95 \times 10^{8} \text{ mg/(sq cm)(min)}; \quad E = 73.5 \text{ kcal/mole.}$$

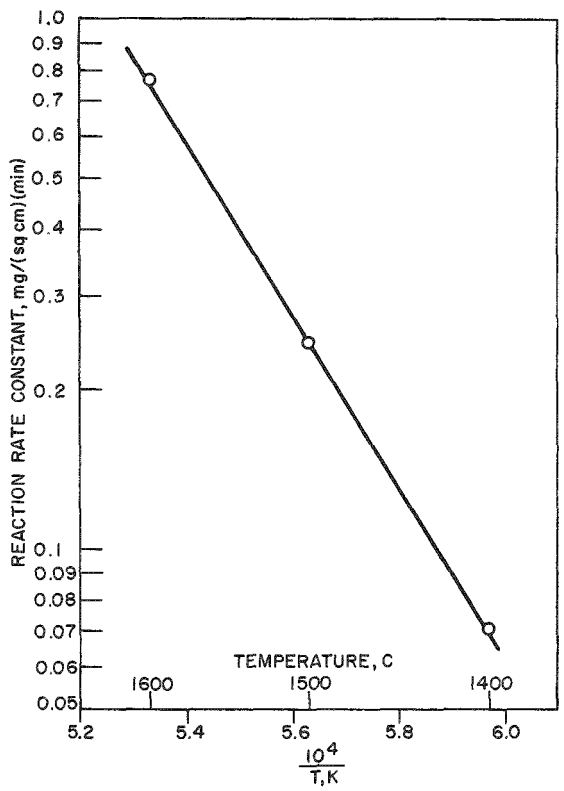

Figure 67

EFFECT OF TEMPERATURE ON THE LINEAR RATE CONSTANTS OF THE ALUMINUM-STEAM REACTION OBTAINED BY THE LEVITATION MELTING METHOD

c. Ignitions

Oxidation results at 1600 C could not be extended to longer times because the specimens ignited. Delayed ignitions occurred in aluminum spheres heated in steam to 1600 C or above; immediate ignition

Table 43

IGNITION DELAY FOR ALUMINUM SPHERES IN STEAM

(Nominal 8-mm spheres in levitation)

Sample Surface Temperature (C)	Ignition Delay (min)
1600	18
1650	9
1700	5
1750	0

occurred when the specimen surface temperature reached 1750 C. Approximate ignition delays at various surface temperatures are given in Table 43.

An ignition begins with the formation of a small hot spot which rapidly spreads across the surface of the sphere. The temperature at the hot spot rises above 2100 C. Burning appears to be similar to the vapor-phase burning previously reported to occur in air at 1750 C (see ANL-6379, p. 208), although the voluminous white smoke was less apparent during burning in steam. Evidently, the rapidly flowing moist steam carried smoke particles away as soon as they were formed.

The occurrence of delayed ignitions at temperature below 1750 C may be a result of the experimental procedure. Sample temperature is measured and controlled by means of a two-color optical pyrometer which is focused on the outer oxide surface. The molten metal core of specimen pellets may reach significantly higher temperatures than the outer oxide surface because of the insulation afforded by the oxide films. Attempts will be made to compute the metal core temperature at the moment of ignition by considering the presence of the oxide film, estimating its thermal conductivity and thickness, and computing the rate of heat loss from the outer oxide surface.

3. Studies of the Aluminum-Water Reaction in TREAT
(R. O. Ivins, F. J. Testa, P. Krause)

Studies were continued of metal-water reactions initiated by nuclear reactor bursts in the TREAT reactor at the National Reactor Testing Station, Idaho. The method consists of exposing a fuel specimen immersed in water to a neutron pulse from the TREAT reactor. The objectives of this program are:

1. to determine the extent of reaction between the metal and water;
2. to determine the fuel temperature and pressure history during the excursion;
3. to determine the physical damage that occurs as a result of the transient; this includes metallographic and particle size evaluations.

Nine aluminum-clad, 77 w/o aluminum-23 w/o fully enriched uranium plates have been subjected to destructive transients in TREAT during the quarter. These plates had nominal dimensions of 0.06 in. by 0.5 in. by 1.4 in. Both of the cladding layers and the core were 20 mils thick. The plates, placed in high-pressure autoclaves, were each submerged in 45 cc of distilled water in a 20-psia helium atmosphere. They were subjected to single bursts of energy ranging from 174 cal/g to 794 cal/g (based on the total weight of both core and clad material).

Chromel-alumel thermocouples were wired to the surface of some of the plates; however, the temperature traces indicated only an intermediate temperature between that of the metal surface and the water. During the transients run at the higher reactor energies, pressure transducers were used to record the pressure history. No significant pressure rises were noted. The autoclaves were lined with a thin sheet of stainless steel in some of the runs which could be removed and unrolled to show the particles of molten metal which became attached to the liner. The results of these experiments are summarized in Table 44.

Table 44

BEHAVIOR OF ALUMINUM CLAD, 77 w/o ALUMINUM-23 w/o URANIUM (FULLY ENRICHED) PLATES IN TREAT

TREAT Transient CEN	Fuel Wt (g)	Reactor Pulse		Calc Energy Input (cal/g of plate)	Peak Temp (Adiabatic) (C)	Extent of Metal-Water Reaction (%)	Xe^{133} Released (% of Xe^{133} produced)	Appearance of Fuel after Transient	Average Particle Size,[a] d_{SV} (mils)
		Period (msec)	Internal Power (Mw-sec)						
109	1.9685	104	169	174	660	0.10	0.02	Plate intact. Central region shows melting.	-
110	1.9434	96	238	245	690	0.13	0.02	Plate bulged, indicating extensive melting.	~500
111	1.9192	80	350	361	1170	0.30	2.8	Plate melted into a single spherical drop.	~450
112	1.9546	50	417	430	1440	3.9	27.7	Plates melted and fragmented.	~300
117	2.2526	52	512	527	1820	11.0	33.5		44.6
118	2.3370	50	560	577	2010	11.0	37.7		24.2
113	1.9628	53	633	652	2220	10.4	35.6		~100
119	2.1908	42	710	731	2330 (vapor)	13.6	35.4		21.8
120	2.2301	42	770	794	2330 (vapor)	36.9	49.0		18.6

[a] Average particle size diameters presented as Sauter mean diameter, $d_{SV} = \frac{\sum_i n_i d_i^3}{\sum_i n_i d_i^2}$. Except for numbers preceded by ~, which were estimated, these values were determined by sieve screen analysis.

The appearance of the plates after irradiation showed the effects of the increasingly destructive energy inputs. Figure 68 shows the first four plates (transients CEN 109 to 112) after irradiation. In CEN 109 at 174 cal/g fission energy input, only slight melting occurred. The integrated reactor power and fission energy input were increased in succeeding experiments, and the original shape of the plates was lost due to melting. Above an energy input of 430 cal/g, the plates were fragmented.

Figure 68

FOUR ALUMINUM-CLAD, 77 w/o ALUMINUM-23 w/o URANIUM (FULLY ENRICHED) CORE PLATES AFTER TREAT TRANSIENT BURSTS

(Original dimensions: 0.06 in. by 0.5 in. by 1.4 in.)

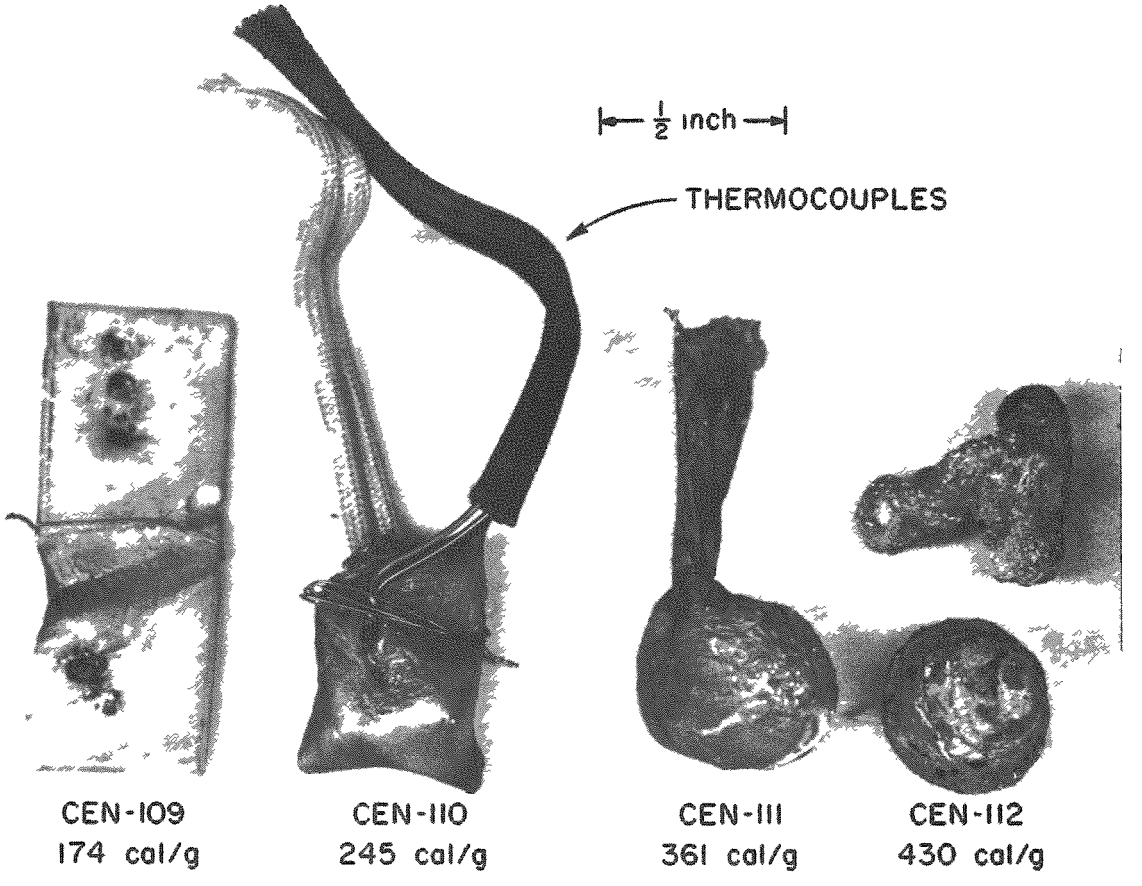

Figures 69, 70, 71, 72, and 73 contain photographs of the fragmented plates from CEN 117, CEN 118, CEN 113, CEN 119, and CEN 120, as well as macrographs and micrographs of the fragments. In these experiments the plates were fragmented into pieces at energy inputs of 527, 577, 652, 731, and 794 cal/g, respectively. The particle size distribution obtained by sieve screen analysis is also shown in Figures 69 through 73. The average particle diameter was determined as the Sauter mean diameter, d_{sv}, which is defined as the diameter of a spherical particle having the same surface to volume ratio as the entire fragmented sample. The average particle diameters were 44.6, 24.2, 100, 21.8, and 18.6 mils for CEN 117, CEN 118, CEN 113, CEN 119, and CEN 120, respectively. For the other runs in which little or no fragmenting occurred, mean particle diameters were estimated by visual examination. These values also are listed in Table 44.

Figure 69

TREAT TRANSIENT CEN-117: 2S ALUMINUM-CLAD, 77 w/o ALUMINUM-23 w/o URANIUM (FULLY ENRICHED) PLATE

FRAGMENTED PLATE AFTER TRANSIENT AT 527 cal/g

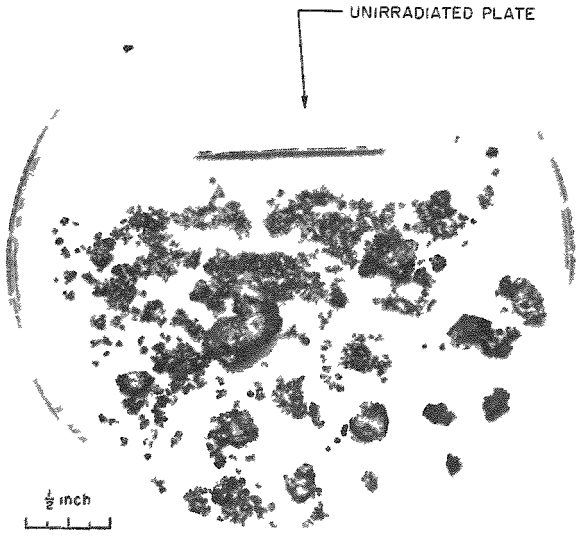

108-5770

MACROGRAPH OF FRAGMENT

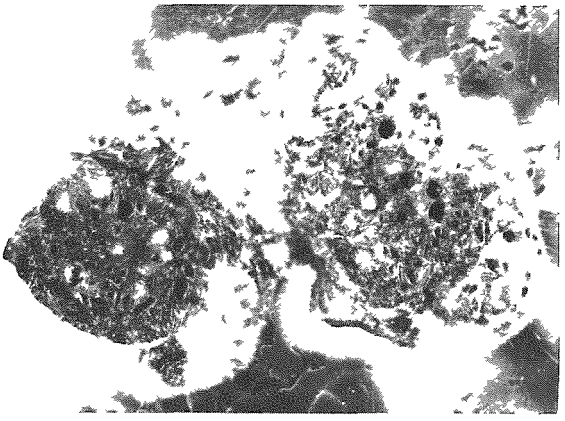

5X

PARTICLE SIZE DISTRIBUTION

d_{sv} = 44.6 mils

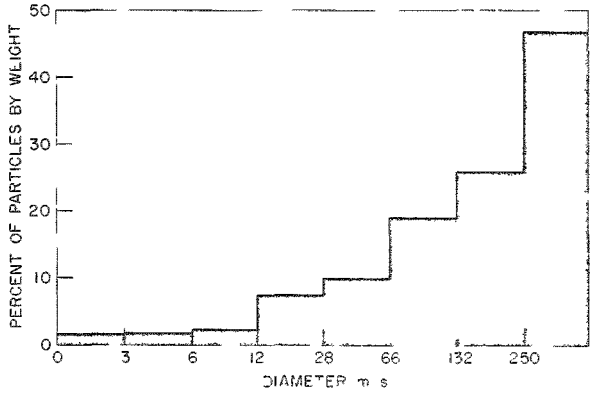

MICROGRAPH OF FRAGMENT

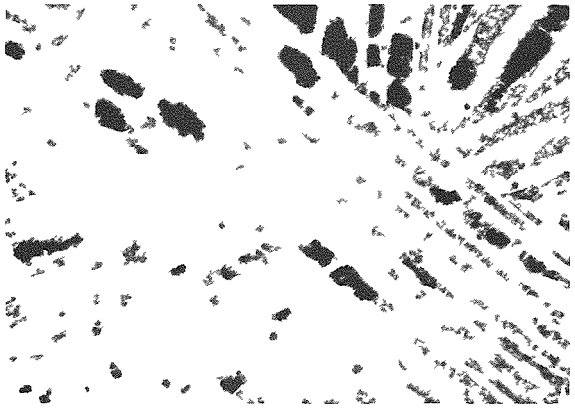

125X

Figure 70

TREAT TRANSIENT CEN-118: 2S ALUMINUM-CLAD, 77 w/o ALUMINUM-23 w/o URANIUM (FULLY ENRICHED) PLATE

FRAGMENTED PLATE AFTER TRANSIENT AT 577 cal/g

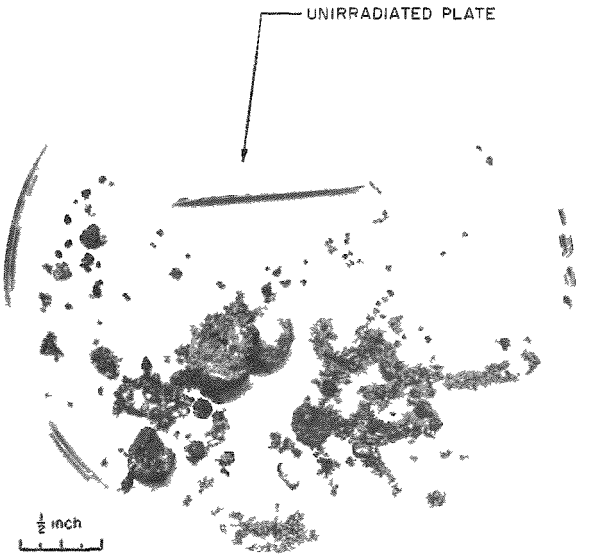

108-5771

MACROGRAPH OF FRAGMENT

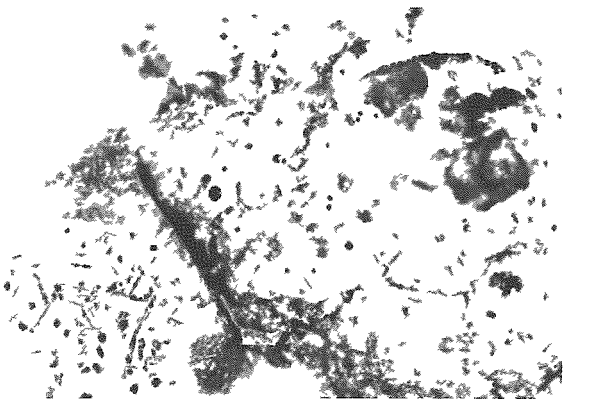

5X

PARTICLE SIZE DISTRIBUTION

d_{sv} = 24.2 mils

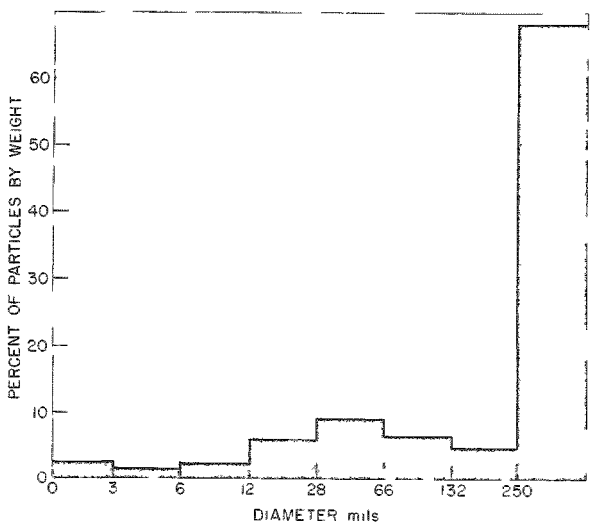

MICROGRAPH OF FRAGMENT

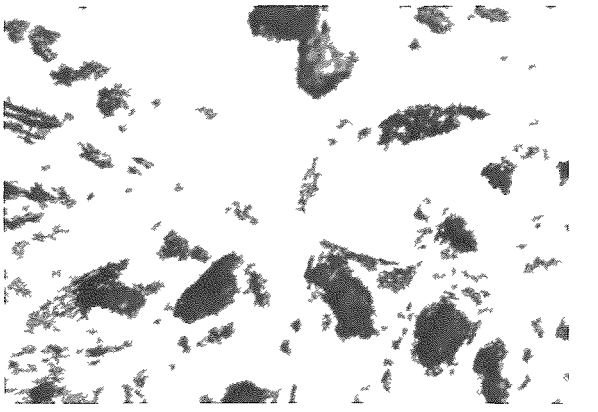

125X

Figure 71

TREAT TRANSIENT CEN-113: 2S ALUMINUM-CLAD, 77 w/o ALUMINUM-23 w/o URANIUM (FULLY ENRICHED) PLATE

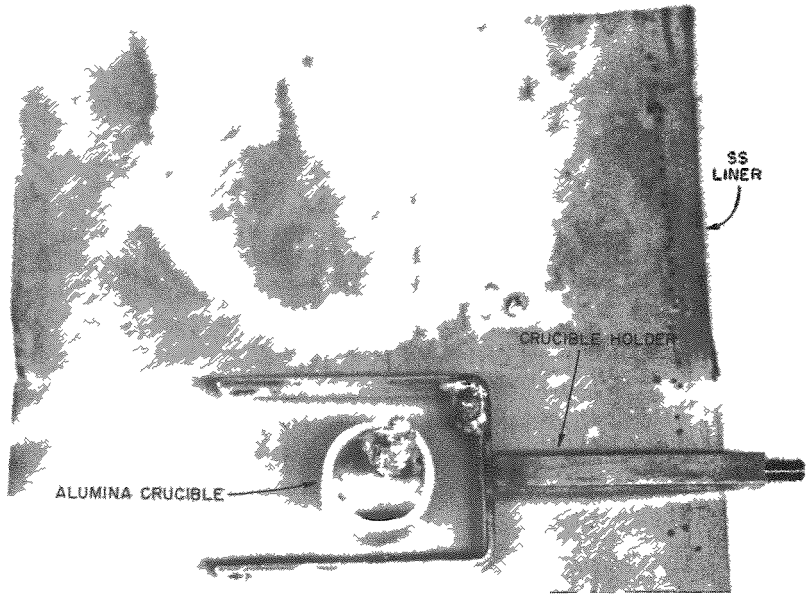

108-5565

FRAGMENTED PLATE AFTER TRANSIENT AT 652 cal/g

(Portions of the plate were found to have adhered to inner parts of the autoclave)

MACROGRAPH OF FRAGMENT

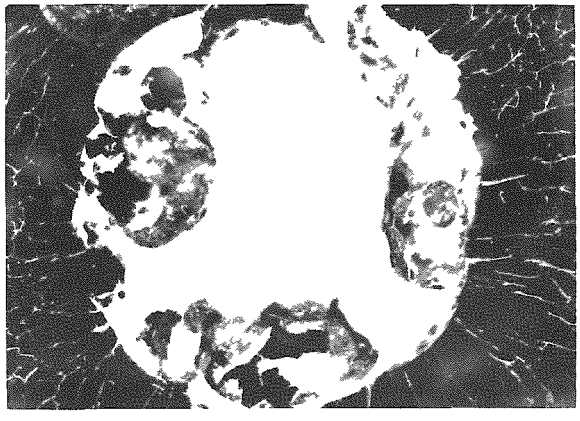

5X

MICROGRAPH OF FRAGMENT

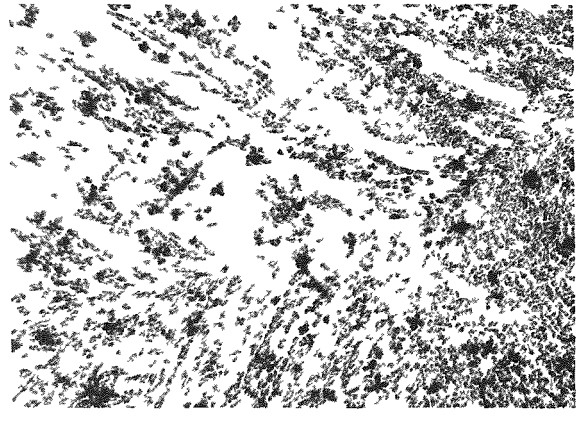

125X

Figure 72

TREAT TRANSIENT CEN-119: 2S ALUMINUM-CLAD, 77 w/o ALUMINUM-23 w/o URANIUM (FULLY ENRICHED) PLATE

FRAGMENTED PLATE AFTER TRANSIENT AT 731 cal/g

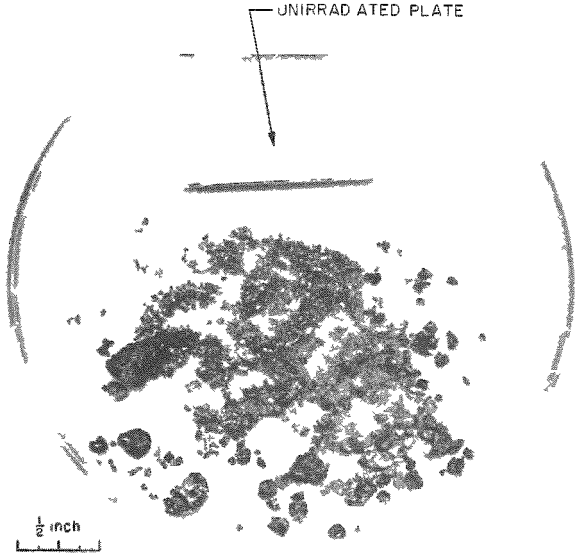

108-5772

MACROGRAPH OF FRAGMENTS

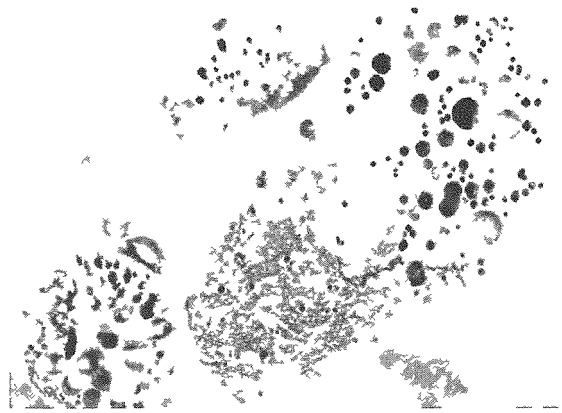

5X

PARTICLE SIZE DISTRIBUTION

d_{sv} = 21.8 mils

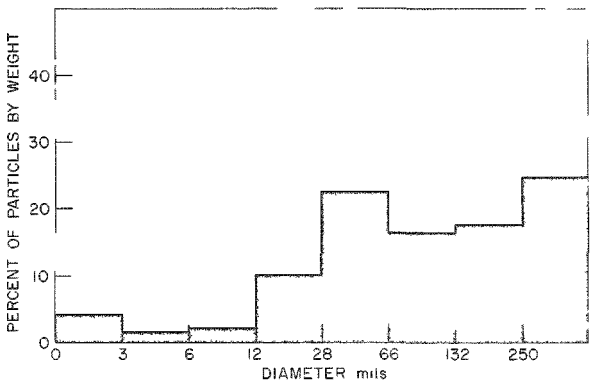

MICROGRAPH OF FRAGMENT

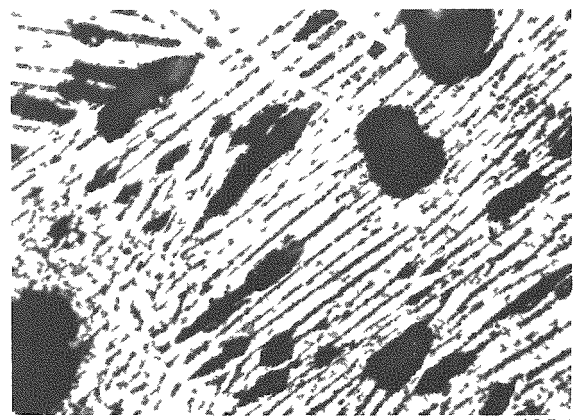

125X

Figure 73

TREAT TRANSIENT CEN-120: 2S ALUMINUM-CLAD, 77 w/o ALUMINUM-23 w/o URANIUM (FULLY ENRICHED) PLATE

FRAGMENTED PLATE AFTER TRANSIENT AT 794 cal/g

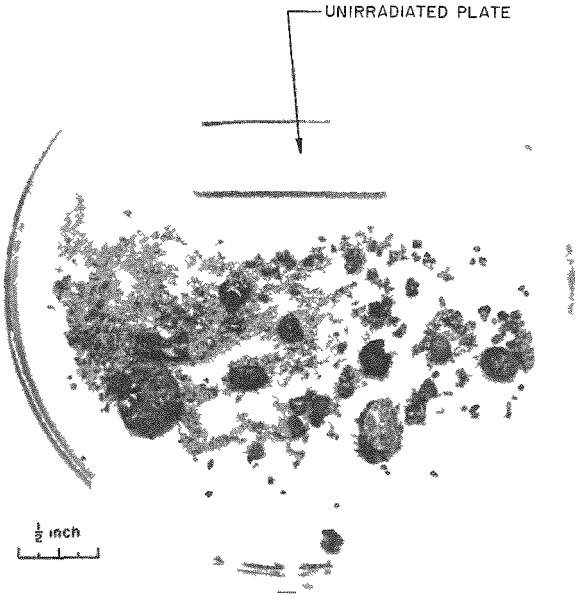

108-5773

MACROGRAPH OF FRAGMENTS

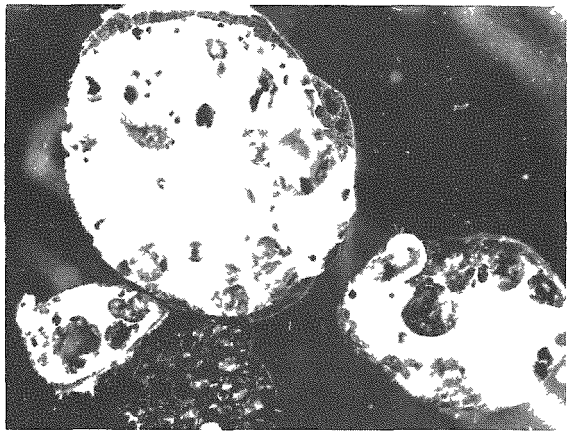

5X

PARTICLE SIZE DISTRIBUTION

d_{sv} = 18.6 mils

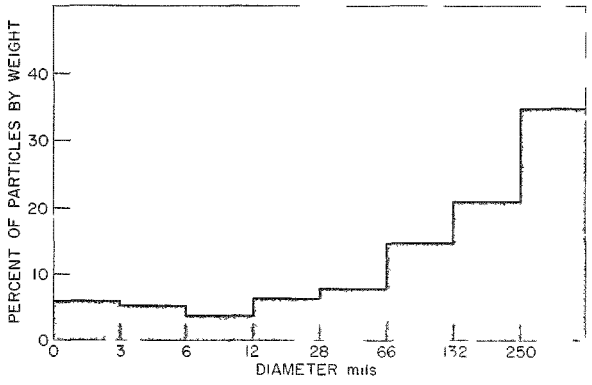

MICROGRAPH OF FRAGMENT

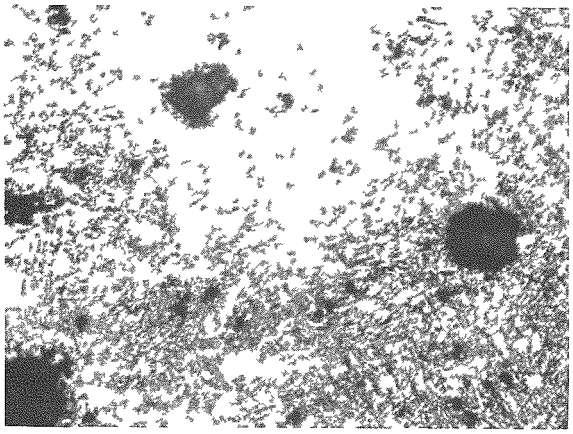

125X

A photomicrograph of the cross section of an unirradiated plate is shown in Figure 74. The core material had three phases, two of which were probably intermetallic compounds of uranium and aluminum (UAl_4 and possibly UAl_3) plus the aluminum phase. Macrographs and micrographs of various portions of the plates irradiated in experiments CEN 110, 111, and 112 are shown in Figure 75.

Figure 74

PHOTOMICROGRAPH OF UNIRRADIATED PLATE - CROSS-SECTIONAL VIEW SHOWING BOTH CLADDING AND CORE

(etched with 0.5 percent HF)

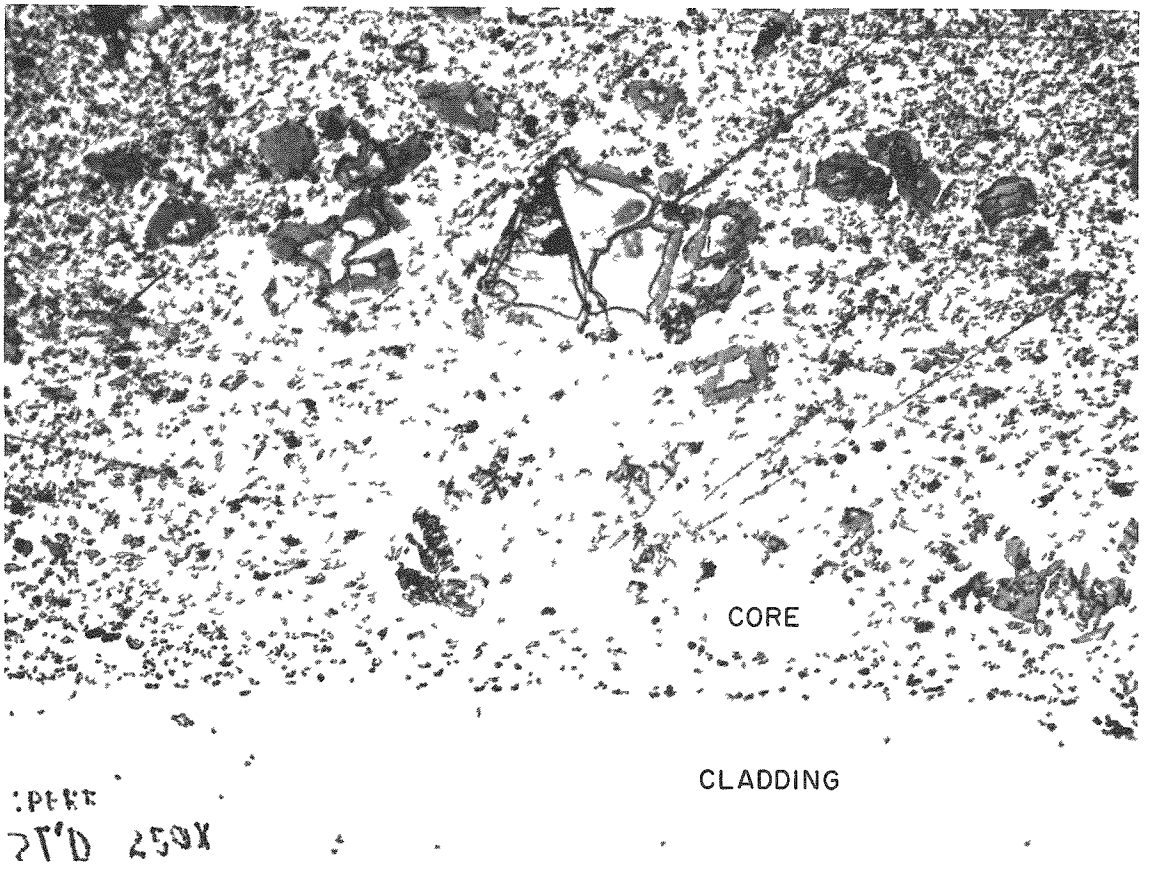

ANL-108-6125 250X

Some striking differences are apparent in the metallurgical appearance of the fuel samples, which was dependent on the reactor energy to which they were subjected. The samples that received energies less than 430 cal/g had no well-defined phases but appeared to be a porous agglomeration of small rounded crystals. At energies above 430 cal/g but below 794 cal/g, large slab-like crystals were present which were randomly arranged in a many-phased matrix. At 794 cal/g, the material

Figure 75

TREAT TRANSIENTS CEN-110, CEN-111, AND CEN-112: PHOTOMACROGRAPHS AND PHOTOMICROGRAPHS OF 2S ALUMINUM-CLAD, 77 w/o ALUMINUM-23 w/o URANIUM (FULLY ENRICHED) PLATES AFTER IRRADIATION

MACROGRAPHS

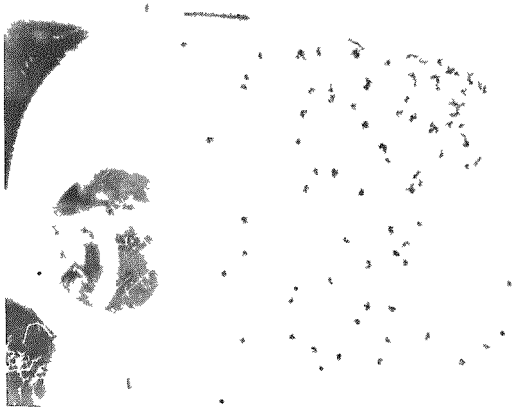

6X

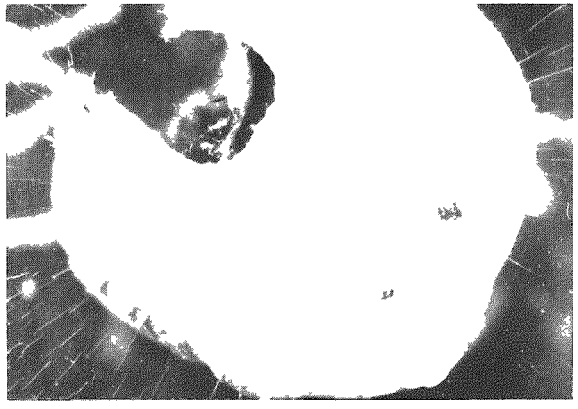

5X

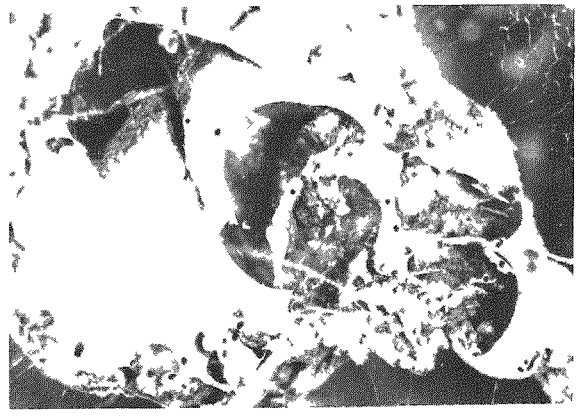

5X

MICROGRAPHS

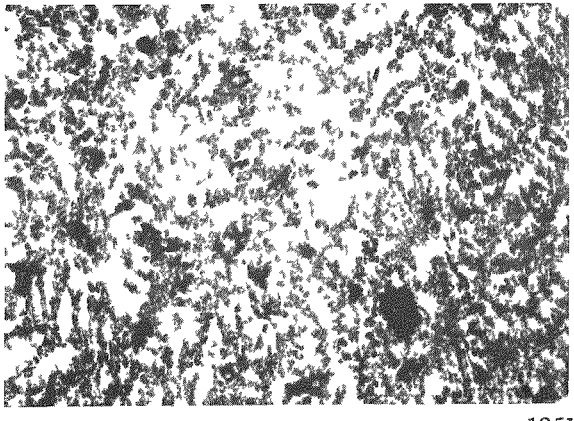

125X

CEN-110 (245 cal/g)

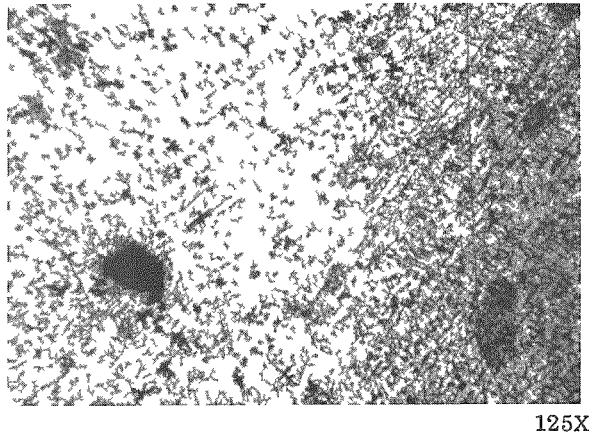

125X

CEN-111 (361 cal/g)

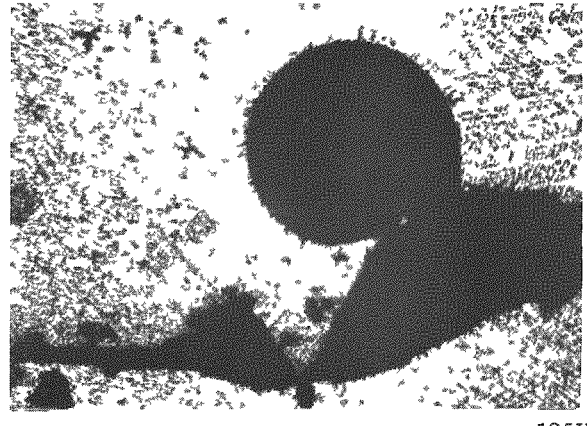

125X

CEN-112 (430 cal/g)

appears to be an eutectic with small, finely dispersed phase fields. The examination of the fuel plates after irradiation revealed that the uranium was dispersed throughout the material in all of the fully melted plates. No pure cladding material could be found. Also, the porosity of the material had greatly increased. The large spherical pores formed indicating the presence of a gas which was probably hydrogen, since only a very small quantity of fission product gases were generated by the irradiation.

Figure 76

TREAT EXPERIMENTS: PERCENT OF METAL REACTED VERSUS NUCLEAR ENERGY INPUT FOR ALUMINUM-CLAD, 77 w/o ALUMINUM-23 w/o URANIUM (FULLY ENRICHED) PLATES

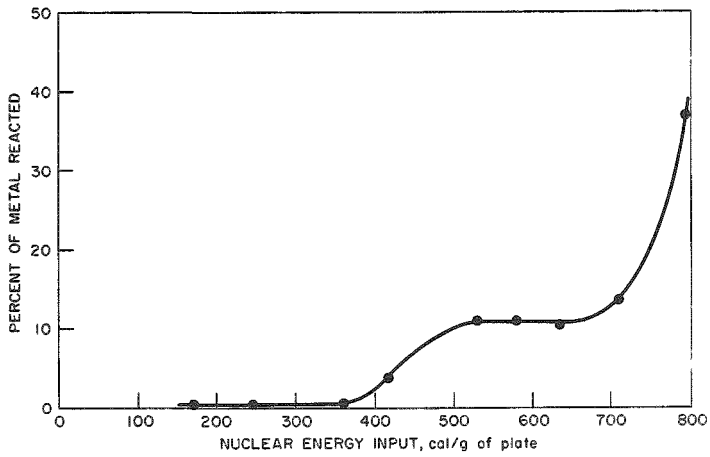

The percent of metal reacted, as determined by hydrogen analysis of a gas sample from each experiment, is plotted as a function of nuclear energy input to the plates in Figure 76. The energy input was determined on the basis of 2.8 fissions per microgram of uranium-235 per watt-second of reactor energy. This value was determined by zirconium-95 fission product analysis of natural uranium foils placed next to the crucible holding the specimen. A correction for flux depression has been made through use of the data from the experimental work of Lewis.[51] The total weight of clad and core material was used in calculating nuclear energy input values.

The extent of reaction apparently increased in two steps as the nuclear energy input was increased. Up to an energy input of 430 cal/g, there was very little reaction - less than 0.5 percent. When the energy input to the plates was greater than 430 cal/g and less than 794 cal/g, the extent of metal reaction was approximately 11 percent. At an energy input of 794 cal/g, the extent of reaction increased markedly in a single experiment.

The peak temperature reached was estimated to be between 1200 and 1400 C for the transient at 430 cal/g. This is less than the adiabatic temperature because of heat losses. At an energy input of 794 cal/g (Transient CEN 120), the peak temperature was estimated to be above 1800 C. The internal parts of the autoclave were covered with a fine white powder in Transient CEN 120. The powder was probably Al_2O_3, which suggests that vapor-phase burning had been initiated.

---

[51] Lewis, W. B., Flux Perturbations by Materials under Irradiation, Nucleonics 13, 82 (Oct 1955).

The data appear to correlate well with the results of isothermal studies of the aluminum reaction by the levitation melting method reported in the preceding section. Slow oxidation of aluminum in steam occurring at 1300 C and below according to the cubic law would account for the lack of significant reaction in the in-pile studies below an energy input of 430 cal/g. The vigorous oxidation of aluminum in steam reported to occur between 1400 and 1750 C according to a linear law might then be identified with the in-pile specimens that received energy inputs between 430 and 794 cal/g. The vapor-phase ignitions at temperatures above 1750 C would then account for the large amount of reaction occurring during the most vigorous transient of the series.

It is expected that a more rigorous correlation between the results of the two experimental methods can be achieved by a mathematical study with a computer. A similar study, concerned with the zirconium-water reaction, was successful in correlating isothermal oxidation rates with results obtained by the condenser-discharge method (see ANL-6548).

V. ENERGY CONVERSION*

Two methods of directly converting nuclear energy into electricity are being studied. One method involves the use of regenerative emf cells, the other method concerns itself with studies of the thermocouple effect.

A. Regenerative Emf Cell

(C. E. Crouthamel, M. Foster, C. E. Johnson, R. Heinrich, R. Eppley, J. Allen, G. McCloud)

Work is continuing on the development of a regenerative cell for the conversion of heat into electricity in a closed cyclic system. These studies are being made in three high-purity helium glove boxes in which oxygen and nitrogen impurities are less than 10 ppm for each element and water is less than 1 ppm.

The present studies include the following:

(a) Phase-diagram investigations of liquid salt and metal systems. During the past quarter the binary salt system lithium hydride-lithium chloride has been studied.

(b) Investigations of bimetallic cells. The high-temperature behavior of the cells has been observed, and emf data at various temperatures for the lithium-bismuth cells have been obtained.

The problem of fabrication of metal diaphragms with suitable properties for the diffusion of hydrogen in the hydride cell is currently being studied by the Advanced Materials Technology Division of the Battelle Memorial Institute on an Argonne National Laboratory subcontract.

1. Inert Helium Atmosphere Purifier

The necessity of a very high-purity inert atmosphere for successful work in the regenerative cell program has been discussed previously (see ANL-6543, p. 196).

The second model of the helium-purification unit has been in operation throughout the past quarter. This unit has been described in detail in ANL-6652. Working drawings of the unit are included in the report.

Lithium metal and clear crystals of lithium hydride have been handled in the boxes at room temperature. No visible reaction on the surface of the bright lithium metal sample could be detected until the second day

*A summary of this section is given on pages 28 to 29.

of exposure, when a slight darkening of the metal was noted. Lithium hydride crystals showed no evidence of reaction after several days of exposure to the box atmosphere. In addition to monitoring water vapor in the box atmosphere by the phosphorus pentoxide cell, which was described in the previous quarterly, ANL-6596, p. 202, and in ANL-6652, gas chromatographic samples have been analyzed at periodic intervals during the past quarter. The gas chromatographic analysis showed that the concentrations of oxygen and nitrogen were each below 5 ppm in the boxes. Water content of the boxes remained consistently below 1.0 ppm, as indicated by the phosphorus pentoxide cell monitor, and below the detection limits (5 ppm) of the gas chromatographic equipment.

2. Heating and Cooling Curve Phase Studies
(C. E. Johnson and J. Allen)

Currently, phase studies are being made of various systems that are of interest in the development of the lithium hydride regenerative cell. The determination of the solid-liquid equilibrium is an important technique in obtaining necessary thermodynamic and physical data. The free energies of dilution or activity coefficients, degree of dissociation in solution, heat capacity, solubility limits, eutectic composition, and freezing points are all of interest in the design and operation of the regenerative cell. The apparatus that is being used in these studies was described in the previous quarterly (ANL-6596, p. 203).

Figure 77

LITHIUM HYDRIDE-LITHIUM CHLORIDE PHASE DIAGRAM

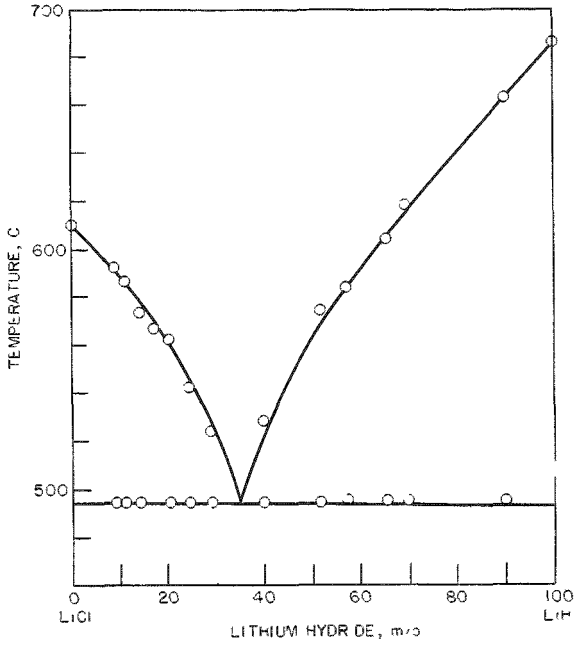

During the past quarter the lithium hydride-lithium chloride system has been investigated. Different salt compositions were used to obtain the tentative phase diagram for this system (see Figure 77). A single eutectic, melting at 496 C, was observed at 33 m/o lithium hydride. There was no evidence of compound formation or of solid solution.

The lithium hydride was prepared from lithium metal of 99.99 percent purity obtained from Foote Mineral Company.* The impurity analysis supplied by the Foote Mineral Company was 0.003 percent sodium, 0.0028 percent potassium, 0.003 percent chlorine, and 0.0031 percent nitrogen. The lithium hydride was prepared by

*Foote Mineral Company, 410-418 West Chelten Bldg., Philadelphia, Pa.

contacting the molten lithium metal with hydrogen purified as needed by diffusion through a silver-palladium valve heated to 400 C. The lithium, held in a pure iron cup, was reacted at 750 C for 12 hr with hydrogen at a pressure of about 1000 mm Hg. The material was cooled and transferred under vacuum to the helium atmosphere box. Clear crystalline lithium hydride was broken free of the iron cup and weighed into a Type 347 stainless steel cup.

Purified lithium chloride was also weighed into the stainless steel cup and the whole was introduced into the furnace well which is connected to the floor of the helium box and which, at this point, contained the purified helium-box atmosphere. Before heating of the sample, the furnace well was isolated from the box (by placing a cover over the well), evacuated, and refilled with hydrogen (purified by passage through the silver-palladium valve) to about 800-900 mm Hg pressure. The sample was heated to melt all the pure components and held in the liquid state for about one hour. The temperature was then decreased and the first break in the cooling curve was observed. The sample was remelted and a second cooling-curve run was made to locate again the first break in the curve. This procedure was repeated until the location of the first break was consistent, after which a complete cooling curve was determined. This procedure was followed to insure that complete mixing of the components of the system had occurred.

3. Bimetallic Cells
(M. Foster, R. Eppley)

As a part of a systematic study of the thermodynamic properties of bimetallic cells which may be of interest in a regenerative cell system, measurements are being made of the emf of the cell Li/LiCl-KCl (eutectic)/Li-Bi (liquid alloy) as a function of temperature and lithium content in the bismuth alloy. The results that have been obtained for this cell are still considered incomplete.

The liquid anode and liquid cathode both were contained in porous beryllium oxide crucibles. The crucibles were in contact with the molten lithium chloride-potassium chloride electrolyte, which was contained in a tantalum cup. Stainless steel solid wires contacted the anode and cathode melts to permit passage of the electric current.

In the first cells tested, the mole fraction of lithium in the cathode was 0.05. In operation of the cell, some difficulty was experienced in obtaining data for temperatures above approximately 450 C. At the higher temperatures, the cell voltage became increasingly unstable. Moreover, the observed emfs of two successive cells were found to differ by as much as 0.030 v, the slopes of the emf-temperature plots, however, were the same. The temperature coefficient was found to be positive in both cells, i.e., the emf increased with increasing temperatures. The

relationship between the emf ϵ and the temperature for the two cells is given by the following equations:

$$\text{First Cell: } \epsilon = 0.743 + 2.44 \times 10^{-4} T \text{ (over the range from 625 to 839 K)} \quad ; \tag{1}$$

$$\text{Second Cell: } \epsilon = 0.742 + 2.79 \times 10^{-4} T \text{ (over the range from 633 to 720 K)} \quad . \tag{2}$$

The porous beryllium oxide crucibles used as electrode containers were found to disintegrate after use. This problem was investigated by temperature cycling the potassium chloride-lithium chloride eutectic in one of the beryllium oxide crucibles. It was observed that the molten salt mixture wetted the crucible throughout its porous structure. The cracking of the crucible wall was attributed to the mechanical forces which developed as a result of the volume change that occurred during the freezing of the electrolyte. No adverse effects were noticed when lithium metal alone was heated in a beryllium oxide crucible.

The status of the Battelle Memorial Institute (BMI) contract for the manufacture of metal diaphragms has been reviewed periodically in this quarter. Alloy preparation of iron-molybdenum alloys up to 20 w/o molybdenum have been cast successfully at Battelle using a graphite mold. Iron-molybdenum diaphragms of 5 and 10 w/o molybdenum have been successfully bonded to 347 stainless steel holders. Three samples of each diaphragm have been received from BMI and are now being evaluated. Gas-pressure bonding of niobium and vanadium to stainless steel holders has not produced a good bond. Attempts are being made to pressure bond 1-mil silver-palladium foil to "clean" niobium sheet. If this is successful, it would alleviate the problem of the formation of an oxide barrier on the hydrogen gas side of the niobium diaphragm. Electron beam welding of vanadium to stainless steel holders has not yet been successful. Cracks have appeared in the vanadium diaphragms, but not in the weld area.

B. Thermoelectricity Research

(R. K. Edwards, H. M. Feder)

Studies in thermoelectricity are under way to contribute to the future technological development of direct conversion of nuclear reactor heat energy into electrical power by means of the thermocouple effect.

Liquid thermocouple systems and refractory solid thermocouple materials are being studied. The liquid systems are being investigated because they offer certain experimental advantages; the refractory solids are being investigated because they are of particular interest to reactor energy conversion.

1. Liquid Systems

(R. K. Edwards, P. Danielson)

The thermoelectric properties of liquid systems are of importance since their study should contribute to the extension of solid-state theory to the liquid state. At the present, there are only meager data in the literature on the electrical transport properties of liquid systems. However, it is evident that the electrical classes used to describe solids are each also represented by liquids.[52] The semiconductors and semimetals, liquid or solid, are of particular interest as possible conversion materials. The semimetals have received less attention as to the controlled modification of their electronic structures, although an analysis by Klemens[53] has indicated the nature of the desired electron distribution.

Liquid binary systems offer a wide latitude for the study of composition dependencies. Solid-state investigations of the transport properties of binary semiconductors are generally limited to very narrow composition ranges by virtue of narrow ranges of phase stability.

The binary liquid systems from the indium-antimony-bismuth triad were chosen for the initial investigation, for solid-state combinations of elements listed in this region of the periodic table have led to a number of semiconducting phases with interesting electrical properties. The two systems indium-antimony and indium-bismuth are isoelectronic and have electron:atom ratios which vary with composition. The third system, antimony-bismuth, is one in which the electron:atom ratio is constant with composition. The study of the triad should permit some isolation of electron:atom ratio effects.

The present report will present the results of a partially completed study of the variation of the Seebeck coefficient (thermoelectric power) with composition in the binary systems of the selected triad. The apparatus and standard procedures adopted for the general investigation are first described.

Experimental Apparatus - The arrangement of the electrical circuit for the measurement of Seebeck coefficients in the liquid alloys is shown schematically in Figure 78. The liquid alloy, A, has a temperature gradient between the two isothermal regions, T_a and T_b. A short piece of tungsten wire dips into each of the isothermal regions of the alloy. Each tungsten wire is connected to a short length of molybdenum ribbon. The

---

[52] Ioffe, A. F., and Regel, A. R., Progress in Semiconductors, Edited by A. F. Gibson, John Wiley and Sons, Inc., New York (1960) Vol. 4, p. 237.

[53] Klemens, P. G., Theoretical Requirements for Thermoelectric Materials, Westinghouse Research Report 929-8904-R2 (July 12, 1961).

two ribbons are, in turn, connected to platinum and platinum-10 percent rhodium wires of thermocouple grade. The platinum and platinum-10 percent rhodium wires are joined (all joins hereafter noted are of "thermal free solder") to silver wires and each junction is immersed in an individual mineral oil bath contained within a Pyrex tube. The Pyrex tubes are immersed in a common ice bath to maintain the reference temperature, T_0. The silver lead wires, 1, 2, 3, and 4, connect to a double-pole, multiple position-selector switch (silver components). The lead wires from the switch to the potentiometer are also of silver. A type K-3 potentiometer and a type 2430 galvanometer from Leeds and Northrup Company are used for the measurements.

Figure 78

SCHEMATIC ARRANGEMENT FOR MEASUREMENT OF SEEBECK COEFFICIENT RELATIVE TO PLATINUM

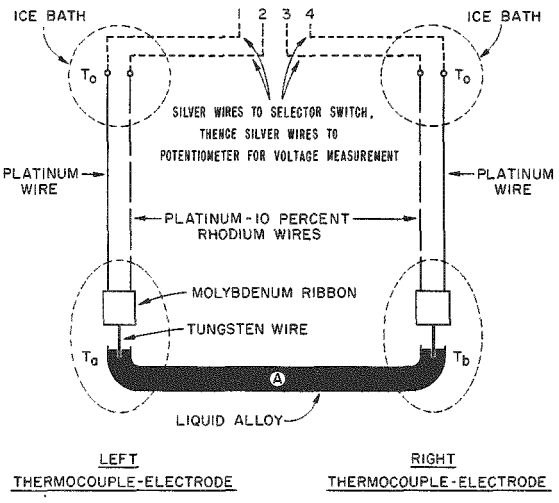

The selector switch could be used to obtain the voltage between any desired pair of wires. Thus, the voltage at 1-2 yields the temperature T_a. Similarly, the voltage at 3-4 yields T_b. The difference between these two observations is the ΔT for the liquid A, and the average of T_a and T_b is T_m for which the thermal voltage measurements on A apply. The measurement at 1-4 is the thermal voltage of alloy A relative to platinum for the given ΔT and T_m. Similarly, the measurement at 2-3 gives the thermal voltage of alloy A relative to platinum-10 percent rhodium for the same ΔT and T_m. It follows that the difference between these last two measurements also leads to a value of ΔT. The latter values of ΔT were used in the calculations of Seebeck coefficients since these ΔT values arise from smaller numbers and also correspond more nearly in time with the 1-4 observation used in the final evaluation of the Seebeck coefficients. Values of ΔT obtained from the two sets of observations should, of course, agree in steady-state conditions; however, because slightly drifting conditions are generally encountered and because the measurements are not simultaneous, disagreement between the two values of ΔT is mostly a measure of the rate of thermal drift between observations. As a matter of procedure, only sets of measurements with values of ΔT that disagreed by less than 0.2 C were considered satisfactory.

The thermocouple electrodes indicated schematically in Figure 78 are of specialized construction. One electrode is shown in detail in Figure 79. The thermocouple wires are welded to molybdenum ribbon which is welded to tungsten wire, and the assembly is enclosed within a

quartz-glass envelope. A vacuum-tight seal is made by fusing the quartz-glass around the molybdenum ribbon. The seals made by the fusion of the quartz-glass around the tungsten wire and around the thermocouple wires in the vicinity of their junction with molybdenum are very close but generally not vacuum-tight. For this reason the envelopes were evacuated and sealed off by means of epoxy glue to prevent oxidation of the molybdenum joins of the couple wires.

Figure 79

THERMOCOUPLE ELECTRODE

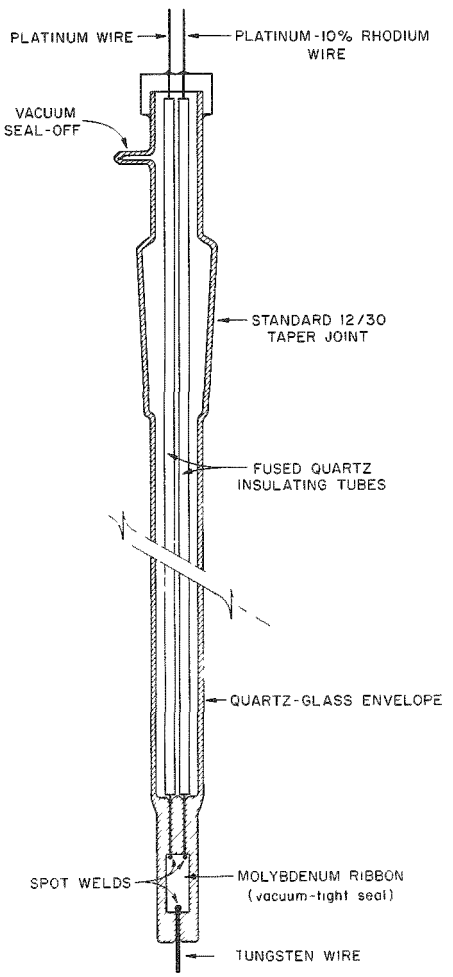

Tungsten was used to contact the liquid alloys since it is more generally compatible with the elements of the systems to be studied. The platinum-platinum-10 percent rhodium couple was used because of its greater temperature range and particularly because platinum is more stable and is better characterized in its thermoelectric properties than are other materials available for high-temperature use.

A drawing of the quartz-glass cell used to contain the liquid alloys is shown in Figure 80. The cell, with the two thermocouple-electrodes in place, is shown within one-half of the split "H-furnace," the forward (hinged) half of which is shown open as required when a new cell is being installed. The furnace is mounted on a pivot tube whose axis (into the paper) is indicated. The furnace can be rotated 180° about this axis to empty the cell at the conclusion of a series of measurements. The shape of the reservoir sections of the cell with regard to the axis of rotation is such that complete pouring of the contents from one side of the cell to the other (without holdup) can be made as desired in mixing or emptying operations. A bellows-type flexible stainless steel tube is joined at the semi-ball joint of the cell. This allows the cell to be connected, through valves, to either a vacuum pumping system or a source of purified helium gas.

Concentric metallic pipes passed from the furnace through the pivot axis mount. All of the thermocouple lead-out wires passed through the outer annulus and the power leads passed through the centermost pipe. Figure 81 shows a photograph of the furnace-cell portion of the apparatus. The network of small pipes coming from the H-furnace are copper shielding tubes for a number of monitoring thermocouples.

Figure 80

QUARTZ-GLASS CELL WITH THERMOCOUPLE ELECTRODES

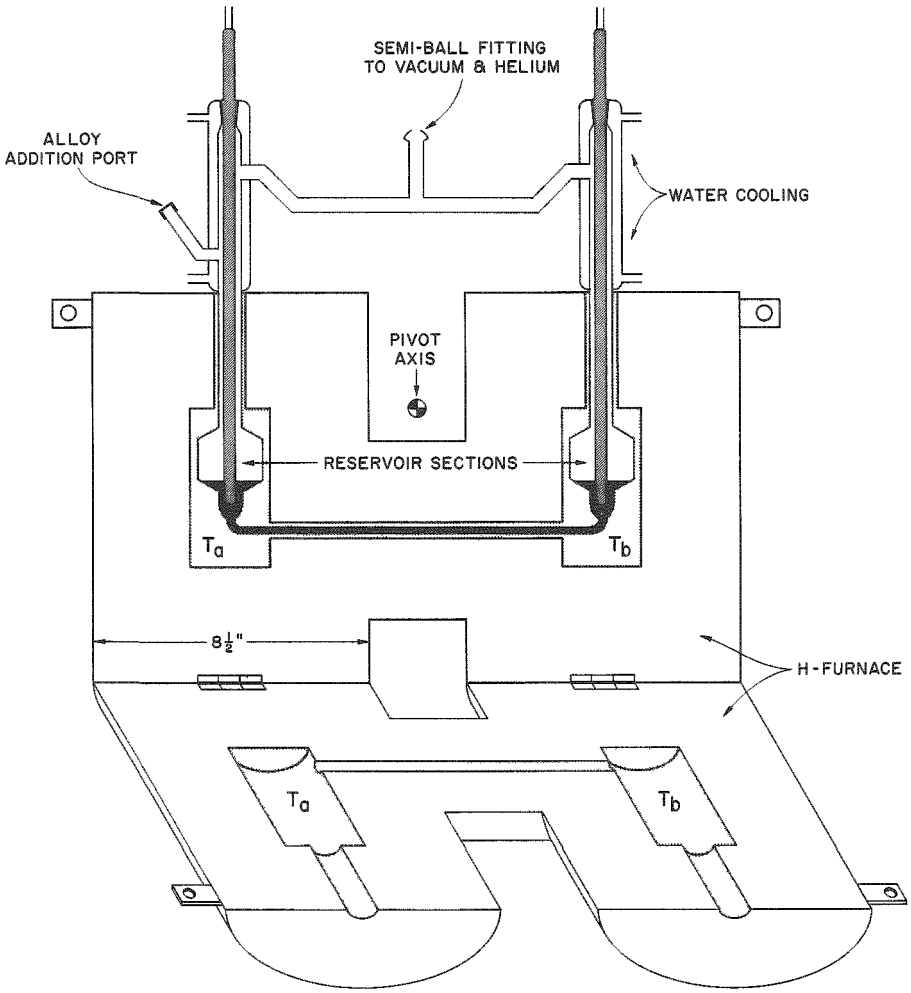

Figure 81

H-SHAPED FURNACE USED IN THE STUDY OF
THERMOELECTRIC PROPERTIES
OF LIQUID ALLOYS

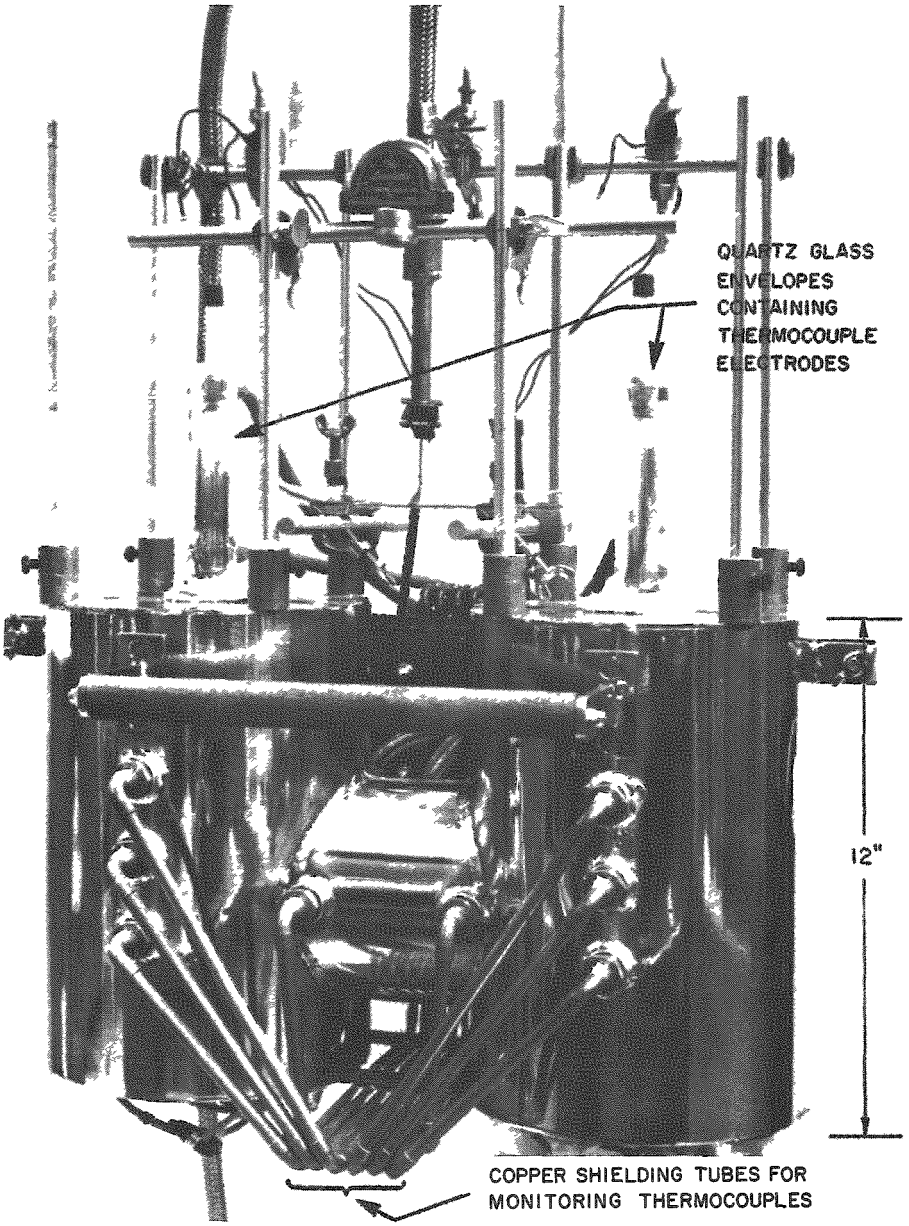

ANL-108-5828

Experimental Procedure - The cleaned cell and electrodes were degassed in operating position at the highest temperatures for the planned run. The cell was cooled and indium (99.999+%), antimony (99.999%), or bismuth (99.999%) was added through the addition port. Approximately one gram-atom of the pure metal was introduced for the initial run of a given series, and compositions were then successively altered by additions of the pure alloying element out to a composition of approximately 50-60 a/o. The process was then repeated starting now with the other component.

After the initial introduction of the pure component, the addition port cap was put on and the system was subjected to vacuum pumping while being heated. Degassing pressures were kept below 1×10^{-5} mm Hg and final pressures at operating temperatures were about 3×10^{-6} mm Hg, as measured by an ionization gauge which was situated about 8 ft from the cell along the $\frac{3}{8}$-in.-ID, flexible stainless steel tube. High-purity helium gas, which was purified further by being passed through a charcoal trap cooled in liquid nitrogen, was admitted to a pressure of one atmosphere in order to minimize losses of metal by vaporization.

Desired composition changes were effected by additions of the appropriate alloying component through the additions port against a strong counterflow of helium gas. The system was then quickly evacuated (about 10^{-4} mm Hg within a minute) and helium was again introduced into the system. Mixing of the cell contents was thorough. The mixing was easily accomplished by pouring the contents of the cell from one side of the cell to the other twelve times or more by tilting the furnace about its pivot mount.

Evaluation of Measurements - For each composition four sets of measurements, meeting the criterion set above for the rate of temperature drift, were taken with $T_a - T_b = 100$ C, and averaged. These are conveniently designated "normal" as to temperature gradient. Then the furnace temperatures were "reversed" and the procedure repeated for $T_b - T_a = 100$ C. The same mean temperature was maintained in both cases. Calculation of the Seebeck coefficient can then be carried out in such a manner that extraneous voltage contributions can be eliminated, as may be seen by referring to Figure 82.

In the figure, both the platinum-liquid alloy and the platinum-10 percent rhodium-liquid alloy voltages are plotted against their difference voltage for a given liquid composition in the indium-antimony system at a constant $T_m = 750$ C. The difference voltages are a measure of $T_a - T_b$. A residual extraneous voltage is evident since the two curves show finite vertical ordinate values at $T_a - T_b = 0$. The linearity of the two curves in Figure 82 is excellent, and it is apparent that Seebeck coefficient values (relative to platinum) may be best obtained by taking the

slope of the appropriate line (converting the abscissa to temperature units) over a larger temperature interval rather than trying to use small ΔT observations to approximate a differential. It can be shown that for regions in which the Seebeck coefficients of platinum and platinum-10 percent rhodium are linear with temperature, as reported by Nystrom,[54] a straight line signifies that the absolute Seebeck coefficient of the liquid derived from the slope of the line is dependent only on T_m and is then independent of the intervals of $T_a - T_b$ used.

Figure 82

SEEBECK VOLTAGES DEVELOPED FOR VARYING TEMPERATURE INTERVALS ALL ABOUT A GIVEN MEAN TEMPERATURE, 750 C

(Liquid alloy of antimony/indium ratio 0.4748/0.5252)

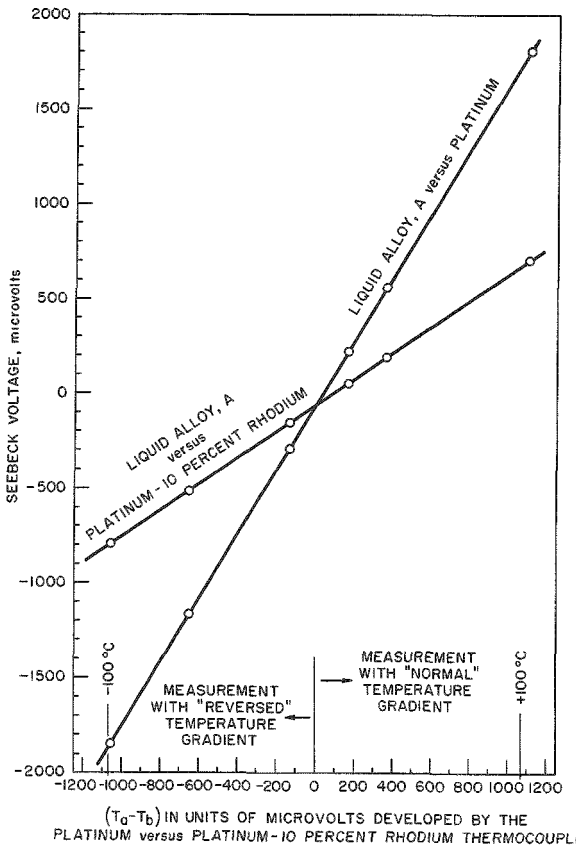

Under these circumstances it becomes an advantage to carry out the measurements using the larger ΔT intervals in order to decrease percentage errors. The procedure adopted for the general investigation was to consider the slope of the line adequately determined by two sets of observations at a given T_m, the one at a normal ΔT of 100 C and the other at a reversed ΔT of 100 C. The derived Seebeck coefficients, relative to platinum, were then adjusted to absolute values by allowing for the contribution of platinum, using Nystrom's[54] values. The latter values were found to be in agreement with values obtained by Rudnitskiy[55] in his work with "thermocouple grade" platinum. It is to be borne in mind that Cusack and Kendall,[56] however, derived values for platinum which are more negative by as much as 0.8 microvolt per degree. If these values were used to correct for the contribution of platinum, the absolute values of the Seebeck coefficients in the current report would be more negative

---

[54]Nystrom, J., Arkiv. Mat., Astron., Fysik, 34A, 1 (1948).

[55]Rudnitskiy, A. A., AEC-tr-3724, Physics and Mathematics, A translation by the United States Atomic Energy Commission, Technical Information Service, of (Aleksandr Alekseevich Rudnitskii, Izdatel'stvo Akademii Nauk SSSR, Moskva, 1956).

[56]Cusack, N. and Kendall, P., Proc. Phys. Soc. (London), 72, 898 (1958).

by this amount. The relative values of the Seebeck coefficients for a given binary system are not influenced by the choice of absolute values for the reference material, and the main interest in the work is in the relative values.

Results - Sufficient information has been obtained in the three systems to provide for some tentative comparisons, although the study is not yet complete.

In Figure 83 are shown the Seebeck coefficient values for the antimony-bismuth system at the mean temperature 750 C. All points were established by both normal and reversed temperature gradient observations to eliminate any extraneous voltage contributions as described in the procedure above.

Figure 83

ABSOLUTE SEEBECK COEFFICIENTS IN THE LIQUID SYSTEM ANTIMONY-BISMUTH AT 750 C

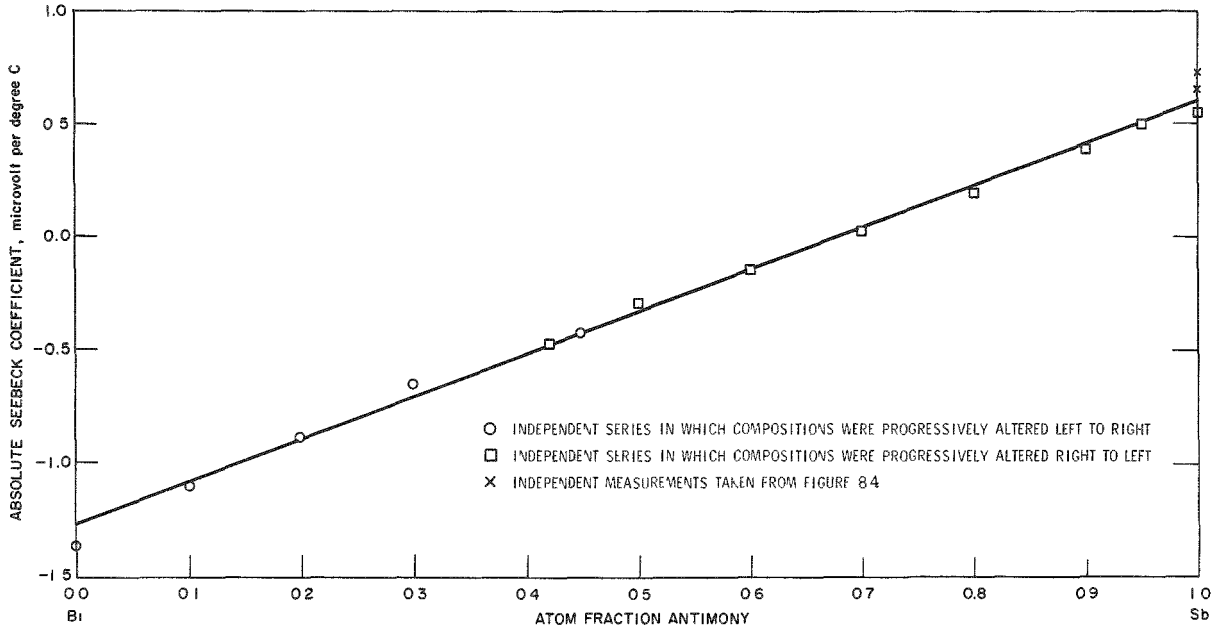

The Seebeck coefficient values for the indium-antimony system are shown in Figure 84, also for 750 C. However, some of the points (solid squares) were determined by only a single direction of the temperature gradient. For these, the plotted values are values which have been corrected by an assumed constant extraneous voltage term determined at each of the two compositions indicated by the open squares and found there to be a constant. Otherwise, all points were determined by both normal and reversed gradient observations. The inset for this figure shows some measurements made toward the close of the left-to-right series with a view to noting any sequential factors in the measurements.

Figure 84

ABSOLUTE SEEBECK COEFFICIENTS IN THE LIQUID SYSTEM INDIUM-ANTIMONY AT 750 C

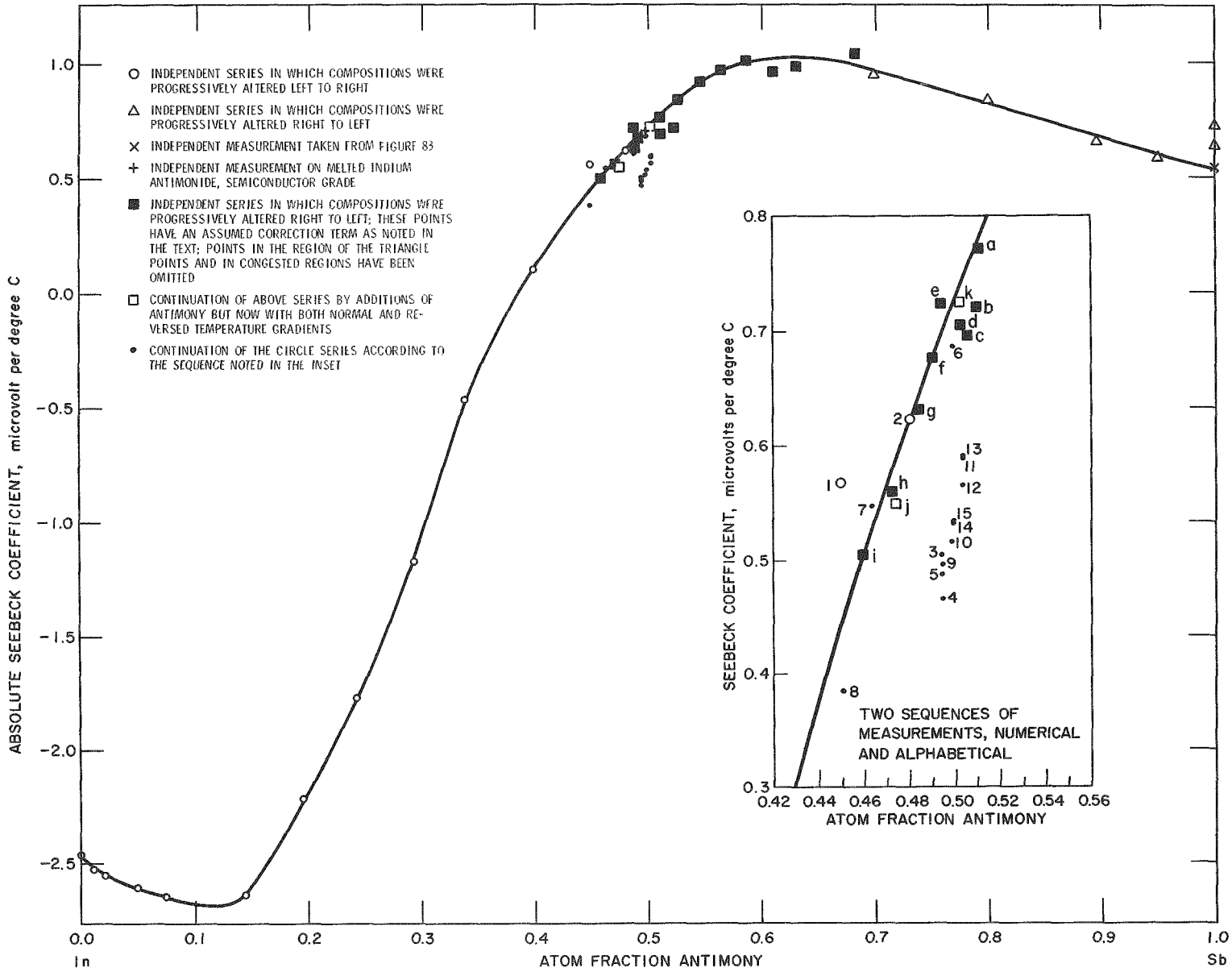

The Seebeck coefficient values for the indium-bismuth system are shown in Figure 85 for the mean temperature 450 C instead of 750 C (because of a temporary power limitation). All points, except the one denoted "x," were obtained from measurements which involved only a single direction of the temperature gradient. The single point (at 100 percent bismuth) was from a later run with new material and was carried out with both normal and reversed gradient observations. From the good agreement of the latter point with the other values, it would appear that no significant correction term is implied; however, this cannot be considered to have been established. Later measurements in the 750 C range are planned; meanwhile, the relative shape of the curve is considered of significance for comparison purposes.

Figure 85

ABSOLUTE SEEBECK COEFFICIENTS IN THE LIQUID SYSTEM INDIUM-BISMUTH AT 450 C

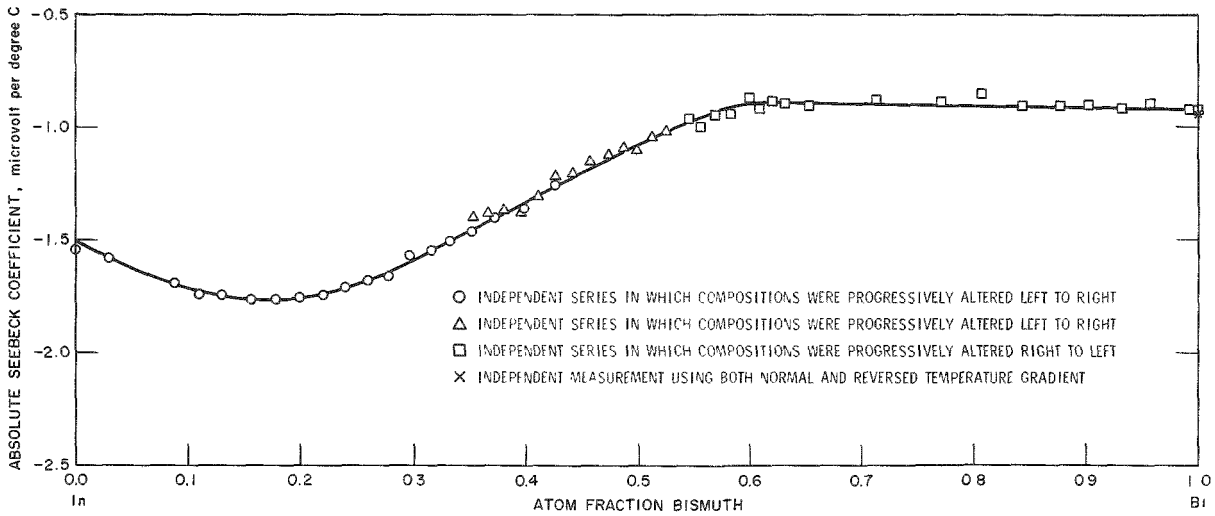

Discussion - A number of factors need to be considered before more than a qualitative evaluation of the meaning of the results is appropriate. Thus, liquid indium antimonide (atom fraction = 0.5) has been studied by Blum and Ryabtsova.[57] They have reported a Seebeck coefficient of -35 microvolts per degree and that this value was constant with temperature in the range 530 to 700 C. The work of Blum and Ryabtsova was carried out in a cell which was open to the atmosphere during measurements. Some work reported by Fischer-Colbrie and Littebrant[58] on indium antimonide of "unspecified impurity" yielded positive values in the

[57] Blum, A. I. and Ryabtsova, G. P., Soviet Physics Solid State 1, 692 (1959).

[58] Fischer-Colbrie, E. and Littebrant, E., General Electric Electronics Laboratory Technical Information Series R59ELS 39, (Electronics Laboratory Technical Information, Bldg. 3, Electronics Park, Syracuse, New York).

liquid state ranging from 5 microvolts per degree at the melting point to about 38 microvolts per degree (short extrapolation) at 750 C. These discrepancies suggested that the variable behavior in our own data in this composition region (see inset in Figure 84) might be associated with unknown impurity factors. A check measurement was carried out in which melted indium antimonide of semiconductor grade was used. The Seebeck coefficient value is plotted in Figure 84 and it is seen to be in good agreement with the other values.

At present, it is interesting to compare qualitatively the three systems studied. The antimony-bismuth system yields a simple linear dependence of the Seebeck coefficient on the atom fraction composition. For comparison purposes, it is reasonable to consider this system to have a constant electron:atom ratio since the two elements have similar outer electron structures. The indium-antimony and indium-bismuth systems yield complex relationships between the Seebeck coefficient values and alloy composition. This relationship, though complex, is quite similar for the two systems. The similarity of the two curves is attributed to the similarity of the outer electronic structures of bismuth and antimony. The complexity of the relationship is attributed to the fact that the electron:atom ratios change with composition.

2. Refractory Solid Thermocouple Systems
(M. Tetenbaum and F. Mrazek)

Materials possessing high melting points and low vapor pressures are desirable if energy-conversion devices are to be used at high temperatures, such as might be encountered in current nuclear reactor systems. The lanthanide and actinide sulfide systems are highly refractory and have phases with carrier concentrations in the semiconducting range. The uranium and thorium sulfide systems and their solid solutions have been selected for the initial studies.

It has been found that the relative Seebeck coefficient values for uranium monosulfide had been assigned incorrect signs and, as a consequence, the derived absolute Seebeck coefficient values shown in two previous reports (ANL-6569, p. 157, Figure 57 and ANL-6596, p. 209, Figure 80) require correction. These values then become positive in sign and of magnitudes decreased by twice the contribution of the reference material, platinum, to yield the values shown in Figure 86. The data from Electro-Optical Systems, Inc.[59] was also incorrectly shown in the cited earlier figures, but is correctly shown in Figure 86.

[59] Jordan, C. B., High Temperature Semiconducting Compounds for Thermoelectric Power Generation, Bimonthly Progress Report No. 4, June 15-August 1962, EOS-1592-2M-4, Final Comprehensive Report, Dec. 15, 1960 through Dec 15, 1961, EOS-1592-Final, Electro-Optical Systems, Incorporated, Pasadena, California.

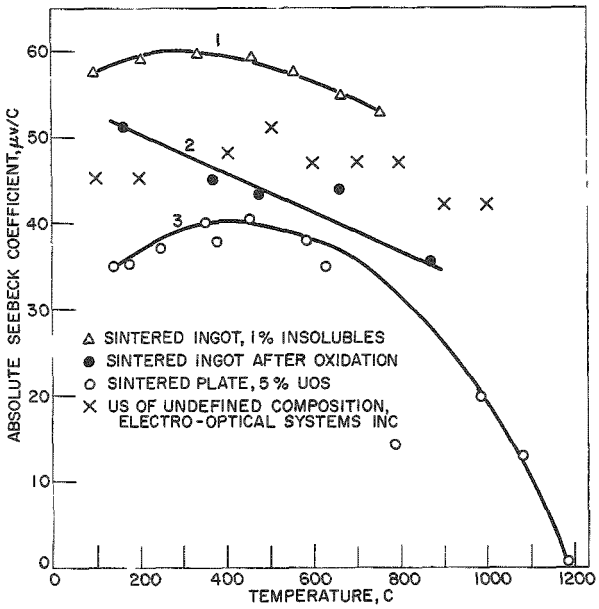

Figure 86

ABSOLUTE SEEBECK COEFFICIENT VERSUS TEMPERATURE FOR VARIOUS SPECIMENS OF URANIUM MONOSULFIDE

The experimental conditions which existed during the measurement sequences, 1, 2, 3 are explained in the text on page 209 of ANL-6596.

Kazmierowicz and Kanter[60] find, from the latest evaluation of their measurements, positive Hall coefficients for uranium monosulfide rather than negative values. Thus, their values reported in ANL-6543, p. 205 and ANL-6569, p. 159, Table 44 are to be considered as positive. The dominant current carriers in uranium monosulfide are therefore positive holes rather than electrons.

A series of Seebeck coefficient measurements were made with the arc-melted slab of uranium monosulfide (insolubles: ~16 percent UOS) which had yielded favorable figure-of-merit values (see ANL-6477, p. 216) and the equipment (Z meter) for the measurement of the figure of merit at Westinghouse. The surface of the specimen, which had become somewhat tarnished from previous handling, was "cleaned" by heating the specimen in vacuum at 1800 C for approximately 15 min. This heat treatment yielded a specimen with a bright shiny surface. A duplicate set of Seebeck measurements was obtained in the following manner: The specimen was removed from the Seebeck apparatus upon completion of the initial run. The specimen was again cleaned by means of the high-temperature vacuum treatment described above, and returned to the Seebeck apparatus.

The results of the duplicate sets of measurements of Seebeck coefficients as a function of temperature are shown in Figure 87. It is apparent that agreement between the two sets of measurements is good, and that the Seebeck apparatus is capable of yielding reproducible data.

The results of Seebeck coefficient measurements as a function of temperature for sintered specimens of uranium monosulfide, thorium

[60]Kazmierowicz, C. W., and Kanter, M. A., Solid State Science Division, Argonne National Laboratory, private communication, April 13, 1963.

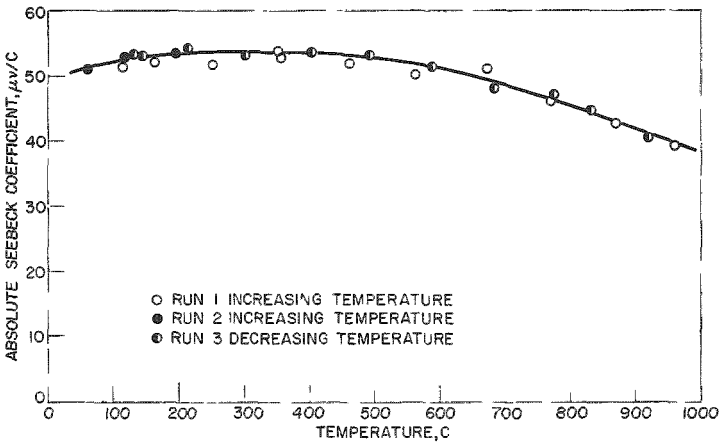

Figure 87

ABSOLUTE SEEBECK COEFFICIENT VERSUS TEMPERATURE FOR ARC MELTED URANIUM MONOSULFIDE

monosulfide, and a 50-50 m/o uranium monosulfide-thorium monosulfide solid solution are shown in Figure 88. The sintered uranium monosulfide pellet (density about 85 percent of theoretical) was obtained from a relatively pure batch of uranium monosulfide which had an oxysulfide content of about 0.1 percent. The sintered thorium monosulfide pellet (density about 80 percent of theoretical) was prepared by using thorium monosulfide powder obtained from the Metallurgy Division. The insoluble content of the thorium monosulfide was approximately five percent. The uranium monosulfide-thorium monosulfide solid solution in the form of a sintered pellet (density about 84 percent of theoretical) was obtained from the Metallurgy Division.

Figure 88

ABSOLUTE SEEBECK COEFFICIENT VERSUS TEMPERATURE FOR URANIUM MONOSULFIDE, THORIUM MONOSULFIDE AND 50-50 m/o URANIUM MONOSULFIDE-THORIUM MONOSULFIDE SOLID SOLUTION

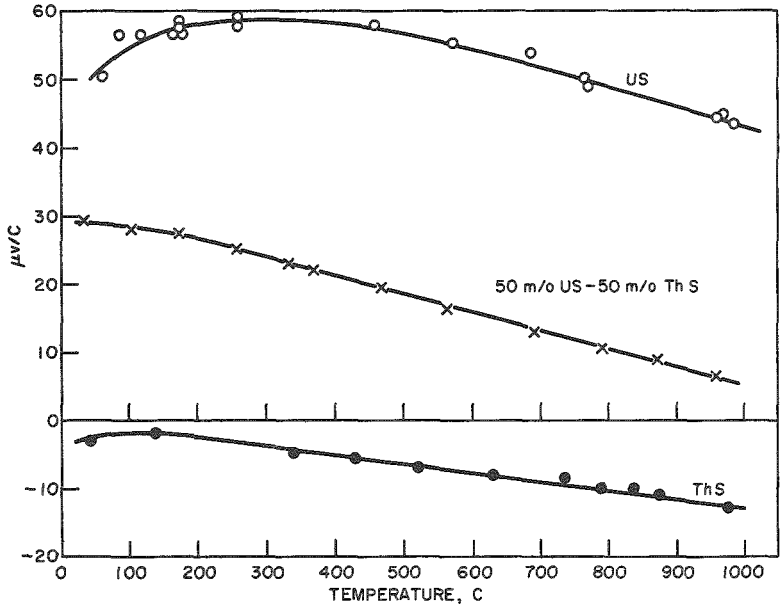

The results shown on Figure 88 suggest that the thermoelectric power decreases with increasing thorium monosulfide concentration in the uranium monosulfide-thorium monosulfide solid solution system. From resistivity and Hall measurements, it appears that thorium monosulfide is more metallic than uranium monosulfide. The trend shown in Figure 88 may reflect, therefore, the increase in the metallic nature of the solid solution with increasing thorium monosulfide content. Further thermoelectric parameter measurements will be made on other compositions in this system.

Simultaneous Seebeck coefficients and resistivity measurements as a function of temperature have been made with a sintered plate of uranium monosulfide containing approximately 5 percent uranium oxysulfide (UOS). The potential probes consisted of platinum wires wrapped around two parallel grooves which had been cut around the perimeter of the slab by means of Elox techniques. Prior to these measurements, the specimen was cleaned by means of the high-temperature vacuum treatment described above. The results of Seebeck coefficients and resistivity measurements are shown in Figures 89 and 90, respectively. In addition, the product $\alpha^2\sigma$, where α is the Seebeck coefficient and σ the electrical conductivity, is plotted versus temperature in Figure 91.

Figure 89

ABSOLUTE SEEBECK COEFFICIENT VERSUS TEMPERATURE FOR SINTERED SLAB OF URANIUM MONOSULFIDE

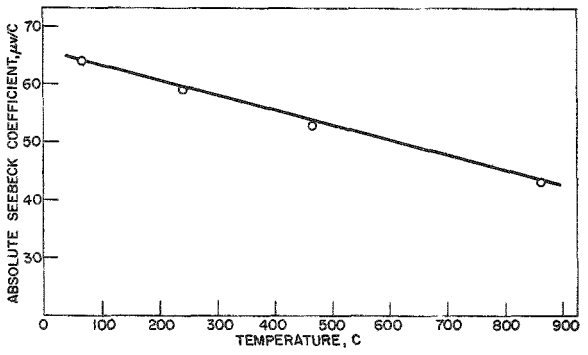

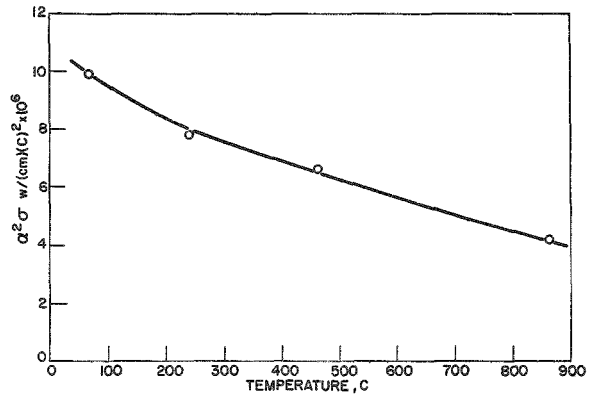

Figure 90

RESISTIVITY VERSUS TEMPERATURE FOR URANIUM MONOSULFIDE

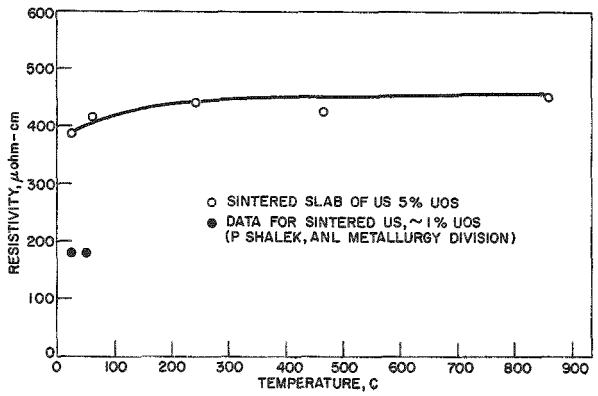

Figure 91

DEPENDENCE OF $\alpha^2\sigma$ ON TEMPERATURE FOR SINTERED SLAB OF URANIUM MONOSULFIDE

(Sample contained about 5% UOS)

The Seebeck coefficient values shown in Figure 89 are higher than the values which were previously obtained from a similar slab of this material and which are shown in Figure 86. The slab used in the earlier studies had not been cleaned after fabrication. In addition, the earlier Seebeck measurements were made under less refined experimental conditions.

It is apparent from Figure 90 that the resistivity of our uranium monosulfide specimen increased but slightly with temperature. For comparison, values obtained by Shalek[61] are also shown in Figure 90. A similar trend of resistivity with temperature was found with the cerium sulfide system.[62]

We can conclude from the above thermoelectric parameter measurements that uranium monosulfide, thorium monosulfide, and their solid solution behave somewhat like a metal.

Some recent thermal conductivity values measured over a limited temperature range by McElroy[63] of Oak Ridge National Laboratory with a sintered specimen of uranium monosulfide (one percent insolubles) supplied by Argonne allows the calculation of approximate figure-of-merit values for our sintered slab of uranium monosulfide from the data shown in Figures 89, 90, and 91. The results of the calculations are summarized below:

Temp (C)	Thermal Conductivity [w/(cm)(C)]	Figure of Merit ($K^{-1} \times 10^4$)
40	0.0914	1.3
75	0.0990	1.0
125	0.0850	1.2

These figure-of-merit values are roughly comparable with the values found with the promising refractory cerium sulfide system in the same temperature range, and are approximately 5 to 10 times lower than the figure-of-merit values obtained with lead telluride (maximum operating temperature ~600 C).

---

[61]Shalek, P., Metallurgy Division, Argonne National Laboratory, private communication.

[62]Ryan, F. M., I. N. Greenberg, F. L. Carter, and R. C. Miller, J. Appl. Phys., 33, 864 (1962).

[63]McElroy, P. L., Oak Ridge National Laboratory, private communication.

VI. DETERMINATION OF NUCLEAR CONSTANTS*
(C. Crouthamel)

Measurements of neutron cross sections of interest to the reactor program are continuing. Both low-intensity monoenergetic neutrons derived from the (p,n) reaction in a Van de Graaff accelerator and the intense continuous spectra from nuclear reactors are being used, depending upon the sensitivity required for the measurement.

This report contains a discussion of two series of experiments. The first is a series of runs in the Transient Reactor Test Facility (TREAT) designed to measure the rate of double neutron capture by rhodium to form 36-hr rhodium-105 and to derive the pile neutron capture cross sections of the short-lived intermediates, rhodium-104m and rhodium-104. Radiochemical results of isotope buildup and fission studies in EBR-I (Mark III) are also presented. Data are given on uranium-238 capture and fission cross sections. Data on plutonium-240 capture supplement the information previously reported for plutonium-239, uranium-233 and uranium-235 in the same loading.

A. Double Neutron Capture Experiments
(E. H. Dewell)

The TREAT (Transient REActor Test) facility at the National Reactor Testing Station (ANL Idaho Division) offers an unusual opportunity for studying the behavior of samples exposed to very high neutron fluxes for short periods. Among other phenomena, the capture cross sections of the short-lived radioactive species which can be produced *in situ* from a stable target may be studied in TREAT.

The equations for such reactions can be written

$$A \xrightarrow[\sigma_A]{(n,\gamma)} B \xrightarrow[\sigma_B]{(n,\gamma)} C \quad .$$

$$B \xrightarrow{\beta^-} D$$

The differential equations for each of the species involved become

$$\frac{dN_A}{dt} = -N_A \phi \sigma A \quad ; \tag{1}$$

$$\frac{dN_B}{dt} = N_A \phi \sigma_A - N_B (\lambda_B - \phi \sigma_B) \quad ; \tag{2}$$

$$\frac{dN_C}{dt} = N_B \phi \sigma_B - \lambda_C N_C \quad , \tag{3}$$

* A summary of this section is given on page 29.

where N_i represents the numbers of atoms of species i involved, λ_i their respective decay constants, σ_i their respective capture cross sections, and ϕ is the reactor flux.

If B is postulated to be short-lived, it can never accumulate to any large degree in any system. There is, accordingly, little hope of getting good measurements for its cross sections unless the quantity $\phi\sigma_B$ can be made sufficiently large with respect to λ_B that a fair fraction of the B atoms formed are converted by (n,γ) reaction to C rather than into the ordinary decay product, D. Even when this situation occurs, some very sensitive measurement of C must be available. Since C is isotopic with A and B, it cannot be separated chemically from either of them; hence, it probably cannot be detected unless it, too, is radioactive and has a short enough half-life that its decay can be observed. Its half-life must be much longer than that of B, however, since B is initially many million-fold more active than C. Measurement of C must wait on the decay of B. There is, however, another possibility, that is, the measurement of an active daughter of C may be made rather than the measurement of C itself. This route has not shown promise in the current work, however.

If Equations 1 to 3 are solved together, the decay rate of C at the close of an exposure t time units long is given by

$$\lambda_C N_C = \lambda_C \phi \sigma_B \frac{N_A \phi \sigma_A}{\lambda_B + \phi \sigma_B} \left[\frac{1}{\lambda_C - (\lambda_B + \phi \sigma_B)} \left(e^{-\lambda_C t} - e^{-(\lambda_B + \phi \sigma_B)t} \right) + \frac{1}{\lambda_C} \left(1 - e^{-\lambda_C t} \right) \right]. \quad (4)$$

It is readily apparent that, for comparable exposure times, the decay rate of C is proportional to the product of the two capture cross sections, σ_A and σ_B. Since these are small numbers, the amount of C generated is extremely small. The decay rate is also proportional to the square of the reactor flux. Hence, it is necessary to increase the flux as high as possible for double capture studies.

Several target materials are suitable for study in TREAT-rhodium in particular. It is monoisotopic, rhodium-103 being the lone stable isotope. The rhodium equations are

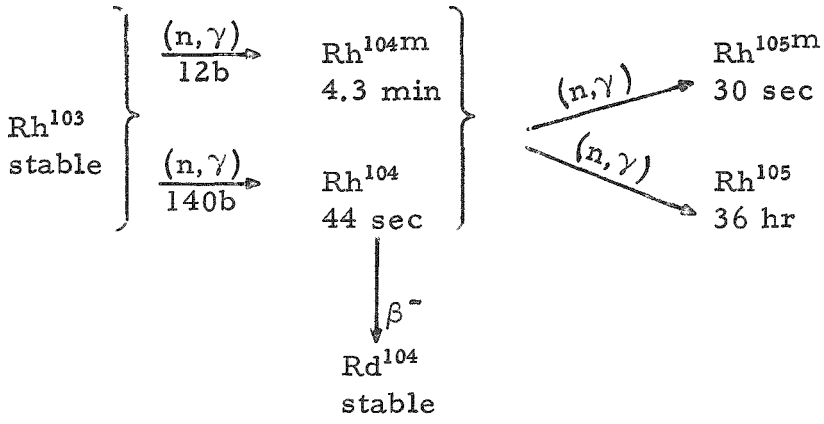

After an exposure, the rhodium-104 activities die out with the 4.3-min half-life of the metastable state, leaving the 36-hr rhodium-105 as a measure of the number of double captures taking place.

If rhodium were available completely free of contaminating elements, the measurements would be straightforward. The reaction-born rhodium-105 has a 0.320-Mev gamma ray in its decay scheme, which makes it easy to measure by means of conventional gamma-ray spectrometry. Rhodium occurs in nature in ores containing most of the platinum metals, from which it is difficult to separate. In particular, it retains traces of iridium with remarkable tenacity. This would not be serious except for the fact that iridium has a pair of resonance capture peaks at energies a little above thermal neutron energies ($\sigma_{c,0.65ev}$ = 5000b, $\sigma_{c,1.3ev}$ = 6000b). The first produces 74-day iridium-192, and the second produces 19-hr iridium-194. Iridium, therefore, activates strongly in a pile spectrum. Both of these emitters have gamma rays of 0.32-Mev energy and can be expected to mask the rhodium-105 gamma rays completely. Moreover, if the rhodium contains any ruthenium, an alternate path for rhodium-105 production exists via the reaction

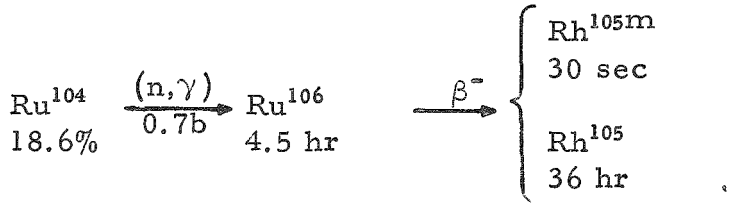

The rhodium-105 produced by the latter reaction adds to any rhodium-105 produced by double neutron capture to give high values for the cross sections of rhodium-104, -104m. Clearly, the lower the ruthenium level, the more accurately the desired cross sections of rhodium can be measured. The actual requirements in this regard cannot be calculated directly, but a rough estimate shows that 10 ppm of ruthenium would add about 10 percent to the rhodium-105 level expected from the irradiation of rhodium-104, assuming that the cross sections for rhodium-104 and -104m are near 50 b. One

unpublished set of values[64] places the two cross sections at 800 ± 100 b and 40 ± 30 b for the 4-min and 42-sec isomers, respectively.

A sample of rhodium sponge of nominal 99.995% purity was obtained from the Johnson-Matthey Company. Activation analysis showed strong lines for sodium, chlorine, iodine, and iridium. Ruthenium lines have not been unambiguously identified yet, and work is continuing on this point. A number of other samples of rhodium were also examined in which the impurity levels were higher. Iridium was common to all samples; sodium and the halogens were usually observed, along with traces of gold and antimony.

Several exposures of rhodium in TREAT have been completed. Because of the overwhelming presence of iridium-192, and -194 activities, even in the case of the sample obtained from the Johnson-Matthey Company, it was necessary to dissolve the exposed material by means of a potassium acid sulfate fusion, to convert the rhodium to the anionic chloro complex, and to separate it from iridium by anion exchange. The procedure was based on a method worked out by Berman and McBryde[65] for microgram quantities of rhodium and iridium. Scaling up to the 100-mg level for the pile experiments was not very successful, but decontamination factors of 10 or so were observed. Three passes through the column gave sufficient decontamination so that the rhodium-105 level could be obtained from the composite decay curve of the residual iridium and rhodium activities.

Calibration experiments are in progress to provide the data needed to convert the observed rhodium count rates to absolute disintegration rates. Sufficient rhodium-105 for this purpose can easily be obtained, using the ruthenium reaction already discussed. These data will permit the desired cross sections to be calculated.

B. Capture and Fission Reactions in EBR-I
(C. E. Crouthamel, R. R. Heinrich, G. H. McCloud)

The previous reports of data from EBR-I Mark III irradiations, made in ANL-6569, p. 162, and ANL-6596, p. 212, gave the horizontal and vertical variations of the capture and fission cross sections for uranium-233, uranium-235, plutonium-239, and also the (n,2n) reactions per 10^6 uranium-233 atoms as a function of reactor position. The significance of these data to the fast breeder reactor program was discussed, and the Mark III loading was briefly described. Where the data were a repetition of EBR-I Mark I and Mark II irradiation data, the two sets of data were compared and discussed. These data which are in a relatively raw and inconvenient form for general application, will be reduced, by means of a computer, to monoenergetic neutron cross-section values by the use of the known reactor neutron-energy spectrum and neutron multigroup calculations,

[64] Unpublished data from Chalk River reported in BNL-325, 2nd ed., Suppl. 1, p. 2, Jan. 1, 1960.

[65] Berman, S. S., and McBryde, W. A. E., Can. J. Chem. 36, 845 (1958).

as described by Yiftah, Okrent, and Moldauer.[66] It is planned to report the data in this form when the calculations are completed.

The data presented here essentially complete the chemical analysis of the Mark III samples.

The data from the vertical and horizontal loading of highly depleted uranium-238 are summarized in Table 45. Mass analysis of the batch of uranium-238 used in these irradiations showed an initial uranium-235 content of 100 ppm. In the core and inner blanket, the number of fissions from uranium-235 is less than 0.2 percent of the total. Figures 92 through 97 give capture, fission, and alpha values for uranium-238 and allow comparison

Table 45

VERTICAL AND HORIZONTAL VARIATIONS OF σ_c/σ_f OF URANIUM-238 IN EBR-I, MARK III

Vertical Loading

Vertical Distance from Midplane (in.)	Position of Sample in Reactor	Captures per 10^6 U^{238} atoms	Fissions[a] per 10^6 U^{238} atoms	$\alpha(\sigma_c/\sigma_f)$
9.86	upper bl.	26.7	2.88	9.27
7.86	upper bl.	42.3	6.96	6.08
5.86	upper bl.	61.0	19.8	3.08
3.87	core	69.7	69.8	0.999
1.87	core	75.7	110.0	0.688
-0.13	core	78.3	118.1	0.663
-2.12	core	-	106.4	-
-4.12	core	57.9	57.8	1.00
-6.11	lower bl.	43.4	16.6	2.61

Horizontal Loading

Distance from Reactor Axis (in.)				
0.93	core	78.3	118.1	0.663
3.80	core	75.4	65.7	1.15
4.60	inner bl.	58.9	29.0	2.03

[a] U^{238} contained 100 ppm U^{235} and negligible quantities of other fissile isotopes. Fission was determined by Cs^{137} monitoring, assuming a yield of 5.5 percent and a half-life value of 30.0 yr.

[66] Yiftah, S., Okrent, D., and Moldauer, P. A., Fast Reactor Cross Sections, Pergamon Press (1960), p. 5.

Figures 92-97

URANIUM-238 CAPTURE, FISSION, AND ALPHA IN EBR-I, MARK III

Horizontal Loading: Samples were near (± 1/2 in.) vertical midplane of core
Vertical Loading: Samples were about one inch from horizontal midplane of core

× previous data, Mark II irradiations.[67] o current data, Mark III irradiations

Figure 92
Horizontal Loading-Capture

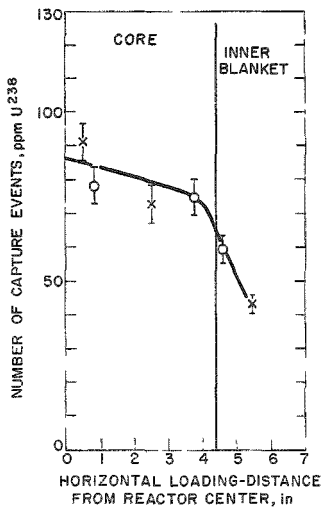

Figure 93
Vertical Loading-Capture

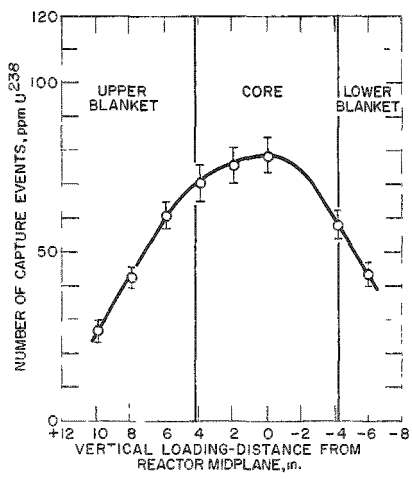

Figure 94
Horizontal Loading-Fission

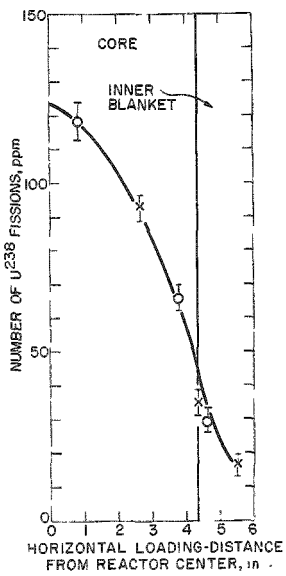

Figure 95
Vertical Loading-Fission

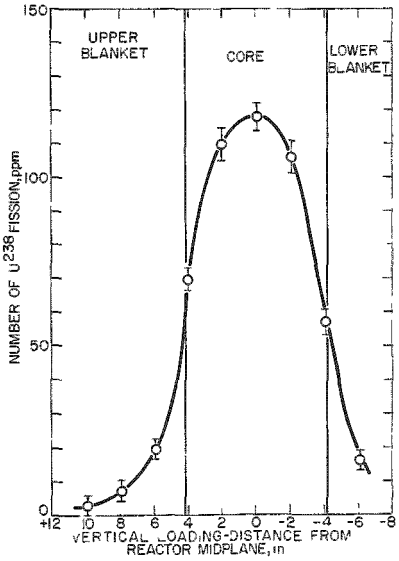

Figure 96
Horizontal Loading-Alpha, σ_c/σ_f

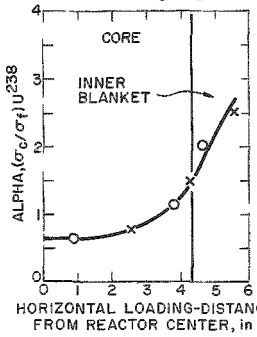

Figure 97
Vertical Loading-Alpha, σ_c/σ_f

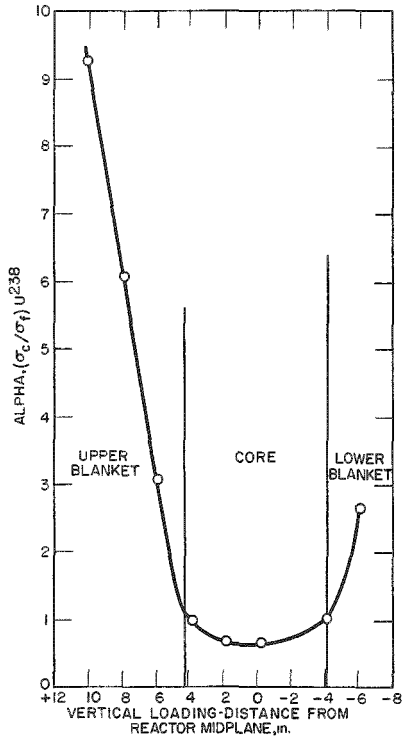

with previous results obtained by Kafalas and Heinrich[67] for horizontal loadings of uranium-231. The data for fissions in the reactor core are in very good agreement with the previous results for Mark II.[67] This undoubtedly results from the relatively low temperatures* at which these samples were irradiated, since the number of fissions is measured by a cesium-137 determination. Such measurements can be erroneously low if the samples are subjected to extremely high temperatures and if a vapor-escape path is available, since cesium-137 itself and its 3.8-min xenon precursor are both volatile. As was noted in ANL-6556, p. 364, some overheating of the uranium-235 and plutonium-239 samples apparently occurred in the Mark I samples with a consequent loss of cesium fission product.

The capture events in the uranium-238 were determined by counting the alpha activity of the plutonium-239 with a solid-state alpha spectrometer, whereas the previous results[66] were obtained with the Frish grid proportional gas spectrometer. The capture results of the two sets check within the experimental error (±5 percent standard deviation).

The Mark III loading contained, in the core of EBR-I, samples of U^{238}, U^{233}, U^{235}, Pu^{239}, and Pu^{240}. The Pu^{240} samples were analyzed only for the capture events. Table 46 summarizes the fission and capture data obtained at positions near the core center. Since all these samples were exposed to similar neutron spectra, the observed alpha (σ_c/σ_f) values can be compared directly; these are the values for the most energetic spectrum in the reactor.

Table 46

CENTER-OF-CORE RESULTS FOR EBR-I, MARK III IRRADIATIONS

Isotope, X	Fissions per 10^6 atoms	Captures per 10^6 atoms	$\alpha = \sigma_c(X)/\sigma_f(X)$
U^{233}	1420	79.0	0.0556
U^{235}	985	123	0.125
U^{238}	118	78.3	0.663
Pu^{239}	1170	87.5	0.0747
Pu^{240}	-	108	-

[67] Kafalas, P., and Heinrich, R. R., Capture and Fission Patterns of U^{238} in EBR-I (Mark II), Nuclear Sci. and Eng. 4, 698 (1958).

*The fission rate for U^{238} is nearly five-fold less than that for Pu^{239} and U^{235}. The temperature attained by the sample is correspondingly lower.

VII. ROUTINE OPERATIONS
(H. G. Swope)

A. Waste Processing
(H. G. Swope, K. Bremer, B. Kullen and R. Juvinall)

Routine Operations

A total of 49,255 gal of liquid radioactive wastes was processed during October, November, and December, 1962. The processing methods and volumes were as follows:

Process		Volume (gal)
Evaporation and Concentration		32,132
Filtration		8,435
Ion Exchange (cation only)		8,435
Absorption into Vermiculite		253
	Total	49,255

Special Problems
(R. Juvinall and B. Kullen)

This is the final progress report for the processing of liquid radioactive waste by the Chemical Engineering Division. During December, 1962, dismantling of the equipment and its transfer to the Plant Services Department was begun. Henceforth, the liquid radioactive wastes as well as the solid wastes will be processed by Plant Services Department. A topical report will be prepared by the Chemical Engineering Division on the operation of the liquid radioactive waste treatment facility over the past twelve years.

The amounts of wastes processed by the various methods in 1962 are shown in Table 47.

B. High-level Gamma-irradiation Facility
(H. G. Swope, N. Ondracek, G. Teats and V. Lemke)

The year 1962 was the seventh full year of operation of the Argonne High-level Gamma-irradiation Facility. Table 48 summarizes work in Rack M-1. There were 2,443 samples (equivalent to a No. 2 sized can) irradiated in 1962, as compared with 5,234 samples in 1961. In addition, 1,547 special dosimetry samples were run during the year. Rack M-2 also was used from March through August 1962.

Table 47

SUMMARY OF RADIOACTIVE LIQUID WASTES PROCESSED DURING 1962

1962 Quarterly Period	Volume, gal																		
	Struthers-Wells Evaporator									30-gal Concentrator			Cation Exchange (HCR-H+)						
	Retention Tanks	Decon. Soln.	Misc. Aqueous	GIF Pool Water	Cim-Cool	Flocculation	D-34 Sludge	Regen. Soln.	Adam's Filter Cake	Evap. Bottoms	Misc. Aqueous	Distillation Org.	R.T.	EBWR	Filtration	Flocculation	Absorption into Vermiculite	Neutralization of HF Waste	Totals
Jan.-March	2,190	12,270	822	476	605	200	1,300	2,470	1,050	1,697	-	62	-	-	-	1,120	372	-	24,634
April-June	9,990	11,873	832	490	330	-	2,210	1,710	1,355	1,209	160	-	-	21,520	21,520	-	791	171	74,161
July-Sept.	25,480	11,348	661	435	700	-	-	2,935	1,564	1,477	-	-	9,950	2,300	12,250	-	478	288	69,866
Oct.-Dec.	19,155	6,760	445	390	305	-	-	2,730	1,045	1,066	236	-	8,435	-	8,435	-	253	-	49,255
Totals	56,815	42,251	2,760	1,791	1,940	200	3,510	9,845	5,014	5,449	396	62	18,385	23,820	42,205	1,120	1,894	459	217,916

Abbreviations

GIF - High Level Gamma Irradiation Facility

R.T. - Retention Tanks

H.F. - Hydrofluoric acid wastes

EBWR - Experimental Boiling Water Reactor Wastes

Table 48

ARGONNE HIGH LEVEL GAMMA-IRRADIATION FACILITY

1962 Summary (Rack M-1)

	No. of Samples[a]				Total Day Units[b] in Rads				Total Night Units[b] in Rads			
	QMC	Educ. Inst.	Fed. Govt	ANL	QMC	Educ. Inst.	Fed. Govt	ANL	QMC	Educ. Inst	Fed. Govt.	ANL
January	155	0	0	21	309	0	0	237	0	0	0	1,404
February	125	25	0	25	205	22	0	344	4	0	0	2,028
March	93	5	0	57	123	11	0	306	0	10	0	1,220
April	122	16	0	30	185	49	0	457	0	30	0	2,177
May	30	3	0	18	40	14	0	450	0	14	0	1,791
June	68	13	0	30	84	44	0	565	0	0	0	2,423
July	77	0	0	15	108	0	0	351	0	0	0	1,628
August	723	60	0	14	2,275	83	0	579	0	19	0	2,467
September	205	10	0	26	720	20	0	850	0	58	0	3,043
October	167	1	0	28	308	2	0	667	0	45	0	2,531
November	39	5	0	16	94	8	0	477	0	72	0	1,639
December	68	3	30	120	121	2	24	490	0	6	8	2,049
Total	1,872	141	30	400	4,572	255	24	5,773	4	254	8	24,400
	Grand Total 2,443				10,624				24,666			

[a] Equivalent to a No. 2 size can (3-7/16 in. in diam x 4-9/16 in. high).

[b] Includes loadings and reimmersions. One unit = 2×10^6 rad.